THE FRACTIONATION, CARBONISATION AND CHARACTERISATION OF ELECTRO-SPUN LIGNIN FIBRES

by INAM UR RAHMAN KHAN

A thesis submitted to the
University of Birmingham
for the degree of
DOCTOR OF PHILOSOPHY

School of Metallurgy and Materials
College of Engineering and Physical Sciences
University of Birmingham
March 2020

UNIVERSITY OF BIRMINGHAM

University of Birmingham Research Archive

e-theses repository

This unpublished thesis/dissertation is copyright of the author and/or third parties. The intellectual property rights of the author or third parties in respect of this work are as defined by The Copyright Designs and Patents Act 1988 or as modified by any successor legislation.

Any use made of information contained in this thesis/dissertation must be in accordance with that legislation and must be properly acknowledged. Further distribution or reproduction in any format is prohibited without the permission of the copyright holder.

Abstract

Polyacrylonitrile (PAN) continues to be the primary precursor that is used for the production of carbon fibres. However, PAN is derived from petroleum and it is not a sustainable precursor in the long-term. This current research was focused on identifying bio-based precursors that could be used as an alternative for the production of fibrous preforms that could subsequently be carbonised.

In the first instance, lignin was purchased from Domtar PC sales centre (Germany) and it is referred to as softwood Kraft lignin (BioChoice®) in the thesis. Lignin was chosen because of its high aromatic content, availability and it is known to cross-link. The as-received lignin was characterised using a range of analytical techniques. The analyses indicated the presence of impurities such as small concentrations of carbohydrates and inorganics. The carbohydrates and inorganic content in the BioChoice® lignin were found to be 4.4% and 1.3%.

Two methods were considered to reduce the carbohydrate and inorganic contents in the as-received and these were acid-washing and solvent fractionation. The acid-washing was carried out using nitric acid. The solvent fractionation of as-received lignin was carried out using acetone; this was extended to include ethanol and propanol. The inorganic content in the BioChoice® lignin was reduced from 1.3% to 0.1% after solvent fractionation in acetone. However, the inorganic content after acid-washing was 0.34%. Solvent fractionation was found to be simpler and time-efficient for removing the inorganic content in lignin when compared with acid-washing and hence, it was adopted as a preferred method to purify the lignin prior to electro-spinning.

The majority of the initial electro-spinning experiments were undertaken using acetone-fractionated lignin using a binary solvent of acetone and dimethyl sulfoxide but the reproducibility was not consistent. The majority of the studies in the literature with regard to producing fibres with lignin have involved the use of synthetic polymer blends. For example, polyvinyl alcohol, polyvinyl acetate, polyethylene oxide and PAN. In the current study, a novel

approach of electro-spinning with a 100% blend of acetone-soluble and ethanol-soluble lignin was demonstrated for the first time. These fractions were electro-spun using a mixture (2:1) of acetone and dimethyl sulfoxide. The electro-spun fibres inspected in this study were found to be void-free with a relatively uniform and circular cross-section. From the numerous micrographs that were inspected, there was no evidence to suggest the presence of fused fibres.

The above-mentioned electro-spun fibres had a random orientation, as is the case with conventional electro-spinning using a ground conductor. In this study, a new ground electrode made from graphite was designed to enable the electro-spinning of aligned fibres. A series of detailed experiments were undertaken to derive the heat-treatment regime for the as-spun fibres. This was necessary to prevent fibre fusion during subsequent oxidative and carbonisation treatments.

The optimum heat treatment for the as-spun 100% lignin fibres was found to be drying at 140 °C in a vacuum oven for 6 hours prior to thermo-stabilisation at 250 °C in air and carbonisation in nitrogen. The sp^2 graphitic content in the carbonised fibres, as inferred by Raman spectroscopy, was found to be in the order 1000 °C < 1200 °C < 1500 °C.

The BioChoice® lignin was obtained from a commercial source and the decision was made to extract lignin from coir. Coir was chosen because it has the highest lignin content of all plant matter. The procedures and protocols for the extraction were developed and the lignin was characterised as mentioned previously. The lignin was electro-spun using a binary solvent of acetone and dimethylsulfoxide. It is proposed that coir with its high lignin content (32%) can be used as a renewable and sustainable precursor for the production of preforms for the production of carbon fibres.

Acknowledgements

I would like this opportunity to sincerely thank first and foremost Professor Fernando for his continued supervision and guidance through-out my PhD research. The invaluable discussions and meetings with Professor Fernando helped me to inculcate this research with the remit of developing experimental methods and finding solutions to the challenges faced during the PhD research. I would also like to thank and acknowledge Professor Fernando for his time and comments to improve my thesis.

I am extremely grateful to Dr Kukureka for his time, support and advice on improving my thesis. In addition, I would like to thank Dr Machavaram for helping me during my PhD. Moreover, I would also like to acknowledge and appreciate the help I received during my PhD study from the University staff members namely Mr Frank Biddlestone, Dr Cecile Le Duff and Mr Paul Stanley. Their kindness and willingness to assist in the instrumentation problems was invaluable towards the completion of my PhD.

Finally, I would like to express gratitude to my family and friends especially my parents for their love and support. Their prayers and continuous moral support have encouraged and guided me through the PhD study.

Contents

Abstract iii

Acknowledgements v

List of Figures xiv

List of Tables xxiv

List of Abbreviations xxvii

Chapter 1 Introduction and Motivation 1

1.1 Carbon Fibre 1

1.2 Carbon Fibre Precursors 2

1.2.1 Carbon Fibre from Polyacrylonitrile (PAN) 3

1.2.2 Heat Treatment 5

1.2.2.1 Thermo-stabilisation 5

1.2.2.2 Carbonisation 7

1.3 Carbon Fibres from Lignin 8

1.4 Aims and Objectives 9

1.5 Structure of the Thesis 10

Chapter 2 Literature Review 12

2.1 Ligno-cellulosic Biomass 12

2.2 Composition and Structure of Lignin 15

2.3 Isolation of Lignin from Biomass 19

2.3.1 Kraft Lignin 22

2.3.2 Soda Lignin (Alkali Lignin) 23

2.3.3 Sulfite Pulping (Lignosulfonate) 24

2.3.4 Milled Wood Lignin 26

2.3.5 Cellulolytic Enzyme Lignin 26

2.3.6 Steam Explosion Lignin 26

2.3.7 Organosolv Lignin 26

2.3.8 Ionic Liquid Treatment 27

2.4 Fractionation of Lignin 28

2.4.1 Lignin Solubility 28

2.5 Characterisation of Lignin for Structural Analysis 30

2.5.1 Pyrolysis 30

2.5.1.1 Pyrolysis-Gas Chromatography-Mass Spectrometry (Py-GC-MS) 31

2.5.2 Nuclear Magnetic Resonance Spectroscopy (NMR) 33

2.6 Carbon Fibres Derived from Lignin 36

2.6.1 Fibre Spinning 43

2.6.1.1 Melt-spinning and Dry-spinning 43

2.6.1.2 Wet-spinning and Dry Jet-Wet spinning 48

2.6.1.3 Electro-spinning 52

2.7 Structural Changes During the Heat Treatment of Lignin 63

2.7.1 Thermo-stabilisation 63

2.7.2 Carbonisation 68

Chapter 3 Materials and Methods 70

3.1 Lignin 70

3.1.1 Softwood Kraft (BioChoice®) Lignin 70

3.1.2 Lignin from Coir 70

3.1.3 Lignin Blending with Tannic Acid 70

3.2 Chemicals and Solvents 70

3.2.1 Sulphuric acid 70

3.2.2 Nitric acid 70

3.2.3 Solvents 70

3.2.4 Chemicals 71

3.3 The Characterisation of Softwood Kraft Lignin using TAPPI Standards 72

3.3.1 Moisture Content and Sample Preparation 72

3.3.2 Ash Content 72

3.3.3 Acid Insoluble Lignin (Klason Lignin) 73

3.3.4 Acid Soluble Lignin 73

3.4 Design of Experiments for the Diluted Acid Treatment of Lignin 74

3.4.1 Signal to noise ratio (S/N) of minimising the ash content 76

3.4.2 Analysis of Variance 76

3.4.2.1 Degrees of Freedom 77

3.4.2.2 Total Variation (S_T) 77

3.4.2.3 Percentage Contribution (%) 77

3.5 SAMPLE PREPARATION AND SOLVENT FRACTIONATION OF LIGNIN 77

3.6 Characterisation of Lignin Using Conventional Techniques 78

3.6.1 Particle Size Distribution 78

3.6.2 Elemental Analysis 79

3.6.4 Scanning Electron Microscopy 79

3.6.5 Differential Scanning Calorimetry 80

3.6.6 Dynamic Vapor Sorption 81

3.6.7 Gel Permeation Chromatography 81

3.6.8 Thermogravimetric Analysis 82

3.6.9 Pyrolysis-Gas Chromatography-Mass Spectrometry 82

3.6.10 Fourier Transform Infrared Spectroscopy 83

3.6.11 UV/Visible Spectroscopy 83

3.6.12 Proton Nuclear Magnetic Resonance Spectroscopy 83

3.6.13 Quantitative Carbon Nuclear Magnetic Resonance Spectroscopy 84

3.6.14 Quantitative Phosphorous Nuclear Magnetic Resonance Spectroscopy 86

3.7 Preparation of Lignin Solutions for Electro-spinning 87

3.7.1 Viscosity of Lignin Solutions 87

3.7.2 Electrical Conductivity of Lignin Solutions 87

3.7.3 Electro-spinning of Lignin Solutions 87

3.8 Thermo-stabilisation of Electro-spun Lignin Fibres in Air or Nitrogen 89

3.8.1 Characterisation of the Thermo-stabilised Electro-spun Lignin Fibres 91

3.9 Carbonisation of Thermo-stabilised Lignin Fibres 91

3.9.1 Characterisation of Carbonised Lignin Fibres 93

3.9.1.1 Fibre Morphology 93

3.9.1.2 Fibre Diameter Distribution 93

3.9.1.3 Electrical Conductivity 93

3.9.1.4 Raman Spectroscopy 94

3.9.1.5 X-ray Diffraction 94

3.10 Electro-spinning of Lignin-Tannic Acid Solution 95

3.11 Coir Fibre and Coir Pith 96

3.11.1 Cryo-milling of Coir Fibre and Pith 97

3.11.2 Quantification of the Lignin Content in Coir Fibres and Pith 97

3.11.3 Extraction of Lignin from Coir Fibre 98

3.11.4 Characterisation of Lignin from Coir Fibre 99

3.11.5 Electro-spinning of Lignin Extracted from Coir Fibres 99

Results and Discussion

Chapter 4 Solvent Fractionation and Characterisation of Softwood Kraft Lignin 100

4.1 Softwood Kraft Lignin 100

4.2 ANOVA Analysis 102

4.3 The Composition of the Ash in Softwood Kraft Lignin 105

4.4 Analysis of Moisture Content in Lignin using DSC 106

4.5 Moisture Sorption Characteristics of As-received (BioChoice®) Lignin 112

4.6 Solvent Fractionation of Lignin 114

4.7 Characterisation of Lignin using Gel Permeation Chromatography 115

4.8 Differential Scanning Calorimetry of Fractionated Lignins 118

4.9 The Effect of Molecular weight on the Glass Transition Temperature 125

4.10 Thermogravimetric Analysis of Fractionated Lignins 128

4.11 Pyrolysis-Gas Chromatography-Mass Spectrometry 133

4.12 Scanning Electron Microscopy 136

4.13 Fourier Transform Infrared Spectroscopy 138

4.14 Ultraviolet/Visible Spectroscopy 142

4.15 Proton Nuclear Magnetic Resonance Spectroscopy (1H NMR) 145

4.16 Carbon Nuclear Magnetic Resonance Spectroscopy 148

4.17 Derivation of the Empirical Formula for Lignin 150

4.18 Phosphorous Nuclear Magnetic Resonance Spectroscopy (^{31}P NMR) of Lignin 152

4.19 Structural Evaluation of Lignin 157

4.20 Summary 160

Chapter 5 Electro-spinning and Carbonisation of Lignin Fibres 161

5.1 Optimising the Electro-spinning Parameters 161

5.2 Thermo-stabilisation of BioChoice® Electro-spun Lignin (95ASL-5ESL) Fibres 172

5.2.1 Elemental Analysis of Electro-spun Fibres from 95ASL-5ESL 181

5.2.2 Thermal Analysis of 95ASL-5ESL Electro-spun Lignin Fibres 183

5.2.2.1 Differential Scanning Calorimetry 183

5.2.2.2 Thermogravimetric Analysis of 95ASL-5ESL Electro-spun Lignin Fibre 189

5.2.3 Fourier Transform Infrared Spectroscopy of Electro-spun Lignin Fibres 193

5.2.4 Solid State NMR (^{13}C CP/MAS NMR) Spectra of Lignin (95ASL-5ESL) Fibres 196

5.2.5 Evaluation of Chemical Structure of Lignin Fibres During Thermo-stabilisation in Air 198

5.3 Carbonisation of the Electro-Spun ASL-ESL Lignin Fibres 201

5.3.1 Fibre diameter distribution 203

5.3.2 Electrical Conductivity of Electro-spun ASL-ESL Carbonised Lignin Fibres 206

5.3.3 Raman Spectroscopy of Electro-spun ASL-ESL Carbonised Lignin Fibres 207

5.3.4 X-ray Diffraction of Electro-spun ASL-ESL Carbonised Lignin Fibres 210

5.4 Electro-spinning of Lignin with Tannic Acid 211

5.5 Summary 213

Chapter 6 Quantification, Extraction, Characterisation and Electros-pinning of Lignin from Coir 214

6.1 Characterisation of Coir Pith and Fibres 214

6.1.1 Scanning Electron Microscopy 214

6.1.2 Particle Size Distributions for Cryo-milled Coir Pith and Fibres 217

6.1.3 The Compositions of Coir Pith and Coir Fibre 219

6.2 Elemental Composition of Alkali Lignin from Coir and its Molecular Weight Distribution 221

6.3 Thermal Analysis of Alkali Lignin Extracted from Coir Fibres 223

6.4 Spectral Analysis of Alkali Lignin Extracted from Coir Fibres 226

6.4.1 Ultraviolet/Visible Spectroscopy 226

6.4.2 Fourier Transform Infrared Spectroscopy of Alkali Lignin Extracted from Coir Fibre 227

6.4.3 Proton Nuclear Magnetic Resonance Spectroscopy of Alkali Lignin from Coir Fibre 231

6.4.4 ^{13}Carbon Nuclear Magnetic Resonance Spectroscopy of Alkali Lignin from Coir Fibre 232

6.4.5 ^{31}Phosphorous Nuclear Magnetic Resonance Spectroscopy of Alkali Lignin Extracted from Coir Fibre 233

6.5 Electro-spinning of Alkali Lignin Extracted from Coir Fibres 235

Chapter 7 - Conclusions and Future Work 237

7.1 Conclusions 237

7.1.1 Solvent Fractionation and Characterisation of Softwood Kraft lignin 237

7.1.2 Electro-spinning and Carbonisation of Lignin-based Fibres 238

7.1.3 Quantification, Extraction and Electrospinning of Lignin from Coir 239

7.2 Future Work 240

Appendices 242

Appendix A: Experimental Method for Atomic Force Microscopy and Surface Wettability 242

Appendix A1: Atomic Force Microscopy 242

Appendix A2: Surface Wettability 243

Appendix B: Results and Discussion for AFM and Surface Wettability 244

Appendix B1: Atomic Force Microscopy of Electro-spun ASL-ESL Lignin Fibres 244

Appendix B2: Wettability of Electro-spun ASL-ESL Carbonised Lignin Fibres 247

Appendix C: List of Structures 249

Appendix D: Chemical Structure and Solubility of Bio-based Precursors 254

Appendix E: Thermogravimetric Analysis and Properties of Bio-based Precursors 256

References **258**

List of Figures

Figure 1.1 Schematic illustration of the production of PAN-based carbon fibres (18). 3

Figure 1.2 Co-monomers typically used in the polymerisation of acrylonitrile (17). 4

Figure 1.3 Chemical structure of Polyacrylonitrile and its repeat unit. 5

Figure 1.4 Proposed mechanism for the thermo-stabilisation of PAN (27-30). 6

Figure 1.5 Conversion of stabilised PAN fibres to carbon fibres (8, 18, 27-30). 7

Figure 1.6 Estimated production costs per kg for production of carbon fibres from lignin and PAN-based precursors (2, 38). 8

Figure 2.1 Chemical structures on the: top row - the main building blocks/precursors of lignin and they are referred as monolignols; and bottom row - the corresponding polymeric units found in structure of lignin (59-62). 16

Figure 2.2 Resonance stabilisation of radicals over delocalised aromatic ring and aliphatic side chain to form interunit linkages (63). 16

Figure 2.3 Structure of softwood lignin consisting of phenyl propanoid units and common lignin interunit linkages (35). 17

Figure 2.4 A summary of common procedures including by ionic liquids treatments (ILs) that are used for the isolation of lignin from ligno-cellulose (72). 19

Figure 2.5 The main extraction methods used for the isolation of lignin from biomass (62, 73). 20

Figure 2.6 Estimated production of lignin from extraction procedures in 2015; the total is 1.2 million tonnes (76). 21

Figure 2.7 Typical functional groups present in the structure in Kraft lignin (35). 23

Figure 2.8 Cleavage of the α-ether bond in lignin during the soda process (82). 23

Figure 2.9 The sulfonation of softwood lignin using the acidic sulfite process (84). 24

Figure 2.10 GC chromatogram of volatile products released during the pyrolysis of lignin at 150 °C, 200 °C , 250 °C and 300 °C (146). 32

Figure 2.11 HSQC spectrum of softwood Kraft lignin with the assignment of structural features for the: (a) aliphatic; region and (b) aromatic region (163). 35

Figure 2.12 Schematic illustration of a manufacturing process for lignin based-carbon fibres (3, 5, 67, 112, 177, 184-193). 36

Figure 2.13 Schematic illustration for fibre spinning: (a) melt-spinning (206, 209); and (b) dry-spinning (188). 44

Figure 2.14 SEM micrographs of carbon fibres from organosolv hardwood from yellow poplar (YP)/switchgrass (SG) lignin blends: (a) 50% YP: 50% SG, and (b) 85% YP:15% SG 46

Figure 2.15 (a-b) SEM micrographs of carbon fibres produced from acetylated softwood Kraft lignin by dry-spinning (188). 47

Figure 2.16 Schematic illustration of a conventional setup for wet-spinning (194, 227). 48

Figure 2.17 (a-b) SEM micrographs of lignin/PAN blends: (a) without lignin; and (b) with 0.2% lignin in the coagulation bath (189). 49

Figure 2.18 Conventional setup for dry jet-wet spinning (181). 50

Figure 2.19 (a-d) SEM micrographs of softwood Kraft lignin/cellulose fibres made using dry jet-wet spinning (191). 51

Figure 2.20 Schematic illustration of a typical electro-spinning setup for producing randomly orientated micro-to-nano diameter fibres (249, 253-255). 53

Figure 2.21 Schematic illustration of several types of charged jets that can be ejected from the Taylor cone (249, 262). 56

Figure 2.22 (a-c) Schematic illustrations of electro-spinning setups with modified collector used for the fabrication of uniaxially aligned fibres: (a-b) shows the influence of rotating drum with cellophane tapes and conductive copper wire (265); (c) shows the effect of introducing conductive strips inside the rotating cylinder (267); and (d) represents SEM micrographs of the aligned fibres from (c). 58

Figure 2.23 Schematic illustration of collector modifications used for fabrication of uniaxially aligned fibres with the corresponding fibre micrographs; (a-c) shows use of silicon (Si) conductive strips with the corresponding SEM images (251); and (d-g) shows the use of step-based aluminium conductive strips with the associated SEM images (268). 59

Figure 2.24 (a-b) SEM micrographs of lignin/PEO electro-spun and thermo-stabilised fibres at 250 °C in air for 1 hour: (a) unfused fibre morphology from HW/PEO blend; and (b) fused fibres from a mixture HW/LW with PEO (184). 60

Figure 2.25 SEM micrographs of lignin/PEO electro-spun fibres that were carbonised at 1000 °C in nitrogen for 1 hour: (a) unfused fibre morphology from HW/PEO blend; and (b) fused fibres from a HW/LW blend with PEO (184). 61

Figure 2.26 (a-b) SEM micrographs show the morphology of softwood Kraft lignin/PEO fibres mat carbonised directly at 1000 °C without a thermo-stabilisation step (183). 62

Figure 2.27 Mechanism proposed by Norberg et al., to demonstrate homolytic cleavage of the β-O-4 linkage in softwood Kraft lignin followed by rearrangement leading to the formation of stilbene when heated in an air atmosphere to 250 °C (5). 66

Figure 2.28 Homolytic cleavage of the C-O (β-O-4) and O-C (OMe) linkages during heat treatment of softwood lignin up to 350 °C (285, 286, 289). 67

Figure 2.29 The mechanism involving the cleavage of a C-C bond in a dimeric lignin unit and the release of formaldehyde via hydrogen abstraction (222). 67

Figure 2.30 The oxidation reactions occurring during the heat treatment of Kraft lignin in air at 200-250 °C (222). 68

Figure 2.31 The proposed mechanism for the formation of condensed structures in lignin at elevated temperatures (180). 69

Figure 2.32 Model of turbostratic carbon (30). 69

Figure 3.1 Reaction scheme for the acetylation of lignin (299). 85

Figure 3.2 Reaction scheme for the phosphorylation of lignin (165). 86

Figure 3.3 (a) Shows schematic illustration of electro-spinning setup with a flat plate ground-electrode for collecting randomly oriented lignin fibres; and (b) shows photograph of the electro-spinning unit. 88

Figure 3.4 Schematic illustration of collector-plate used for electro-spinning of aligned fibres. 89

Figure 3.5 The furnace assembly used for the heat treatment of lignin fibres. 92

Figure 3.6 (a-e) Images of coir with (a-c) showing soaking of coconut husk in water and extracted coir fibres and coir pith; (d-e) shows the as-received coir fibre bundle and coir briquette. 96

Figure 3.7 Illustration of the steps that were taken for reducing the particles size for coir fibre and coir pith using cryo-milling. 97

Figure 4.1 (a-b)The Taguchi analysis of parameters involved with the plots for (a) means and (b) S/N ratios for the performance measure. 102

Figure 4.2 (a-d) Residual plots for the ash content. 104

Figure 4.3 Tukey confidence interval plot of pH factors. 104

Figure 4.4 The elemental composition of the ash in oxidised as-received lignin. 105

Figure 4.5 The first cooling and heating DSC thermograms for as-received lignin (ARL), vacuum dried (Vac 80 °C) and freeze-dried lignin: (a) cooling; and (b) heating. 108

Figure 4.6 Second cooling and heating DSC thermograms for as-received lignin (ARL), vacuum dried (Vac 80 °C) and freeze-dried lignin: (a) cooling; and (b) heating. 110

Figure 4.7 Moisture uptake experiment for as-received lignin: (a) drying cycle at 80 °C for 6 hours; and (b) followed by moisture sorption-desorption isotherm with respect to change in relative humidity at 25 °C. 113

Figure 4.8 Molecular weight distribution traces for as-received lignin: (a) soluble; and (b) insoluble lignin fractions. 116

Figure 4.9 DSC traces for first heating scan of as-received lignin: (a) soluble; and (b) insoluble fractions using acetone, ethanol and 1-propanol. 119

Figure 4.10 DSC traces for the second heating scan of as-received lignin: (a) soluble; and (b) insoluble fractions. 121

Figure 4.11 DSC traces for the 3rd heating scan of as-received lignin: (a) soluble; and (b) insoluble fractions. 123

Figure 4.12 Glass transition temperature of as-received (ARL), soluble and insoluble lignin fractions in each heating scan. 124

Figure 4.13 The application of the Fox-Flory model where the T_g (reported for each heating scan) is plotted against the reciprocal of number average of molecular weight (Mn) for the fractionated lignin (soluble and insoluble lignin fractions) including the parent lignin. 126

Figure 4.14 Mass loss (TGA) and DTG data for as-received lignin. 128

Figure 4.15 (a-b) TGA and DTG traces for as-received lignin: (a) soluble; and (b) insoluble fractions. 130

Figure 4.16 Plot showing the char residue at 900 °C as function of the Mw for soluble lignin fractions. 132

Figure 4.17 PY-GC-MS chromatogram for as-received lignin (ARL) with acetone soluble (ASL) and acetone insoluble (ALR) fractions pyrolysed at (a) 320 °C and (b) 1000 °C. 133

Figure 4.18 Morphology of as-received (ARL), soluble and insoluble lignin fractions. 136

Figure 4.19 FTIR spectra of as-received lignin: (a) solvent soluble, and (b) insoluble fractions. 138

Figure 4.20 FTIR spectra for: (a) as-received lignin (ARL) and acetylated lignin (Ace-ARL); and (b) deconvoluted carbonyl peak for Ace-ARL sample. 141

Figure 4.21 UV/vis spectra of (a) soluble and (b) insoluble lignin fractions including as-received lignin. 142

Figure 4.22 ^{1}H NMR of as-received (ARL) lignin. 145

Figure 4.23 ^{13}C NMR of (a) as-received (ARL) and (b) acetylated lignin. 148

Figure 4.24 ^{31}P NMR of as-received lignin (ARL). 152

Figure 4.25 Plot the guaiacyl (G) lignin moieties concentration against the char content for the soluble and insoluble lignin fractions. The linear regression equations have been included for the two classes of materials. 156

Figure 4.26 The structural components of lignin moieties as identified by PY-GC-MS, ^{31}P NMR, ^{1}H NMR and UV/Vis. 157

Figure 4.27 The structural moieties in lignin compiled from the literature where ^{1}H NMR and ^{13}C NMR in relation with 2-D NMR was used (151, 152, 163, 164, 174, 386, 387). 158

Figure 4.28 The structural moieties in the lignin as identified by ^{31}P NMR spectroscopy including ^{13}C NMR, ^{1}H NMR and UV/Vis. 159

Figure 5.1 (a-g) SEM micrographs of electro-spun lignin fibres: (a-b) shows solvent rich morphology for experiment 1 (Table 5.1) with the lowest polymer concentration; (c-d) shows morphology of beaded-fibres emanating from experiment 2; (e-f) shows smooth and circular fibre morphology and this corresponds to experiment 3 with a viscosity of 0.42 Pa.s; and (c-d) shows morphology of fused fibres from experiment 4. 164

Figure 5.2 (a-f) Electro-spun lignin fibres using 95ASL–5ESL in acetone/DMSO: (a) macroscopic appearance of the deposition area (randomly oriented fibres); and (b-f) magnified SEM micrograph of fibres produced using the 52.8 wt% total polymer solution concentration. 166

Figure 5.3 (a-d) Modified (a) parallel plate collector for alignment with SEM images (b) x500, (c) x2500 and (d) x5000 magnifications. 167

Figure 5.4 Orientation of the aligned 95ASL-5ESL electro-spun lignin fibres. 168

Figure 5.5 (a-b) DSC traces for electro-spun ASL-ESL lignin fibres: (a) as-spun, and (b) vacuum dried at 140 °C. 170

Figure 5.6 (a-b) SEM micrographs of electro-spun ASL-ESL lignin fibres that were dried under vacuum at 140 °C for 6 hours. 171

Figure 5.7 (a-f) Micrographs showing the macroscopic morphology of the electro-spun ASL-ESL lignin fibre where the initial drying was carried out in a vacuum oven at: (a-b) 100 °C; (c-d) 120 °C; and (e-f) 140 °C respectively. 173

Figure 5.8 (a-f) Micrographs of electro-spun lignin fibres (95 ASL-5 ESL)- that were subjected to drying in a vacuum oven for 6 hours at: (a-b) 160 °C; (c-d) 180 °C; and (e-f) 200 °C respectively. 175

Figure 5.9 (a-f) Micrographs of electro-spun lignin fibres (95ASL-5ESL) that were previously dried at 140 °C in a vacuum oven and then thermo-stabilised in air or nitrogen at 150 °C, 180 °C and 200 °C. 179

Figure 5.10 (a-d) Micrographs of thermo-stabilised electro-spun lignin fibres (95ASL-5ESL) in air or nitrogen at: (a and b) 220 °C; and (c and d) 250 °C respectively. 180

Figure 5.11 Elemental composition (carbon, hydrogen and oxygen) for electro-spun lignin fibres from 95ASL-5ESL. 181

Figure 5.12 (a-b) DSC traces for the first heating scan for 95ASL-5ESL lignin fibres thermo-stabilised at 150 °C, 180 °C, 200 °C, 220 °C and 250°C: (a) in air; and (b) in nitrogen. 184

Figure 5.13 (a-b) DSC traces for the second heating scan for 95ASL-5ESL lignin fibres thermo-stabilised at 150 °C, 180 °C, 200 °C, 220 °C and 250°C: (a) in air; and (b) in nitrogen. 186

Figure 5.14 (a-b) DSC traces for the third heating scan for 95ASL-5ESL electro-spun lignin fibre thermo-stabilised at 150 °C, 180 °C, 200 °C, 220 °C and 250°C: (a) in air; and (b) in nitrogen. 188

Figure 5.15 (a-b) Thermal analysis of ASL-ESL electro-spun lignin fibres that were thermo-stabilised in air or nitrogen: (a) TGA; and (b) DTG curves. 191

Figure 5.16 (a-b) FTIR spectra of ASL-ESL electro-spun lignin fibres that were heat-treated at selected temperature: (a) in air; and (b) nitrogen. 195

Figure 5.17 Solid state ^{13}C CP/MAS NMR spectra for the ASL-ESL electro-spun lignin fibres that were heat-treated in nitrogen and air at 250 °C. 196

Figure 5.18 Homolytic cleavage of α-O-4 and β-O-4 in dibenzodioxocin; the numerical values of the bond dissociation energies (kJ/mol) are indicated (147). 198

Figure 5.19 Postulated mechanism for the release of formaldehyde from a phenylcoumaran structural unit (147). 199

Figure 5.20 Postulated reaction of β-aryl structure with bond dissociation energies for β-O-4 (kJ/mol) (112). 200

Figure 5.21 Structure of phenanthrene and naphthalene. 200

Figure 5.22 Colour changes in the electro-spun ASL-ESL lignin fibres before and after heat treatment at specified temperatures. 201

Figure 5.23 Electro-spun and carbonised (ASL-ESL) lignin fibres after carbonisation at 1000 °C, 1200 °C and 1500 °C with magnifications of x1000 and x2500. 202

Figure 5.24 Micrographs showing transverse sections of electro-spun (ASL-ESL) lignin fibres after carbonisation at 1000 °C, 1200 °C and 1500 °C. 203

Figure 5.25 (a-f) Histogram plots for the diameter distribution for the electro-spun (ASL-ESL) lignin fibres: (a) as-spun; (b) vacuum-heated at 140 °C; (c) thermo-oxidative stabilised at 250 °C; and carbonised at (d) 1000 °C; (e) 1200 °C and (f) 1500 °C in nitrogen. The histograms have been overlaid with a normal diameter distribution curve for each data set. 204

Figure 5.26 Average fibre diameter distribution for the electro-spun ASL-ESL lignin samples including the carbonised sample. 205

Figure 5.27 Raman spectra of electro-spun and randomly orientated lignin fibre mats that were carbonised at 1000 °C, 1200 °C and 1500 °C in nitrogen for 1 hour. 207

Figure 5.28 X-ray diffraction results for ASL-ESL lignin fibres carbonised at 1000 °C, 1200 °C and 1500 °C in nitrogen for 1 hour. 210

Figure 5.29 (a-b) SEM images of electro-spun lignin-based fibres (95 ASL-5 TA). 212

Figure 5.30 Micrographs showing transverse sections of electro-spun (ASL-ESL) lignin fibres after carbonisation at 1500 °C. 212

Figure 6.1(a-d) SEM micrographs of as-received coir pith showing: (a-b) a flaky morphology attributed to the cellulose microfibrils (374); and (c-d) a compacted version of the flaky morphology which is thought to be comprised of agglomerates of cellulose microfibrils and lignin particles (374, 417). 215

Figure 6.2 (a-d) SEM micrographs of as-received coir fibres: (a-b) transverse section; and (c-d) surface morphology. 216

Figure 6.3 (a-d) SEM micrographs showing morphologies of: (a-b) cryo-milled coir pith; and (c-d) cryo-milled coir fibres. 217

Figure 6.4 (a-b) Particle size distribution for: (a) cryo-milled coir pith; and (b) cryo-milled coir fibre. 218

Figure 6.5 Elemental composition of the ash in oxidised coir pith and fibres. 220

Figure 6.6 Alkali lignin extracted from coir fibre. 221

Figure 6.7 (a-b) SEM micrographs alkali lignin extracted from coir fibre. 222

Figure 6.8 (a) TGA and (b) DTG data for coir fibre, coir pith, Klason and alkali lignin. 224

Figure 6.9 DSC traces of heating scans of alkali lignin. 226

Figure 6.10 UV/Visible spectra of BioChoice® and alkali lignin that was extracted from coir fibres. 227

Figure 6.11 (a-b) FTIR spectra of: (a) coir pith and fibre; and (b) alkali, BioChoice® and Klason lignin. 228

Figure 6.12 ^{1}H NMR of alkali lignin from coir fibres. 231

Figure 6.13 ^{13}C NMR of alkali lignin that was extracted from coir fibre. 232

Figure 6.14 ^{31}P NMR of alkali lignin extracted from coir fibre. 233

Figure 6.15 SEM micrographs of electro-spun fibres from lignin extracted from coir. 235

Figure A.1 Schematic illustration of the basic AFM setup to characterise the topography imaging of the electro-spun and carbonised lignin fibres. 243

Figure A.2 Schematic illustration of the contact angle measurement involving a drop of deionised water of the surface of an electro-spun and carbonised lignin fibre mat. 244

Figure B.1 Topography of lignin samples with (a-b) shows the topography and the profile of randomly orientated vacuum dried lignin electro-spun; (c) shows 3-D profile of electro-spun profile; (d) shows the calculation of surface roughness (f) show the comparison of surface roughness for different heat treated lignin samples measured along the fibre axis. 245

Figure B.2 Topography of (a) aligned singled electro-spun fibre with (b) its profile height and 3D image of electro-spun fibre. 246

Figure B.3 Contact angle measurement with (a) showing a water droplet on carbonised electro-spun lignin fibre mat and (b) shows the processing of image for theta (θ) measurement using ImageJ software. 247

Figure C.1 Structures of carbohydrates (cellulose and hemicellulose), tannic acid and daemonorops (dragons' blood) resin. 249

Figure C.2 Structures of pyrolysis products (Py-GC-MS) discussed in Chapter 4. 250

Figure C.3 Structures of pyrolysis products (Py-GC-MS) discussed in Chapter 4. 251

Figure C.4 Structures of products discussed in results and discussion section (Chapter 4 and Chapter 6). 252

Figure C.5 Structures of products discussed in results and discussion section (Chapter 4 and Chapter 6). 253

Figure E.1 TGA data of bio-based precursors including lignin. 256

List of Tables

Table 1.1 Comparison of properties of reinforcing fibres and typical metal alloys (9-12). 1

Table 2.1 Approximate compositions of specified biomass materials; the data are reported in weight %. 14

Table 2.2 Approximate weight-percentage of lignin interunit linkages and their corresponding dimer structures in softwood lignin(68, 69). 18

Table 2.3 A summary of conditions used for the extraction of lignin (74, 77, 82, 85-88). 25

Table 2.4 Examples of the solvents used commonly for the dissolution of lignin along with their Hildebrand solubility parameters and polarity indices (119-126). 29

Table 2.5 The pyrolysis types based upon processing parameters and the respective yields (129, 131). 30

Table 2.6 Properties of lignin-based carbon fibres obtained using specified spinning techniques and heat treatments. 38

Table 2.7 Processing parameters influencing the electro-spinning process. 55

Table 3.1 Factors and level of factors involved in the Taguchi (DoE) study for the acid-washing of lignin. 74

Table 3.2 The factors involved in the Taguchi (DoE) method for the acid washing of lignin. 75

Table 3.3 Summary of the heating regimes that were used to identify the optimum conditions for the thermo-stabilisation of electro-spun lignin fibres in air or nitrogen. 90

Table 4.1 The composition of the softwood Kraft lignin used in this study (BioChoice® lignin) and characterised in accordance with TAPPI211 and TAPPI222 (for pre-dried lignin). 100

Table 4.2 ANOVA analysis of the ash content for as-received softwood Kraft lignin. 103

Table 4.3 Physico-chemical properties of as-received (BioChoice®) lignin. 106

Table 4.4 The enthalpy of vaporisation including the peak area (J/g) and the T_g of as-received lignin. 111

Table 4.5 Solubility and solvent fractionation yields with their respective ash contents for each fraction. 115

Table 4.6 Molecular weights of BioChoice® lignin samples. 117

Table 4.7 The T_g of as-received lignin and fractionated samples. 125

Table 4.8 Char content (%) at 900 °C including the peak mass-loss of lignin at specific temperatures for as-received lignin including the soluble and insoluble lignin fraction. 131

Table 4.9 Main phenolic products from the pyrolysis of lignin at 320 °C and 1000 °C. 135

Table 4.10 FTIR spectral assignments for specific functional groups for lignin samples compiled from the reported literature (100, 101, 346, 376). 140

Table 4.11 Extinction coefficients for as received (BioChoice ® lignin) and fractionated lignin samples at 280 nm. 144

Table 4.12 The assignments of chemical shifts in the ^{1}H NMR spectra for as-received lignin (ARL). 146

Table 4.13 Integration and assignment of ^{13}C NMR chemical shifts for acetylated as-received lignin (Ace-ALR). 150

Table 4.14 Empirical formula for C_9 lignin unit derived from elemental composition and methoxyl content as inferred via ^{13}C NMR. 151

Table 4.15 Hydroxyl group content for lignin (mmol/g) calculated from the ^{31}P NMR spectra. 154

Table 5.1 The viscosity and electrical conductivity of the concentrations of lignin solutions (ASL-ESL) used in the electrospinning experiments. 162

Table 5.2 Elemental analysis of 95ASL-5ESL electro-spun lignin fibres. 182

Table 5.3 The glass transition temperatures for 95ASL-5ESL electro-spun lignin fibres thermo-stabilised in air and nitrogen. 185

Table 5.4 Char content of lignin fibres at 900 °C, DTG max peak and the mass loss of 50% at specific temperatures. 192

Table 5.5 Electrical properties of the carbonised ASL-ESL lignin fibres that were carbonised in nitrogen at 1000, 1200 and 1500 °C for 1 hour. 206

Table 5.6 Analysis of the position of the D and G-band in the Raman spectra for the carbonised lignin fibres and the FWHM for these bands along with their intensity and area ratios. 209

Table 6.1 Particle size distribution analysis for cryo-milled coir pith and cryo-milled coir fibre. 219

Table 6.2 The composition of coir pith and coir fibre in accordance with TAPPI methods. 220

Table 6.3 Elemental composition and molecular weight of alkali lignin. 223

Table 6.4 Char residue at 900 °C and maximum DTG peak temperature of biomass including Klason and alkali lignin. 225

Table 6.5 FTIR spectral assignments for specific functional groups for lignin samples compiled from the reported literature (100, 101, 346, 376). 230

Table 6.6 Hydroxyl group content in alkali lignin from coir fibre (mmol g^{-1}) moieties using ^{31}P NMR. 234

Table B.1 Contact angle of electro-spun and carbonised lignin fibres. 248

Table D.1 Chemical structure and solubility of bio-based precursors including lignin. 254

Table E.1 Char and ash content of bio-based precursors including lignin. 257

List of Abbreviations

PAN	Polyacrylonitrile
DMF	Dimethylformamide
DMSO	Dimethyl sulfoxide
PEO	Poly(ethylene oxide)
PVA	Polyvinyl alcohol
PET	Polyethylene terephthalate
CNC or NCC	Cellulose nanocrystals or nanocrystalline cellulose
ILs	Ionic liquids
CNF	Carbon nano-fibres
CNT	Carbon nano-tubes
T_g	Glass transition temperature
M_w	Weight average molecular weight
M_N	Number average molecular weight
PDI	Polydispersity index
SEM	Scanning electron microscopy
TAPPI	Technical Association of the Pulp and Paper Industry
DVS	Dynamic vapour sorption
GPC	Gel permeation chromatography
DSC	Differential scanning calorimetry

TGA	Thermogravimetric analysis
DTG	Derivative thermogravimetry
UV/Visible	Ultraviolet/visible spectroscopy
FTIR	Fourier transform infrared spectroscopy
NMR	Nuclear magnetic resonance
^{1}H NMR	Proton Nuclear magnetic resonance
^{13}C NMR	Carbon Nuclear magnetic resonance
^{31}P NMR	^{31}P Nuclear magnetic resonance
PY-GC-MS	Pyrolysis gas chromatography mass spectrometry
XRD	X-ray diffraction
TMS	Tetramethylsilane
TMDP	2-chloro-4,4,5,5-tetramethyl-1,3,2- dioxaphospholane
DoE	Design of experiments
AFM	Atomic force microscopy
ARL	As-received lignin
ASL	Acetone soluble lignin
ALR	Acetone (insoluble) lignin residue
ESL	Ethanol soluble lignin
ELR	Ethanol (insoluble) lignin residue
1-PSL	1-propanol soluble lignin

1-PLR	1-propanol (insoluble) lignin residue
TA	Tannic acid

Chapter 1 Introduction and Motivation

1.1 Carbon Fibre

Carbon fibre is an attractive engineering material mainly due to its specific tensile strength & stiffness, low thermal expansion, high electrical and thermal conductivity, good chemical resistance, elevated temperature tolerance and fatigue resistance (1-4). Its low density and high strength offers a wide range of applications as a reinforcement in composites for automotive, aerospace, military, energy and sporting goods industries (5-7). Carbon fibres (CFs) by definition have to contain more than 90 wt% of carbon and other heteroatoms whilst graphite fibres constitute 99 wt% of carbon (8, 9). The importance and significance of carbon fibre-based materials can be appreciated by comparing their mechanical properties with conventional engineering metal alloys as shown in Table 1.1. These values show that carbon fibres have superior mechanical properties as compared to the metal alloys (10).

Table 1.1 Comparison of properties of reinforcing fibres and typical metal alloys (9-12).

Material	**Tensile strength (GPa)**	**Young's modulus (GPa)**	**Density (kg/m^3)**	**Thermal conductivity (W/m·K)**	**Electrical resistivity (μΩ·m)**
PAN-based CF	3.5-6.4	200-500	1.70-1.80	14-45	11-18
Pitch-based CF	1.3-3.1	150-965	1.80-2.20	36-1000	1.1-12.1
Rayon-based CF	0.5-1.2	40-100	1.40-1.50	-	1-15
Lyocell Based CF	0.9-1.1	90-100	-	-	-
E-glass fibre	3.5	70	2.54	13	10^{18}-10^{19}
Aramid fibre (Kevlar 49)	2-3	127-135	1.47	0.04	-
Steel alloy	1-1.5	200	7.80	50	0.72
Aluminium alloy	0.5-0.8	72-76	2.70	205	0.003

1.2 Carbon Fibre Precursors

Carbon fibres are manufactured by carbonising suitable precursor fibres at temperatures ranging from 1000-2000 ˚C while the use of temperatures above 2000 ˚C results in graphitised fibres. Polymeric materials yielding a carbon residue without degrading during pyrolysis are generally considered to be potential precursors for the production of carbon fibres (11). The conventional precursors for the carbon fibres are as follows;

- Polyacrylonitrile (PAN)
- Pitch-based CFs
    - mesophase pitch
    - Isotropic pitch
- Cellulose-based CFs
    - Rayon
    - Lyocell
- Phenolic resin-based CFs

Carbon fibres produced from these precursors can be classified into various types depending on the processing parameters during carbonisation. These include processing temperature, the type of precursor used and the intended application. Carbon fibres with low strength and modulus typically 1-100 GPa are produced at a processing temperature of 300-1000 ˚C. These fibres are used as general-purpose grade. The high strength and intermediate to high modulus (200-450 GPa) carbon fibres are manufactured at higher temperatures 1000-2000 ˚C. The graphitised carbon fibres yielding a higher modulus (>450 GPa), carbon content and higher electrical conductivity but with reduced tensile and compressive strengths are obtained at processing temperatures above 2000 ˚C. These fibres are termed ultra-high modulus fibre (12-14). PAN is the most commonly used precursor among the conventional precursors, in fact 90% of the carbon fibres produced worldwide are manufactured from PAN (12).

1.2.1 Carbon Fibre from Polyacrylonitrile (PAN)

Carbon fibres from PAN were first produced in 1950s (15, 16). PAN consists of a theoretical yield of 67% by weight and gives high carbon content of approximately 55% upon pyrolysis (17). A general process used for manufacturing carbon fibres from PAN is summarised in Figure 1.1. The polymer solution is shaped into a fibre precursor form by extruding the solution directly into a coagulation bath (wet-spinning process) or by introducing an air gap between the spinneret and the bath (dry-spinning process). The fibres are washed, dried and stretched before commencing heat treatment. The fibres are thermo-stabilised during heat treatment followed by the conversion into carbon or graphitised fibres. Thermo-stabilisation is an exothermic oxidation process carried out in air typically in a temperature range of 200-300 °C which is below the polymer's degradation temperature. During this process, the polymer undergoes cross-linking reactions which enhance its capability to remain in a fibre form. The oxidised fibres are then converted into carbon and graphitised fibres in an inert atmosphere over a temperature range of 1000-3000 °C. During the whole process, the fibre experiences stretching and tensioning to increase the molecular orientation which enhances the mechanical properties of the carbon fibres produced. During the heat treatment process, the polymer goes through significant reactions including the evolution of gases leading to change in molecular structure and physico-chemical properties. The changes in the structure of PAN during the heat treatment regime and the effect of tensioning will be discussed in Section 1.2.3.

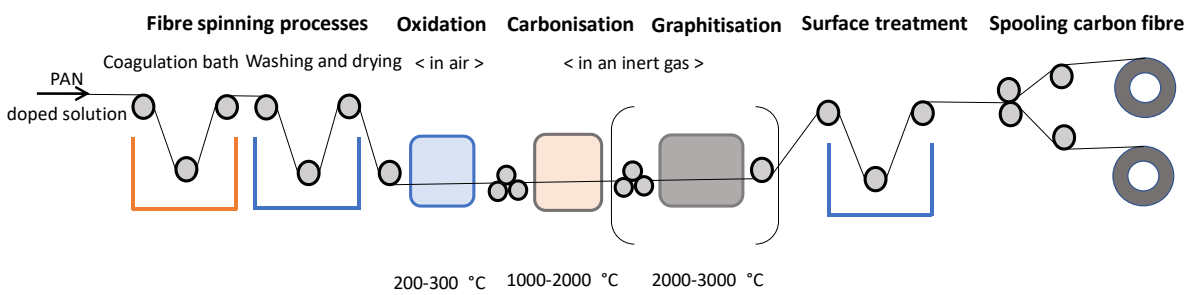

Figure 1.1 Schematic illustration of the production of PAN-based carbon fibres (18).

Polyacrylonitrile is an aliphatic polymer which is derived from radical co-polymerisation of at least 85% of its main monomer acrylonitrile along with other co-monomers (17). PAN derived from 100% acrylonitrile is generally not used for manufacturing carbon fibres due to its higher melting point which is close to its degradation temperature. The nitrile groups in the PAN homopolymer have strong intermolecular interactions leading to chain entanglement and high solvent resistance, thus hindering its spinnability (17). Therefore, acrylonitrile is co-polymerised with other linear chain co-monomers to improve its spinnability and processability at lower melting temperatures. PAN derived from co-monomers aid in the stabilisation steps with a lower residence time and in achieving increased molecular orientation. The co-monomers with acidic groups also act as catalyst and assist in cyclisation reaction during thermo-stabilisation. Increased molecular orientation improves the tensile strength and modulus of carbon fibres. Some of the co-monomers used for PAN polymerisation along with acrylonitrile are shown in Figure 1.2.

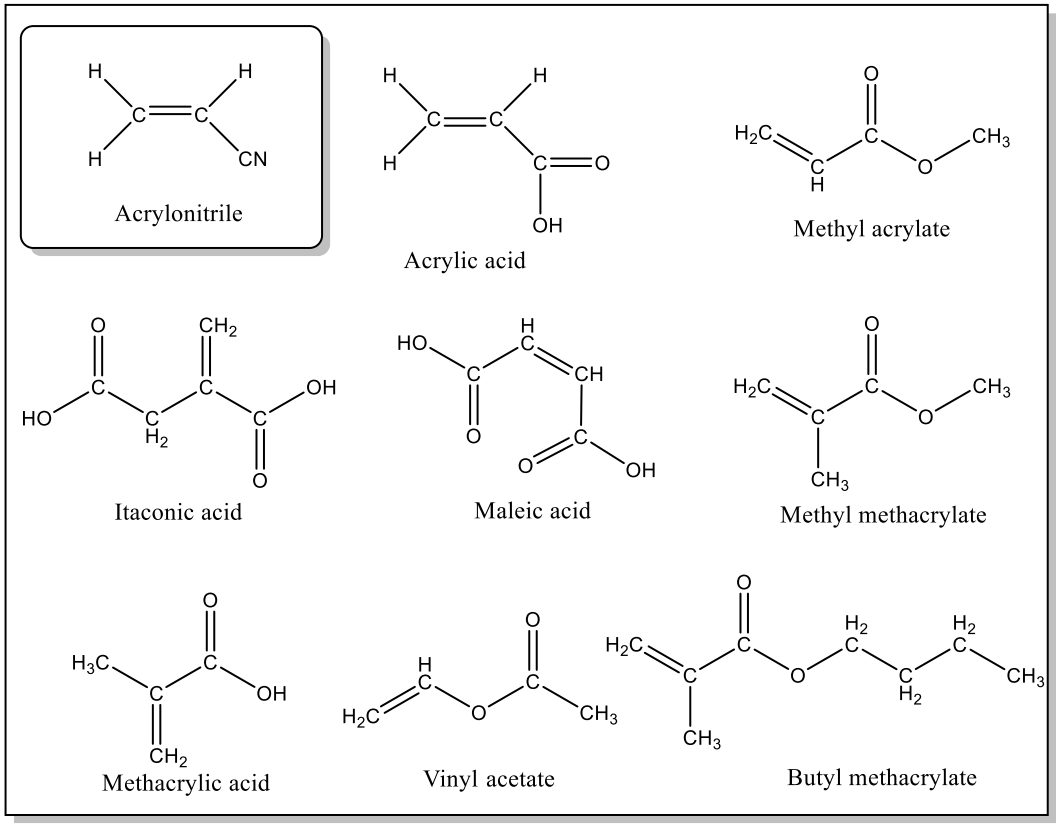

Figure 1.2 Co-monomers typically used in the polymerisation of acrylonitrile (17).

1.2.2 Heat Treatment

1.2.2.1 Thermo-stabilisation

Thermo-stabilisation is a critical step in the manufacturing of high-quality carbon fibres. During this process, the precursor fibre undergoes physico-chemical changes via exothermic oxidation, cyclisation reactions, dehydrogenation and cross-linking reactions (9). Thermo-stabilisation is carried out at a slow heating rate in air because the heat generated during cyclisation and oxidation reactions can lead to overheating and chain scission causing fibres to fuse and introduction of defects (19). The runaway reactions during thermo-stabilisation step are prevented by employing a slow heating rate and with the inclusion of co-monomers which have lower activation energy than the cyclisation reaction (12). The structure of polyacrylonitrile is shown in Figure 1.3. The nitrile groups are responsible for strong intermolecular interaction and the ladder-type structure formed during stabilisation (20).

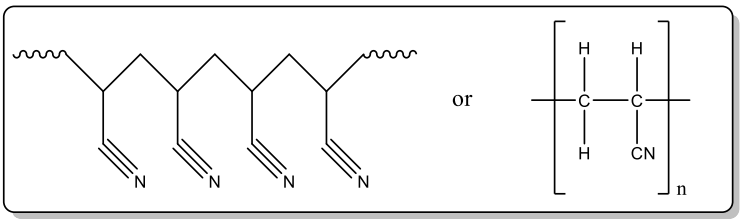

Figure 1.3 Chemical structure of Polyacrylonitrile and its repeat unit.

The mechanisms involved in thermo-stabilisation have been explained by several researchers (21-28). However, these explanations continue to be a subject of debate. One of the widely reported mechanism found in literature is shown in Figure 1.4 (28-30). It is believed that the nitrile (CN) groups in the polyacrylonitrile are responsible for exothermic cyclisation reaction forming a ladder-type structure (28). It is still unclear whether dehydrogenation or cyclisation occurs. These reactions covert the PAN into hexagonal cyclised C-N rings. The dehydration of C-C bonds during cyclisation takes place and contributes to the weight loss of PAN fibre. The cyclised rings are oxidised by the incorporation of several oxygen moieties including carbonyl groups

(C=O), hydroxyl (OH) groups with inclusion of bridging ether groups and carboxylic groups (27-29). This oxidation step promotes the intermolecular rearrangement cross-linking reactions which aid in the thermal stability of the precursor fibre and prevents the fibres from fusing (28). The formation of carbon dioxide (CO_2), carbon monoxide (CO) and water (H_2O) occurs during oxidative thermo-stabilisation (20).

The stabilisation steps are critical in rendering the precursor fibres suitable to withstand high temperature treatment during carbonisation and graphitisation steps (14, 20). During thermo-stabilisation, fibres remain under tension and their diameter is reduced. The stretching increasing the molecular orientation. This process results in high strength and modulus of carbon fibres (14). The precursor fibres undergo a colour change during stabilisation from white to pale yellow and reddish brown at the end of stabilisation and eventually turn black during carbonisation (28).

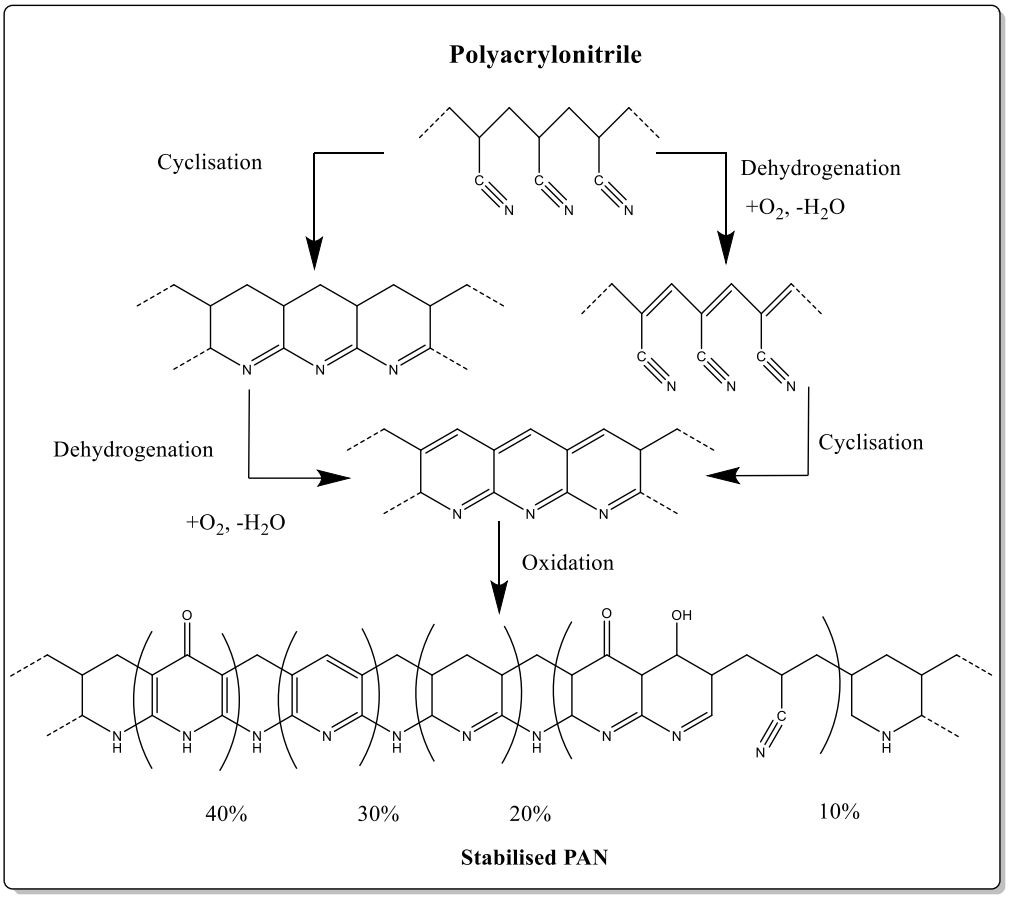

Figure 1.4 Proposed mechanism for the thermo-stabilisation of PAN (27-30).

1.2.2.2 Carbonisation

The stabilised fibres are carbonised in nitrogen or argon atmosphere under tension. The fibres lose weight upon dehydrogenation and evolution of gases, shrink and undergo structural changes during carbonisation (20). The stretching of fibres during carbonisation reduces the shrinkage and aids in maintaining the fibres orientation along its length (19). The carbonisation temperature depends on the intended application. The fibres carbonised at 1500-1600 °C usually have high strength with a well orientated carbon with a turbostratic structure (19). Upon graphitisation, the crystallinity increases in the fibre direction and the defects in the turbostratic structure are healed (19). The graphitised fibres are formed by the conversion of defects and disordered carbon structure into a crystalline graphitised structure via high temperature treatment (19, 20, 28).

The structural changes that occur during the conversion of stabilised PAN fibres to carbon fibres is shown in Figure 1.5. At a temperature below 700 °C, the evolution of toxic gases such as hydrogen cyanide (HCN), CO and ammonia (NH_3) occur (19, 29). At temperatures above 700 °C, denitrogenation takes place with the evolution of volatiles gases such as methane (CH_4), water, hydrogen, CO and CO_2 (8, 20, 29, 30).

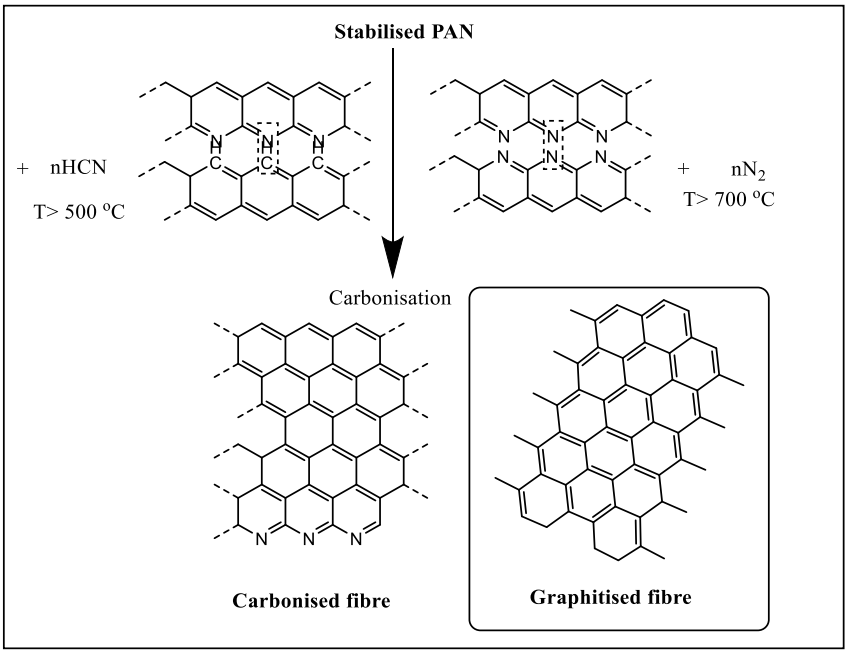

Figure 1.5 Conversion of stabilised PAN fibres to carbon fibres (8, 18, 27-30).

1.3 Carbon Fibres from Lignin

Several factors are involved in reducing the dependence on petroleum-based precursors for the production of carbon fibres that needs to be addressed. These issues are mainly related to the cost, need to find a renewable source and the toxicity of gases released during carbonisation (2, 5). The main cost associated with production of carbon fibres is attributed to the PAN precursor as shown in Figure 1.6. The cost distribution presented in Figure 1.6 is for wet-spinning of PAN precursor and the melt-spinning of lignin. However, the total cost distribution estimated by Baker *et al.*, (2) reported a significantly higher cost for the production of PAN-based carbon fibre ($25.14/kg for wet-spinning and $17.40/kg for melt-spinning). The cost for the production of lignin-based carbon fibres using melt-spinning was estimated to $4/kg. Hence there is an increased interest in engineering industries to look for cost-effective alternative precursors for the production of carbon fibres. Lignin is currently produced in large quantities, approximately 50 million tonnes per year by paper and pulp industry alone (31, 32). Currently, the full potential of lignin is not realised and only a small portion is being used commercially for products such as adhesives, binding agents and raw materials for chemicals (32, 33). Only 1-2% lignin in the world is utilised and the remainder is burned as fuel for energy generation (31, 34, 35). Lignin has been long considered to be a potential low-cost alternative precursor for carbon fibres (5, 7, 36, 37).

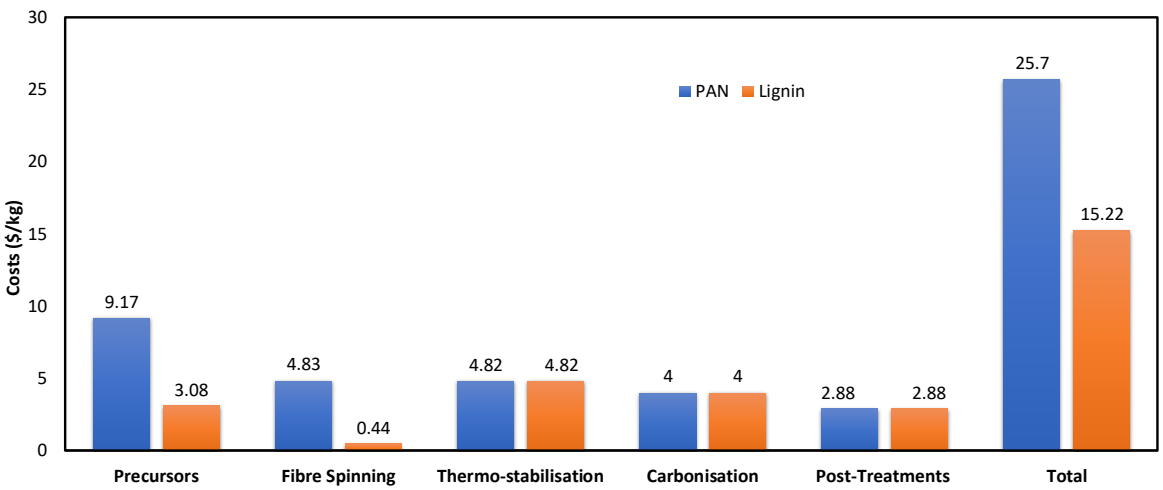

Figure 1.6 Estimated production costs per kg for production of carbon fibres from lignin and PAN-based precursors (2, 38).

1.4 Aims and Objectives

The aims and objectives of this proposed research project are as follows:

(i) To quantify impurities in industrially produced lignin (softwood Kraft lignin) and purify lignin via dilute acid treatment.

(ii) To perform solvent fractionation of softwood Kraft lignin to aid electro-spinning.

This was conducted using organic solvents to inspect the effect of solvent fractionation on reducing impurities and the resulting changes to the physico-chemical properties.

(iii) To investigate a novel approach based on the lignin/lignin blending and to determine optimum conditions for electro-spinning lignin without any synthetic polymer blend, in a non-toxic solvent system.

This study evaluated the production of lignin fibres in random and unidirectional alignment through a modified electro-spinning setup.

(iv) To investigate heat-treatment of electro-spun lignin fibres.

This included a detailed study of heat-treatment regime of lignin-based fibres to evaluate the effect of atmospheric and temperature conditions on the fibre morphology. These effects were correlated with the changes in their thermal and structural properties. A methodology was developed for the thermo-stabilisation of lignin fibres.

The influence of carbonisation temperature on their properties were also explored.

(v) To evaluate the viability of lab-based extraction of lignin from coir to produce electro-spun fibre.

This included research on determining the composition of lignin-rich coir and the quantification of lignin in coir. The lignin was extracted, characterised and used for electro-spinning.

1.5 Structure of the Thesis

Chapter 2

Chapter 2 represents the literature review which summarises a range of topics that are relevant to this research. This includes the sources of lignin, composition of biomass and various extraction procedures used in biorefinery (pulp and paper) and laboratory-scale. The effect of these extraction procedures on the structure of lignin and its physico-chemical properties is also discussed in detail. This chapter also gives an insight into the fractionation of lignin to improve its processability as a precursor for spinning fibres. The properties of lignin-based carbon fibre produced using various fibre spinning processes are also presented. This is followed by a review on fibre spinning techniques including electro-spinning which is a prime focus in this study. The structural changes in lignin during heat treatment are also discussed in this chapter.

Chapter 3

Chapter 3 provides a detailed experimental methodology for the research undertaken. This includes quantification of impurities and dilute acid treatment for the purification of lignin, solvent fractionation and techniques used for the characterisation of industrially produced lignin (softwood Kraft lignin). This chapter also includes the methodologies for electro-spinning and the investigation of heat-treatment regimes for producing lignin-based carbon fibre. The methods used for the characterising the physico-chemical properties of lignin-based fibres are also presented. This chapters includes the procedure for determining the biomass composition, lab-based extraction of lignin from biomass (coir), characterisation and electro-spinning of the extracted lignin.

Chapter 4

Chapter 4 represents the results and discussion and it provides an insight into the impurities in softwood Kraft lignin and the effect of acid treatment in reducing such impurities. This

chapter discusses the impact of solvent fractionation in the purification of lignin and its physico-chemical properties which plays an important role in the fibre spinning processes.

Chapter 5

Chapter 5 presents a novel approach for the electro-spinning of 100% solvent fractionated lignin without any non-lignin polymer blends. The optimum conditions required to electro-spin lignin are discussed. This chapter also reports on the conditions required for thermo-stabilisation which are important for producing lignin-based carbon fibres with smooth and circular morphology. The properties of the carbonised lignin fibres are discussed in this chapter.

Chapter 6

Chapter 6 includes the results of the quantification and composition of biomass (coir fibre and coir pith). The extraction, characterisation and electro-spinning of lignin from coir fibre are summarised in this chapter.

Chapter 7

Chapter 7 provides the conclusion reached from the results generated in this research. This chapter also presents pathways to expand on the current research and recommendations for future work.

Appendices

Appendices (A-E) are included and these represent small but focused aspects of the research undertaken. List of chemical structures which are discussed in this study are shown in Appendix C.

Chapter 2 Literature Review

This chapter presents an overview of the literature in the context of the current research undertaken on the production of carbon fibres from lignin. This includes ligno-cellulosic biomass composition, the postulated structure of lignin and the extraction procedures used globally for the extraction of lignin from biomass. The impact of the various extraction procedures on the physico-chemical properties of lignin, characterisation techniques utilised for elucidating the structure are reviewed along with the need for pre-treatment procedures for fibre formation. This chapter also presents a review on the fractionation of lignin to facilitate fibre spinning methods including electro-spinning. The structural changes during heat-treatment for the conversion of lignin-based fibre into carbon fibres are also discussed.

2.1 Ligno-cellulosic Biomass

Ligno-cellulosic biomass is mainly composed of lignin and polysaccharides. It is the most abundant renewable source of carbon in the world. Ligno-cellulosic biomass is primarily used in the paper and pulp industries as a renewable resource. It is also used in production of value-added chemicals such as sugars, bioethanol, vanillin, carboxylic acids and hydrocarbons (39, 40). Lignin is a naturally occurring bio-polymer found in the plant kingdom as a major component of plants along with cellulose and hemicellulose (41, 42). Lignin is an integral part of cell walls existing in the vascular system of plants including arborescent plants, herbaceous and agricultural biomass (43). There are two main types of cell walls that exist in plants. They are termed as primary and secondary cell walls. The primary cell walls are relatively thin and consist of growing cells and are mainly composed of cellulose, hemicellulose, pectins and proteins. The secondary cell walls are thicker, stronger and comprised of cellulose, hemicellulose and lignin (39). The lignin that is present in the cell walls is responsible for three primary functions (43):

- It reduces the permeation of water across the cell wall in the xylems and thus plays a vital role in the internal transport of water, nutrients and metabolites.

- It provides rigidity and hydrophobicity to the cell wall making it resistant to impact, bending and compression.
- It acts as a protecting layer to the cell wall by resisting an attack from the enzymes released by microorganisms.

Lignin is of great interest due to its properties and abundance (41). The presence of lignin has been verified in leaves, roots, foliage and tissues associated with the stem. The lignin content and its chemical composition can vary from the type of tree, growing conditions, species and the location within a tree, with high content in wood and low in juvenile shoots (41, 42, 44, 45). The lignin content in selected plants species is compiled in Table 2.1. The content is known to vary from hardwood (angiosperms), softwood biomass (gymnosperms) and agricultural residues. The average lignin composition in biomass is typically estimated to be between 10-25 wt% (39).

Table 2.1 Approximate compositions of specified biomass materials; the data are reported in weight %.

	Cellulose	Hemicellulose	Lignin	Extractives	Ash	Ref.
Softwood biomass						
Pine	32.1	14.2	31.2	15.6	2.4	(46)
Spruce	45.6	20.0	28.2	5.9	0.3	(47)
Japanese cypress	44.9	14.9	33.0	-	-	(48)
Fir	55.6	12.7	25.1	-	-	(49)
Lodgepole pine	45.0	23.6	28.1	5.0	0.3	(50)
Japanese cedar	38.6	23.1	33.8	4.0	0.3	(47)
Eastern red cedar	40.3	17.9	35.9	-	0.3	(51)
Harwood biomass						
Poplar	42.6	16.6	25.6	-	-	(52)
French oak	22-50	17-30	17-30	2-10	0.2	(53)
English oak	41.1	22.2	29.6	3.8-6.1	0.3	(53)
Agricultural waste						
Rice Straw	30.3-38.2	19.8-31.6	7-12.8	-	8-15.6	(54)
Wheat straw	33.7	19.1	19.8	-	9.7	(55)
Coir	24.7	12.3	40.1	-	2.6	(56)
Banana skin	13.2	14.8	14	-	-	(57)
Sugarcane bagasse	38.6	27.9	17.8	2.7	8.8	(58)

With reference to Table 2.1, it is seen that coir has the highest lignin content.

2.2 Composition and Structure of Lignin

Lignin is a complex biopolymer which is made up of three main precursors as shown in Figure 2.1. These are referred to as phenylpropanoid units or C_9 units; p-coumaryl alcohol, coniferyl alcohol and sinapyl alcohol. They differ from each other at the C-3 and C-5 positions due to the substitution of the methoxyl group (OCH_3). The numbering around the ring follows the rule that if there is only one OCH_3 attached to the aromatic ring, it will be on the C-3 position but not C-5 (42). As shown in Figure 2.1 (i), the aliphatic groups (side chain) are attached at the C-1 position, whilst the phenolic hydroxy (OH) group is attached at the C-4 position (para-position). The side chain is classified as α, β, and γ, with C-α being the one connected to the C-1 position of the aromatic (aryl) ring. These three alcohols are also termed as monolignols which undergo oxidative polymerisation in the biosynthesis of lignin and subsequently classified into three main monomeric units which constitutes the structure of lignin. The unit which is formed from p-coumaryl alcohol is known as p-hydroxyphenyl (H) lignin and it has no methoxyl group attached to it. The lignin unit which is formed from coniferyl alcohol is known as guaiacyl (G) unit having one methoxyl group. The lignin unit which is formed from sinapyl alcohol is referred to as syringyl (S) lignin with two methoxyl groups (43).

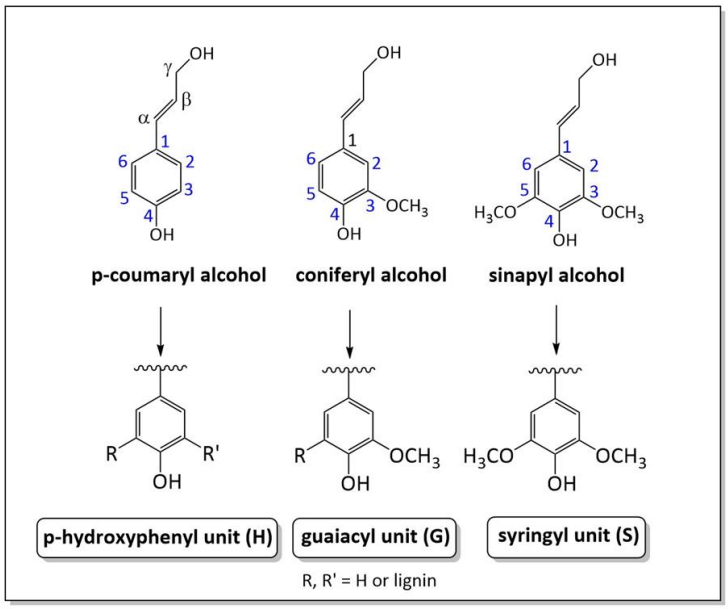

Figure 2.1 Chemical structures on the: top row - the main building blocks/precursors of lignin and they are referred as monolignols; and bottom row - the corresponding polymeric units found in structure of lignin (59-62).

The biosynthesis of lignin polymerisation proceeds via an oxidative radical coupling through a mechanism of dehydrogenative polymerisation. This hypothesis is also referred to as a lignification process and it is reported widely in the literature (40, 41). The process is initiated via a hydrogen abstraction from the hydroxyl group on the para-position leading to a phenoxy free-radical. This free-radical is delocalised over the aromatic ring and the aliphatic side chain leading to resonance stabilisation. The resonance stabilised structure of the lignin unit is shown in Figure 2.2.

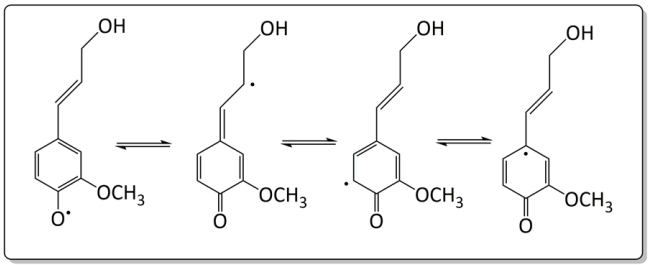

Figure 2.2 Resonance stabilisation of radicals over delocalised aromatic ring and aliphatic side chain to form interunit linkages (63).

The most stable free-radical structure couple together to form a linkage and this accounts for the growth of the lignin network. As aforementioned, these linkages are formed via the oxidative free-radical coupling of monomers and more importantly, with an end unit of the polymer, resulting in a condensed lignin structure (42). There are mainly two types of linkages in lignin, ether bonds (C-O-C) and carbon-carbon bonds (C-C) (41, 42). The common linkages found in softwood lignin are shown in Figure 2.3 and their approximate weight-percentage presented in Table 2.2.

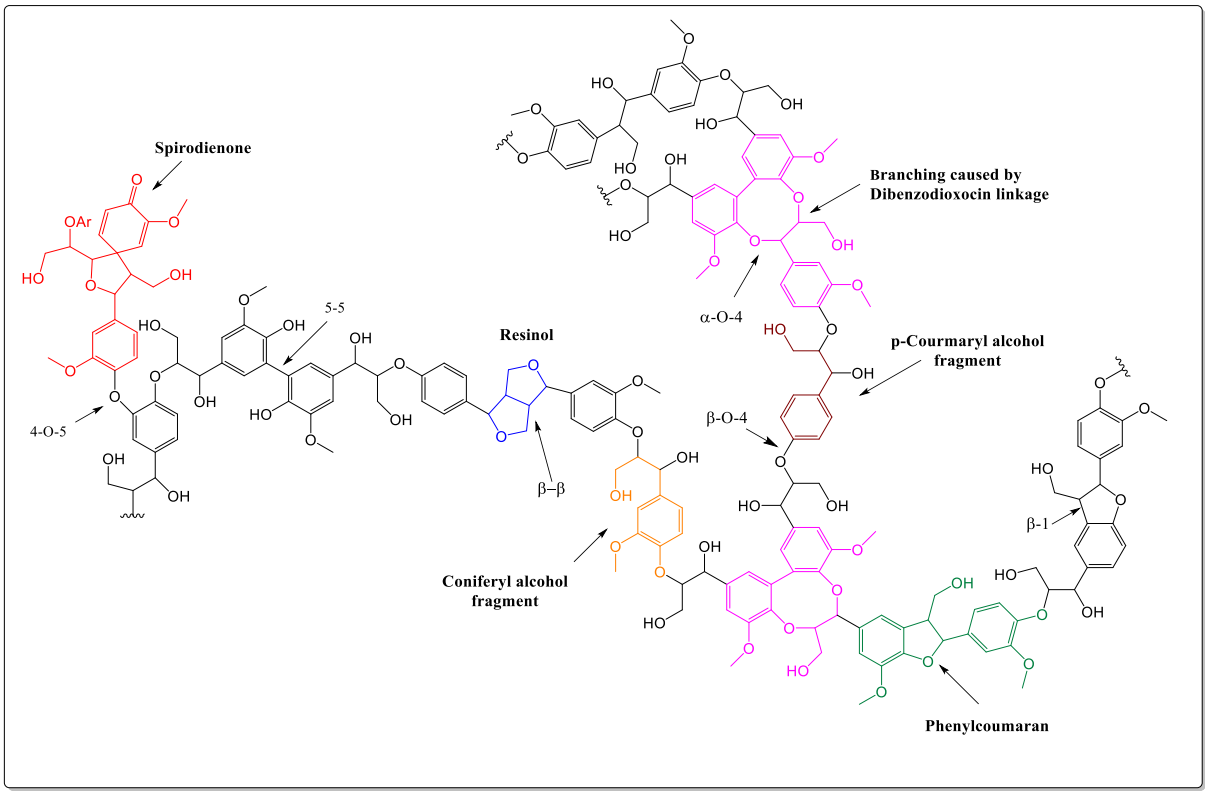

Figure 2.3 Structure of softwood lignin consisting of phenyl propanoid units and common lignin interunit linkages (35).

The structure of the softwood lignin is shown in Figure 2.3. Its shows the phenylpropanoids (lignin monomeric units) which are linked together by ether (C-O-C) or carbon (C-C) linkages. Guaiacyl (G) units (~95%) are largely present in softwood lignin with low concentration of p-hydroxyphenyl (H) and syringyl (S) units (41, 42, 62, 64, 65). The existence of the lignin dimeric units with defined linkages has been verified using techniques such as NMR, FTIR spectroscopy and pyrolysis-GC-MS. The presence of the functional groups and linkages shown in Figure 2.3

accounts for its complex heterogenous structures and it also makes it an attractive material suitable for various applications, including the production of carbon fibres (66, 67).

Table 2.2 Approximate weight-percentage of lignin interunit linkages and their corresponding dimer structures in softwood lignin(68, 69).

Linkage type	**Dimer structure**	**Approximate weight (%)**
β-O-4	Phenylpropane β-aryl ether	45-50
5-5	Biphenyl and dibenzodioxocin	18-25
β-5	Phenylcoumaran	9-12
β-1	1,2-Diaryl ether	7-10
α-O-4	Phenylpropane α-aryl ether	6-8
4-O-5	Diaryl ether	4-8
β-β	β-β-linked structures (pinoresinol)	3

2.3 Isolation of Lignin from Biomass

Lignin can be isolated from ligno-cellulosic biomass via chemical (65), physical (70) and biochemical (62) treatments. The origin of the biomass source, extraction methods used, as well as the pulping process has a major influence on the purity, final structure, functional groups and corresponding physico-chemical properties of lignin (62, 71). The procedure for the extraction of lignin can be classified in two categories: (a) the dissolution of lignin leaving behind the other constituents as an insoluble residue; and (b) the dissolution of components such as cellulose and extractives (via hydrolysis) leaving the lignin as an insoluble residue. Figure 2.4 shows the common processes used for the isolation of lignin and the subsequent impact on the compositional modifications (72).

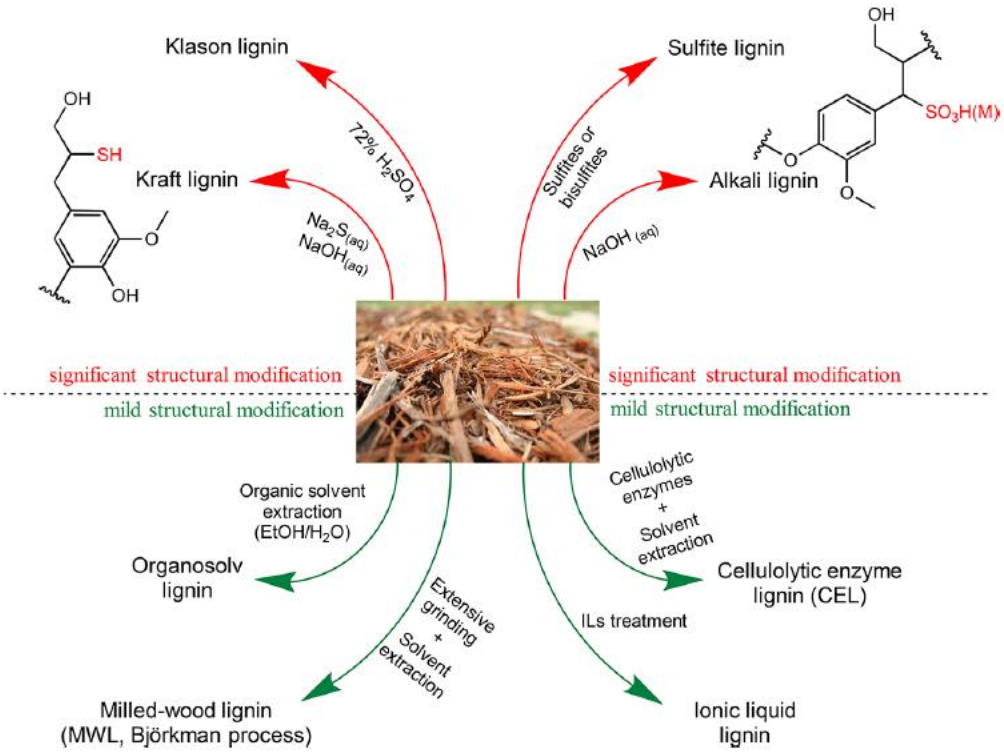

Figure 2.4 A summary of common procedures including by ionic liquids treatments (ILs) that are used for the isolation of lignin from ligno-cellulose (72).

Lignin that is extracted from the pulping industries is generally classified into two main categories: (i) sulfur-included; and (ii) sulfur-free processes. With reference to Figure 2.5, these two processes are further sub-classified into four main pulping procedures depending on the isolation conditions employed; primarily based on the pH, chemical composition of the reagents and the temperature (62, 65).

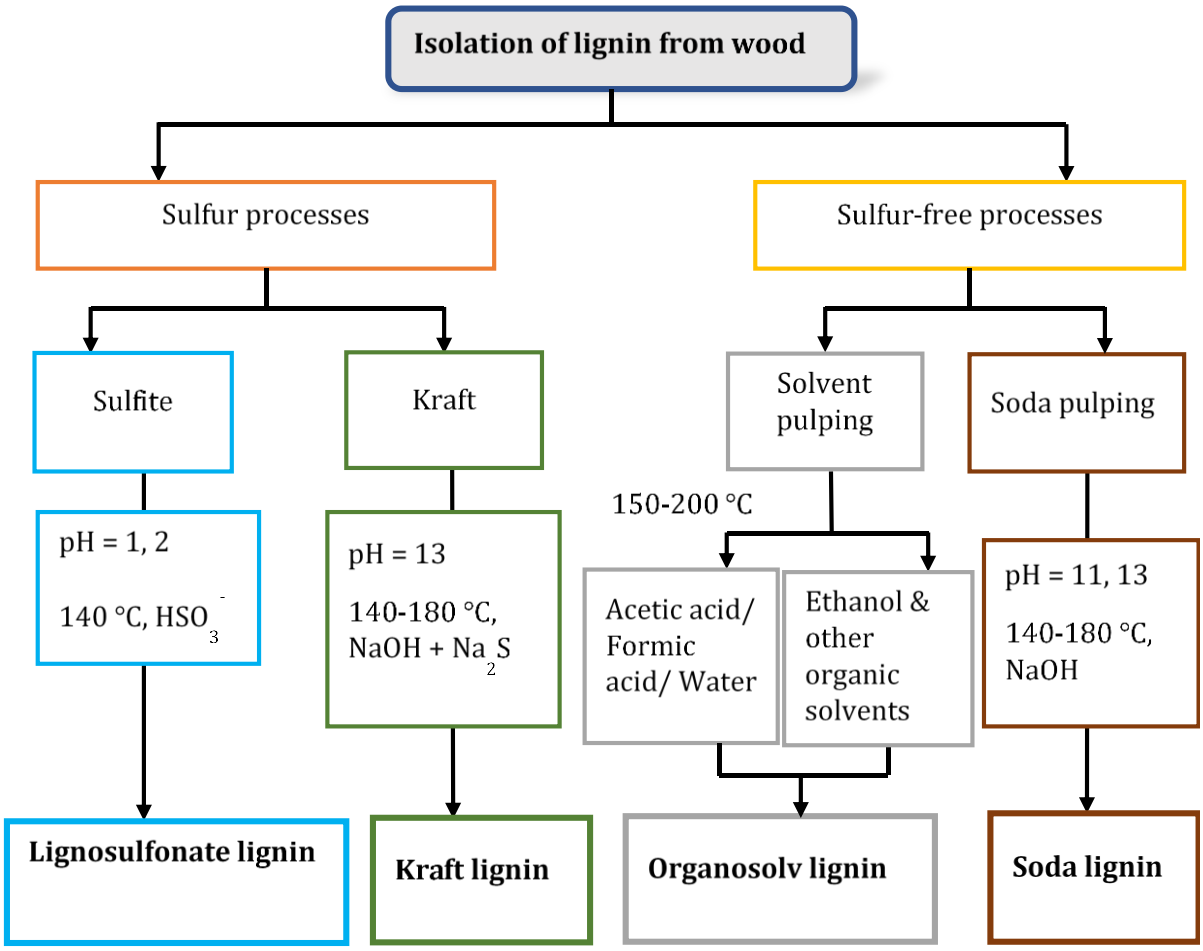

Figure 2.5 The main extraction methods used for the isolation of lignin from biomass (62, 73).

The lignin extracted using the Kraft, sulfite and soda pulping processes are also termed as technical lignins (62). These are used in pulping procedures worldwide. The procedures adopted using these pulping processes and the resulting change in the physico-chemical properties are discussed in the following section.

Kraft pulping process is the most generally used method for the isolation of lignin from wood. Currently, the annual Kraft pulp production is estimated to be around 130-150 million tons (74-76). However only 75,000 tonnes (6%) lignin is recovered from the Kraft pulp and the rest is utilised as a fuel for energy generation. The estimated production of lignin in the world from various extraction procedures for the year 2015 is shown in Figure 2.6 (76). The total production of lignin is estimated to be 1.2 million tonnes in 2015 from a potential source of 141 million tonnes. Currently, the lignosulfonate process predominates the production of lignin with an estimation of 1 million tonne per year (93%). The biorefinery industries are responsible for producing lignin (such as organosolv lignin, steam explosion lignin, etc.) and other components such as vanillin, cellulose, hemicellulose, bioethanol and nano-cellulose. Lignin produced from biorefinery in 2015 is minute and estimated to be only 3000 tonnes (0.25%). This large source of lignin extraction from biorefinery remains untapped. However, due to the emergence of new technologies and advancements in pulp processes such as Lignoboost technology in 2013 (Plymouth, USA), 2015 (Kotka, Finland), and LignoForce in 2016 (Hilton, Canada) for recovering lignin; Kraft process is forecasted to overtake lignosulfonate process as a preferred method of extraction procedure by 2025 (76).

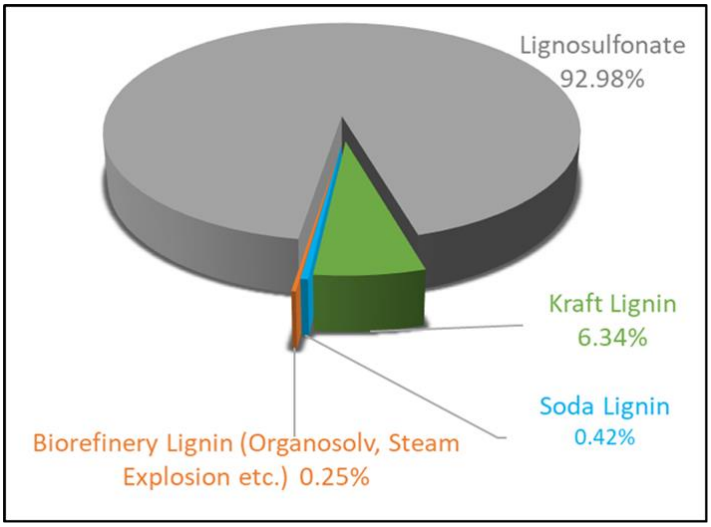

Figure 2.6 Estimated production of lignin from extraction procedures in 2015; the total is 1.2 million tonnes (76).

2.3.1 Kraft Lignin

The Kraft manufacturing process begins with the treatment of wood chips in a solution of sodium hydroxide (NaOH) and sodium sulfide (Na_2S) between 150-180 °C for 1-2 hours. This method is able to dissolve 90-95% lignin present in wood (35, 77). A solution containing lignin and other extractives including hemicellulose is called black liquor - a complex mixture of dissolved organics and fibrous materials (78). Lignin is isolated from the black liquor through a modified process known as Lignoboost (62, 73, 79-81). The lignoboost process involves the precipitation of black liquor using carbon dioxide (CO_2) as an acid and subsequently washing with sulfuric acid (H_2SO_4) to obtain a high-purity lignin (73).

During Kraft pulping, two main reactions occur: (a) depolymerisation including the cleavage of lignin-hemicellulose bonds; and (b) condensation reactions (82). In Kraft pulping, delignification proceeds through depolymerisation via cleavage of α and β-ether bonds which results in increased solubility of the resulting fragments (73). The cleavages of ether bonds lead to the formation of quinone methide, a reactive intermediate responsible for the repolymerisation reactions. The condensation reaction proceeds with addition of hydroxy (OH^-) and sulfide (HS^-) anions and carbanions (from phenolic structures) to quinone methide or formaldehyde (77, 83). This type of reaction leads to the introduction of new functional groups in softwood lignin including thiol groups with the existence of lignin-carbohydrate linkages also been reported in Kraft lignin as shown in Figure 2.7 (35).

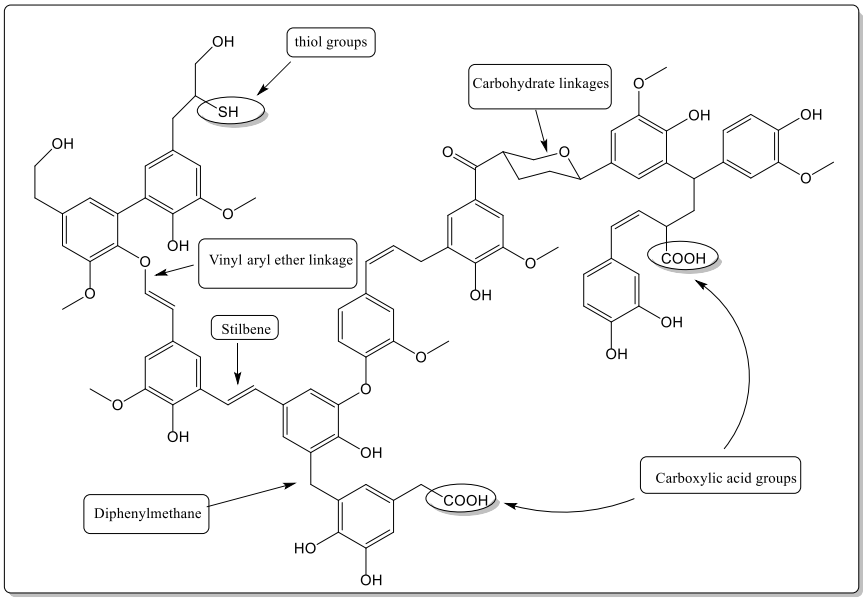

Figure 2.7 Typical functional groups present in the structure in Kraft lignin (35).

2.3.2 Soda Lignin (Alkali Lignin)

Soda pulping is primarily used for the extraction of lignin from non-woody plant matter such as wheat straw, sugarcane bagasse, kenaf, sisal and flax (77, 82). This process is carried out in an aqueous alkaline medium of NaOH (or lime and calcium hydroxide) between 140-180 °C under high pressure (10 psi). The lignin is recovered through precipitation at pH 11-13. During the pulping process, delignification proceeds through the depolymerisation of lignin which involves the cleavage of α and β-ether linkages as shown in Figure 2.8. The depolymerisation of lignin via the cleavage of ether bonds and intermolecular cross-links between lignin and hemicellulose leads to an increase in the solubility and formation of quinone methide. This contributes to further depolymerisation of lignin and it results in the formation of stilbene or styryl moieties by condensation reactions (77, 82).

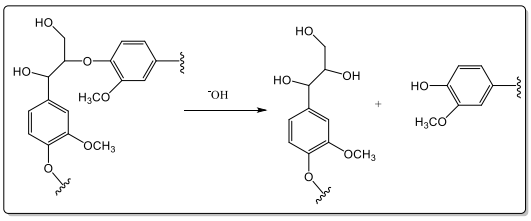

Figure 2.8 Cleavage of the α-ether bond in lignin during the soda process (82).

2.3.3 Sulfite Pulping (Lignosulfonate)

In sulfite pulping, the lignin is isolated from the biomass by reaction with sulfur dioxide (SO_2) which reacts with water to form sulfonic acids. The sulfurous acids such as sulfites or bisulfites typically contain calcium or magnesium sulfite in acidic, netural or alkaline media (84). The pulping is carried out between 125-175 °C with pH ranging from 1-5 for 3-7 hours (61, 74, 82). The process cleaves the α and β-ether linkages leading to the formation benzylium cations (α-cation) followed by sulfonation as shown in Figure 2.9. These cations trap sulfonic acids resulting in the formation of ligno-sulfonic acid. The lignin is extracted from the liquor by addition of excess lime followed by treatment with alkylamines. This process is called Howard's process and it is the mostly widely used extraction method for ligno-sulfites providing a yield of 90-95% (74). The ligno-sulfite lignin has quite a distinct physico-chemical property compared to Kraft lignin. This includes its solubility in water unlike Kraft lignin and contains a high percentage of sulfur groups ranging from 4-8%.

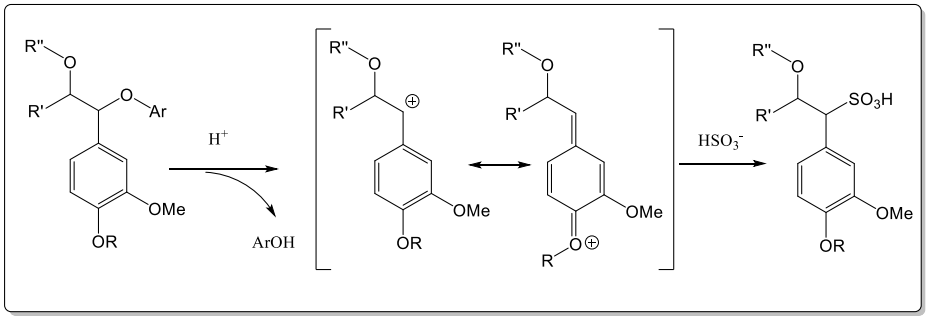

Figure 2.9 The sulfonation of softwood lignin using the acidic sulfite process (84).

There are several other procedures employed in the extraction of lignin from ligno-cellulosic biomass and these are summarised in Table 2.3. These procedures are described briefly:

Table 2.3 A summary of conditions used for the extraction of lignin (74, 77, 82, 85-88).

Extraction process	Solvent/Reagents	Conditions	Classification
	Lignin quantitative analysis		
Acid hydrolysis of Polysaccharides	H_2SO_4	72 wt. % H_2SO_4 (dilution to 3% boil at 100 °C for 3 hours)	Klason lignin (Acid Insoluble lignin)
	Extraction procedures		
Kraft	$NaOH/Na_2S$	140-170 °C	Kraft lignin
Sulfite	Mg or Ca and HSO_3^-	125-170 °C	Lignosulfite
Soda	NaOH	160-170 °C	Soda lignin
Enzymatic treatment	Cellulolytic enzymes digestion (followed by solvents extraction (EtOH or dixoane/ H_2O)	Temperature depending on the solvent system used	Cellulolytic enzyme lignin
Hydrothermal Process	Steam /acetic acid	1380-20,000 Pa, 180-280 °C for 1-20 minutes	Steam Explosion lignin
Aqueous Alkaline	NaOH, Ca $(OH)_2$	40-160 °C	Alkaline lignin
Extensive mechanical disintegration with solvents treatment	Dioxane/H_2O Dioxane with NaOH	~175 °C	Milled wood lignin (MWL)
Liquid hot water	H_2O followed by enzymatic hydrolysis	160-240 °C with optimum pressure	Liquid hot water lignin
Dilute acid hydrolysis	H_2SO_4 (HCl, H_3PO_4,	0.5-1.4 %, 165-195 °C for 3-12 minutes	Dilute acid lignin
Ionic liquid treatment	Ethyl-methylimidazolium acetate [EMIM][OAc] 1-Butyl-3-methylimidazolium bromide [BMIM][Br]	~170-190 °C for 1-3 hours	Ionic liquid lignin

2.3.4 Milled Wood Lignin

The milled wood lignin extraction method was developed by Bjorkman (74), where biomass was subjected to extensive grinding and milling followed by solvent extraction. The solvent extraction of lignin is generally achieved using a dioxane/water mixture. The lignin is dissolved in acetic acid/water mixture followed by precipitation in deionised water (89-91).

2.3.5 Cellulolytic Enzyme Lignin

Enzymes such as cellulysin cellulase, celluclast and spezyme derived from *Trichoderma* are used to treat milled biomass to hydrolyse polysaccharides. The residual biomass is treated subsequently by solvent extraction typically composed of a dioxane and water mixture. This is followed by precipitation and purification in water and acid media (74, 77, 89, 92, 93).

2.3.6 Steam Explosion Lignin

Steam explosion lignin is obtained from hydrothermal processing of biomass at temperatures between180-280 °C under pressure in the range 1380-20,000 Pa for a set time. This process results in producing acetic acid which leads to the solubilisation of hemicellulose. In some cases, ethanol and acid (H_2SO_4) is used in steam explosion. The lignin is separated from cellulose in the wood residue by using alkali (NaOH) or organic solvents such as ethanol followed by precipitation and purification (74, 77, 82, 89, 94, 95).

2.3.7 Organosolv Lignin

The production of organosolv lignin involves the extraction of lignin directly from biomass using a range of organic solvents including low and high-boiling point solvent mixtures. The low boiling point solvents used are generally alcohols and carboxylic acids. These include ethanol, methanol, acetone, solvent/water mixtures, acetic and formic acids. Examples of typical high-boiling point

solvents used for the isolation of lignin includes 1,4-butane-di-ol, tetrahydrofurfuryl alcohol and ethylene glycol (74, 82, 88).

The use of catalysts (acids or base) with organic solvents produced lignin of high yield and purity. The delignified biomass solution is subjected to precipitation followed by evaporation of organic solvents and further purification to produce organosolv lignin. The main factors that influence the delignification of biomass in the organosolv processes are the composition of the solvents, duration of the extraction procedure and the processing temperature (89).

2.3.8 Ionic Liquid Treatment

Ionic liquids (ILs) such as molten salt hydrates have been used to treat ligno-cellulosic biomass to dissolve lignin. The ILs have good thermal stability, miscibility and can solubilise cellulose, lignin and other extractives depending on parameters such as the processing temperature, extraction time, biomass type, particle size including the cation and anion pair in the ILs used. The lignin and hemicellulose were also found to be solubilised by treatment with ILs in a process known as Ionosolv (74). This process involve the precipitation of lignin and its separation by the addition of water leaving cellulose as an insoluble residue (74).

Lee *et al.* (96) found that lignin can be isolated selectively from wood using ethyl-methylimidazolium acetate [EMIM][OAc]. Fort *et al*. (97) observed that 1-butyl-3-methylimidazolium chloride [EMIM][Cl] was able to dissolve both cellulose and lignin, from which cellulose could be separated from the other components by means of precipitation and treatment with solvents. ILs can also be used for the fractionation of lignin to solubilise Kraft lignin. Pu *et al*. (98) observed that the solubility of lignin using ILs is governed by the presence of the anion in the IL. They suggested that the imidazolium cations are largely responsible for the dissolution of cellulose. The solubility of softwood lignin using ILs is influenced by anion present in the order: $MeSO_4^- > Cl^- \sim Br^- >> PF_6^-$(77, 98).

2.4 Fractionation of Lignin

The main drivers for the fractionation of lignin include: (i) to purify or refine lignin by solvent extraction followed by drying under vacuum to remove volatile contaminants (3, 99); (ii) to improve the miscibility and compatibility of lignin in common solvents and other polymers (iii) to obtain high and low-molar mass fractions (100, 101); and (iv) to modify the chemical and structural properties of lignin in a more controlled manner (101).

The fractionation of lignin involves three main steps: (i) extraction with organic solvents (31, 101-103); (ii) selective precipitation at reduced pH values (31, 101, 102, 104); and (ii) membrane ultrafiltration (31, 101, 102, 105). Fractionation of lignin by solvent extraction is a commonly used method to alter the lignin properties for desired needs (100, 103, 106-111). Lignin is partially soluble in most of the common solvents as shown in Table 2.4 (81, 101, 102, 112, 113).

2.4.1 Lignin Solubility

The solubility of a polymer in a solvent is governed by factors such as the molecular weight, polydispersity, chemical structure, composition, conformation, processing conditions and the type of solvent (114). The Hildebrand solubility parameter (δ) of a polymer in a solvent is expressed as the square root of the total cohesive energy density (115) according to Equation 1:

$$\delta = \left(\frac{E}{V}\right)^{1/2} = \left(\frac{\Delta H_v - RT}{V}\right)^{1/2} \qquad \text{Equation 1}$$

where E is its measurable energy of vaporisation, V is the molar volume of the pure solvent, ΔH_v refers to the enthalpy of vaporisation, R is the universal gas constant and T is the absolute temperature (115). It has been reported that the ability of a solvent to swell or dissolve different types of isolated lignins increases as the hydrogen bonding capacities of the solvents increase (116, 117). The solubility of lignin increases as the Hildebrand solubility parameter approach a value of around 11 $MPa^{1/2}$ (117, 118). Some of the solvents with their ability to dissolve lignin are shown in Table 2.4. The polarity index is generally defined as the dielectric constant or dipole

moment of the solvent. The polarity indices of the solvents are relative to that of water (10.2), hence the solvents with indices value closer to that of water are considered polar solvents (119). For instance, hexane and petroleum ether are considered non-polar solvents with a polarity index value of 0.1 (119, 120).

Table 2.4 Examples of the solvents used commonly for the dissolution of lignin along with their Hildebrand solubility parameters and polarity indices (119-126).

Solvents	**Chemical Formula (functional groups)**	**Boiling points (°C)**	**Solubility**	**Hildebrand Solubility Parameter $(MPa)^{1/2}$**	**Polarity Index**
Acetone	H_3CCOCH_3	56.3	Partially soluble	19.7	5.1
n-Butanol	C_4H_9OH	117.7	Partially soluble	28.7	3.9
Chloroform	$CHCl_3$	61.2	Partially soluble	18.7	4.1
Dichloromethane	CH_2Cl_2	39.8	Partially soluble	20.2	3.1
Dimethyl sulfoxide (DMSO)	H_3CSOCH_3	189	Completely soluble	26.4	7.2
Dimethyl formamide (DMF)	$(CH_3)_2NCH$	152.8	Completely soluble	24.9	6.4
1,4-Dioxane	$C_4H_8O_2$	101.2	Partially soluble	20.5	4.8
Ethanol	CH_3CH_2OH	78.3	Partially soluble	26.2	5.2
Ethyl acetate	$C_4H_8O_2$	77.1	Partially soluble	18.2	4.4
Methanol	CH_3OH	64.7	Partially soluble	29.7	5.1
n-propanol	$CH_3CH_2CH_2OH$	95	Partially soluble	24.9	4.0
Tetrahydrofuran	C_4H_8O	66	Partially soluble	18.5	4.0

2.5 Characterisation of Lignin for Structural Analysis

2.5.1 Pyrolysis

This section is concerned with the characterisation of lignin with regards to the elucidation of its chemical structure. Pyrolysis can be classified into three types: fast pyrolysis, intermediate and slow pyrolysis, depending on the processing conditions as shown in Table 2.5. Fast pyrolysis is at heating rate of approximately 200-2000 °C/seconds with dwell times in the region of 1-10 seconds (127-130). This is said to result in higher yield of pyrolysis liquids, also referred to as bio-oil with evolution of gases and a lower char content. The slow pyrolysis is carried out at heating rates between 1-20 °C/seconds with longer residence time, resulting in a higher char content and the production of non-condensable gases (128, 129, 131-134).

Table 2.5 The pyrolysis types based upon processing parameters and the respective yields (129, 131).

Pyrolysis	Dwell time	Temperature °C	Yield %		
			Bio-oil	Char	Gas
Fast	1-2 s	500	75	12	13
Intermediate	10-30 s	500	50	25	25
Slow	Hours/Days	400	30	35	35

The bio-oil which is a liquid fraction from biomass after pyrolysis and it is also termed as tar. The composition of bio-oil depends on the source and the pyrolysis conditions. It is used as feedstock for the synthesis of chemicals such as adhesives, resins, polymers and it is also utilised as a biofuel for renewable energy generation (135). The gaseous products that are generated include CO, CO_2, CH_4 and H_2. The char can be used as fuel, bitumen additive, asphalt binder/modifier and as activated carbon including the production of carbon fibres, carbon nanotubes and carbon black (61, 128, 131, 136-142).

2.5.1.1 Pyrolysis-Gas Chromatography-Mass Spectrometry (Py-GC-MS)

Pyrolysis combined with analytical techniques such as FTIR spectroscopy (Py-FTIR) and/or gas-chromatography and mass spectrometry (PY-GC-MS) has been used to study the evolved gases and products during the heat treatment of lignin. The thermochemical decomposition of materials in pyrolysis is analysed using hyphenated techniques where an inert gas is used to transfer the released products or gases into the GC. These products are separated by the GC based on their retention times and the molecular weight of the fragments detected by MS (127, 143-145).

Kim *et al*. (146) studied the decomposition products of milled wood lignin at 150 °C, 200 °C, 250 °C and 300 °C using Py-GC-MS; the output of their study is shown in Figure 2.10. The liberation of decomposed products was initially detected at 250 °C. At 300 °C, the decomposition of lignin accelerated, and this is reflected by a significant increase in concentration of products released. The depolymerised products identified by MS were shown to be phenolic G, S and H mono-lignol units (144, 147).

The pyrolysis of lignin between 200-400 °C gives rise to primary pyrolysis products such as G, S, H-lignin units and coniferyl alcohol due to ether linkages cleaving (147). It is believed that the increase in the release products between 250-300 °C is attributed to the cleavage of dominant β-O-4 linkages. The β-O-4 linkages are thermally labile above 200 °C and tend to cleave at the terminal ends. This cleavage could lead to chain scission including the cleavage of aliphatic side chain and functional groups. This is said to responsible for the evolution of various phenolic products at 300 °C, which are originally from derived from lignin monomeric units (146, 147).

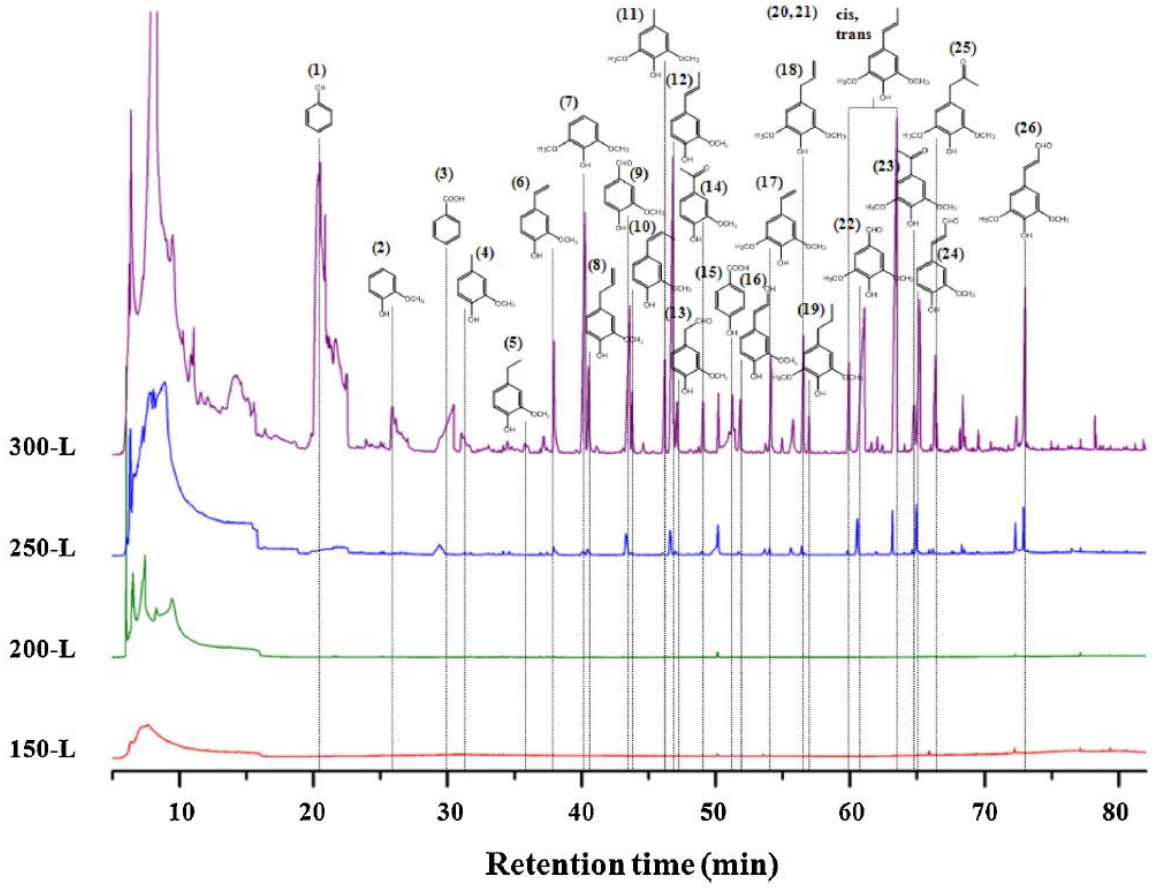

Figure 2.10 GC chromatogram of volatile products released during the pyrolysis of lignin at 150 °C, 200 °C , 250 °C and 300 °C (146).

Kim *et al*. (148) also studied the effect of pyrolysis products at 400 °C, 500 °C, 600 °C and 700 °C on the yield of products released. Above 400 °C, the secondary pyrolysis reactions occur where G-lignin units are converted into catechols, o-cresols and phenols (149). They reported a gradual increase in the yield of pyrolysis products between 400-700 °C for Kraft lignin. This was attributed to increased decomposition of pyrolysed products and the evolution of non-condensable gases. Therefore, the pyrolysis procedure generates phenolic monomers, oligomers along with the release of CO_2, CO, CH_4 and H_2O through demethoxylation, demethylation and dehydrogenation (128, 147, 150). The mechanisms associated with the structural changes during lignin heat-treatment is discussed in Section 2.7.

2.5.2 Nuclear Magnetic Resonance Spectroscopy (NMR)

The structural elucidation of complex macromolecules such as lignin is possible through NMR techniques. In comparison to the others structural characterisation techniques such as Infrared (IR), UV (ultraviolet visible) and Raman spectroscopy, NMR offers a more detailed insight into the identification and structural evaluation of lignin with the quantification of lignin moieties. The most widely used NMR techniques for the structural elucidation of lignin are 1D homonuclear NMR which includes Proton NMR (^{1}H NMR), Carbon NMR (^{13}C NMR) and Phosphorous NMR (^{31}P NMR) (103, 151-156). Among these, ^{1}H NMR is the reliable and an efficient method for the structural characterisation of lignin because of the proton isotopic natural abundance (100%) and it offers better sensitivity and resolution in the resultant spectrum. However, the complete identification and quantification of lignin by ^{1}H NMR is hindered due to the limited chemical shift range (0-13 ppm) along with extensive overlapping of the signals and proton-coupling effects (157-159).

The evaluation of the structure of lignin by ^{13}C NMR offers detection of signals at a wider chemical range (0-200 ppm) with no coupling effects. However, it is not sensitive as compared to proton NMR owning to the low ^{13}C isotopic natural abundance (1.1%). Therefore, to acquire ^{13}C NMR spectra of lignin with an improved resolution, a sample with a higher lignin concentration is required along with longer acquisition time. Typically, 20,000-30,000 scans with scan intervals of 1-2 seconds is used (103, 152, 160, 161). It has been well established that upon derivatisation of lignin via acetylation, the ^{13}C NMR shows better spectral resolution to distinguish and determine the structural moieties present in lignin. It also enables the quantification of specific lignin moieties including lignin-rich hydroxyl (OH) groups and it is capable of differentiating aliphatic and aromatic hydroxyl groups. Nevertheless, the ^{13}C NMR of lignin is insufficient for a complete structural elucidation due to signal overlapping of peaks specifically in the region designated to lignin interunit linkages, side chain and lignin-carbohydrates complexes. This overlapping of the

signals also hinders the integration of the peaks and subsequent quantification of the structural units of lignin (151, 152, 162-164).

^{31}P NMR provides a method for the quantification of lignin monomeric units and condensed C-5 substituted moieties including various other functional groups such as aliphatic hydroxyl and carboxylic groups. The hydroxyl groups in are phosphorylated upon derivatisation allowing ^{31}P NMR to detect the phosphorous nucleus (100%) and generate a spectrum (154, 155, 165).

As stated previously, the limitations of 1D NMR do not allow for the comprehensive structural elucidation of lignin. Hence, 2D NMR techniques are used as they can overcome the overlapping of resonances when seen using 1D NMR. The most commonly used 2D NMR techniques for the structural evaluation of lignin are heteronuclear single-quantum coherence (HSQC) (152, 163, 166-172), heteronuclear multiple bond coherence (HMBC) (173), heteronuclear multiple-quantum coherence (HMQC) (164, 174) and total correlation spectroscopy (TOCSY) (175). Among these techniques, 2D HSQC NMR is widely reported technique used for the structural evaluation of lignin in combination with 1D NMR (^{1}H NMR, ^{13}C NMR and ^{31}P NMR). It allows for an accurate assignment of various structural moieties including the identification of lignin interunit-linkages, side chain and lignin-carbohydrate complexes. It also facilitates the quantification of distinct structural features and the moieties of lignin (152, 163, 171, 172).

The 2D HSQC NMR of softwood Kraft lignin reported by Crestini *et al*., (163) is shown in Figure 2.11. The y-axis represents the signal for ^{13}C nuclei and x-axis shows the signals corresponding to the ^{1}H nuclei. This can also be considered as a ^{1}H-^{13}C spectrum where the peak for a specific proton is considered as being attached to the corresponding ^{13}C nuclei. Figure 2.11 (a) corresponds to the aliphatic region with chemical shift ranging from 0-6 ppm for the ^{1}H and 10-90 ppm for ^{13}C nuclei respectively. The signals allow for distinct assignments to the corresponding structures denoted by symbols α, β and ϒ are attributed to

signals due to specific carbon or hydrogen in the aliphatic side chain. Hence 2D HSQC NMR enables the elucidation of the structure of lignin by overcoming effects of overlapping signals and it allows for a distinct assignment of aliphatic side chain, interunit linkages and lignin-carbohydrates complexes (162, 176). The signal for methoxyl group is denoted as OMe.

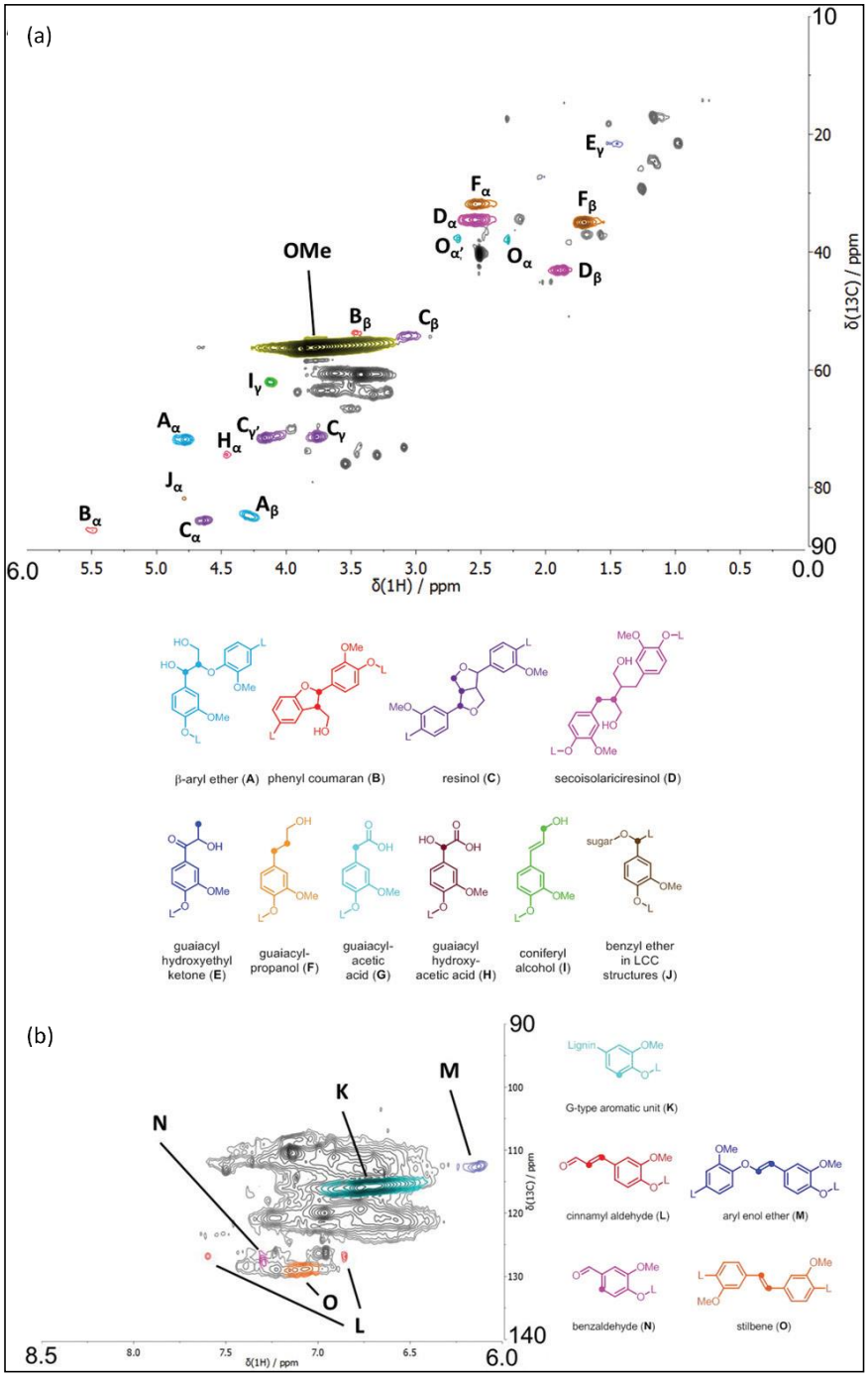

Figure 2.11 HSQC spectrum of softwood Kraft lignin with the assignment of structural features for the: (a) aliphatic; region and (b) aromatic region (163).

Figure 2.11 (b) shows the aromatic region with chemical shift ranging from 6-8.5 ppm for the ^{1}H nucleus and 90-140 ppm for the ^{13}C nucleus. This allows the identification of specific aromatic units with different functional groups (such as aldehydes) including classification of conjugated side chain and lignin interunit linkages.

2.6 Carbon Fibres Derived from Lignin

Lignin-based carbon fibres (LCFs) or lignin-based carbon nanofibres (LCNFs) are manufactured using fibre spinning techniques as summarised in Figure 2.12. The lignin is first purified by washing it with an acid to reduce the carbohydrates content, inorganic impurities and volatile contaminants (89, 151, 177, 178). These impurities affect the fibre spinnability and influence its physico-chemical properties (177, 179, 180). The lignin is fractionated or chemically modified and blended with co-polymers to aid in the fibre spinning processes and to improve the desired properties (158, 181-183). The source, type of lignin and extraction procedures greatly influence the processability during fibre spinning (67, 184). The precursor fibres are then subjected to prolonged heat-treatment to convert them into carbon fibres.

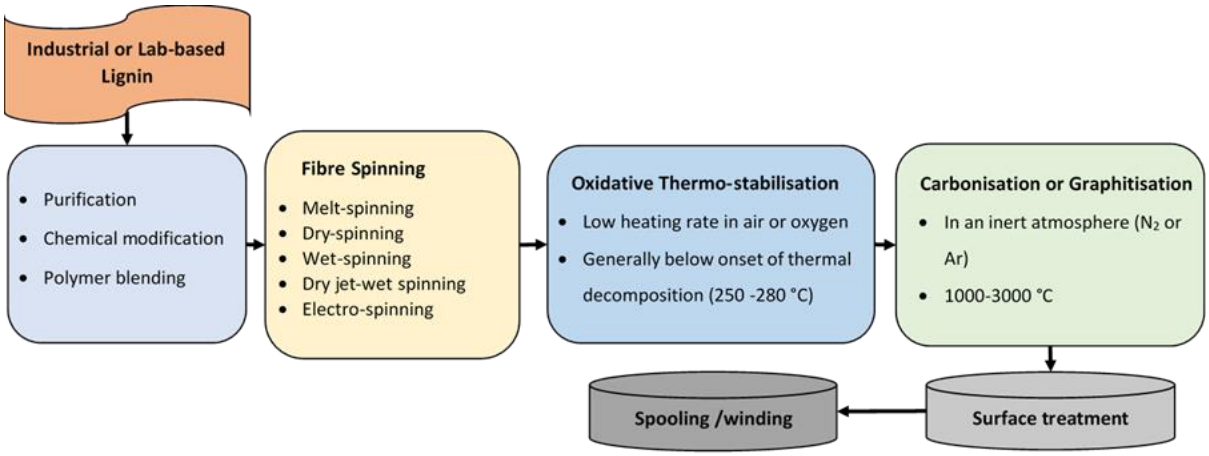

Figure 2.12 Schematic illustration of a manufacturing process for lignin based-carbon fibres (3, 5, 67, 112, 177, 184-193).

Common fibre spinning techniques are used to produce lignin-based fibres with diameters ranging from few micrometres to tens of nanometres (184, 194). These techniques include melt-spinning (5, 179, 187, 195), wet-spinning (189, 190, 194, 196), dry jet-wet spinning (181, 191, 192), dry-spinning (188, 197) and electro-spinning (67, 182, 184, 198-200). The mechanical properties of lignin fibres produced using specified spinning processes are summarised in Table 2.6. The mechanical properties of electro-spun lignin fibres that are subsequently carbonised is also presented in Table 2.6.

Table 2.6 Properties of lignin-based carbon fibres obtained using specified spinning techniques and heat treatments.

Material	**Fibre spinning method**	**Thermo-oxidative stabilisation**	**Carbonisation under an inert atmosphere**	**Tensile strength (MPa)**	**Young's modulus (GPa)**	**Diameter (µm)**	**Ref.**
Softwood & Hardwood Kraft lignin blends	Melt-spinning	0.2 °C/minute 250 °C for 1 hour	1°C/minute to 600 °C -3 °C/minute to 1000 °C	233-377	25-33	36-78	(187, 201)
Softwood Kraft Lignin (Acetylation)	Dry-spinning	250 °C for 1 hour	1000 °C	1040 ± 100	52 ± 2	6.0 ± 1	(188, 197)
Hardwood kraft lignin	Melt-spinning	12-180 °C/hour 250 °C for 1 hour	180 °C/hour 1000 °C for 1 hour	422 ± 80	40 ± 11	46 ± 8	(202)
Hardwood kraft lignin/ PEO	Melt-spinning	12-180 °C/hour 250 °C for 1 hour	180 °C/hour 1000 °C for 1 hour	458 ± 97	59 ± 8	33 ± 2	(202)
Alcell Organosolv lignin	Melt-spinning	12-180 °C/hour 250 °C for 1 hour	180 °C/hour 1000 °C for 1 hour	388 ± 123	40 ± 14	31 ± 3	(202)

Organosolv hardwood lignin from birch wood (acetylation)	Melt-spinning	0.5 °C/minute 250 °C for 1 hour	3 °C/minute 1000 °C for 1 hour	355 ± 53	39.1 ± 13.3	14 ± 1	(203)
Steam Exploded hardwood lignin	Melt-spinning	0.5-2 °C/minute	5 °C/minute to 1000 °C	660 ± 230	40.7 ± 6.3	7.6 ± 2.7	(204)
Hardwood pyrolytic lignin	Melt-spinning	0.3 °C/minute 280 °C for 1 hour	3 °C/minute for 1000 °C for 1 h	855 ± 159	85 ± 37	29-50	(150)
Softwood kraft lignin (Esterification)	Melt-spinning	0.25 °C/minute 250 °C for 1 hour	10 °C/minute 1000-2200 °C	400-750	31.7-41.1	11.2-18.5	(179)
Organoslov Hardwood (yellow poplar) and switchgrass lignin	Melt-spinning	0.05-0.5 °C/minute 250 °C for 30 minutes	5 °C/minute 1000 °C for 15 minutes	229 - 747	33.2-41.8	17-32	(186)
Softwood kraft lignin and Cellulose (Ionic liquids solvation)	Dry/Jet-Wet Spinning	0.2 °C/minute 200 °C, 1 °C/minute 250 °C for 1 hour	1 °C/minute 600 °C, 3 °C/minute 1000 °C	810 ± 160	64 ± 4.6	14 ± 0.9	(191)
Harwood kraft lignin	Melt-spinning	12-180 °C/hour	180 °C/hour	605	61	46 ± 8	(37)

		250 °C for 1 hour	1000 °C				
Harwood kraft lignin/SPP	Melt-spinning	12-180 °C/hour 250 °C for 1 hour	180 °C/hour 1000 °C	167-332	28-57	47-63	(37)
Harwood Kraft lignin/PET	Melt-spinning	12-180 °C/hour 250 °C for 1 hour	180 °C/hour 1000 °C	669-703	61-94	31-45	(37)
Hardwood acetic lignin	Melt-spinning	30 °C/hour 250 °C for 1 hour	180 °C/hour 1000 °C	5.8 ± 1.7	0.84 ± 0.29	26 ± 2	(205)
Softwood acetic lignin	Melt-spinning	30 °C/hour 250 °C for 1 hour	180 °C/hour 1000 °C	26.4 ± 3.1	3.59 ± 0.43	84 ± 15	(205)
Softwood Kraft lignin (Fractionation with successive organic solvents, methanol/dichloromethane fraction)	Electrospinning (26% lignin in DMF with 1 wt% PEO)	0.2 °C/min 250 °C for 1 hour	1 °C/min to 600 - 3 °C/min to 1000 °C	53.0 ± 22	6.9 ± 1	0.32 ±0.03	(182)

Softwood Kraft lignin (Fractionation with successive organic solvents)	Electrospinning (25% lignin in DMF with 1 wt% PEO, 5 wt% with NCC)	0.2 °C/minute 250 °C for 1 hour	1 °C/minute to 600 - 3 °C/minute to 1000 °C	33.7 ± 6	8.0 ± 1.4	0.41 ±0.05	(182)
Alkali lignin extracted from Corn stalk by dissolution with NaOH followed by successive precipitation using HCl at pH 2, pH 4, pH 6, pH 8 and pH 10	Electro-spinning (50% Lignin in DMF with 50% PAN)	0.5 °C/minute 220°C for 12 hours	4 °C/minute to 1000 °C for 240 minutes	13.2 ± 3 (pH 2) 14.9 ± 2 (pH 4) 15.6 ± 3 (pH 6) 17.3 ± 2 (pH 8) 21.1 ± 3 (pH 10)	2.6 ± 0.4 (pH 2) 3.1 ± 0.2 (pH 4) 3.8 ± 0.4 (pH 6) 3.8 ± 0.1 (pH 8) 4.5 ± 0.1 (pH 10)	0.42± 0.04 (pH 2) 0.34± 0.04 (pH 4) 0.4 ±0.03 (pH 6) 0.23± 0.03 (pH 8) 0.19 ±0.02 (pH 10)	(177)

Softwood Kraft lignin (Fractionation with successive organic solvents, methanol/dichloromethane fraction resulted in low (F_{1-3}) and high-molecular weight (F_4) soluble fractions	Electro-spinning (28 wt% of F_4 lignin in DMF with 0.2 wt% PEO or a 70/30 wt% ratio of F_4/ F_{1-3} dissolved at 30 wt% lignin in DMF with 0.2 wt% PEO	5 °C/minute to 250 °C for 1 hour	20°C/minute to 250 °C -10 °C/minute to 600, 800 or 1000 °C	74.1 ± 14.6	4.1 ± 1.4	0.63±0.09	(184)

2.6.1 Fibre Spinning

2.6.1.1 Melt-spinning and Dry-spinning

Melt-spinning is a spinning technique to manufacture fibres which does not require the use of solvents. This process generally initiates with the melting of polymer granules or powder in the extruder. The polymer is melted and homogenised in the extruder and it flow through narrow channels into a filter. The molten polymer is transported to the melt-spinning unit under pressure which is equipped with spinneret. It is extruded using a controlled feed rate through a spinneret and is solidified in a quenching chamber with air cooling. The filaments are drawn at high-speeds typically in the range between 50-4000 m/minute by passing through multiple rollers and collecting them on a winding unit (195, 204). Figure 2.13 (a) shows a schematic illustration for a conventional setup for melt-spinning (206).

There are several parameters which can influence continuous melt-spinning. These includes; the nature of the polymer material, extrusion rate and temperature, the residence time of the fluid in the heater chamber, diameter of spinneret holes, spinning path length, take-up velocity and cooling conditions (206).

Ziabicki (207) proposed that certain conditions are needed to be fulfilled for the continuous spinning without fibre breakage. These conditions were said to depend on the continuity of flow and the tensile stress on the melt-stream which should not exceed the tensile strength of the filament.

There are other factors which needs to be considered not only for melt-spinning but also for solution spinning techniques. These factors relate with fluid flow behaviour (e.g. shear flow and elongational flow), spinnability and flow instabilities. A fluid is considered to be spinnable if stead-state, continuous elongation of the fluid jet proceeds without breakage under given deformation conditions (208).

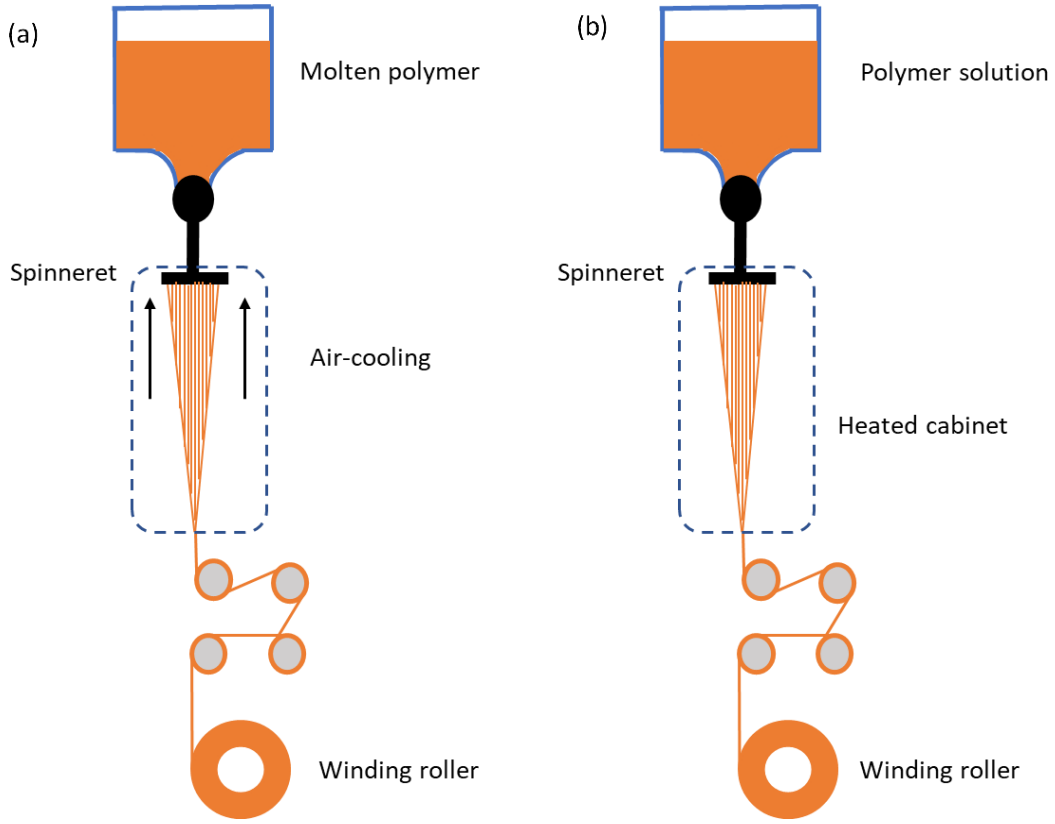

Figure 2.13 Schematic illustration for fibre spinning: (a) melt-spinning (206, 209); and (b) dry-spinning (188).

For melt-spinning of lignin, it is reported that it needs to become fusible (an ability of material to flow) without undergoing thermal degradation or condensation reactions (187). Thermal degradation or depolymerisation can produce volatiles which can lead to defects and have an adverse effect on the fibre morphology and its properties. Whilst condensation reaction can limit lignin's thermal mobility and affect its melt flow characteristics during fibre spinning (186).

In order to improve the thermal mobility and spinnability of lignin, it is chemically modified (179, 197, 204, 210-212) and/or blended with other polymers (213-215) and plasticisers (186, 202). Blending with other polymers is a straightforward method to improve the processing of lignin. However, the miscibility between the polymer blends play an important role in the spinnability and fibre properties. For example, if the blend is immiscible it can result in unfavourable fibre properties such as hollow or porous carbon fibre (37, 216). In the past, PEO has been used to

blend with lignin as it forms a miscible blend. However, the difficulty associated with the thermo-stabilisation of lignin-PEO fibres needs to addressed (202). In recent years, PEO has been extensively used as a plasticiser with lignin where between 0.2-1 % PEO is used to facilitate fibre spinning (182, 184). The role of PEO in the aiding fibre spinning is discussed in Section 2.6.1.3.

Fibres formed by melt-spinning from lignin/lignin blends have also been reported where infusible softwood lignin is blended with a fusible hardwood lignin. Examples of this include: blending of softwood Kraft lignin and hardwood Kraft lignin by Nordstrom *et al*. (187); Hosseinaei *et al*. reported organosolv hardwood lignin blended with switchgrass lignin (186); and Yue *et al*. (217) made carbon fibres from organosolv switchgrass and hardwood lignin blend. It is believed that hardwood lignin plasticises softwood lignin which in turn helps with thermal mobility and fibre spinnability. Hardwood lignins are found to be easily spinnable in comparison to the softwood lignin which are difficult to process (179). However, hardwood lignins are difficult to thermo-stabilise and takes a much longer time (218, 219). The higher concentration of G-units in softwood lignin and its highly condensed structure leads to an increase in the rate of thermo-stabilisation and a decrease in the time for conversion to carbon fibres (220). This is thought to be due to C-5 position in the G-units of lignin which promotes cross-linking and condensation reactions (180). Similarly, in previous years, Kraft lignin was considered unsuitable as a precursor for spinning because of the presence of inorganic impurities and the high concentration of carbohydrates (89, 178). However, different approaches have been reported over the years for the removal of impurities in Kraft lignin and to improve its spinnability (187). Therefore, it is important to find the solutions for overcoming these difficulties with regard to spinning softwood lignin. It is worth noting that the Kraft process can provide an abundant and economical source of technical lignin (180).

Mainka *et al*., (221) reported on the production of carbon fibres made from pelletised hardwood lignin. The lignin fibres were made using melt-spinning and thermo-stabilised with residence

times of approximately 100-150 hours between 200-300 °C, prior to carbonisation. Figure 2.14 (a-b) shows micrographs of carbon fibres reported by Hosseinaei *et al.*, (186) where the fibres were made from melt-spinning of a blend of organosolv hardwood and switchgrass lignin. The lignin fibres were thermo-stabilised at 250 °C with heating rate of 0.05 °C/minute and holding time of 30 minutes before carbonisation. Hardwood lignins are also considered to be melt-spinnable due to their relatively low glass transition temperature (T_g) and melt viscosity in comparison to softwood lignin (201). It was reported that the slow heating is required during thermo-stabilisation for hardwood lignin to achieve cross-linking and it was necessary to maintain the temperature below the T_g (1, 201, 222). If the operating temperature is above the T_g during thermo-stabilisation, it causes the fibres to fuse and affect its properties. It was also observed that the slow heating results in an increase in the T_g (1, 188, 202, 223). The mechanical properties of melt-spun lignin fibres are reported in Section 2.6.

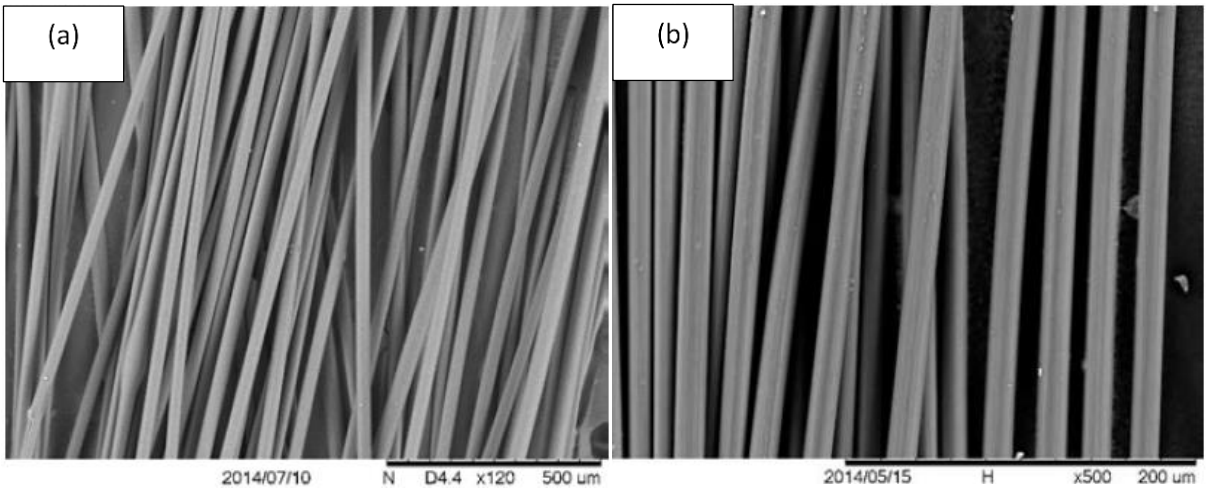

Figure 2.14 SEM micrographs of carbon fibres from organosolv hardwood from yellow poplar (YP)/switchgrass (SG) lignin blends: (a) 50% YP: 50% SG, and (b) 85% YP:15% SG

The dry-spinning is another fibre spinning technique which was explored for the production of lignin-based carbon fibres. Figure 2.13 (b) shows a conventional setup for the dry-spinning process. It can also be classified as a solution spinning technique. A high concentration of polymer

is dissolved in a solvent. The viscous solution dope is extruded vertically from a syringe or barrel through a spinneret to the heating cabinet. The skin on the filaments are formed by the evaporation of solvents from the viscous dope. Commercially, for the production of PAN fibres by dry-spinning, a hot primary inert gas at approximately 350-400 °C is used to remove the solvent. A secondary inert gas is used to cool the filament and recover the solvent. The solvent is recovered using condensation and it is recycled. The parameters that can influence the dry-spinning of lignin are the dope temperature, dope concentration, winding speed, feed rate and the temperature of the heated cabinet (209, 224).

Zhang *et al.*, (188) reported on the production of carbon fibres made from chemically modified softwood Kraft lignin using a custom-designed dry-spinning unit. Figure 2.15 shows SEM micrographs of the lignin fibres they produced. The lignin was acetylated and dissolved in acetone to prepare a 75 wt% lignin solution and transported to a spinning barrel equipped with spinneret (12-hole die, with an orifice diameter of 75 μm each). Dry-spinning was carried out at temperatures ranging from 25-52 °C. However, the procedure for the chemical modification of lignin is expensive and it is not clear if this method is capable of producing lignin fibres in a continuous manner (186, 220).

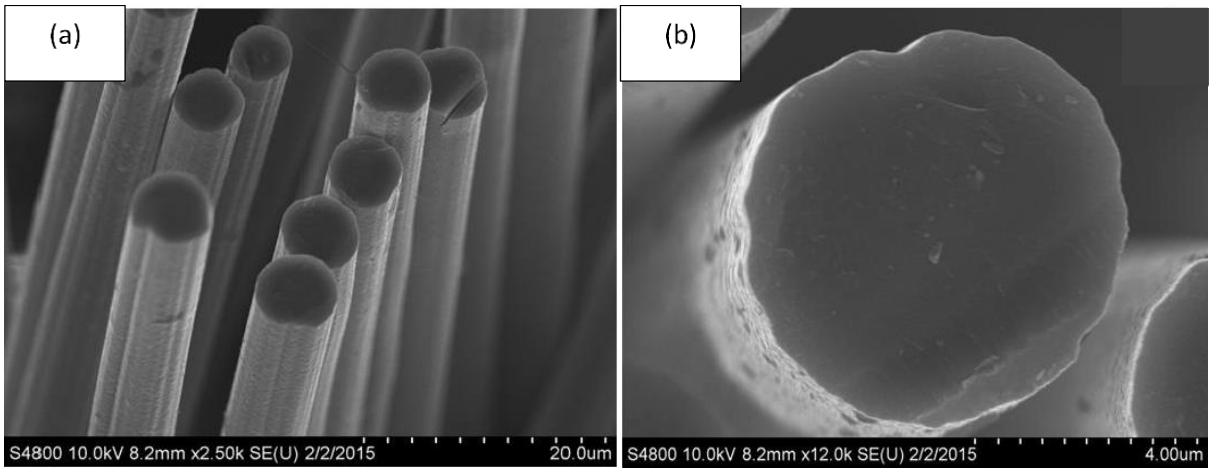

Figure 2.15 (a-b) SEM micrographs of carbon fibres produced from acetylated softwood Kraft lignin by dry-spinning (188).

2.6.1.2 Wet-spinning and Dry Jet-Wet spinning

The wet-spinning process is a conventional method that is used for producing PAN fibres where a polymer solution is extruded into a non-solvent (194). The polymer solution is prepared by dissolving it in a solvent. The optimum concentration of the polymer is dictated by its solubility in the solvent and the required viscosity for fibre spinning (225, 226). The process consists of pumping a polymer solution, controlled by a motorised feeding unit, through a spinneret and into a coagulation bath. The filaments are solidified in a bath with the removal of solvent to form continuous fibres which are washed, dried and stretched and spooled. Figure 2.16 shows a schematic illustration of wet-spinning setup (194, 227).

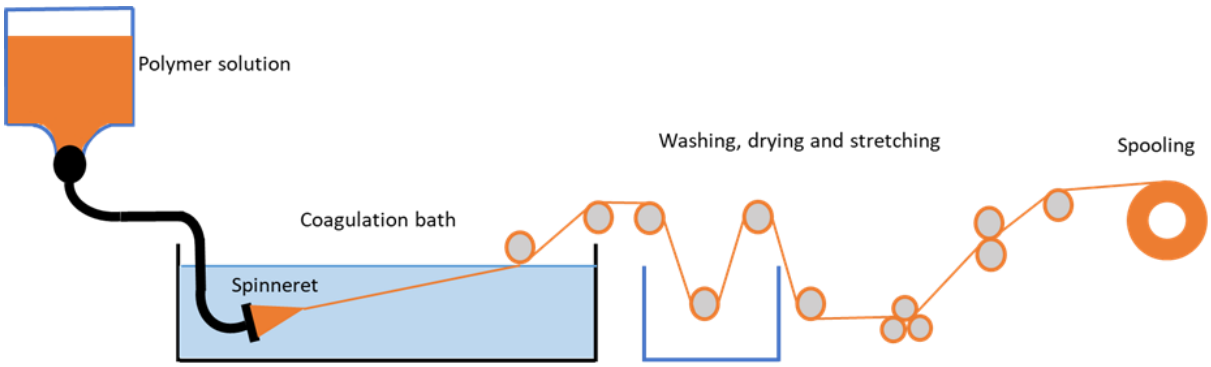

Figure 2.16 Schematic illustration of a conventional setup for wet-spinning (194, 227).

With reference to Figure 2.16, the polymer solution is filtered and degassed to homogenise it and to remove air bubbles which allows continuous fibre spinning. The conversion of the polymer solution into fibres in the coagulation bath is governed by several parameters. These include, the composition of the coagulation bath, temperature, extrusion rate and winding speed (228-230). Fibre formation from a polymer solution is a result of diffusional interchange between the filament and the non-solvent in the coagulant bath (231). This diffusion results in mass transfer by the removal of the solvent from the polymer solution into the coagulant bath (208). The effect of paraments such as the diffusion coefficient of the solvent and the nature of the non-solvent in the coagulant bath, on the fibre morphology, has been explored extensively in the literature. In

some cases, simulations and experiments were used to study the diffusion mechanisms and fibre properties (231, 232).

Jin *et al.*, (189) reported on the wet-spinning of lignin/PAN polymer solutions in a DMSO-water coagulation bath. They observed voids in the fibre cross-section. These voids were said to increase in size with an increase in the lignin content. The presence of these voids in the spun fibres is highly undesirable as it has a detrimental effect on the properties of the lignin fibres (194). However, with the addition of low concentration (0.2%) of lignin in the coagulation bath, it resulted in the elimination of the voids. This addition of lignin in low concentrations is thought to counter balance the diffusion of lignin from the fibres. Figure 2.17 (a-b) shows micrographs from the wet-spinning of lignin/ PAN blends without and with lignin concentration in the coagulation bath respectively.

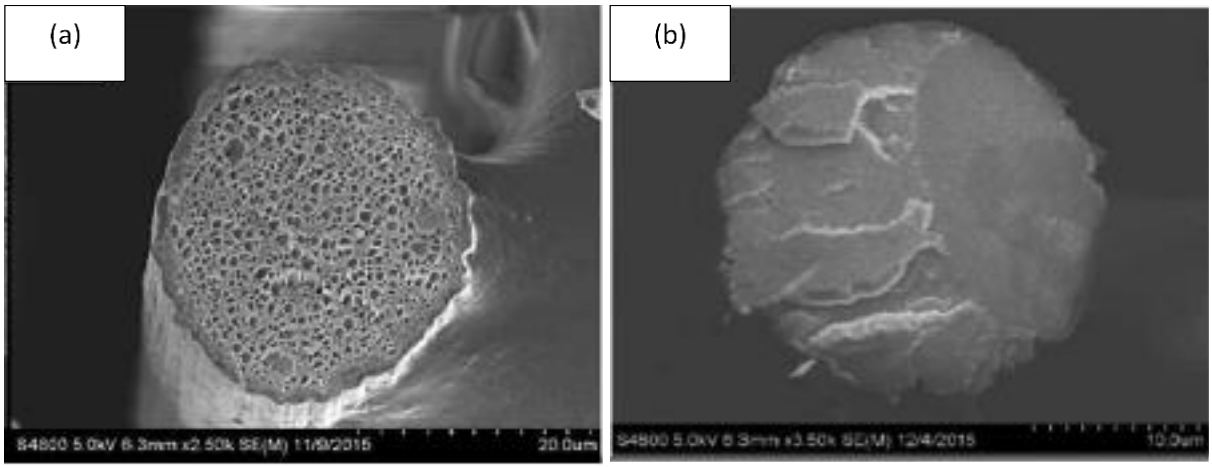

Figure 2.17 (a-b) SEM micrographs of lignin/PAN blends: (a) without lignin; and (b) with 0.2% lignin in the coagulation bath (189).

The washing, drying and stretching of the fibres aids in removing the impurities and to enhance orientation of molecular chains in the fibre axis. This orientation of the molecular chains lead to an increase in the mechanical properties of the spun fibres (233).

Figure 2.18 shows a conventional setup for dry jet-wet spinning. This setup for solution spinning is similar to the wet-spinning process but with a distinct difference in that, an air-gap is present between the spinneret and the coagulation bath (181). The gap length for producing lignin fibres is typically between 10-30 mm (181, 191, 192). Liu *et al.*, (192) reported the dry jet-wet spinning of PAN/lignin solutions into a methanol coagulant bath at -50 °C. The fibres produced when lignin was present in the coagulation bath showed improved mechanical properties. In addition, the incorporation of lignin was found to promote cross-linking and lead to shorter time for fibre thermo-stabilisation.

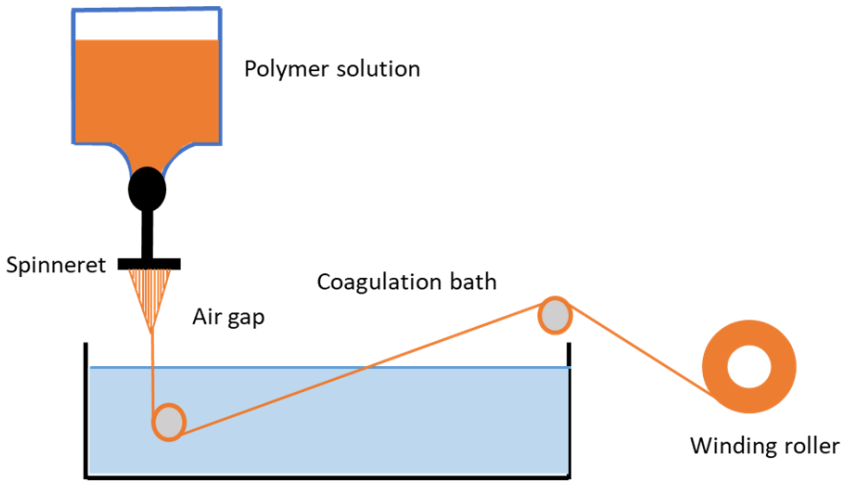

Figure 2.18 Conventional setup for dry jet-wet spinning (181).

Dry jet-wet spinning is known to produce fibres with Young's moduli 2-4 times greater than those fibres prepared by the wet spinning process (234). Bengtsson *et al.*, (191) reported on the dry jet-wet spinning of softwood Kraft lignin/cellulose dissolved in 1-ethyl-3-methylimidazolium. Figure 2.19 (a-d) shows micrographs of surface and transverse sections they obtained: (a-b) neat cellulose carbon fibre; and (c-d) softwood Kraft lignin/cellulose carbon fibre. Previous studies have reported that lignin fibres produced using dry jet-wet spinning largely show void-free fibres in comparison to wet-spinning (181, 191, 192).

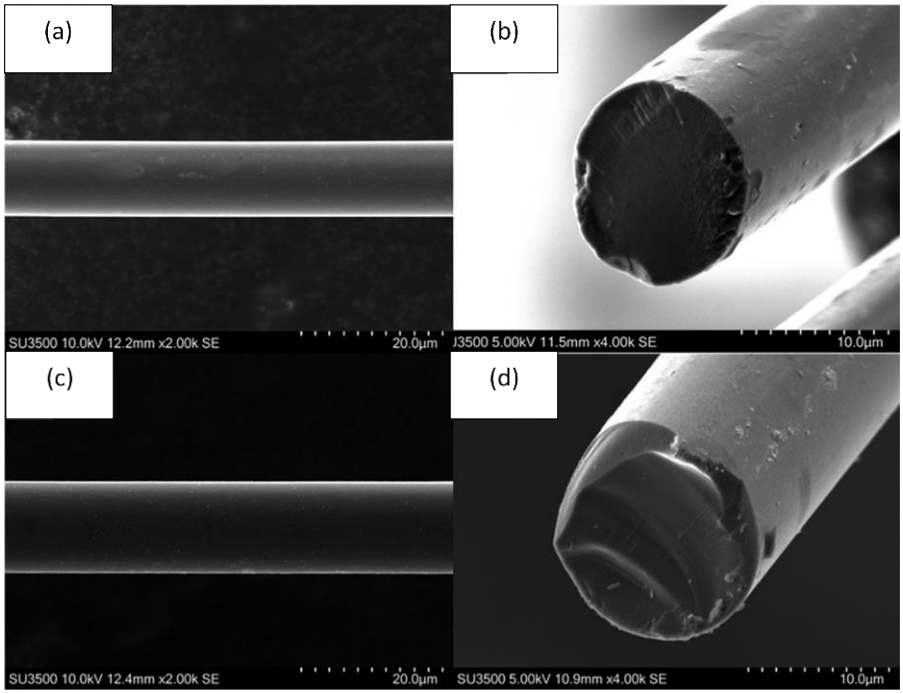

Figure 2.19 (a-d) SEM micrographs of softwood Kraft lignin/cellulose fibres made using dry jet-wet spinning (191).

2.6.1.3 Electro-spinning

Electro-spinning is another cost-effective solution (or melt) spinning method to produce nano-fibres preforms that are subsequently carbonised to produce carbon nano-fibres (CNFs) (235-238). The applications of lignin-based CNFs include nano-composites (239), tissue scaffolds for biomedical applications (240), sensors (241), filtration (180), lithium ion batteries (242), sodium ion batteries (243), fuels cells (244), double layer capacitors (245) and dye-sensitized solar cells for energy storage and batteries related applications (246).

The basic setup for electrospinning is illustrated in Figure 2.20 where the syringe contains a polymer solution (or melt) which is driven to the tip of the needle typically using a controllable dispensing unit (syringe pump). A high-voltage source is used to electrically charge the polymer solution of an appropriate viscosity. As the applied voltage is increased, the intensity of the electric field increases, a charged fluid of hemispherical shape droplet emerges at the tip of the needle which is held by its surface tension (235). This induces charges on the surface of the droplet. The pendant droplet transforms into a conical shape, known as the Taylor cone upon stretching due to the increase in the electrostatic field (247). At an appropriate applied voltage, the electrostatic forces increase the repulsion between the mutual charges and overcome the surface tension of the polymer solution, and a jet of the polymer solution is ejected from the surface of the Taylor cone. Firstly, this jet is linear for 2-3 cm and it is also termed as the jet length (straight jet) as shown in Figure 2.20 (248, 249). The jet then experiences instability due to a combination of forces such as a viscoelastic force, Coulomb force, a surface tension force, an air drag force, a gravitational force and an electric force exerted by the externally applied electric field (250). The bending instability causes the jet (solution) to follow a spiral loop. This is also known as whipping. The bending instability stretches the jet to become thin and long. During this stage, the solvent is evaporated leaving a solidified, continuous and randomly-oriented fibres on the grounded or negatively charged collector (180, 235, 251, 252).

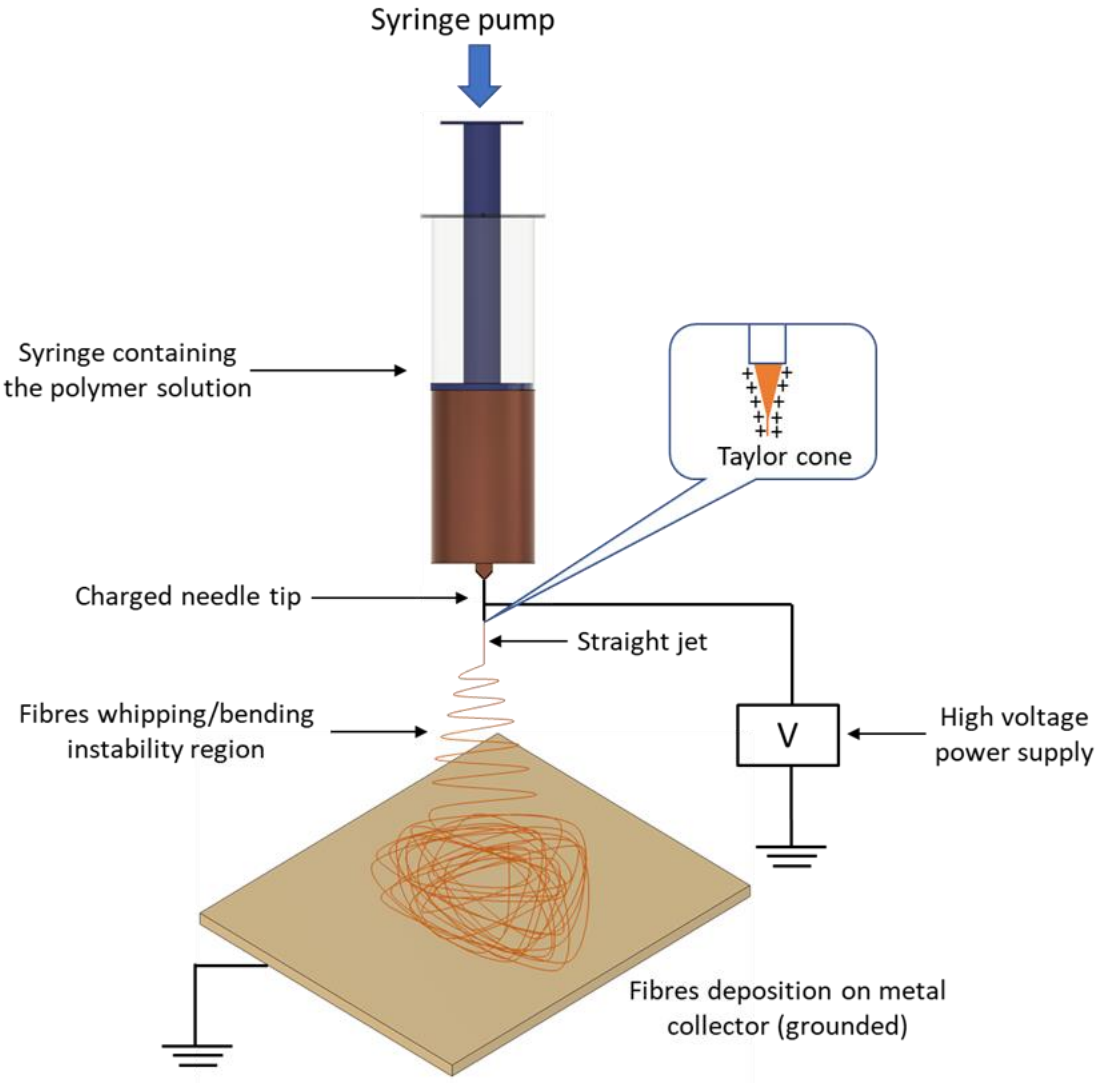

Figure 2.20 Schematic illustration of a typical electro-spinning setup for producing randomly orientated micro-to-nano diameter fibres (249, 253-255).

There are several parameters involved in the electro-spinning process as shown in Table 2.7. The electro-spinning of specific polymers solution is generally possible at appropriate viscosities as governed by the molecular weight distribution. The resulting fibre diameter increases with increasing molecular weight (256). Generally, the viscosity of the polymers solution increases with increasing molecular weight (67). The fibre diameter is also found to be increased with the polymer concentration (257). Dallmeyer *et al*. (2010) reported the fabrication of several technical lignins via polymer blending with 1 wt% polyethylene oxide (PEO) in dimethylformamide (DMF).

The molecular weights of these lignins were between 2200-3700 g/mol with that of softwood and hardwood Kraft lignins were 3700 g/mol and 2500 g/mol respectively (67). They reported a linear correlation between an increase in the fibre diameter with increasing lignin concentration. They also observed that different lignins with the same concentration lead to varying viscosities. This can be attributed to the lignins having different molecular weight distributions. This also suggest that lignins with different structures and composition greatly influence the properties of the solution and the parameters for electro-spinning (67).

Chang *et al*., (255) investigated the effect of the electro-spinning processing parameters on the formation of ligno-sulfonate fibres. They observed that the solution concentration was the most significant contributor towards electro-spinning. In addition, the concentration of the electro-spinning solution was also found to have the strongest effect on the fibre diameter distribution. Furthermore, they found a moderate effect from the applied voltage, syringe-to-collector (working distance) distance and flow rate on electro-spinning. The gauge of the needle had a minor effect on the fibre diameter.

The electrical conductivity, viscosity, volatility (solvents) and surface tension of lignin solutions have also been found to influence the electro-spinning process, including the morphology and diameter of the electro-spun fibres (258-260). Lallave *et al*., (260) demonstrated the use of coaxial electro-spinning when using low volatile solvents such as ethanol for dissolving lignin. In this instance, the primary needle contained the lignin solution with ethanol whilst the secondary needle contained only ethanol. The coaxial needle can compensate the evaporation of the solvents from the solution during electro-spinning. The ambient temperature and humidity are also influential variables. Humidity is known to induce porosity and alter the morphology of the spun fibres (254). Controlling the parameters cited in Table 2.7 can aid in generating conditions which favour the production of nano-fibres of uniform size distribution, composition and morphology.

Table 2.7 Processing parameters influencing the electro-spinning process.

Processing Parameters		
Polymer solution properties	**Processing variables**	**Ambient Parameters**
Molecular weight (67, 256) Viscosity (258, 259) Surface tension (258, 259) Electrical conductivity (258, 259) Polymer concentration (67, 257) Volatility (evaporation) of the solvent/solution (260)	Flow Rate (255) Applied Voltage (255) Working distance (separation between the charged tip and the collector) (255, 261) Needle gauge size (255) Type of collector (261)	Temperature (261) Humidity (254)

The nature of bending instabilities during the formation of fibres using electro-spinning is inherently complex and still not established (249, 262, 263). Hohman *et al.,* (262) discussed the whipping process and proposed a mechanism for it. They said that the charge density of the solution jet interacts with the externally applied electric field to produce the instability. Figure 2.21 (a-f) shows the several types of jets which can emanate from the Taylor cone depending on the magnitude of the applied electrical field. Figure 2.21 (a) shows the dripping mode, this is represented by the emergence of spherical droplets from the Taylor cone and (b) shows the spindle mode, where the jet is stretched and elongates to form thin fibres before breaking into droplets. Figure 2.21 (c) shows an oscillating mode where the jet is twisted and breaks into drops, and (d) represents the precession mode where the solution-jet loops. Figure 2.21 (e) shows the cone-jet mode which is generally required for electro-spinning and (f) shows the multi-jets emerging from the needle (249, 262).

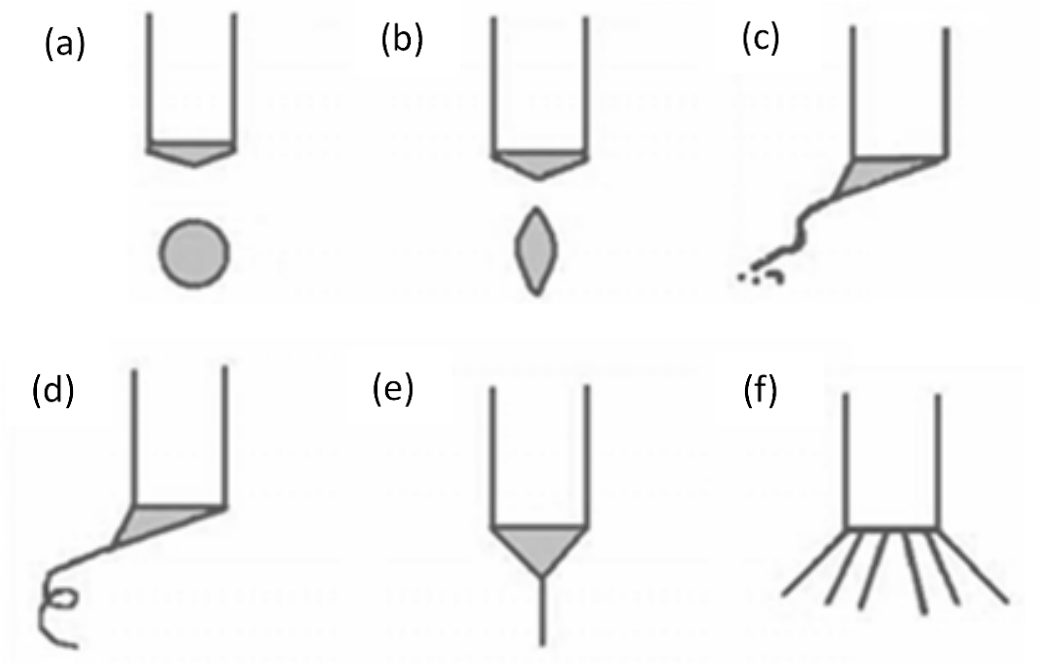

Figure 2.21 Schematic illustration of several types of charged jets that can be ejected from the Taylor cone (249, 262).

The electrostatic repulsion between the fibre due to the presence of residual charge influences the alignment and the orientation of the fibres. According to the desired application and properties, there are several reported techniques to control the orientation of fibres (235, 251, 257, 264-267). These techniques are based on mechanical methods or by controlling the electrical and magnetic field lines assisted by modifying the grounded or negatively charged collector electrode. Some of the techniques employed for controlling the alignment of electro-spun fibres are summarised in the next section.

A rotating drum-based ground electrode has been used for producing uniaxially aligned fibres is shown in Figure 2.22. This method can cause fibre elongation resulting in reduced diameter via mechanical drawing as governed by the rotational speed of the mandrel (264). A balance between the rotational speed of the mandrel and fibre haul-off rate is essential to achieve good alignment without fibre breakage. In another approach, a rotating disk with a chamfered circumference was shown to improve the alignment of the electro-spun fibres. This was attributed to the electrostatic

attraction due to higher charge density at the circumferential edge (266). However, the dimensions required for the aligned fibres is limited due to the constrained spun area on the edge of the disk (235, 266). Kim *et al*., (265) modified a ground mandrel collector by placing cellophane tapes horizontally and vertically on top of horizontally placed copper wire as shown in Figure 2.22(a-b) (265). The direction in which the cellophane tape was placed greatly influenced the orientation of the aligned fibres. This method resulted in highly aligned fibres which were used as a scaffold for biomedical application (265). Figure 2.22 (a-c) shows schematic illustrations of some of the techniques used for the electrospinning setup including collector modifications to enhance the alignment of the electro-spun fibres.

Lei *et al*., (267) reported the use of an insulated hollow PET cylinder with gratings of conductive electrodes inside the cylinder to produce aligned electro-spun fibres as shown in Figure 2.22 (c-d). The needle and the collector were connected to positive and grounds terminals of the power supply. The whipping jet is concentrated inside the cylinder and enables the fibre to align across the electrode gap (267). However, it presents a challenge in collecting the continuous fibres deposited on the drum without disturbing the alignment and to produce these fibres in large scale (235).

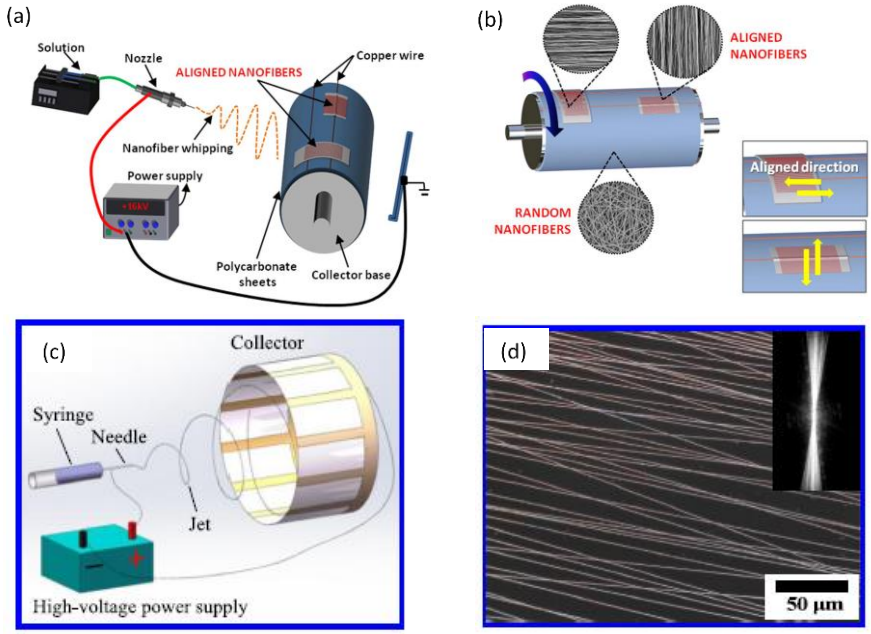

Figure 2.22 (a-c) Schematic illustrations of electro-spinning setups with modified collector used for the fabrication of uniaxially aligned fibres: (a-b) shows the influence of rotating drum with cellophane tapes and conductive copper wire (265); (c) shows the effect of introducing conductive strips inside the rotating cylinder (267); and (d) represents SEM micrographs of the aligned fibres from (c).

Li *at el.*, (2003) used parallel conductive strips with small separation to guide the electro-spun fibre to align perpendicular to the length of two electrodes (251). Figure 2.23 shows a schematic illustration of some the techniques used for modifying the collector to improve the alignment of fibres, along with the corresponding morphologies of the spun fibres. The alignment was achieved by placing two conductive strips such as metals or highly-doped silicon parallel to each other with a defined gap in between. The width of the gap can be from hundreds of micrometres to several centimetres. Beachley *et al.*, (257) reported fibre lengths between 35-55 cm for electro-spun polycaprolactone fibres . The mechanism involved in the alignment of electro-spun fibres across the gap of two electrodes was explained using a detailed study of the electric field strength (251). They reported that the electric field is concentrated in proximity to the two electrodes which splits in two directions that is between the opposite edges of the gap. The positively charged as-spun

fibre experiences electrostatic force of attraction towards the charges induced on the grounded electrodes. This electrostatic force of attraction is in line with electric field and it pulls the fibres towards the electrodes, placing it in perpendicular to the edge of two electrodes. The fibres in the gap region can remain highly charged even after deposition. The electrostatic repulsion due to the retained charges on the deposited fibre and on the upcoming fibre during electro-spinning can lead to further enhancement in alignment. There are several other techniques aimed at improving the alignment of electrospinning reported in the literature. For example, by changing the geometry and arrangement of electrodes such as the use of step-based aluminium strips as a collector (268). Another such technique is based on using an electrode with parallel serrated-edges to align the fibres (241).

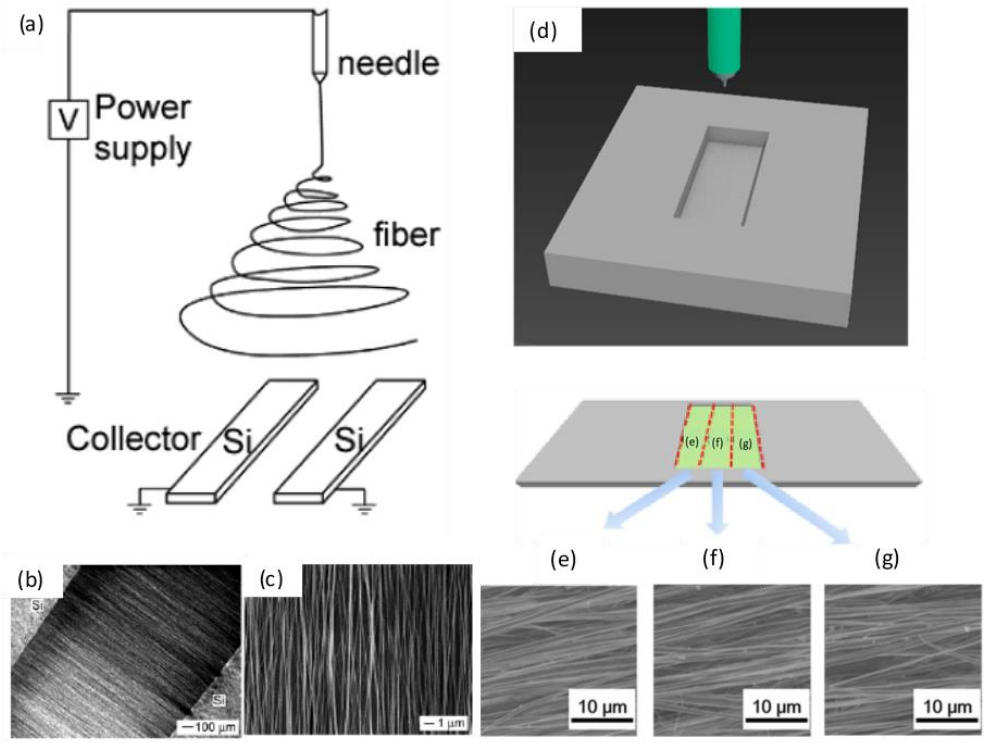

Figure 2.23 Schematic illustration of collector modifications used for fabrication of uniaxially aligned fibres with the corresponding fibre micrographs; (a-c) shows use of silicon (Si) conductive strips with the corresponding SEM images (251); and (d-g) shows the use of step-based aluminium conductive strips with the associated SEM images (268).

Dallmeyer *et al*., (2014) observed that softwood Kraft lignin fractionated using successive solvent treatments resulted in low (LW) and higher (HW) molecular weight lignin fractions (184). Lignin fractions were blended with 0.2 wt% of PEO in DMF. The role of the PEO was classified as a plasticiser which was said to felicitate the electro-spinning of lignin by intermolecular interactions. These interactions were attributed to hydrogen bonding with hydroxyl groups of lignin which was reported to result in a miscible lignin-PEO blend (5, 112, 184, 187). Figure 2.24 (a) shows a SEM micrograph of a HW/PEO blend which resulted in un-fused and circular fibres morphology. Whilst the mixture of 70% HW-30% LW lignin fractions and 0.2% wt PEO resulted in fused fibres as seen in Figure 2.24 (b) . These fibres were thermo-stabilised in air at 250 °C for 1 hour at 5 °C/minute followed by carbonisation at 10 °C/minute in nitrogen to 1000 °C for 1 hour. Figure 2.25 shows the morphology of carbonised lignin/PEO fibres at higher magnification.

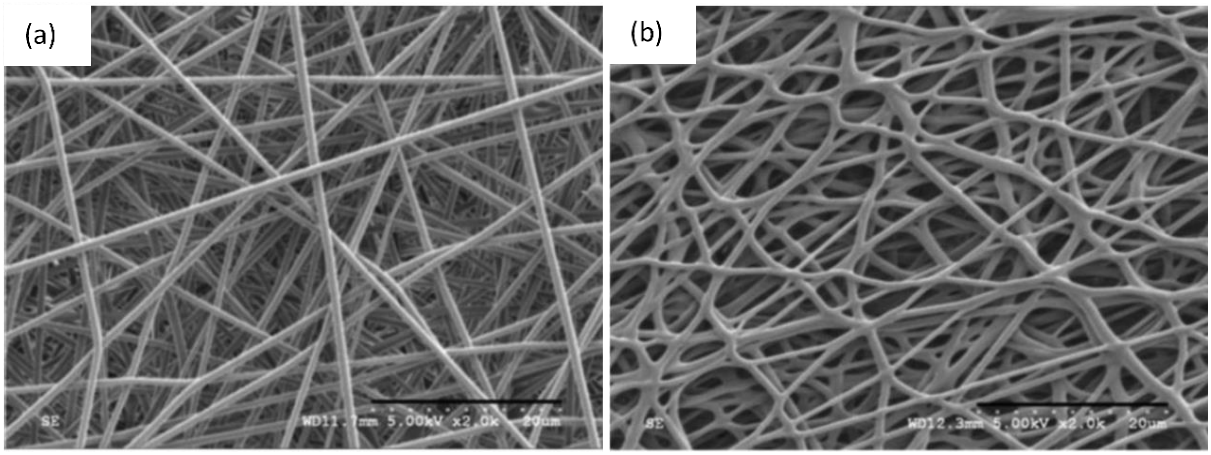

Figure 2.24 (a-b) SEM micrographs of lignin/PEO electro-spun and thermo-stabilised fibres at 250 °C in air for 1 hour: (a) unfused fibre morphology from HW/PEO blend; and (b) fused fibres from a mixture HW/LW with PEO (184).

Figure 2.24 and Figure 2.25 show the effect of molecular weight fractions and heating rate on the morphology of thermo-stabilised lignin/PEO fibres. The formation of fused fibres from low and high-molecular weight lignin/PEO mixture is linked to the higher heating rates employed during thermo-stabilisation. It was reported that the higher heating rates can cause thermal softening of

the materials with the operating temperature (T) being greater than the T_g ($T > T_g$). This can result in fibres becoming tacky and fusing together (183, 184, 269). The high-molecular weight lignin fraction has a higher thermal softening point which prevents the fibres from fusing even at higher heating rates (5, 184, 187, 269). The role of the T_g on the thermo-stabilisation and maintaining the fibre morphology is also discussed in Section 2.6.1.1.

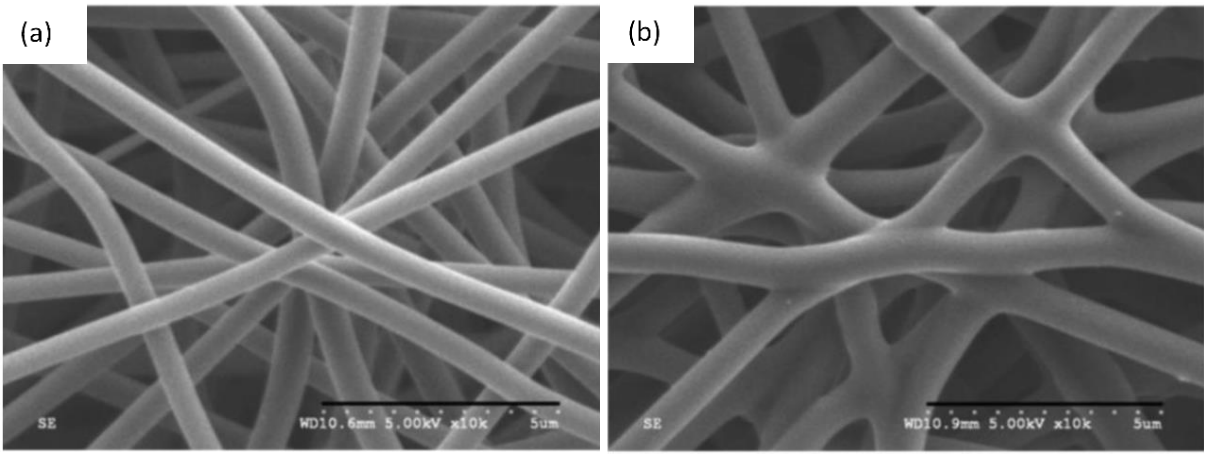

Figure 2.25 SEM micrographs of lignin/PEO electro-spun fibres that were carbonised at 1000 °C in nitrogen for 1 hour: (a) unfused fibre morphology from HW/PEO blend; and (b) fused fibres from a HW/LW blend with PEO (184).

Similarly, Cho *et al.*, (183) investigated the conversion of softwood Kraft lignin/PEO fibres into carbon fibres by skipping oxidative thermal stabilisation step. The as-spun fibres mats were carbonised directly at 1000 °C for 6 minutes with a heating rate of 5 °C/minute under a nitrogen flow (100 ml/minute). They observed significant fibre fusion in the carbonised fibre mat as shown in Figure 2.26 (a-b). However, the degree of fibre fusion decreased, and fibre morphology improved noticeably from fused to interconnected fibres with the addition of small amount (1-5 %) of NCC and by employing a slower heating rate (1-3 °C/minute). This demonstrates the important role of the thermo-stabilisation step in maintaining the fibre structure prior to carbonisation. However, it was reported that the fused fibre morphology tends to improve the

mechanical properties of both thermo-stabilised and carbonised fibres and it also result in the improvement of electrical conductivity of the carbonised fibres (183, 184).

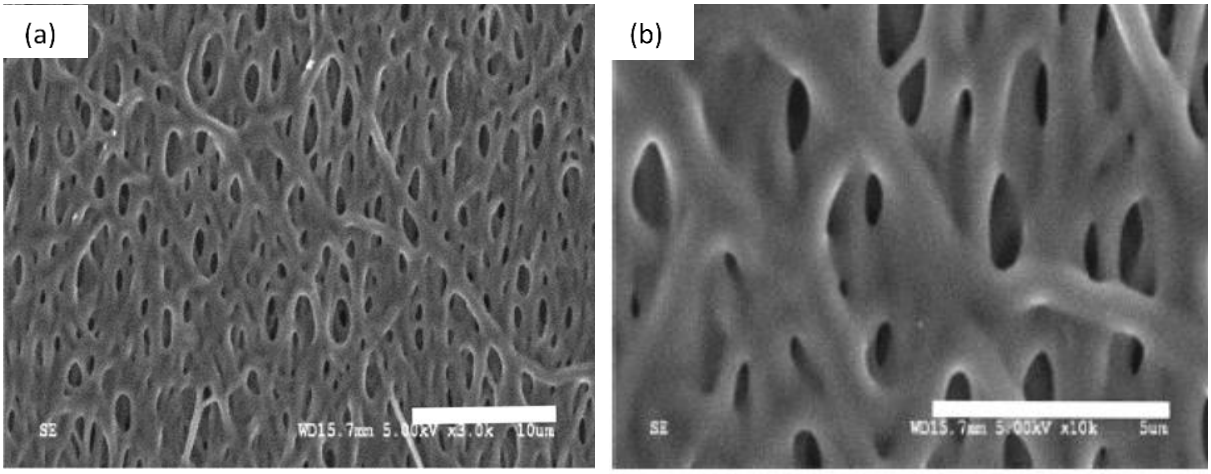

Figure 2.26 (a-b) SEM micrographs show the morphology of softwood Kraft lignin/PEO fibres mat carbonised directly at 1000 °C without a thermo-stabilisation step (183).

A wide range of polymers (PEO, PVA, PAN and cellulose) have been blended with lignin including the reinforcing materials such as carbon nanotubes (CNT), cellulose nanocrystal (CNC or NCC), nanoparticles, nanosheets, active reagents and other binders for the production of CNFs for many applications targeting tailored characteristics such as enhancement in mechanical and electrical properties (180, 183, 246, 270-275). It is believed that the reason for blending lignin with other polymers is to improve its viscoelastic property which in turn aid electro-spinning (186, 215, 276). The difficulty in electro-spinning lignin is linked to its molecular weight distribution, cross-linked structure and intermolecular interaction within the lignin framework. Blending lignin with polymers or plasticisers is thought to facilitate polymer entanglement by disrupting the intermolecular interactions altering lignins viscoelastic properties and in turn improving the electro-spinnability (215, 216, 276, 277). Different solvent systems have been used for electrospinning lignin fibres but DMF is the most commonly used solvent reported in the literature (67, 182, 184).

In recent publications, the research outlook was primarily focused on finding attractive applications for lignin-derived CNFs in the field of energy storage (dye-sensitised solar cells, batteries, capacitors and supercapacitors) and electronic devices. This is due to their aforementioned properties including their porous structure, electrical conductivity and chemical stability (200, 246, 252, 273, 278-284).

2.7 Structural Changes During the Heat Treatment of Lignin

The as-spun lignin fibres are converted to carbon fibres through heat treatment regimes that are generally referred to as thermo-stabilisation and carbonisation. The thermally-initiated chemical changes involve the cleavages of linkages mainly ether bonds (Figure 2.27), demethylation (Figure 2.28), demethoxylation (Figure 2.29), rearrangement of free-radicals via radical coupling or condensation reactions (Figure 2.31), depolymerisation with liberation of gases and carbonisation including formation of new C-C bonds (5, 146, 180, 219, 222, 285, 286). These reactions are detrimental to the composition and structure of lignin fibres during heat treatment. Only a handful of papers have reported and proposed the effect of thermo-stabilisation on the structure of lignin let alone for lignin fibres. Therefore, the effect of heating on powdered lignin samples is also discussed in this section. At time of writing, the author was not aware of any papers or reports on the structural changes in lignin during graphitisation.

2.7.1 Thermo-stabilisation

There are several plausible mechanisms suggested in the literature during thermo-stabilisation but due to the heterogeneity and complex structure of lignin, the suggested mechanisms are still unclear and open for debate (5, 180, 285, 286). These structural changes in lignin during heat treatment along with plausible mechanisms are discussed in the following section.

Cho *et al*., (285) investigated the elemental composition of lignin fibres during thermal oxidative stabilisation at various temperature intervals up to 350 °C. They reported a gradual decrease in the carbon (62.5% to 58.6%) and hydrogen (5.8% to 2.10%) contents as the lignin fibre were

heated in gas chromatography oven to 350 °C at 1-5 °C/minute; the fibre were held at selected temperature for 30-60 minutes in a ramp-hold heat treatment experiment. The oxygen content was observed to increase from 31.7% to 38.9%. The hydrogen content in the lignin fibres was observed to decrease from 5.82% to 2.10% at 350 °C. This can be attributed to the cleavage of hydrogen from C-H or O-H bonds to form free-radical structures that can lead to a cross-linked structure. Solid state ^{13}C NMR spectra showed a significant decrease in the methoxyl (OMe) content at 280 °C with the complete disappearance of the methoxyl peak at 350 °C. The FTIR spectroscopy results showed a significant decrease in the intensities of the hydroxyl (O-H) and C-H groups whilst the intensity of the carbonyl group increased gradually from 230-350 °C.

Li *et al.,* (287) also studied the structural changes of soda lignin during thermo-stabilisation using an air-circulating muffle furnace. They also reported a gradual reduction in the hydrogen content from 5.6% to 3.5%, when the lignin samples were heated at 30 °C/minute from 170 °C to 350 °C and held for 20 minutes at each selected temperature. The oxygen content was observed to increase marginally from 27.7% to 28.7% when heated up to 260 °C. However, it decreased to 27.3% at 350 °C. The hydrogen content decreases gradually from 5.64% to 3.49% between 170-350 °C. They also studied thermal degradation of lignin using TGA-MS from 30-500 °C under an air atmosphere. Their study revealed the evolution of volatiles products such as H_2O, CO_2, CH_3OH and CH_4. The reduction in the hydrogen content during heat-treatment, which was also observed by Cho *et al.*, (285)could be attributed to the evolution of H_2O, CH_3OH and CH_4. The increase in the oxygen content up to 260 °C indicates the occurrence of oxidation reactions to form oxygen-containing functional groups. The gradual drop in the oxygen content from 260 °C to 350 °C can be explained by the evolution of carbon dioxide and carbon monoxide. ^{13}C NMR spectra showed a similar trend to the results reported by Cho *et al.*, (285) where a significant decrease in the methoxyl (OMe) content was observed between 170 °C to 280 °C, and the complete disappearance of this peak at 350 °C. This implies that demethoxylation is one the major reactions involved

during the heat treatment process. The demethoxylation reaction results in the release and the formation of formaldehyde (see Figure 2.29) (219, 288).

Kim *et al*., (146) also reported on the elemental composition of milled wood lignin powder during heat treatment in an inert atmosphere up to 300 °C. They reported a gradual increase in the carbon content from 57.4% to 64.3% whilst the oxygen content was reduced from 36.6% to 29.8%. They observed a reduction in the ^{13}C NMR spectral intensities for the propane side chain and β-O-4 peak. This was said to be indicative of the cleavage of the propane side chain (C_α-C_β-C_γ) and β-O-4 ether linkages. This shows that the atmospheric conditions play an important role in the elemental composition of lignin during heat treatment.

Based on their results, Kim *et al.,* (146) proposed several possible reactions which might occur during heat treatment of lignin. These include:

- cleavage of methoxyl group (OMe) in the G/S lignin units;
- the cleavage of side chain being initiated above 150 °C;
- the cleavage of ether linkages such as α-O-4 and β-O-4 at 250 °C leading to the production of monomeric phenols;
- the generation of free-radical via the homolytic cleavage of the β-O-4 linkage leading to condensation and/or cross-linking reaction which results in the formation of a more condensed structure; and
- hydrogen abstraction reactions involving C-H and O-H functional groups.

The mechanisms associated with the homolytic cleavage of β-O-4 linkages during heat treatment is widely accepted in literature (5, 146, 222, 286). Norberg *et al*., (5) reported a possible reaction of softwood kraft lignin (shown in Figure 2.27) during the heat treatment process with the cleavage of β-O-4 linkages. This cleavage of β-O-4 results in the formation of free-radicals which

undergoes rearrangement reaction leading to the formation of stilbene type structure with loss of water molecules.

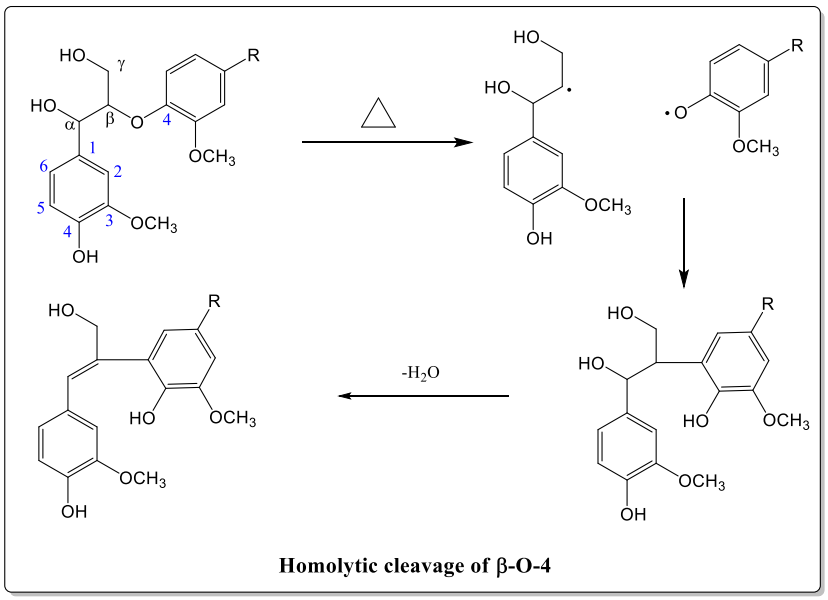

Figure 2.27 Mechanism proposed by Norberg et al., to demonstrate homolytic cleavage of the β-O-4 linkage in softwood Kraft lignin followed by rearrangement leading to the formation of stilbene when heated in an air atmosphere to 250 °C (5).

Faravelli *et al.,* (289) developed a kinetic modelling for the thermal degradation of softwood lignin at temperature above 200 °C. They also proposed the cleavage of β-O-4 as a possible initiation reaction during the pyrolysis of lignin due to their low bond dissociation energy (BDE). This also supports the observation made by Wikberg et al., (286). The BDEs can vary depending on the substituents and the neighbouring atoms. Therefore, chemical reaction schemes shown in Figure 2.28 have been proposed on the basis of the relevant BDEs. The methoxy group (O-CH_3) has similar BDE to β-O-4 and is thought to be cleaved at temperature above 200 °C; this was also apparent in the ^{13}C NMR spectra (285). Examples of other authors who support the mentioned mechanism for homolytic cleavage of the β-O-4 linkage and methoxy group via demethylation can be found in reference (146, 222, 285).

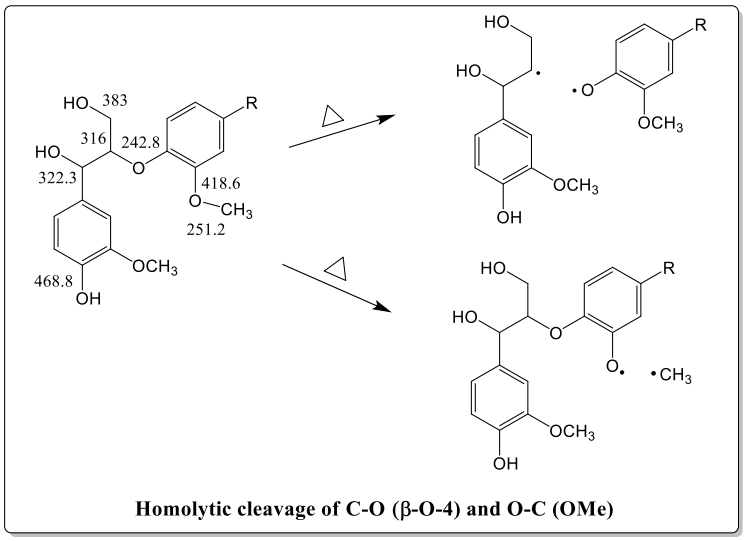

Figure 2.28 Homolytic cleavage of the C-O (β-O-4) and O-C (OMe) linkages during heat treatment of softwood lignin up to 350 °C (285, 286, 289).

The cleavage of carbon-carbon bonds are also reported in the literature and to account for the release of formaldehyde during the thermal degradation of lignin as shown in Figure 2.29. The release of formaldehyde takes place in two ways; either by homolytic cleavage of C-O bonds or by hydrogen abstraction (222).

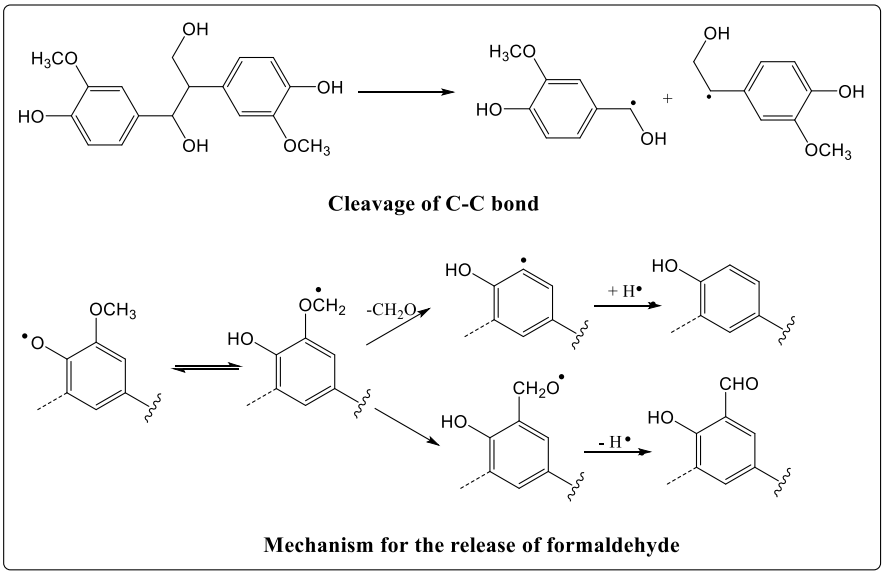

Figure 2.29 The mechanism involving the cleavage of a C-C bond in a dimeric lignin unit and the release of formaldehyde via hydrogen abstraction (222).

Figure 2.30 shows the oxidation reaction which takes place during the heat treatment of Kraft lignin between 200-250 °C in air (222). This type of reaction is also evident through elemental analysis where the increase in oxygen content at temperature below of 260 °C is observed (285, 287). The reaction suggests that oxidation reactions can give rise to the formation of carbonyl, carboxyl and ketone groups in the aliphatic side chain of lignin structure as reported by Braun *et al.*, (222).

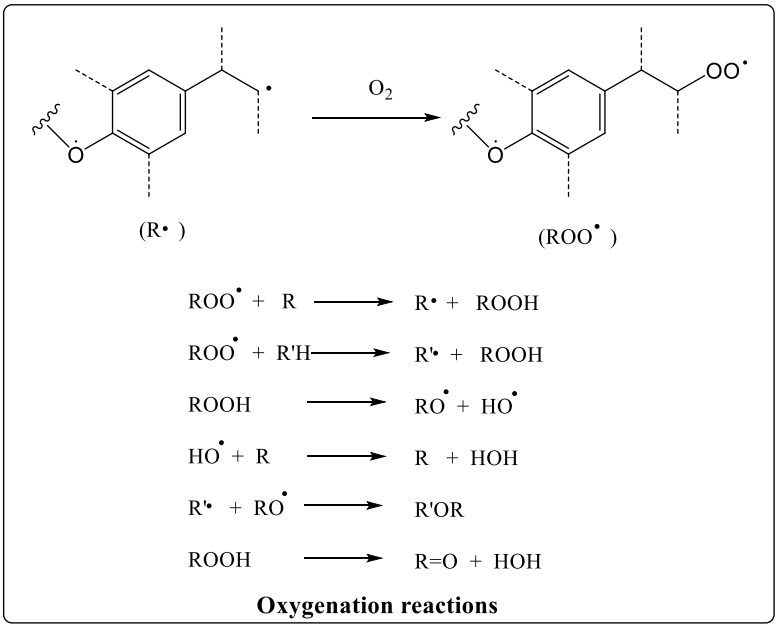

Figure 2.30 The oxidation reactions occurring during the heat treatment of Kraft lignin in air at 200-250 °C (222).

2.7.2 Carbonisation

With reference to the heat treatment of lignin, beyond 250 °C, the oxygen content is reduced, and condensation reactions takes place involving carboxylic acids which leads to the formation of esters or anhydride groups (285, 287). Figure 2.31 shows the proposed mechanism for the formation of condensed structure during heat treatment. The condensation of aromatic groups predominates at temperatures above 400 °C which leads to formation of new thermo-stable C-C linkages and conjugated bonds (147, 180).

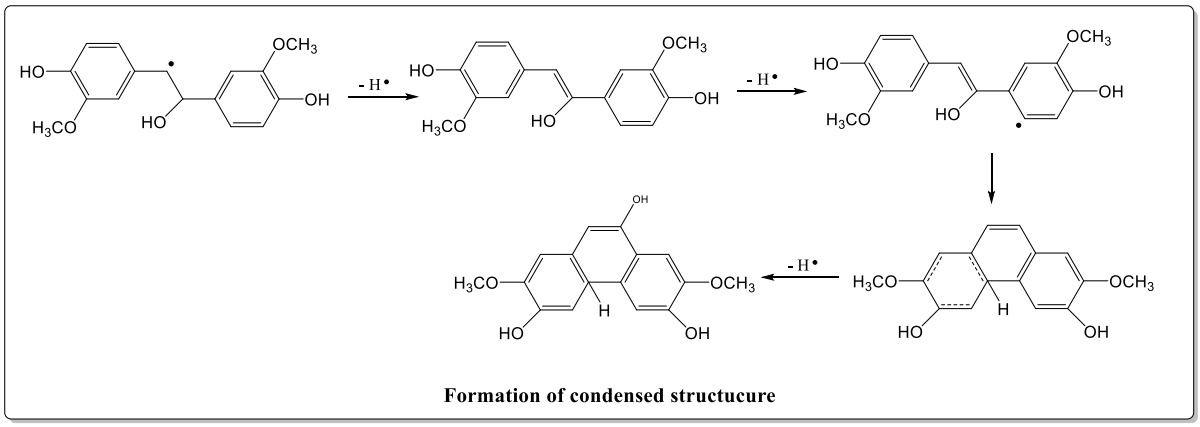

Figure 2.31 The proposed mechanism for the formation of condensed structures in lignin at elevated temperatures (180).

At 200-300 °C, the existence of polyaromatic hydrocarbons such as phenanthrene, naphthalene and anthracene was reported which confirms the formation of condensed aromatic and cyclic structures (218, 219). The structures of these products are shown in Appendix C. During carbonisation, the oxygen and hydrogen content is reduced significantly whilst the carbon content reaches to approximately 97% at 500-1500 °C in nitrogen for 5-10 minutes (218, 219). The oxygen moieties such as carbonyl and carboxyl groups formed at the thermo-stabilisation step are converted to aryl type condensed structures (290). The existence of a turbostratic graphitic structure as shown in Figure 2.32 or highly condensed aromatic structure of carbonised fibres is generally observed through Raman spectroscopy (180, 287).

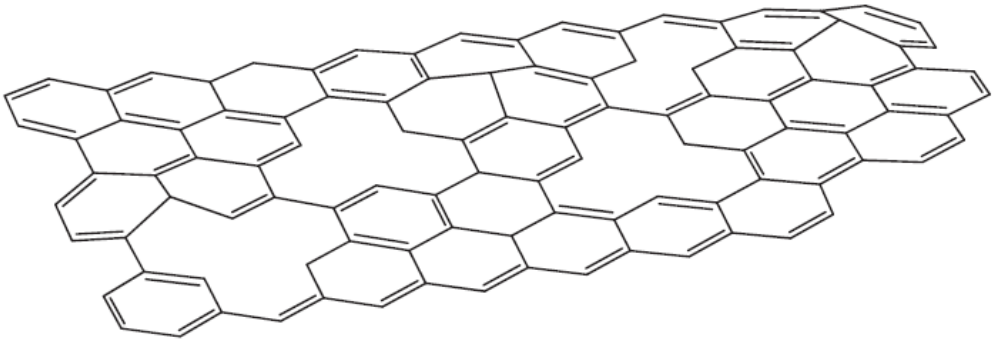

Figure 2.32 Model of turbostratic carbon (30).

Chapter 3 Materials and Methods

3.1 Lignin

3.1.1 Softwood Kraft (BioChoice®) Lignin

Softwood Kraft lignin was purchased from Domtar PC sales centre (Germany). This material was said to originate from Domtar Plymouth Mill (USA) with tradename of BioChoice® lignin and it is understood that it was extracted from Southern pine trees.

3.1.2 Lignin from Coir

Lignin was extracted from coir fibre which were obtained from Hayleys PLC (Colombo, Sri Lanka). The coir was obtained in two forms which are discussed later on in this chapter.

3.1.3 Lignin Blending with Tannic Acid

The tannic acid with a molecular weight of 1701 g/mol was purchased from Sigma-Aldrich (UK), ACS reagent grade, and it was used as a blend with lignin for electro-spinning of lignin.

3.2 Chemicals and Solvents

3.2.1 Sulphuric acid

Sulphuric acid (72 w/w%) was purchased from Fisher Scientific (UK) and it was used for estimating the relative concentration of the lignin in softwood Kraft (BioChoice®) and the quantification of lignin.

3.2.2 Nitric acid

This was purchased from Sigma-Aldrich (UK), 70% ACS reagent grade, and it was used for washing the softwood Kraft lignin to remove inorganic impurities.

3.2.3 Solvents

The solvents used for the fractionation of softwood Kraft lignin were:

(i) acetone (Sigma-Aldrich, UK, 99.5% ACS reagent grade);

(ii) ethanol (Fischer Scientific, UK, 99.8% ACS reagent grade); and

(iii) 1-propanol (Sigma-Aldrich, UK, 99.5% ACS reagent grade).

Dimethyl sulfoxide (DMSO) was purchased from Sigma-Aldrich (UK), 99.9% ACS reagent grade, and it was used for estimating the solubility of softwood Kraft lignin. It was also used to dissolve lignin for purity analysis where the material was characterised by UV/Visible spectroscopy. DMSO was also combined with acetone to form a binary solvent for electro-spinning lignin.

Dimethylformamide (DMF) was purchased from Sigma-Aldrich (UK), 99.9% ACS reagent grade, and it was used for evaluating the solubility of softwood Kraft lignin.

Chloroform (99.8%) and diethyl ether (99.5%) were purchased from Fisher Scientific (UK), ACS reagent grade and they were used for the purification of acetylated lignin.

Deuterated dimethyl sulfoxide (DMSO-d_6) and chloroform-d ($CDCl_3$) were purchased from Sigma-Aldrich (UK), 99.9% ACS reagent grade for preparing lignin solutions for characterisation by nuclear magnetic resonance spectroscopy.

3.2.4 Chemicals

The reagents for that were used for the acetylation and phosphorylation of lignin were acetic anhydride (99.5%), anhydrous pyridine (99.8%) and 2-chloro-4,4,5,5-tetramethyl-1,3,2-dioxaphospholane. These chemicals were purchased from Sigma-Aldrich and Fischer Scientific (UK).

Tetramethylsilane (TMS) was purchased from Sigma-Aldrich, 99.9% ACS reagent NMR grade, and it was used as an internal standard for ^{1}H NMR where it shows a signal at 0 ppm.

Chromium (III) acetylacetonate (99.99%) was used as a relaxation agent whilst 1,3,5-Trioxane (99%) and *N*-hydroxy-5-norbornene-2,3-dicarboximide (97%) were used as an internal standard for ^{13}C NMR and ^{31}P NMR respectively. These chemicals were purchased from Sigma-Aldrich (UK).

The preparation of lignin samples for transmission mode FTIR spectroscopy involved the use of dried potassium bromide (Sigma-Aldrich, UK). The pre-dried KBr powder was mixed and ground with lignin and compressed into 13 mm disks.

3.3 The Characterisation of Softwood Kraft Lignin using TAPPI Standards

Softwood Kraft lignin is known to contain a range of impurities including carbohydrates (151), moisture and inorganic minerals (89). The relative concentration of these materials including the lignin content were quantified using the methods specified by the Technical Association of the Pulp and Paper Industry (TAPPI). The following section presents details of the experimental procedure that were used to determine the moisture ash, acid soluble and acid insoluble lignin contents.

3.3.1 Moisture Content and Sample Preparation

Before the quantification of the lignin, the sample was prepared according to the specified methods (291). The samples are sieved to less than <400 um which is in accordance with TAPPI T257 (291). The moisture content was determined at 105 °C to achieve constant weight in accordance with TAPPI T264 (292).The moisture content was estimated using the Equation 2:

$$\text{Moisture content (\%)} = \frac{Initial\ mass - final\ mass\ after\ drying}{Initial\ mass\ of\ the\ sample} \times 100 \qquad \text{Equation 2}$$

3.3.2 Ash Content

The ash content in the pre-dried (moisture-free) Kraft lignin was determined in accordance with TAPPI T211 om-02 (293). The procedure involved pre-heating alumina crucibles to 525 °C for 60 minutes and cooling them in a desiccator. Approximately 1 gram of lignin was transferred to the pre-dried and pre-weighed crucibles. Alumina lids were placed on the crucibles and they were positioned in a muffle furnace and heated from ambient temperature to 525 °C to carbonise the lignin samples without causing it to ignite. Once the samples had charred, the lid was removed to oxidise lignin samples at 525 °C for 4 hours. Upon cooling to room temperature, it was observed that samples had been converted from a black char to white powdery ash. The mass was recorded

to the nearest 0.001 g using an analytical balance and the ash content was determined using Equation 3:

$$\text{Ash content (\%)} = \frac{Mass\ of\ ash}{Initial\ mass\ of\ moisture-free\ sample} \qquad \text{Equation 3}$$

3.3.3 Acid Insoluble Lignin (Klason Lignin)

The acid insoluble lignin content was determined from the extractive-free biomass subjected to acid hydrolysis with 72% w/w H_2SO_4 according to TAPPI T222 om-02 (294, 295). The carbohydrates were hydrolysed during this process leaving the lignin as an insoluble residue. The procedure involved treatment of 1 gram of moisture free lignin with 20 ml of 72% w/w H_2SO_4 for 2 hours to hydrolyse the carbohydrates. The mixture was diluted with deionised water to 3% H_2SO_4 and boiled for 4 hours under reflux. The mixture was cooled to room temperature, filtered, and the insoluble residue is referred as Klason lignin whilst the filtrate contains acid-soluble lignin.

3.3.4 Acid Soluble Lignin

Depending on the type of lignin, a small amount of lignin is known to be hydrolysed during 72% w/w acid. The amount of acid soluble lignin was quantified using UV/Visible spectroscopy in accordance with TAPPI method (UM 250) (294, 296). The filtrate (acid soluble) from Klason lignin method (in Section 3.3.3) was analysed and compared to a reference of neat 3% H_2SO_4.

A Camspec M550 Double Beam Scanning Spectrophotometer was used to acquire ultraviolet spectra of the acid soluble lignin. Approximately 3 ml was transferred to a quartz cuvette (6030-UV, Hellma UK LTD) with a path length of 1 cm. A reference spectrum was obtained using neat 3% H_2SO_4 which was acquired prior to the sample. The scanning range was from 190-500 nm with a scan interval of 0.5 nm. The acid soluble lignin was then estimated with absorbance at 205 nm (294, 296).

3.4 Design of Experiments for the Diluted Acid Treatment of Lignin

The acid-washing of lignin was carried out using nitric (HNO_3) acid. The parameters that can affect the end product including the type of the acid are as follows: the pH of an acid; lignin to acid solution ratio; duration of the cycle and the number of cycles. In literature, one can often find the use of sulfuric acid and hydrochloric acids for washing lignin to reduce impurities. The pH 2 was used as lowest pH level because more concentrated acid was found to degrade lignin (297).

A Taguchi-based design of experiments (DoE) method was used to identify the optimum parameters for acid washing the lignin. It consisted of nine experiments also referred to as a L_9 DoE orthogonal array. The initial step in the Taguchi method is to design an experimental matrix to evaluate the number of factors, level of design and the interaction of these factors. Table 3.1 shows the factors and level used for the design of experiments.

Table 3.1 Factors and level of factors involved in the Taguchi (DoE) study for the acid-washing of lignin.

Symbol	Factor description	Level		
		1	2	3
A	pH	2	4	6
B	Weight of lignin to liquid ratio (g/ml)	5	50	100
C	Duration of the cycle(s)	15	30	60
D	Number of cycles	1	3	5

The full factorial DoE consisting of similar factors and the number of design level will consist 81 experiments (3^4) which can be time-intensive. Therefore, the Taguchi DoE trials are more applicable as compared to a set of full-factorial experiments. This is due to the reduced number of

experiments which are significantly more economical in terms of experimental time. In this current study fours factors were selected and each factor with three levels of design high, medium, and low were considered. This resulted in nine experiments which are summarised in Table 3.2 detailing the parameters used for acid washing with nitric acid. The selection of the orthogonal array was completed using Minitab-18 software. In this study, the objective was to determine significant factors or optimum combination of factors to reduce the ash content after the combustion of lignin. Approximately 1 g, to the nearest 0.001 g, of moisture-free lignin was transferred into a 500 ml beaker with desired volume of acidified water. The mixture of lignin and acidified water was stirred using overhead stirrer (Pro 40, SciQuip, UK) at 400 rpm for a specified duration. The temperature was between 20 and 25 °C.

Table 3.2 The factors involved in the Taguchi (DoE) method for the acid washing of lignin.

Experiment No.	Factors			
	A = pH	B = Weight to liquid ratio (g/ml)	C = Cycle duration (s)	D = Number of cycles
1	2	5	15	1
2	2	50	30	3
3	2	100	60	5
4	4	5	30	5
5	4	50	60	1
6	4	100	15	3
7	6	5	60	3
8	6	50	15	5
9	6	100	30	1

The robustness and performance of Taguchi method was measured using Taguchi Analysis to identify the controllable and uncountable factors (noise factors) through mean effects and signal-to-noise (S/N) ratio. The S/N ratio is a measurable value and it is used instead of the standard deviation to reduce the variability in the data set.

3.4.1 Signal to noise ratio (S/N) of minimising the ash content

The S/N ratio identifies and determines the significant factors that cause variability in response to the target value. A 'smaller is better' characteristic has been used to determine the significant factors in reducing the ash content in lignin according to Equation 4:

$$S/N = -10\, log\left(\frac{1}{n}\sum_{i=1}^{n} y_i^2\right) \qquad \text{Equation 4}$$

where n refers to the number of measurements or repetitions, and y_i is i^{th} observation of the quality performance which in this case is ash content of lignin. Generally, a greater value of S/N represents a smaller ash content.

3.4.2 Analysis of Variance

The results of the Taguchi DoE method with nine sets of experiments were analysed using the analysis of variance (ANOVA). ANOVA is used to analyse the output of the experiment trails in determining the effect of significant factors and combination of factors, to determine the data variance and analyse the extent of variation that each factor has contributed. The procedure for the ANOVA involves the calculation of the sum of squares, mean squares (variance) and associated F-ratio of significance. In the ANOVA, the total variation (S_T), the sum of squares of each factor (S_t), the percentage contribution and the signal-to-noise ratio (S/N) ratio in achieving the reduced ash content are calculated. The ANOVA was analysed with a confidence level of 95%. This means the significance level was adjusted to 5% which represent the data variance.

3.4.2.1 Degrees of Freedom

In order to design the number of experimental trials using an orthogonal array, the Taguchi design uses the degrees of freedom (DoF) criteria to determine the total number of experiments. The degree of freedom for each factor is defined by number of levels minus one (DoF = No. of levels - 1) whereas the total number of experiments is determined using the sum of degree of factors plus 1 and it is calculated using Equation 5:

$$Total\ number\ of\ experiments, T_{Experiments} = 1 + \sum_{i=1}^{k}(S_k - 1) \quad \text{Equation 5}$$

3.4.2.2 Total Variation (S_T)

The total variation (S_T) refers to the sum of squares of all nine experiments which is expressed according to Equation 6:

$$S_T = [\sum_{i=1}^{N} Y_i^2] - \left[\frac{\left(\sum_{i=1}^{N} Y_i\right)^2}{N}\right] \quad \text{Equation 6}$$

where Y_i is the mean ash content and N is the number of experiments in Taguchi DoE study

3.4.2.3 Percentage Contribution (%)

The percentage contribution of four factors is calculated using the Equation 7:

$$P_i = \frac{S_i}{S_T} \quad \text{Equation 7}$$

where i refers to the number of factors which in this study is equal to 4, S_i and S_T represents the ratio of total variance each factor to total variation (S_T) respectively.

The effect of the significant factors is analysed through main effects and S/N ratio plots for the response from the Taguchi method.

3.5 Sample Preparation and Solvent Fractionation of Lignin

Prior to solvent fractionation, the Kraft lignin was dried in a vacuum oven (Gallenkamp OUA031, Fistreem, UK) at 80 °C for 6 hours under a reduced pressure of 1 bar to remove moisture and low-molecular weight volatiles. The pre-dried lignin was refluxed with the desired solvent (acetone,

ethanol or n-propanol) for 6 hours under constant agitation by bubbling argon gas at 30 ml/minute. The temperature of the solution was maintained close to the boiling points of acetone, ethanol or n-propanol (56 °C, 75 °C and 95 °C, respectively). The lignin-to-solvent ratio was maintained at 1 gram per 15 ml. After refluxing, the solution was cooled to room temperature and filtered under reduced pressure. The filter paper used was Whatman binder-free glass microfilter paper with pore size of 1.2 μm (Sigma-Aldrich, UK). The solvent from soluble lignin fraction was evaporated using a rotary evaporator (RV3, IKA, UK) under a reduced pressure of 200 mbar. The insoluble fraction was deposited on the filter paper. The fractionated lignin including the soluble and the insoluble fractions were dried in a vacuum oven at 80 °C for 6 hours and stored in air-tight container until required.

The ash content of soluble and insoluble lignin fractions was measured in accordance with TAPPI T257 sp-14 (291), T264 cm-07 (292) and TAPPI T211 om-02 (295) methods respectively.

3.6 Characterisation of Lignin Using Conventional Techniques

3.6.1 Particle Size Distribution

A Malvern Mastersizer 2000 (Malvern Panalytical, UK) laser particle size analyser was used to determine the particle size distribution of the lignin samples. Sample with concentration of 2.5 % (w/v) was prepared using 0.25 g of pre-dried lignin in 10 mL of deionised water. The mixture was sonicated for 3 minutes using an ultrasonic bath (Scientific Laboratory Supplies, Ltd, UK). The sample was transferred to the compartment of the particle size analyser that was housed with a stirrer. The stirrer was operated at 2250 rpm. The particle size analyser consisted of an array of detectors where each detector acquired the light scattered from a range of angles. The measurement was made by the detector acquiring 2000 data points for each measurement when the particles passing through the analyser-beam at a particular time. Background data were obtained where the instrument was operated without the dispersed lignin sample. Five

measurements were obtained for each sample. The experiments were carried out approximately at 25 °C.

3.6.2 Elemental Analysis

Elemental analysis of lignin was carried out using a CHNS elemental analyser (model EA111 Carlo Erba Instruments, UK). The samples were freeze-dried for a week prior to conducting the analysis. The oxygen content was determined by subtracting the contribution from C, H, N and S.

3.6.3 Density Measurement

A gas pycnometer (AccuPyc II 1340, Micromeritics, USA) was used to measure the density of the as-received softwood Kraft lignin. The principle of this instrument is based on the gas displacement method to determine volume. Helium was used as a displacement medium. The sample with a mass of approximately 0.4 grams was placed inside the chamber of a known volume. Helium gas was purged into this compartment. The instrument measures the volume required to fill up the chamber and it calculates the density of the sample by dividing the sample mass by its volume. Five measurements were made for each sample.

3.6.4 Scanning Electron Microscopy

A TM3030 PLUS (Hitachi, Japan) scanning electron microscope was used to study the morphology of the lignins and ash. The instrument was operated using an acceleration voltage of 15 kV. The sample was mounted on a SEM stub using an adhesive-backed carbon tape. The samples were coated with gold/palladium alloy for 3 minutes using Emscope SC500 (Quorum Technologies, USA). The instrument was operated at 25 mA under a vacuum of 1 mtorr. The instrument contained a built-in silicon drift detector to enable energy dispersive X-ray (EDX) data to be acquired and to assign the elements present. In this instance, the samples were not sputter-coated with the gold/palladium alloy. A total of 5 measurements were taken at different locations on the sample.

3.6.5 Differential Scanning Calorimetry

The differential scanning calorimetry (DSC) experiments were performed on a power compensated Diamond DSC (Perkin Elmer, UK) and DSC 1 (Mettler Toledo, UK). The instruments were calibrated using indium, tin and gallium. Approximately 10 mg of the lignin was transferred to an aluminium pan and crimped with a lid. A crimped pan without the lignin was used as the reference. The sample and the reference lids were pierced with two holes to permit the release of volatiles during the heating cycle. The DSC 1 (Mettler Toledo) was operated in a nitrogen atmosphere where the flow rate of 50 cm^3/minute. The samples were cooled from 25 °C to -80 °C at 10 K/minute and this was followed by heating from the sample -80 to 200 °C at 10 K/minute. Two successive cooling and heating cycles were conducted. With reference to determine the efficient method as a drying procedure to remove moisture and low-molecular weight volatiles from as-received (BioChoice®) lignin, two methods were investigated: a freeze-drying method; and drying lignin in a vacuum oven.

With respect to freeze-drying, the as-received (BioChoice®) lignin powder was placed inside the round bottom flask. The flask was dipped in liquid nitrogen for approximately two minutes before placing it under vacuum for 7 days. For drying in a vacuum oven (Gallenkamp OUA031, Fistreem, UK), the sample was dried at 80 °C for 6 hours under a reduced pressure of 1 bar.

Diamond DSC (Perkin Elmer, UK) was used to determine the glass transition temperature (T_g) of soluble and insoluble lignin fractions. These experiments were conducted in a nitrogen atmosphere where the flow rate was maintained at 50 cm^3/minute. The samples were heated from 25-250 °C at 10 K/minute. The samples were cooled to 10 °C at 10 K/minute and two successive heating/cooling cycles were performed.

3.6.6 Dynamic Vapor Sorption

A dynamic vapor sorption (DVS) instrument (DVS Resolution, Surface Measurement Systems Ltd, UK) was used to determine the moisture sorption-desorption isotherm curve for lignin. The DVS consists of a dual vapor gravimetric analyser to control, maintain and monitor temperature and relative humidity. It recorded the changes in the mass of the sample relative to a change in the humidity at the desired temperature. The DVS apparatus used a controlled flow of dry nitrogen as the carrier gas. The relative humidity was controlled digitally by mixing dry and saturated gas in desired ratio. Approximately 20 mg of the as-received lignin sample was transferred to sample container that was located in a humidity-controlled chamber. The lignin was heated to 80 °C at 0% humidity for 6 hours. The dried lignin was cooled to 25 °C in a closed chamber. The sample was subjected to a change in the relative humidity (RH) from 0% to 95% with increment of 5%. The relative humidity was reduced from 95% to 0% in steps of 5%: the temperature was maintained at 25 °C. The relative change in humidity to monitor the moisture ingress and egress in lignin at a constant temperature.

3.6.7 Gel Permeation Chromatography

The molecular weight distribution of the lignin was carried out using gel permeation chromatography (GPC) by Dr Daniel Lester at the University of Warwick. The samples, including the standards, were dissolved in dimethylformamide (DMF) containing 5 mmol of NH_4BF_4. The instrument was calibrated using polymethylmethacrylate (PMMA) standards with molecular weights in the range of 550-955,000. NH_4BF_4 was used in conjunction with the polar solvents that were used in this study to prevent artificial shoulder appearing on the high-molecular weight region of the distribution (298). This is due to the interaction between the polar groups of the solvent and the polymer.

The molecular weight distribution was obtained using GPC (Agilent 1260 Infinity II-MDS). This instrument was equipped with refractive index detector and UV wavelength of 280 nm). DMF was

used as the mobile phase eluent with a flow rate of 1 ml/minute at 50 °C. A 100 µL of dissolved lignin sample, in DMF, with a concentration of 1 mg/mL was injected into the column. The analysis of the GPC results was carried out by the author at the University of Birmingham.

3.6.8 Thermogravimetric Analysis

Thermogravimetric analysis (TGA) experiments were performed on a Netzsch STA 449 (Netzsch, UK). Approximately 10 mg of the sample was placed in a platinum pan and transferred into the sample chamber. The sample was heated from 25 to 900 °C at10 K/minute under an argon atmosphere. The gas flow rate was maintained at 50 cm^3/minute throughout the experiment.

3.6.9 Pyrolysis-Gas Chromatography-Mass Spectrometry

A CDS 5000 Pyroprobe (Analytix Ltd, USA) was used to heat the samples in two stages. These experiments were conducted by Dr Karen Sam at Analytix Ltd (Bolden, UK). Two heating sequences were used. In the first instance, the sample was heated from 50 °C to 320 °C at 10 K/minute and maintained for 5 minutes at 320 °C. This was followed by heating from 320 °C to 1000 °C at 10 K/minute with a dwell for 5 minutes at 1000 °C. The Pyroprobe was connected to the GC oven at the injector position with a heated transfer line that was maintained at 300 °C to the transfer volatiles released during pyrolysis using a carrier gas. The GC-MS (1310 ISQ GC-MS from Thermo Fischer Scientific, UK) parameters were as follows: helium was used as a carrier gas with split ratio of 75:1 whilst the heated injector of the GC was set to 350 °C. The GC oven was programmed to heat from 40 °C to 325 °C at 10 K/minute with initial hold of 2 minutes at 40 °C and a final hold for 15 minutes at 325 °C. The MSD scan was used with Ion Mode of EI+ with mass ranging from 35 to 600 amu. A NIST 17 mass spectral library was used to assign the peaks observed in the chromatogram. The analysis of the Py-GC-MS results was carried out by the author at the University of Birmingham.

3.6.10 Fourier Transform Infrared Spectroscopy

The Fourier transform infrared (FTIR) spectroscopy experiments were performed on a Nicolet 6700 spectrometer (Thermo Fisher Scientific, UK). Samples for FTIR spectroscopy were prepared by grinding 200 mg of pre-dried KBr with 2 mg of the sample. The ground mixture was transferred to a 13 mm diameter compression mould die (GS03000, Specac, UK) and compressed at 10 bar. A blank disk containing only the pre-dried KBr was also produced as described above. Transmission spectra were obtained from 400-4000 cm^{-1}, with a resolution of 4 cm^{-1} and 100 scans. The blank KBr disk was used to obtain the reference spectra before obtaining that of the sample.

3.6.11 UV/Visible Spectroscopy

A Camspec M550 Double Beam Scanning Spectrophotometer was used to acquire ultraviolet spectra of lignin solutions. Approximately 0.5 mg of lignin was dissolved in 20 ml of DMSO at 20 °C. Approximately 3 ml of the liquid was transferred to a quartz cuvette (6030-UV, Hellma UK LTD) with a path length of 1 cm. A reference spectrum was obtained using neat DMSO prior to evaluating the sample. The scanning range was from 190-500 nm with a scan interval of 0.5 nm.

The Beer-Lambert law was applied to obtain the extinction coefficient (ε) at a given wavelength (~280 nm) as shown in Equation 8:

$$\text{Absorbance (A)} = log_{10}(I_0/I) = \varepsilon \; x \; c \; x \; L \qquad \text{Equation 8}$$

Where I_0 is the intensity of incident light at given wavelength and I is that of the light transmitted, L is the path length of the quartz cuvette (10 mm) and c is the concentration of lignin used.

3.6.12 Proton Nuclear Magnetic Resonance Spectroscopy

Proton nuclear magnetic resonance (^{1}H NMR) spectroscopy of lignin was obtained using Bruker NEO 500 MHz spectrometer (Bruker, USA) equipped with a liquid nitrogen cooled cryoprobe. Approximately 10 mg of lignin was dissolved in 0.6 ml of d_6-DMSO. The sample was transferred

from the sample vial to NMR tube. Tetramethylsilane (TMS) was used as the internal standard. ^{1}H NMR spectra of lignin was acquired using 64 scans at 25 °C with relaxation delay of 4 seconds.

3.6.13 Quantitative Carbon Nuclear Magnetic Resonance Spectroscopy

The acetylation of lignin was completed prior to conducting carbon nuclear magnetic resonance (^{13}C NMR) analyses. The reaction scheme for the acetylation of lignin is shown in Figure 3.1 (299). The lignin was acetylated by using the following procedure. Firstly, the lignin was dried in a vacuum oven as described previously. Approximately 2 grams of lignin was transferred to a 250 ml three-neck round bottom flask. 40 ml each of pyridine and acetic anhydride (1:1, v/v) were added drop wise to the flask. The solution was agitated by bubbling nitrogen gas. In addition, the mixture was stirred continuously using a magnetic stirrer. The solution was refluxed at room temperature (22 °C) for 24 hours. 500 mL of ethanol was added at the end of the refluxing period. The ethanol was subsequently removed using a rotary evaporator under reduced pressure. This procedure was repeated at least five times to ensure that the by-product, acetic acid and any unreacted reagents were removed from the mixture. The acetylated lignin was purified by dissolving it in 40 ml of chloroform and precipitating with diethyl ether. The acetylated product was washed up to five times with diethyl ether (157). Finally, the acetylated lignin was dried in a vacuum oven at 80 °C for 6 hours and it was stored in airtight container and placed in a desiccator until required.

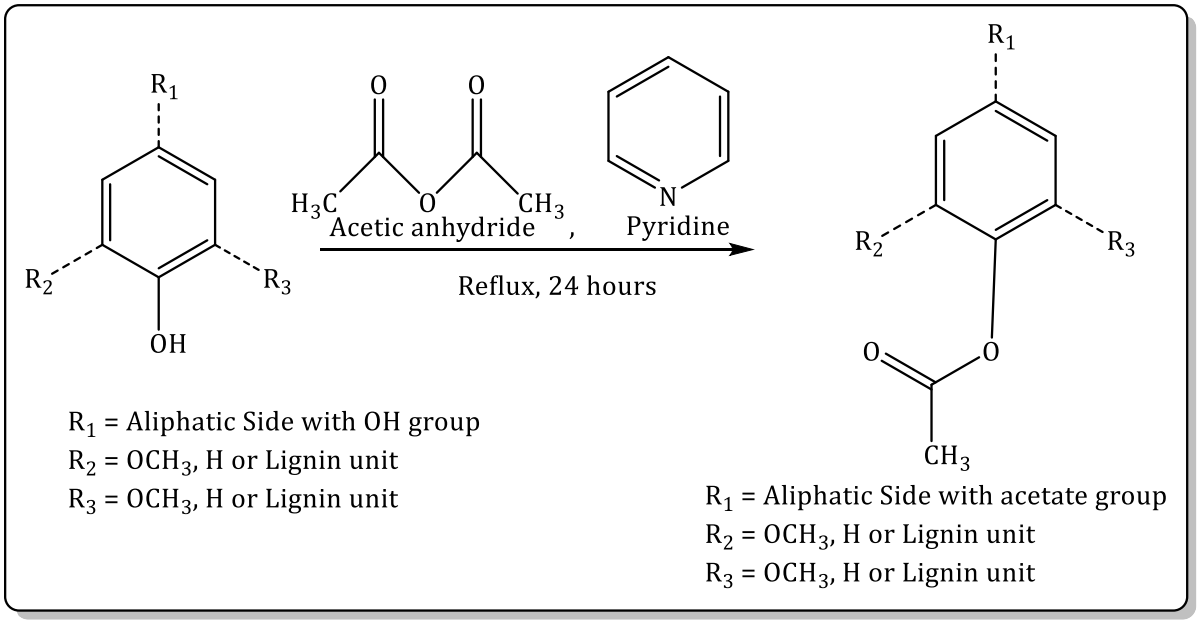

Figure 3.1 Reaction scheme for the acetylation of lignin (299).

The quantitative ^{13}C NMR spectra of lignin was obtained using pre-dried lignin (without acetylation) and acetylated lignin. Approximately 120 mg of the lignin was dissolved in 500 µL of DMSO-d_6, and 60 µL of the relaxation agent and 40 µL of the internal standard, 1,3,5 trioxane were added. The total concentration of lignin was 20% (w/v). The integration of the carbon moieties was based on the aromatic region (163-102), which was used as reference of 6.12 carbon atoms assuming that it contains 6 aromatic carbon atoms with 0.12 of vinylic carbon atoms (103). Therefore, the results are reported as aromatics per C_9 lignin.

Quantitative and qualitative ^{13}C NMR spectra were obtained using a Bruker NEO 500 MHz spectrometer with respect to ^{1}H and it was equipped with nitrogen cooled cryoprobe. A total of 28000 scans were acquired at 25 °C with a relaxation delay of 2 second (300, 301).

3.6.14 Quantitative Phosphorous Nuclear Magnetic Resonance Spectroscopy

Quantitative phosphorous nuclear magnetic resonance (^{31}P NMR) spectroscopy of as-received and lignin fractions was undertaken using established methods (165, 302-305). ^{31}P NMR spectra were obtained using a Bruker NEO console with an operating frequency of 500 MHz and equipped with nitrogen-cooled cryoprobe. A total of 256 scans were acquired at 25 °C with relaxation delay of 25 seconds. Approximately 40 mg of the pre-dried lignin was added to specimen vial followed by a 1 mL of mixture of anhydrous pyridine and deuterated chloroform (1.6:1, v/v respectively) at room temperature. 50 µL of a relaxation agent, chromium (III) acetylacetonate was added followed by the addition of 100 µL of the internal standard, N-hydroxy-5-norbornene-2,3-dicarboximide. 100 µL of the phosphorylating reagent, 2-chloro-4,4,5,5-tetramethyl-1,3,2-dioxaphospholane (TMDP) was added to the mixture and stirred manually and transferred to an NMR tube. The reaction scheme for the phosphorylation reaction is shown in Figure 3.2 (165).

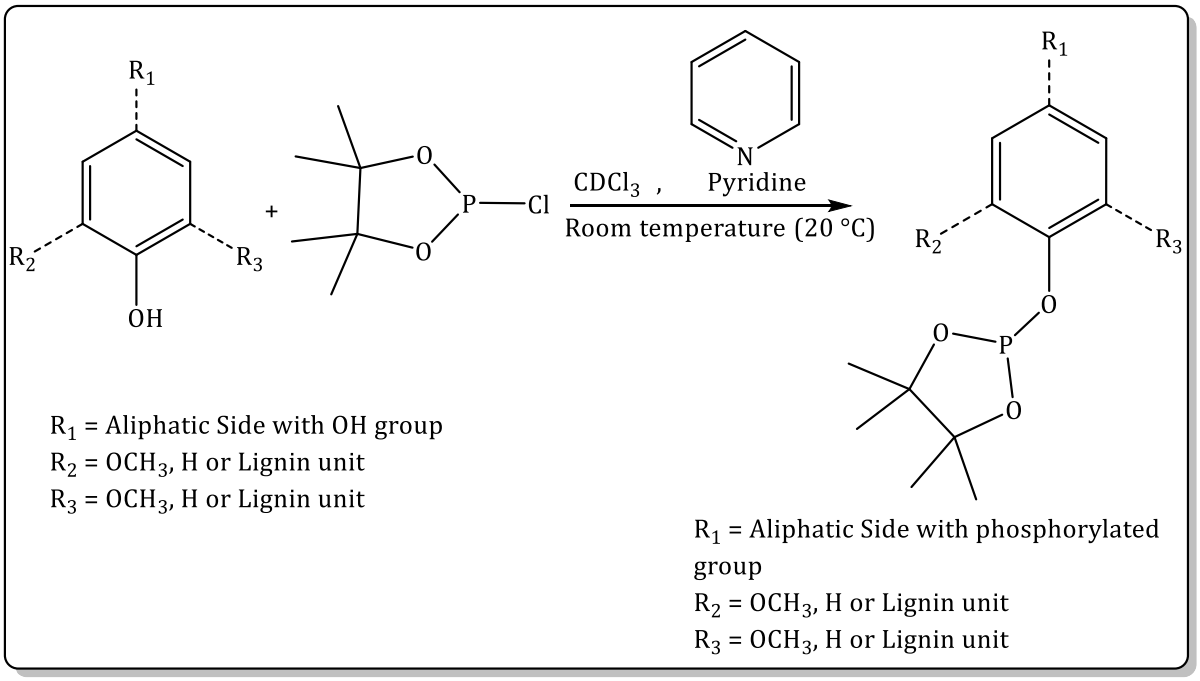

Figure 3.2 Reaction scheme for the phosphorylation of lignin (165).

3.7 Preparation of Lignin Solutions for Electro-spinning

Solutions of fractionated acetone soluble (ASL) and ethanol soluble (ESL) lignin were made using a 2:1 (v/v) ratio of acetone and DMSO. Four different concentrations of lignin were prepared: 48.2 wt%; 50.4 wt%; 52.8 wt%; and 55.4 wt% in order to identify the optimum concentration for electro-spinning. The acetone soluble lignin fraction (ASL) concentration was kept at 95 wt.% with ESL making up the remainder. The solution was homogenised using a magnetic stirrer for 6 hours and then stored in an airtight container until required.

3.7.1 Viscosity of Lignin Solutions

A HR-1 discovery hybrid rheometer (TA instruments, USA) was used to determine the viscosity of the lignin solutions using a 40 mm diameter parallel-plate geometry. The viscosity was determined by subjecting the polymer solution to a shear rate in the range of 0.1 to 100 s^{-1} at 25 °C. A solvent trap was used to minimise evaporation of the solvents.

3.7.2 Electrical Conductivity of Lignin Solutions

A Jenway 4510 (Cole-Parmer, UK) conductivity meter was used to measure the conductivity of the polymer solutions. The conductivity meter was calibrated at 25 °C using a standard solution of sodium chloride supplied by Hannah instruments (USA). Ten measurements of lignin solutions were obtained and averaged.

3.7.3 Electro-spinning of Lignin Solutions

The electro-spinning of lignin solutions was carried out using a custom-built electro-spinner consisting of disposable syringe and needle assembly (Teflon tube with Luer lock adapter, Cole Parmer, UK) a controllable feed liquid dispenser (AL1010, World Precision Instruments, UK) and a flat-tip needle of 25G (0.254 mm diameter, Adhesive Dispensing Ltd, UK). Figure 3.3 (a-b) shows a schematic illustration and a photograph of a custom-designed electro-spinning unit that was used to produce lignin fibres. The needle was connected to the positive terminal of a high-voltage power supply (Laboratory bench power supply, Genvolt, UK). The electro-spun fibres were

collected on an aluminium foil placed on top of a grounded copper plate (10 x 10 x 0.5 cm). The distance from the tip of the needle to the collector plate was kept at 12 cm and the applied voltage was 12 kV. The polymer solution was dispensed at 0.1 µl/minute. The temperature of the chamber was maintained between 25-30 °C with a relative humidity of 30-35%. The electro-spinning operation was carried for 3 minutes.

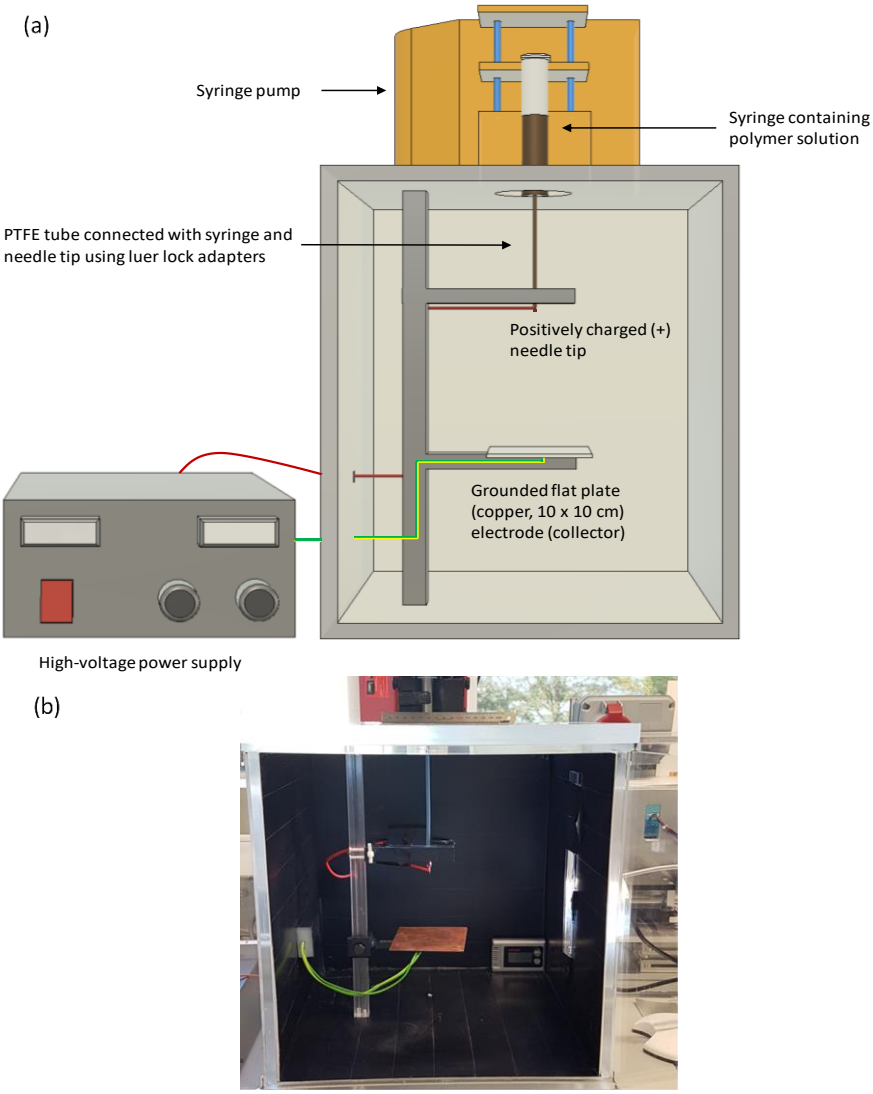

Figure 3.3 (a) Shows schematic illustration of electro-spinning setup with a flat plate ground-electrode for collecting randomly oriented lignin fibres; and (b) shows photograph of the electro-spinning unit.

Figure 3.4 shows the electrode assembly that was used for producing uniaxially aligned electro-spun fibres. This modified setup is based on the parallel-electrode method which was reported

previously by Li *et al.,* (251). The two conductive graphite electrodes with a knife-edged type profile, 3.5 cm distance in between them, were used to align the fibres. The previously mentioned electro-spinning parameters were used to obtain the aligned fibres.

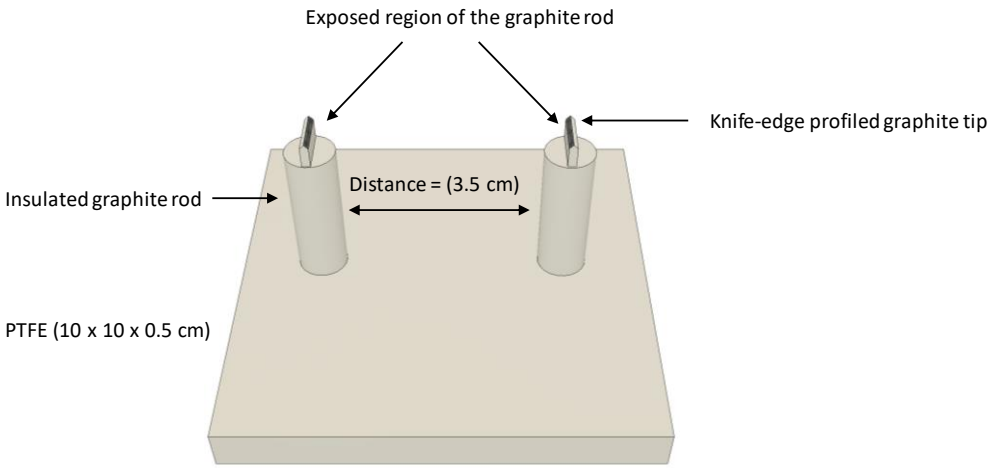

Figure 3.4 Schematic illustration of collector-plate used for electro-spinning of aligned fibres.

The electro-spun fibres including the random and aligned fibres were characterised using the TM3030 Plus SEM. The same procedures were used to study the fibre morphology as described previously in Section 3.6.4. The degree of orientation and fibre diameter distribution was determined using Image J software. Three separate SEM micrographs were used, and the diameter distribution was determined using sixty individual measurements from each image. The orientation distribution of the aligned fibres was also determined using Image J software.

3.8 Thermo-stabilisation of Electro-spun Lignin Fibres in Air or Nitrogen

After conducting a series of preliminary experiments, it was found that electro-spun fibre where the total polymer concentration of 52.8 wt.% of 95ASL-5ESL, produced smooth and circular fibres. Therefore, this concentration was selected for the heat treatment studies in air and nitrogen. Prior to thermo-stabilisation, a method for drying was developed to identify the optimum condition for the removal of excess solvent from the electro-spun fibres. The electro-spun lignin fibres were dried in vacuum oven at 100 °C, 120 °C, 140 °C, 160 °C, 180 °C and 200 °C for 6 hours. The optimum

temperature for vacuum drying the electro-spun fibres was found to be at 140 °C. This was determined by the effect of the vacuum drying temperature on the morphology of the lignin samples. Therefore, treating the lignin fibre at 140 °C in a vacuum oven was selected as the procedure for drying prior to thermo-stabilisation.

The thermo-stabilsation of the pre-dried (140 °C) electro-spun lignin fibre was investigated at 150 °C, 180 °C, 200 °C, 220 °C and 250 °C in air or nitrogen. Table 3.3 shows the five sets of experiments that were used for the thermo-stabilisation investigation. The pre-dried lignin fibres, on aluminium foil, were transferred into a tube furnace (Pyrotherm, UK) using a graphite crucible and heated from 25 °C to 100 °C and held for 1 hour. The fibres were then heated to 150 °C and held for 1 hour. The electro-spun fibres for experiment 1 were removed from the furnace at this stage. Experiment 2 follows the same heating regime but with the final temperature selected as 180 °C. The sequential heating of the remaining samples to 200 °C, 220 °C and 250 °C is summarised in Table 3.3. In all the experiments, the fibres were heated at heating rate of 0.5 K/minute with a gas (nitrogen or air) flow rate of 50 ml/minute.

Table 3.3 Summary of the heating regimes that were used to identify the optimum conditions for the thermo-stabilisation of electro-spun lignin fibres in air or nitrogen.

Experiment	Thermo-stabilisation temperature sequence (°C). The samples were pre-dried at 140 °C in a vacuum oven for 6 hours. The samples were then heated to 100 °C before subjecting them to the following thermal treatment in air or nitrogen.				
1	150 for 1 hour				
2	150 for 1 hour	180			
3	150 for 1 hour	180	200		
4	150 for 1 hour	180	200	220	
5	150 for 1 hour	180	200	220	250 for 1 hour

The thermo-stabilised fibres were characterised using a range of techniques to investigate the physico-chemical properties with a view to study the chemical changes in lignin involved in the control of the morphology of these fibres.

3.8.1 Characterisation of the Thermo-stabilised Electro-spun Lignin Fibres

The morphology of the thermo-stabilised fibres was inspected using scanning electron microscopy as described previously in Section 3.6.4.

Elemental analysis of the thermo-stabilised lignin fibres was carried out as detailed previously in Section 3.6.2.

Thermal analysis of thermo-stabilised electro-spun fibres carried out using DSC (Section 3.6.5) and TGA (Section 3.68).

Sample preparation for FTIR spectroscopy was conducted as outlined in Section 3.6.10.

Solid-state NMR cross-polarisation magic-angle spinning spectra (^{13}C CP/MAS NMR) of the vacuum dried (140 °C) and thermo-stabilised electro-spun lignin fibres at 250 °C in air and nitrogen was acquired using Bruker Avance III HD (Bruker, US) instrument. These experiments were conducted by Dr David Apperley at Durham University. Solid-state ^{13}C NMR spectra were obtained using 3600 scans with a relaxation delay of 1 second and a spin rate of 10 kHz. The chemical shift of neat TMS was used as a reference for solid-state ^{13}C NMR. The analysis of the NMR results was carried out by the author at the University of Birmingham.

3.9 Carbonisation of Thermo-stabilised Lignin Fibres

The electro-spun lignin fibres that were thermo-stabilised at 250 °C in air showed smooth and circular cross-sections. Therefore, the lignin fibres that were thermo-stabilised at 250 °C was used for the carbonisation studies. The carbonisation of the fibres was studied at 1000 °C, 1200 °C and 1500 °C. These samples were heated at 5 K/minute under a nitrogen flow of 50 ml/minute. The

fibres were held isothermally at each temperature for one hour before cooling to room temperature.

Figure 3.5 shows the tube furnace used for the heat treatment of lignin fibres.

Figure 3.5 The furnace assembly used for the heat treatment of lignin fibres.

3.9.1 Characterisation of Carbonised Lignin Fibres

3.9.1.1 Fibre Morphology

The surface and transverse fibre morphologies of the carbonised fibres were inspected using scanning electron microscopy as described in Section 3.6.4. A TM3030 PLUS (Hitachi, Japan) SEM was used to characterise the surface and cross-section morphology of lignin carbonised samples at 1000 °C, 1200 °C and 1500 °C with an acceleration voltage of 15 kV. The sample was mounted on SEM stub using an adhesive carbon tape. The samples were coated with gold/palladium for 3 minutes using a current of 25 mA and a vacuum of 1 mtorr.

3.9.1.2 Fibre Diameter Distribution

The fibres diameter distribution of the lignin fibres, before and after carbonisation, was acquired using ImageJ analysis software. Three micrographs with a magnification of 2500 were selected for each sample and the diameter distribution was determined using sixty individual measurements for each image.

3.9.1.3 Electrical Conductivity

The electrical properties of the carbonised electro-spun lignin fibres were measured using a 4-point probe of RM3000 (Jandel Engineering Limited, UK). Prior to the measuring the electrical resistivity, the equipment was calibrated using a Jandel resistivity standard (Serial no. 74452, Jandel Engineering Limited, UK). The carbonised lignin fibre with a width of 0.5 cm were mounted on a clean glass slide. The sheet or surface resistance of fibres that were carbonised at 1000 °C, 1200 °C and 1500 °C was measured. The sample thickness of electro-spun carbonised mat was averaged from five individual measurements. The spacing or distance between the probes was set at 0.1 cm and the sample measurements were carried out at 24-25 °C and with a relative humidity of 38-40%. Five measurements of the surface resistance (R) were made at different locations on the samples. The resistivity (ohm.cm) in four-point probe method can be measured according to the Equation 9 (198, 306):

$$\rho = \frac{R}{L} A \qquad \text{Equation 9}$$

where ρ is the resistivity and L is the distance between the probe (0.1 cm) and R is the electrical resistance; A is the cross-sectional area of the sample.

3.9.1.4 Raman Spectroscopy

An inVia confocal Raman Microscopy (Renishaw, UK) equipped with a 488 nm laser diode was used to observe the graphitic structure of the carbonised electro-spun fibres. The samples were mounted on the glass microslide. Raman spectra were acquired over a spectral range of 320-3200 cm^{-1} using 100 scans per sample at 10 % laser power. The band intensities including peak area intensity (A) and the peak height intensity (I) were determined from the peaks. The ratio of intensities of D to G are represented by I_D/I_G whilst A_D/A_G shows the area integrated of D to G peak (285, 307).

3.9.1.5 X-ray Diffraction

X-ray diffraction (XRD) of the carbonised lignin fibres was carried out on a Proto AXRD (Proto Manufacturing Inc., US) benchtop diffractometer (CuKα radiation with λ = 1.541 Å). The diffraction intensities were obtained with 2θ ranging from 10 to 110 ° using a step-scan mode with increment of 0.2° per step and the intensities were measured for 3 s in each step.

3.10 Electro-spinning of Lignin-Tannic Acid Solution

Solutions of fractionated acetone-soluble (ASL) and tannic acid (TA) lignin were made using a 2:1 (v/v) ratio of acetone and DMSO solvents. The acetone soluble lignin fraction (ASL) concentration was kept at 95 wt% with tannic acid making up the remainder. The total concentration of the polymer solution was kept at 52.8 wt%. The solution was homogenised using a magnetic stirrer for 6 hours and then stored in an airtight container until required.

The viscosity and conductivity of the ASL-TA solution was measured in accordance with the procedure listed in Sections 3.7.1 and 3.7.2 respectively.

The electro-spinning of 95% ASL-5% TA solution was carried out in a similar fashion as discussed in Section 3.7.3 where the distance from the needle to collector was kept at 12 cm and the applied voltage was 11.8 kV. The polymer solution was dispensed at 0.1 µl/minute. The temperature of the chamber was maintained between 25-30 °C with a relative humidity in the range of 30-35%. The electro-spinning operation was carried for 3 minutes.

3.10.1 Thermo-stabilisation and Carbonisation of Lignin-Tannic Acid Fibres

Prior to thermo-stabilisation, the electro-spun ASL-TA lignin fibres were dried in vacuum oven at 140 °C for 6 hours. The pre-dried lignin fibres (140 °C), on an aluminium foil, were transferred into a tube furnace (Pyrotherm) using a graphite crucible and heated from 25 °C to 100 °C and held for 1 hour. The fibres were then heated to 150 °C, held for 1 hour followed by heating to final temperature of 250 °C where they were held for another 1 hour. During the thermo-stabilisation steps, a heating rate of 0.5 K/minute was used under an air gas flow of 50 ml/minute.

The thermo-stabilised ASL-TA lignin fibres at 250 °C were carbonised at 1500 °C. These samples were heated at 5 K/minute under a nitrogen flow of 50 ml/minute. The fibres were held isothermally at each temperature for one hour before cooling to room temperature. The samples morphology was characterised using SEM.

3.11 Coir Fibre and Coir Pith

The coir used in this research was obtained from Hayleys PLC (Colombo, Sri Lanka). The coir was supplied in two forms; coir bundle consisting of fibres with average length from 15-20 cm and briquettes comprising of compressed coir dust. The fibres were mechanically extracted from the coconut husk whilst the dust was the residual powder which falls off upon the handling of coir fibres and coconut husk. This residual powder which also consist of some short length fibres is compressed into briquettes and is referred here as coir pith. Figure 3.6 (a-c) shows the coconut husk drying and extraction of coir fibre and coir pith. Figure 3.6 (d-e) shows the as-received coir fibre bundle and coir pith briquette.

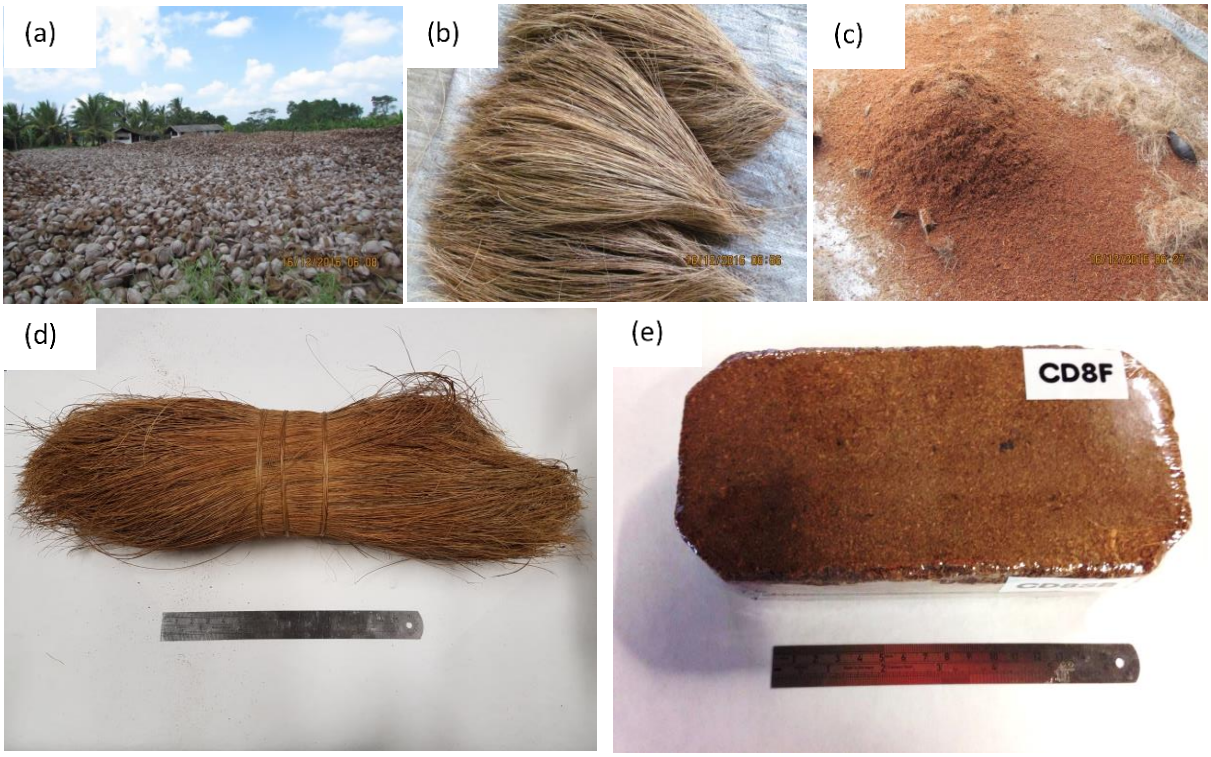

Figure 3.6 (a-e) Images of coir with (a-c) showing soaking of coconut husk in water and extracted coir fibres and coir pith; (d-e) shows the as-received coir fibre bundle and coir briquette.

3.11.1 Cryo-milling of Coir Fibre and Pith

Cryo-milling process was used to grind coir fibre and coir pith to reduce the particle size and to increase the surface area. Figure 3.7 shows the illustration of cryo-milling procedure for coir fibre and coir pith. Coir fibre was cut into short-fibres (20-30 mm) using a guillotine and in a separate procedure lumps of coir pith was removed from coir pith briquette. Coir fibre and coir pith were independently subjected to freeze milling using Freezer/Mill 6750 (Spex SamplePrep, USA). The coir was placed into a hollow Perspex tube along with a steel impactor and tube was closed at both ends with steel end-plugs. Liquid nitrogen was used as cryogenic agent to freeze the sample. The following parameters were used for the cryo-milling process: pre-cooling time of 5 minutes followed by one minute of single cycle with milling frequency of 10 Hz.

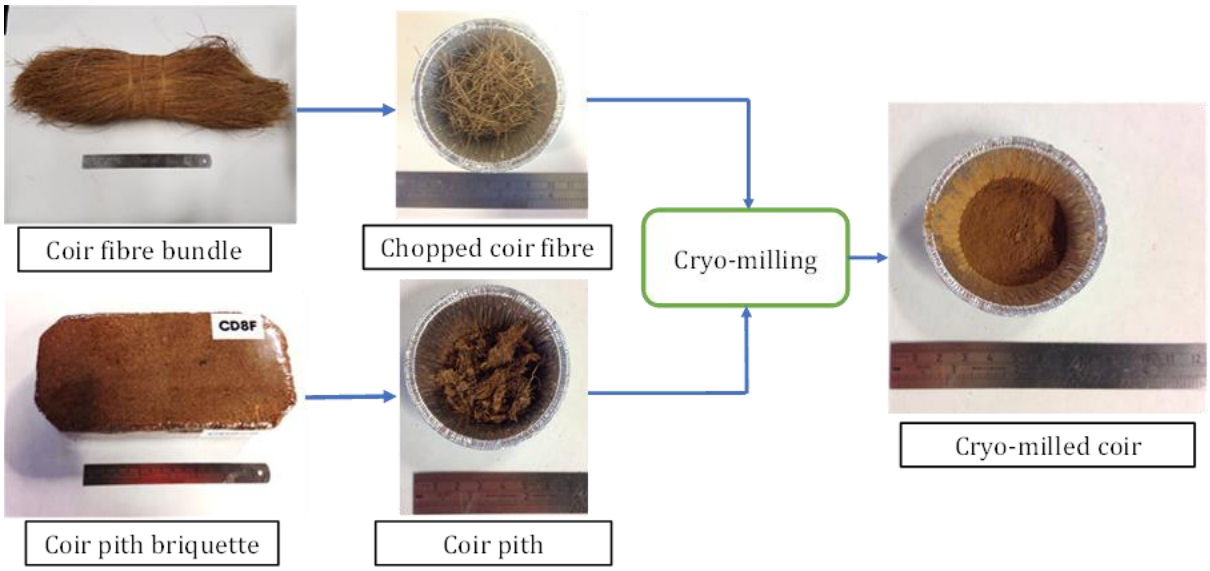

Figure 3.7 Illustration of the steps that were taken for reducing the particles size for coir fibre and coir pith using cryo-milling.

3.11.2 Quantification of the Lignin Content in Coir Fibres and Pith

The composition of the coir fibre and coir pith including the lignin content was determined in accordance with TAPPI standards as described in Section 3.3. In addition, the following TAPPI standard were used to characterise the coir fibres and pith.

- T257 sp-14 Sampling and Preparing Wood for Chemical Analysis (291).
- T264 cm-07 Preparation of wood for chemical analysis (292).
- T204 cm-97 Solvent extractives of wood and pulp (308).
- T211 om-02 Ash in wood, pulp, paper and paperboard combustion at 525 °C (293).
- T222 om-02 Acid Insoluble lignin (Klason lignin) in wood and pulp (295).
- TAPPI Method UM 250 Acid soluble lignin (294).

The moisture, ash, acid insoluble and acid soluble lignin contents in the biomass were carried out using the procedure outlined in Section 3.3.1, 3.3.2, 3.3.3 and 3.3.4 respectively. Prior to the quantification of the composition of the biomass, the sample was sieved as described in Section 3.3.1 (291). Subsequent to this, the samples were subjected to Soxhlet extraction with acetone for 6-8 hours and the residue was washed with boiled deionised water to remove acetone in accordance with TAPPI T264 (292). The acetone-soluble filtrate, also referred as the extractives content, comprises of mainly fatty and resin acids, sterols, waxes and fats. The extractive content was determined from acetone soluble filtrate in accordance with TAPPI T204 (308). The residue was boiled with de-ionised water for 1 hour, filtered to remove the soluble part and the residue was washed again with boiled with de-ionised water. The water-soluble filtrate mainly comprises of tannins, gums, sugars, starches and colouring matter. The residue was defined as extractive-free biomass and the moisture content was determined at 105 °C to achieve constant weight according to the procedure TAPPI T264.

3.11.3 Extraction of Lignin from Coir Fibre

The initial set of experiments showed that the lignin quantified from coir fibres was found to have a higher content (31.6%) than that from coir pith (23.5%). Hence coir fibres were used to extract the lignin. Approximately 60 g of cryo-milled coir fibre was refluxed with 900 mL acetone for 6 hours at 20 °C. The mixture was filtered, and the residue was washed with boiled (100 °C) de-ionised water using a silicon oil bath. The residue was then treated with 1 litre of boiled de-ionised water for 1 hour and after filtration, washed with 1 litre of hot de-ionised water. The purpose of

these treatments was to generate an extractive-free biomass prior to the extraction of lignin. The residue was refluxed with 1.5 M of NaOH (Sigma-Aldrich, UK) for 6 hours at 80 °C. The mixture was agitated by bubbling nitrogen throughout the experiment. The black liquor solution formed during this process was separated from the insoluble residue by filtration under reduced pressure. The filtrate which was composed of lignin and hemicellulose was washed with ethanol five times to separate the hemicellulose from lignin. Upon treating the hemicellulose with ethanol, it precipitated from the black liquor and the mixture was filtered. The filtrate was concentrated using rotary evaporator under reduced pressure. The lignin was precipitated with 20 % H_2SO_4 at pH 2 and dried in vacuum oven at 40 °C for 6 hours. The lignin extracted from the coir fibre was named as "alkali lignin".

3.11.4 Characterisation of Lignin from Coir Fibre

The characterisation of the lignin that extracted from the coir fibres was characterised using the procedures outlined previous in Sections SEM (3.6.4), particle size distribution (3.6.1), elemental analysis and GPC (3.6.2 and 3.6.7), DSC (3.6.5), TGA (3.6.8) , UV/Visible and FTIR spectroscopy (3.6.11 and 3.6.10) , ^{1}H NMR (3.6.12), ^{13}C NMR (3.6.13) and ^{31}P NMR (3.6.14).

3.11.5 Electro-spinning of Lignin Extracted from Coir Fibres

The coir lignin was blended with cellulose acetate (M_n = 30000, Sigma-Aldrich, UK) using a binary solvent consisting of acetone/DMSO (2/1, v/v). The total polymer concentration was 30 wt% with the lignin concentration being maintained at 12 wt%. The solution was homogenised using a magnetic stirrer for 6 hours and it was stored in an airtight container until required. The electro-spinning of coir-lignin was carried using the same equipment and electrospinning unit as previously mentioned in Section 3.7.3. However, the solution was dispensed at 0.2 µl/minutes. The SEM of electro-spun fibres was carried out as described in Section 3.6.4.

Results and Discussion

Chapter 4 Solvent Fractionation and Characterisation of Softwood Kraft lignin

4.1 Softwood Kraft Lignin

The as-received (BioChoice®) lignin was characterised to determine the moisture, ash, lignin and carbohydrates content in accordance with the relevant TAPPI methods as described in Section 3.3 and the results are summarised in Table 4.1. The carbohydrates content was calculated by subtracting the sum of the Klason lignin, ash and acid soluble lignin from 100%. The as-received lignin contained 28% moisture. The total lignin and ash contents were approximately 94% and 1.26%, respectively for pre-dried lignin.

Table 4.1 The composition of the softwood Kraft lignin used in this study (BioChoice® lignin) and characterised in accordance with TAPPI211 and TAPPI222 (for pre-dried lignin).

	Moisture Content (%)	**Ash Content (%)**	**Acid insoluble 'Klason' lignin (%)**	**Acid soluble lignin (%)**	**Carbohydrates (%)**
ARL	28.35	1.26	91.20	3.12	4.42

Softwood Kraft lignin is known to contain a small percentage of carbohydrates which are mainly of sugars (1.98%) such as arabinan(0.26%), glucan (0.12%), galactan (0.76%), and xylan (0.84%) (89, 151, 178). The composition of these sugars has been determined using high-performance liquid chromatography (151, 309). With reference to Table 4.1, the Klason lignin, free of impurities, cannot be dissolved in common organic solvents (acetone, ethanol, DMSO and DMF) and it is primarily only used for quantification purposes (310). This solubility issue has been attributed to the degradation of lignin caused by the use of concentrated inorganic acids used for the hydrolysis of carbohydrates. In order to minimise the degradation of lignin caused by the strength of the acid, and to remove the impurities, a series of experiments were designed to

determine the relative pH values that could be used to "wash" lignin. The term washing is taken to represent the number of times the lignin is treated with an acid at a particular pH.

The Taguchi method described in Section 3.4 was designed to determine the parameters such as pH, lignin-to-acid ratio (g/ml), duration of the washing cycle and the number of cycles. The overall aim of these Taguchi experiments was to minimise the ash content. An indication of the optimum parameters to achieve the lowest ash content was determined by plotting the means and the signal-to-noise ratio as shown in Figure 4.1(a and b). The mean effect plot shows the effect of the parameters that were selected on the response and it identifies the dependant variables. Figure 4.1(a) illustrates that the pH (factor A) has a significant effect on lowering the ash content. The number of cycles used for acid washing has a negligible effect on reducing the ash content. In Figure 4.1(b), a higher signal-to-noise (S/N) ratio implies the parameters that will contribute to obtain a low ash content. This indicates the significant parameters that can reduce the variability with regard to acid washing experiment with a view to minimising the effect of uncontrollable factors. In these analyses, the 'smaller is better' criterion is used. With reference to Figure 4.1(b), pH 2 and pH 4 are seen to be the most significant contributors towards lowering the ash content. The horizontal dotted line in Figure 4.1(b) represents the mean target for minimising the ash content. This is seen by a higher difference in the variability between the data sets for a pH factor to the mean target. Whereas, the other parameters such as the volume of acidified water-to-lignin ratio (B), duration of mixing (C) and the number of cycles (D) have marginal or no significant effect in minimising the ash content.

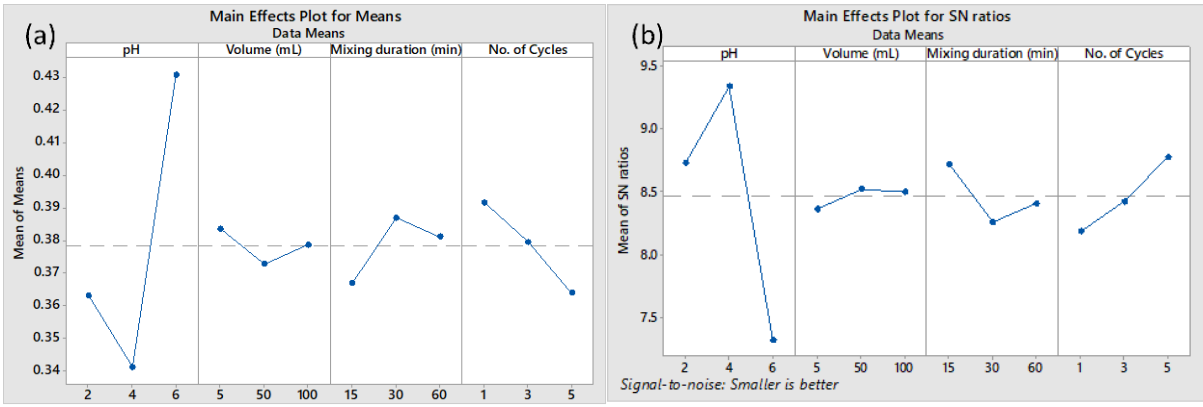

Figure 4.1 (a-b)The Taguchi analysis of parameters involved with the plots for (a) means and (b) S/N ratios for the performance measure.

4.2 ANOVA Analysis

The analysis of variance with the contribution each factor is tabulated in Table 4.2. The ANOVA analysis uses a hypothesis test where the means are equal with a confidence level of 95% for each interval. The F-value is a statistical term that represents the ratio of two variances. This value is determined by the ratio of the means square to the variation within the samples (error mean square) for each factor. The larger value represents a greater dispersion to the mean. On inspecting Table 4.2, it is seen that factor-A (pH), due to its higher value, is responsible for the variation from the mean. The p-value is used to justify the hypothesis test based on the significance level. If the p-value for a specific factor is less than or equal to the significance level, which is denoted by $\alpha = 0.05$, then the null hypothesis is rejected. The p-value for factor-A is less than 0.05, and this suggests it will have a significant contribution in reducing the ash content. The percentage contribution for each factor is determined by the sum of square (SS) divided by the total sum of squares. The percentage contribution confirms that the pH has an important role in reducing the ash content.

Table 4.2 ANOVA analysis of the ash content for as-received softwood Kraft lignin.

Factors	DoF	Adjusted Sum of squares (SS)	Adjusted Mean square (MS)	F-value	P-value	Significance	Percentage contribution
A	2	0.030587	0.015294	8.46	0.009	High	58.22
B	2	0.000360	0.000180	0.10	0.906	No	0.69
C	2	0.002332	0.001166	0.64	0.547	No	4.44
D	2	0.002986	0.001493	0.83	0.468	No	5.68
Error	9	0.016271	0.001808				30.97
Total	17	0.052537					100

The residuals plots shown in Figure 4.2 (a-d) illustrate the data distribution and its fitted linear regression based on ANOVA. A residual is defined as the difference between an observed value and its corresponding fitted value. The residuals can aid in determining the applicability of a model to justify and explain the variations in the observed data. Figure 4.2 (a) shows that the residuals have a normal distribution, and that regression is closely fitted with the majority of the observed data. In Figure 4.2 (b), the histogram shows that the residuals are evenly distributed through the range and are not skewed. The residual against fitted value and observation order plots in Figure 4.2 (c and d) shows a pattern of distribution with a constant variance with some outliers in the data set. The Figure 4.2 (d) also suggests that residuals are uncorrelated with each other.

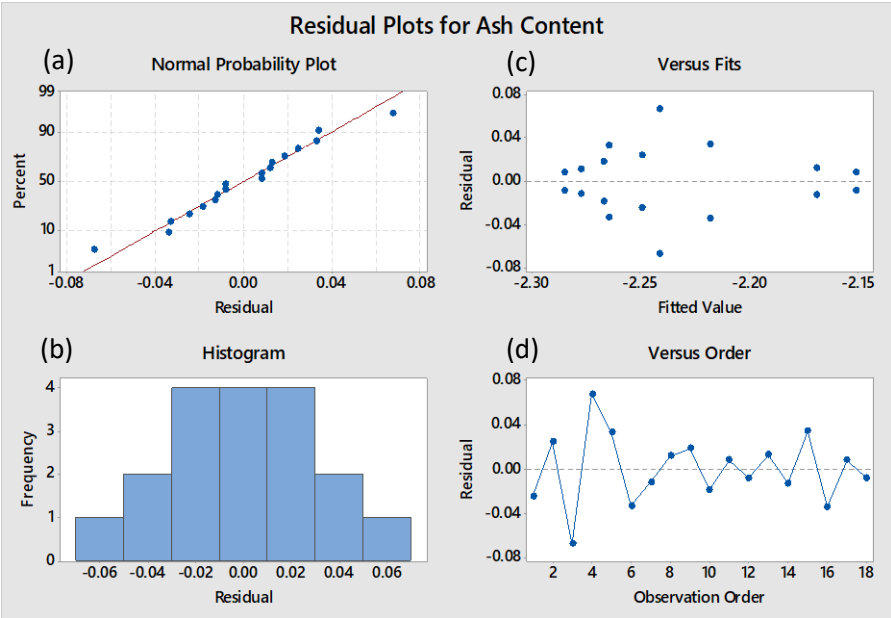

Figure 4.2 (a-d) Residual plots for the ash content.

The ANOVA analysis using a Tukey confidence interval plot depicts the significant levels of a factor as shown in Figure 4.3. The levels which do not share a zero value implies that the corresponding means are significantly different. This indicates that pH 2 and 4 are similar and are the most significant levels for reducing the ash content. Whereas the pH 2 and 6, and pH 4 and 6 are significantly different. Hence, pH 6 has the lowest contribution in minimising the ash content.

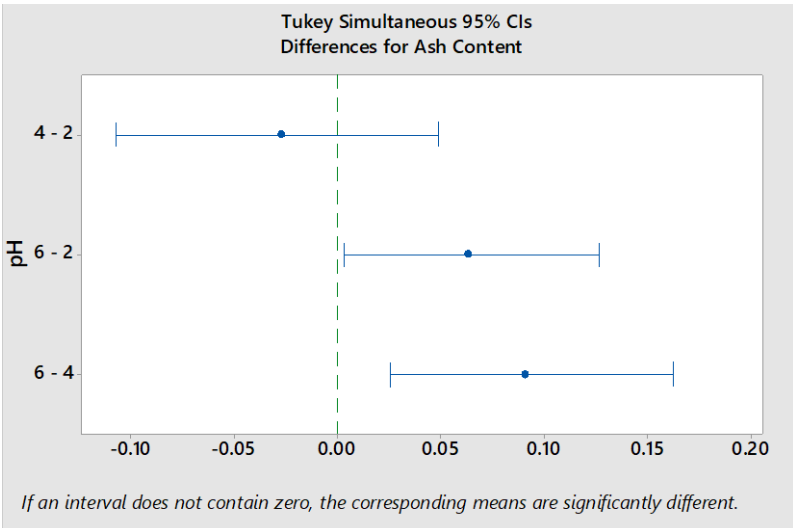

Figure 4.3 Tukey confidence interval plot of pH factors.

4.3 The Composition of the Ash in Softwood Kraft Lignin

Figure 4.4 shows the elemental composition of the ash from as-received BioChoice® lignin obtained using SEM-EDS. The oxygen content is seen to be the highest and this is because lignin is pyrolysed in air (as detailed in Section 3.6.4). This is in agreement that reported in literature (311, 312). The other elements that were detected in relatively higher concentrations were sodium and sulphur with trace amounts of K, Si, Al, Mg, Fe, Ca, Mn, and P. The reasons for the presence of inorganic elements in lignin was discussed in publications (311, 312) where it was reported that the ash may be attributed to the presence of inorganic matter or procedures used during Kraft pulping for the extraction of lignin.

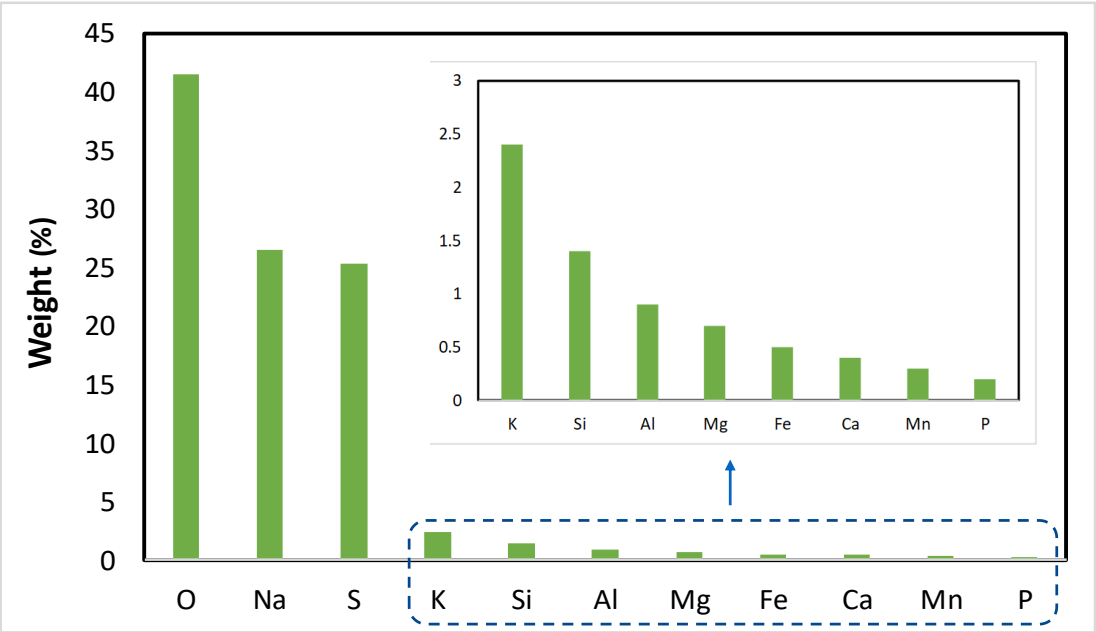

Figure 4.4 The elemental composition of the ash in oxidised as-received lignin.

The physico-chemical properties of the as-received BioChoice® (softwood Kraft) lignin are summarised in Table 4.3. The experimental procedure for determining the particle size distribution, elemental composition and density were outlined in Section 3.6.1, 3.6.2 and 3.6.3 respectively. The particle size distribution of the lignin was measured to be in the range 0.03-158 µm. The standard percentile, d=0.9, indicated that 90% of the lignin is below 52.5 µm. The

elemental composition of the lignin was 65% of carbon which is typical for lignin (151, 313, 314). The density for the lignin used in this study was 1.38 g/cm^3 (313, 315). Relevant physico-chemical data for softwood Kraft lignin are also included in Table 4.3. It is seen that data obtained in the current study agreed with those reported in the literature (315, 316).

Table 4.3 Physico-chemical properties of as-received (BioChoice®) lignin.

	Particle size distribution (µm)				**Elemental composition**				**Density**
	d (0.1)	**d (0.5)**	**d (0.9)**	**Size range**	**C (%)**	**H (%)**	**S (%)**	**O (%)**	**kg/m^3**
ARL	1.38	8.75	52.47	0.03-158.49	64.60	5.73	1.40	28.30	1380

4.4 Analysis of Moisture Content in Lignin using DSC

With reference to the structure of lignin illustrated previously in Figure 2.3 (Section 2.2), it is moisture sensitive due to the presence of polar functional groups and its amorphous nature (317). A number of previous studies reported in the literature have commented on the effects of moisture on the thermal properties of lignin. Most of these studies have tended to cite the T_gs for the second scan of the DSC thermogram, ignoring the characteristics of the first scan (101, 318, 319). The following drying condition were investigated in this current study: (i) freeze drying in liquid nitrogen; and (ii) vacuum drying at 80 °C for 6 hours. As presented previously in Table 4.1, the moisture content in the as-received lignin was found to be approximately 28.3%. The DSC traces for lignin are presented in Figure 4.5 (a-b) where (a) shows the first cooling scan of as-received lignin (ARL), vacuum dried (Vac 80 °C) and freeze-dried lignin. In the ARL cooling scan, three exothermic peaks are observed at -14.2 °C, -22.1 °C and -39.2 °C. An expanded view of the peaks at -22.1 °C and -39.2 °C are shown in the insert. These peaks could be related to water and/or the solvents and chemicals used during isolation of the commercially supplied (as-received) lignin. Previously, three of forms of water have been reported in the ligno-cellulosic

materials: freezing bound water, non-bound free-water and free-water (317, 320-322). The phase change between -10 to -20 °C and -40 was attributed to the free-water and freezing bound water respectively (322). Hatakeyama *et al.,* (321) and Nakamura *et al*., (317) also reported the effects of absorbed water in dioxane lignin and ligno-cellulosic materials relative to that of pure water. They observed that the crystallisation cooling peak at approximately -40 °C in the first scan was due to the freezing of bound water. The bound water was is strongly attracted to hydroxyl groups of lignin via hydrogen bonding. However, it has been suggested that the phase change between -10 to -20 °C may also be attributed to the freezing of bound water (322). Whereas for non-freezing bound water which does not form ice upon cooling and hence no peak is detected in the DSC traces (317, 321). The polar groups such as hydroxyl groups and carboxyl groups are responsible for the attraction of water molecules. It is apparent in Figure 4.5 (a) that vacuum and freeze-dried lignin does not show any freezing peak for water. Thus, it can be assumed that these drying procedures remove the moisture or other volatiles chemical species.

The first heating scan for ARL is shown in Figure 4.5 (b) and it exhibits two peaks centred at approximately 2.8 °C and 116.8 °C respectively. The peak at 2.80 °C is the melting endothermic peak associated with the melting of free-water. This observation was also made by Hatakeyama *et al*., and Nakamura *et al.,* where endothermic peak corresponding to free-water is observed close to 0 °C (317, 321).

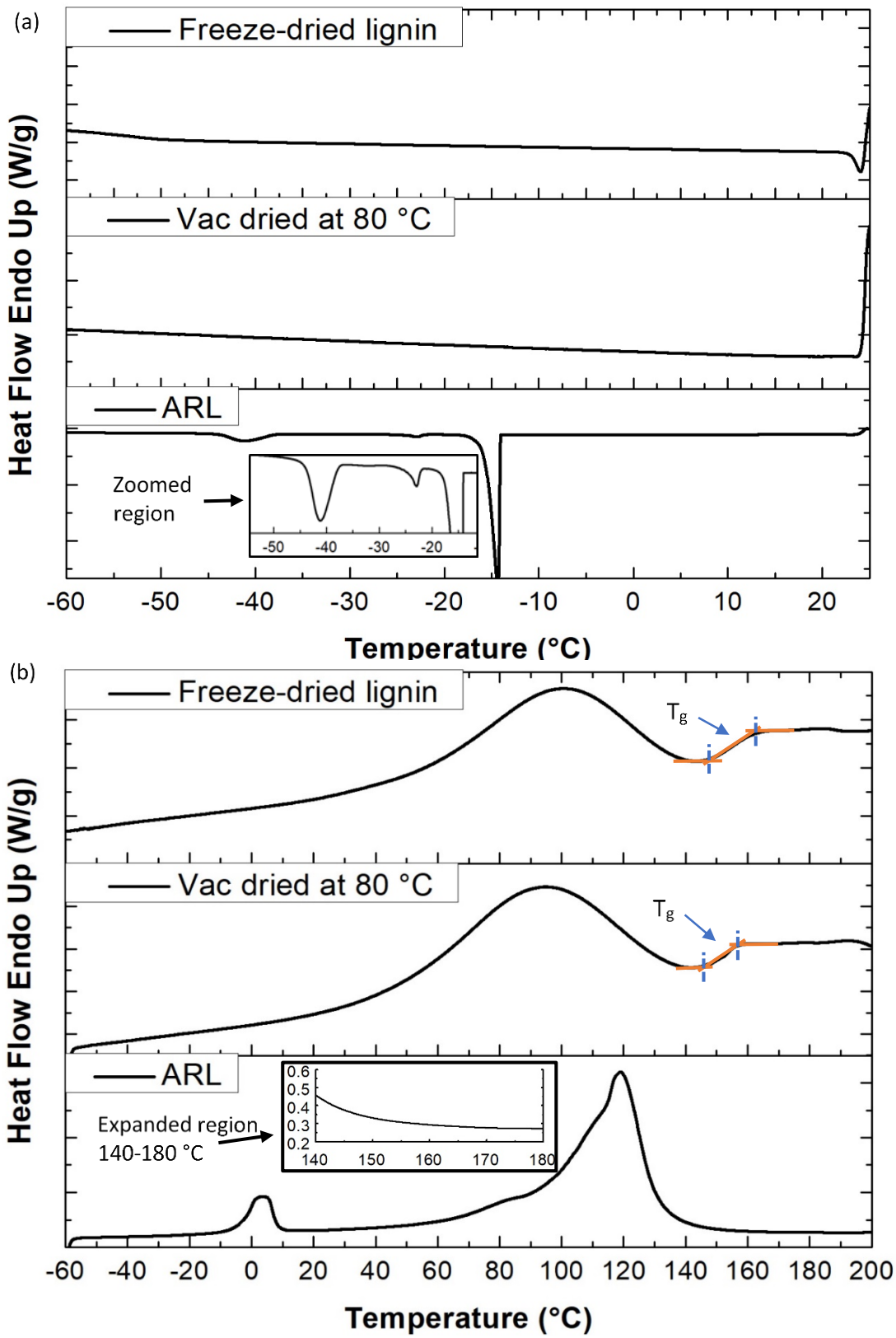

Figure 4.5 The first cooling and heating DSC thermograms for as-received lignin (ARL), vacuum dried (Vac 80 °C) and freeze-dried lignin: (a) cooling; and (b) heating.

The lignin being an amorphous polymer exhibits a distinct glass transition temperature (T_g). The first heating scan with a broad endothermic peak of lignin and T_g is widely ignored in literature (323). The reason for bypassing the first heating scan in literature is that it erases the influential thermal history of the polymer in its glassy state (318, 324). It is also observed that the presence of moisture in polymers can plasticise the material resulting in a reduced T_g. Thus, T_g is widely reported and accepted for the second heating scan (323, 325, 326). This method however presents a challenge and obstacle in determination of the initial state of the material, as lignin goes through morphological changes during the first heating cycle (325). The broad endothermic peak could be due to the evaporation of absorbed water or due to the presence of low molecular weight volatiles in lignin including a possibility of cleavable sulphur (thiol groups) containing species (318, 323, 325). In some cases, such as that for ARL as shown in Figure 4.5 (b), the broad endothermic volatilisation hinders the clear visibility of the sigmoidal variation of heat capacity making it difficult to determine the glass transition temperature in the first heating scan. The first heating scan for freeze dried and vacuum dried lignin shows an endothermic peak and a clear T_g. The reasons for the presence of endothermic peak centred at approximately 100 °C even after drying could be due the evaporation of low-molecular weight volatiles and/or may be attributed to the absorption of moisture during the storage of the sample or whilst preparing it for characterisation.

The second cooling and heating scans are shown in Figure 4.6 (a-b). The crystallisation exothermic peaks are not observed in ARL 2nd cooling scan suggesting that the water and/or other volatiles have been removed. In Figure 4.6 (b), the calculation of the T_g is illustrated for ARL where intersection of two tangent lines are considered for the midpoint-based determination of the T_g. Figure 4.6 (b) shows the second heating scan for ARL where a distinct T_g at approximately 151 °C is seen. This confirms that the sample was relatively free of volatiles and completely dry after the first heating cycle where it was heated to 200 °C, hence no endothermic peaks are observed.

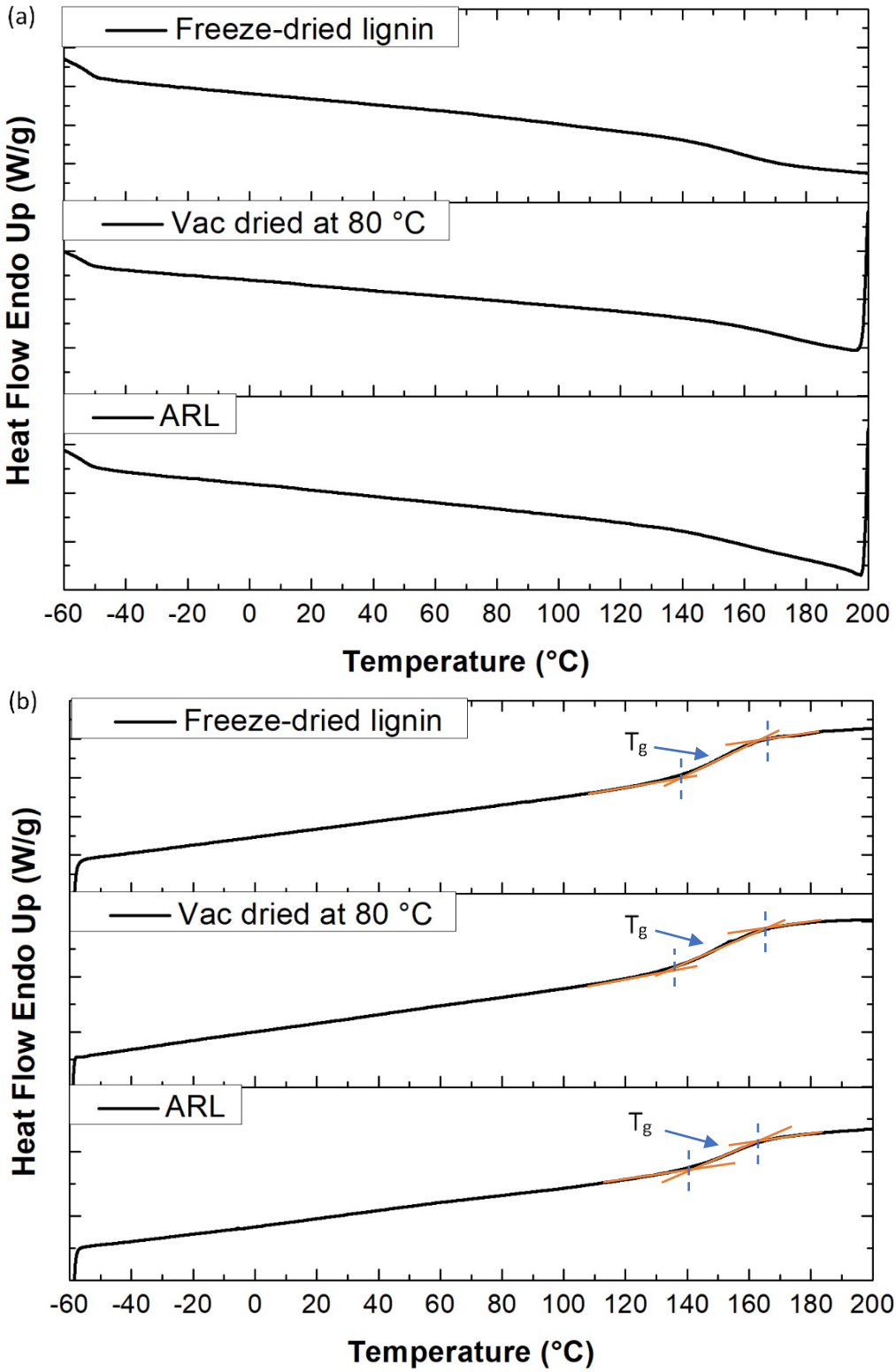

Figure 4.6 Second cooling and heating DSC thermograms for as-received lignin (ARL), vacuum dried (Vac 80 °C) and freeze-dried lignin: (a) cooling; and (b) heating.

A summary of the DSC-1 data are presented in Table 4.4. The effectiveness of the drying procedures on reducing the magnitude of the endothermic peak during the first heating scan, as infered by the integration of the area under the peak gave a value of 487.8 J g^{-1} for the heat of vapourisation. The water content is found to be approximately 22 wt%. This was estimated by dividing the intergrated area with the heat of vaporisation of water (2256.8 J g^{-1}).

Table 4.4 The enthalpy of vaporisation including the peak area (J/g) and the T_g of as-received lignin.

Samples	**Cooling Scan 1**		**Heating scan 1**			**Heating scan 2**
	Peak (°C)	**Peak Area (J/g)**	**Peak (°C)**	**Peak area (J/g)**	**Glass transition temperature, T_g (°C)**	**Glass transition temperature, T_g (°C)**
ARL	-14.2 -22.1 -39.2	-40.3 -1.13 -7.12	2.8 116.8	36.4 487.8	120.1	153.4
Vacuum-dried at 80 °C for 6 hours	-	-	92.2	79.2	150.1	150.8
Freeze-dried lignin	-	-	100.8	85.4	152.8	150.5

4.5 Moisture Sorption Characteristics of As-received (BioChoice®) Lignin

As-received lignin was dried at 80 °C for 6 hours in the DVS sample chamber as described in Section 3.6.6. Figure 4.7 (a) shows the mass-loss during the drying cycle. A mass-loss of approximately 21% was observed due to the moisture which correlates well with the mass-loss observed by DSC. The moisture sorption and desorption isotherm curves relative to the change in relative humidity (RH), at a constant temperature, are shown in Figure 4.7 (b). The sorption curve initially shows a linear relationship in the moisture uptake from 20-50% RH. The actual mechanism of water sorption is still not understood clearly. During the ingress of water vapor, the water molecules are known to be attracted to sorption sites. As mentioned previously, the hygroscopic nature of lignin is attributed to the presence of polar groups. The hygroscopicity is related to the high affinity of binding sites, such as hydroxyl, carbonyl, carboxyl and sulfonic acid groups, in forming hydrogen bonds with water molecules (320, 322, 327, 328). In particular, hydroxyl groups (-OH) are claimed to be a significant contributor towards hygroscopic behaviour (317, 320, 324, 329).

The sudden upward trend could coincide with onset of clustering of water molecules (327, 330). The moisture regain in lignin was found to be 11% at 95% humidity. With reference to Figure 4.7 (b), the water is diffused out at a slower rate in desorption isotherm resulting in a hysteresis. The hysteresis is defined as the difference between desorption and sorption of equilibrium moisture contents at the same humidity. The hysteresis is at a maximum level between 50-70 % RH. Above 70% RH, the sorption isotherm follows an upward trend. The desorption curves show the retention of moisture even at zero relative humidity and at 25 °C.

Moisture can be absorbed by lignin during storage or processing. Water is also known to remain in the polymer matrix even after drying at 100 °C (324). Therefore, lignin needs to be stored appropriately to exclude moisture. Moreover, it can also absorb moisture from the atmosphere.

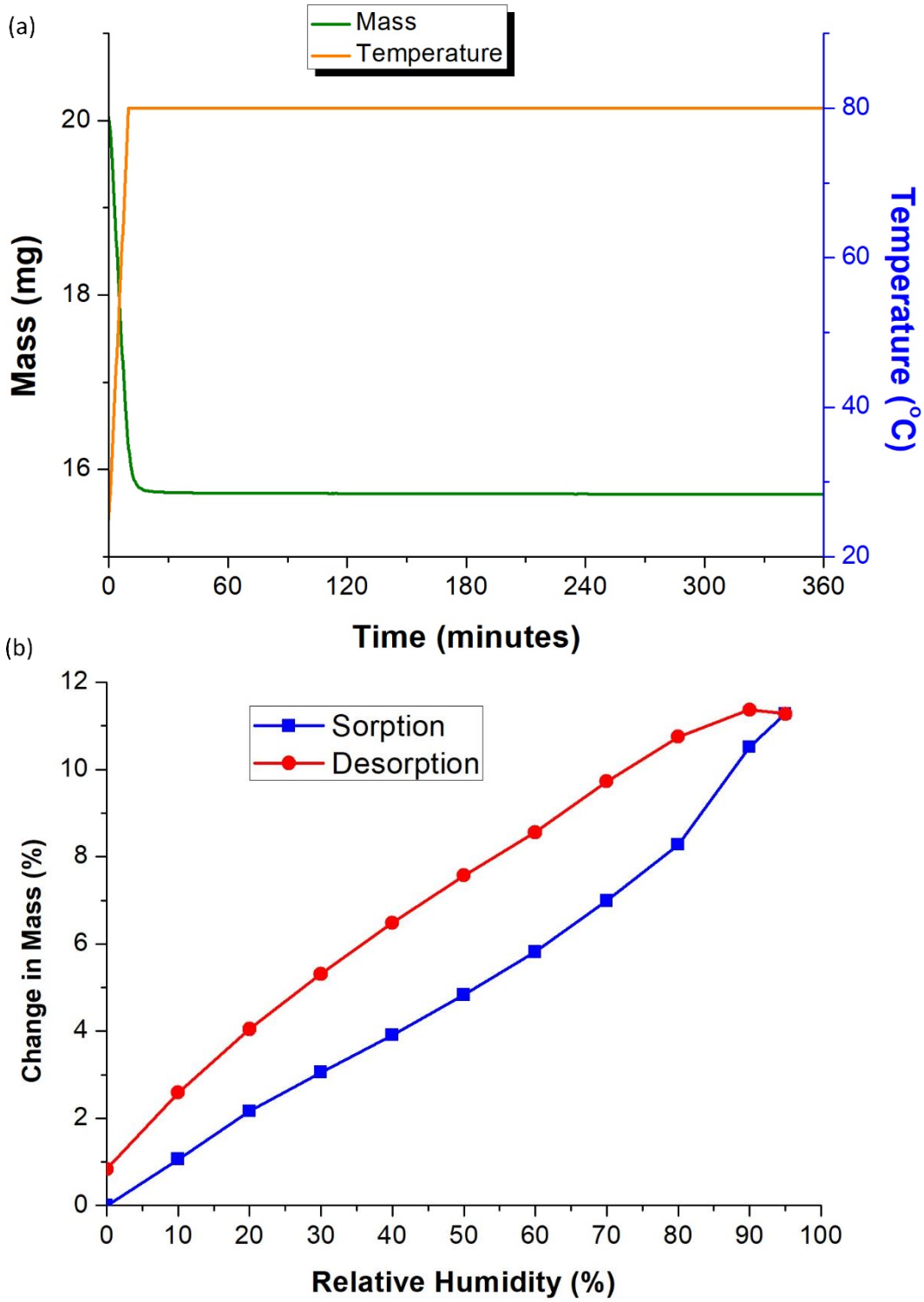

Figure 4.7 Moisture uptake experiment for as-received lignin: (a) drying cycle at 80 °C for 6 hours; and (b) followed by moisture sorption-desorption isotherm with respect to change in relative humidity at 25 °C.

4.6 Solvent Fractionation of Lignin

The effect of treating lignin with a range of solvents on the solubility, yield and ash content is present in Table 4.5. Lignin dissolved completely in DMSO and DMF. It was found to be partially soluble in acetone, ethanol and 1-propanol. The highest yield attained, when fractionating lignin with these three solvents was with acetone. Approximately 56% was recovered as the soluble fraction whilst 1-propanol had the lowest yield. This shows that the affinity between the polymer and solvent not only depends on the solubility parameter but also on the chemical nature of the solvent used. The chemical structure of acetone consists of ketone as a functional group whereas the hydroxyl groups are found in ethanol and n-propanol. The only difference between n-propanol and ethanol is that the n-propanol has an extended carbon chain and hence a lower polarity compared to ethanol. As the structure of lignin consists of polar and non-polar functional groups, the fractionated lignin yields suggest that it has better solubility in polar solvents as compared to non-polar solvents.

As seen in Table 4.5, the ash content for the soluble fraction were in the range 0.1-0.12% whereas that for the as-received lignin and acid-washed lignin were 1.24% and 0.34% respectively. This shows that solvent fractionation can reduce the inorganic impurities as inferred by the ash content in the soluble fractions. The ash content for the insoluble fraction was found to be higher than that of as-received lignin. Hence, it can be concluded that the ash content can be effectively reduced from lignin via solvent fractionation without the need for acid-washing.

Table 4.5 Solubility and solvent fractionation yields with their respective ash contents for each fraction.

Solvents	Fractionation Yields (%)	Ash Content (%)	
		Soluble Fraction	Insoluble Fraction
Dimethylsulfoxide (DMSO)	Completely soluble	-	-
Dimethylformamide (DMF)	Completely soluble	-	-
Fractionation Solvents			
Acetone	56	0.10	2.17
Ethanol	38	0.11	1.99
1-propanol	29	0.12	3.03

4.7 Characterisation of Lignin using Gel Permeation Chromatography

The effect of solvent fraction on the molecular weight distribution of the fractionated samples including the as-received material using size exclusion chromatography (SEC) is shown in Figure 4.8. The samples were dissolved in DMF containing NH_4BF_4 in accordance with the sample preparation method described in Section 3.6.7. The molecular weight distribution data for the samples largely show a mono-modal distribution with minor shoulders appearing on left side of the curve which is indicative of lower molecular weight fractions within the sample. Saito *et al.*, (331) explained the differences observed in the molecular weight distribution of lignin when the GPC analysis was carried out using neat DMF and DMF with a salt such as LiBr. Neat DMF showed a bi-modal peak whilst DMF with LiBr showed a monomodal peak. This observation was attributed to the heterogeneity in the structure of lignin. Neat DMF could also be responsible for both single and aggregated lignin molecules which could result in a high M_w/M_n ratio (PDI). The weight average molecular weight (M_W), number average molecular weight (M_n) and

polydispersity index (PDI) which is the ratio of M_w/M_n for each lignin fraction is calculated and summarised in Table 4.6.

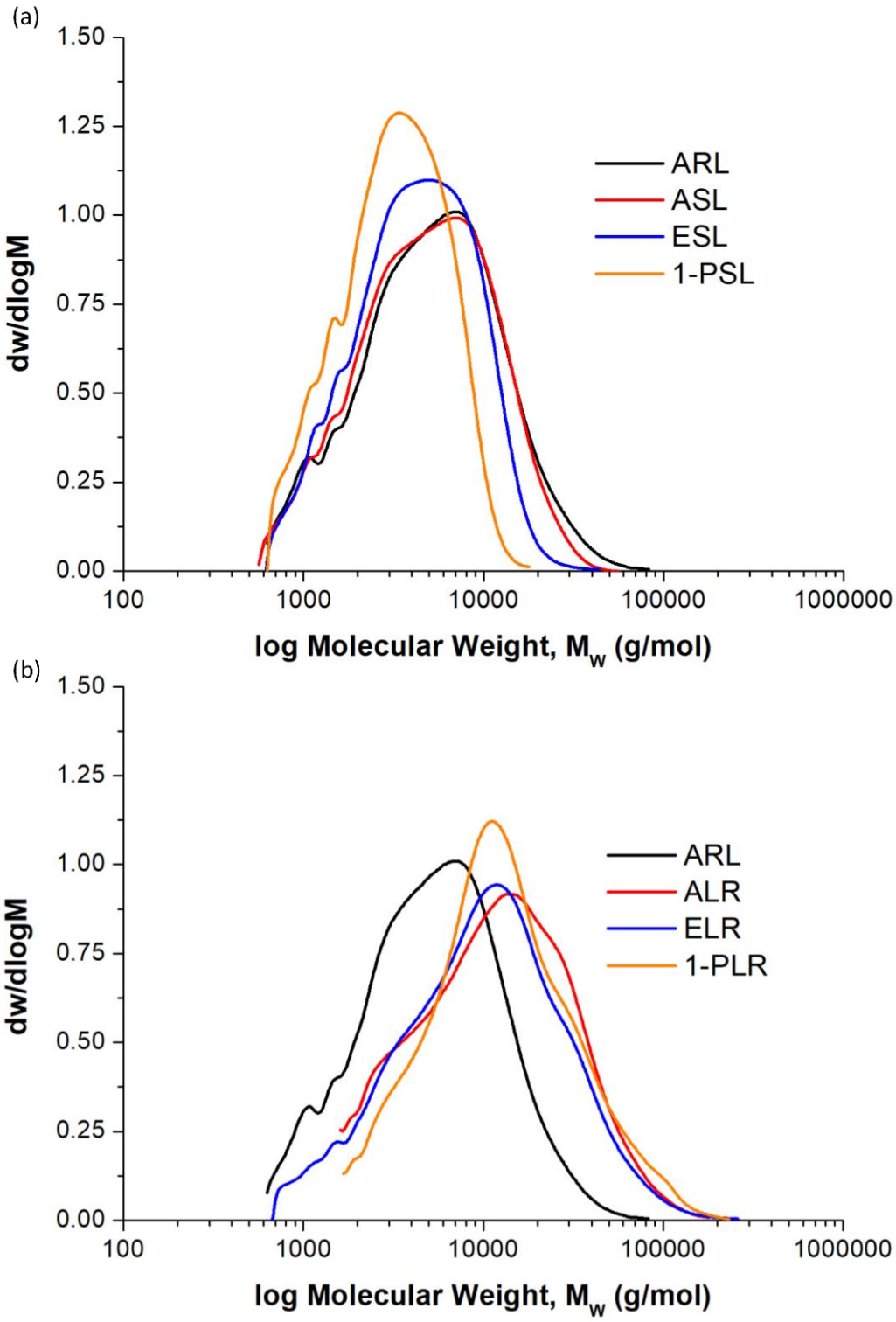

Figure 4.8 Molecular weight distribution traces for as-received lignin: (a) soluble; and (b) insoluble lignin fractions.

The ARL has a molecular weight of approximately 7400 g/mol. The soluble fractions show a narrower distribution with lower molecular weights and longer retention time compared to as-received lignin (ARL). The molecular weight distribution for the soluble fractions was observed in the order of n-PSL<ESL<ASL<ARL. The 1-PSL has the highest intensity with narrower distribution among all the soluble fractions. This indicates that 1-propanol can extract a higher ratio of lowest molecular weight components present in the parent lignin. These low molecular weight fragments are generally comprised of oligomers and chain sections (101, 103, 332). Such low molecular weight fragments are not produced as a result of fractionation but are generally found in parent lignin and their concentration is seemed to be higher in lignin soluble fractions (103). As the polarity of the solvent increases an increase in molecular weight of the soluble fractions was observed. This suggests that more polar solvents like acetone and ethanol have stronger ability in making hydrogen bonds with hydroxyl groups of lignin. Therefore, these solvents tend to extract a larger amount of phenolic-lignin chains in higher proportion as compared to other solvent upon solvent treatment (99, 101).

Table 4.6 Molecular weights of BioChoice® lignin samples.

Samples	**M_w (g/mol)**	**M_n (g/mol)**	**PDI (Mw/Mn)**
As-received lignin (ARL)	7367	3413	2.16
Acetone soluble lignin (ASL)	6700	3357	2.00
Acetone insoluble lignin residue (ALR)	17665	7499	2.36
Ethanol soluble lignin (ESL)	5370	3121	1.72
Ethanol insoluble lignin residue (ELR)	16203	5738	2.82
n-Propanol soluble lignin (1-PSL)	3848	2509	1.53
n-Propanol insoluble lignin residue (1-PLR)	19381	8560	2.26

The insoluble fractions showed a broader distribution with significantly higher molecular weights, shorter retention time and higher polydispersity as compared to as-received lignin. The molecular weight distribution for the insoluble lignin fraction was observed in the order; n-PLR>ELR>ALR>ARL. This trend for the insoluble fractions could be an indication that certain solvents have difficulty in penetrating longer macromolecular chains of the bulky and branched structure of lignin. This hindrance caused could be due to the limited hydrogen bonding and intermolecular interaction between the solvent and the hydroxyl groups of macromolecule chains which play an important role in the solubilisation of lignin (99, 101). The significantly higher molecular weight for the lignin insoluble fractions may also be attributed to the formation of aggregation, since it is known that aggregation can occur in lignin solutions (103, 332). The mechanism proposed for the formation of aggregation is linked to the π-π stacking of aromatic groups (333, 334). The n-PLR had the highest molecular weight of approximately 20000 g/mol. Similar results were reported in the literature where the soluble fraction comprised of low molecular weight whilst high molecular weights were obtained in the insoluble fractions (100, 101, 121, 332, 335, 336).

4.8 Differential Scanning Calorimetry of Fractionated Lignins

In order to study the effect of solvent treatments on the thermal properties of the fractionated lignin samples, DSC experiments were performed on the soluble and insoluble lignin samples. Three ramped heating experiments were performed on each sample in the temperature range, 20-250 °C. DSC trace for the first heating scan of fractionated lignin is shown in Figure 4.9 (a-b). The first scan follows up the same trend as previously mentioned by exhibiting an endothermic peak corresponding to evaporation of water or evaporation of solvents used for fractionation. This endothermic peak is followed by the glass transition which is observed in each scan. In Figure 4.9 (a-b), the method for defining the T_g for the lignin samples in the first heating scan is illustrated for ARL and 1-PLR. The intersection points of the tangent lines are considered for the onset and end-set for the T_g whilst the midpoint of the intersection is reported as the T_g. The same procedure

is followed to determine the T_g of all the other sample. The soluble fractions exhibit a lower T_g and the insoluble fractions show a higher T_g in contrast to as-received lignin.

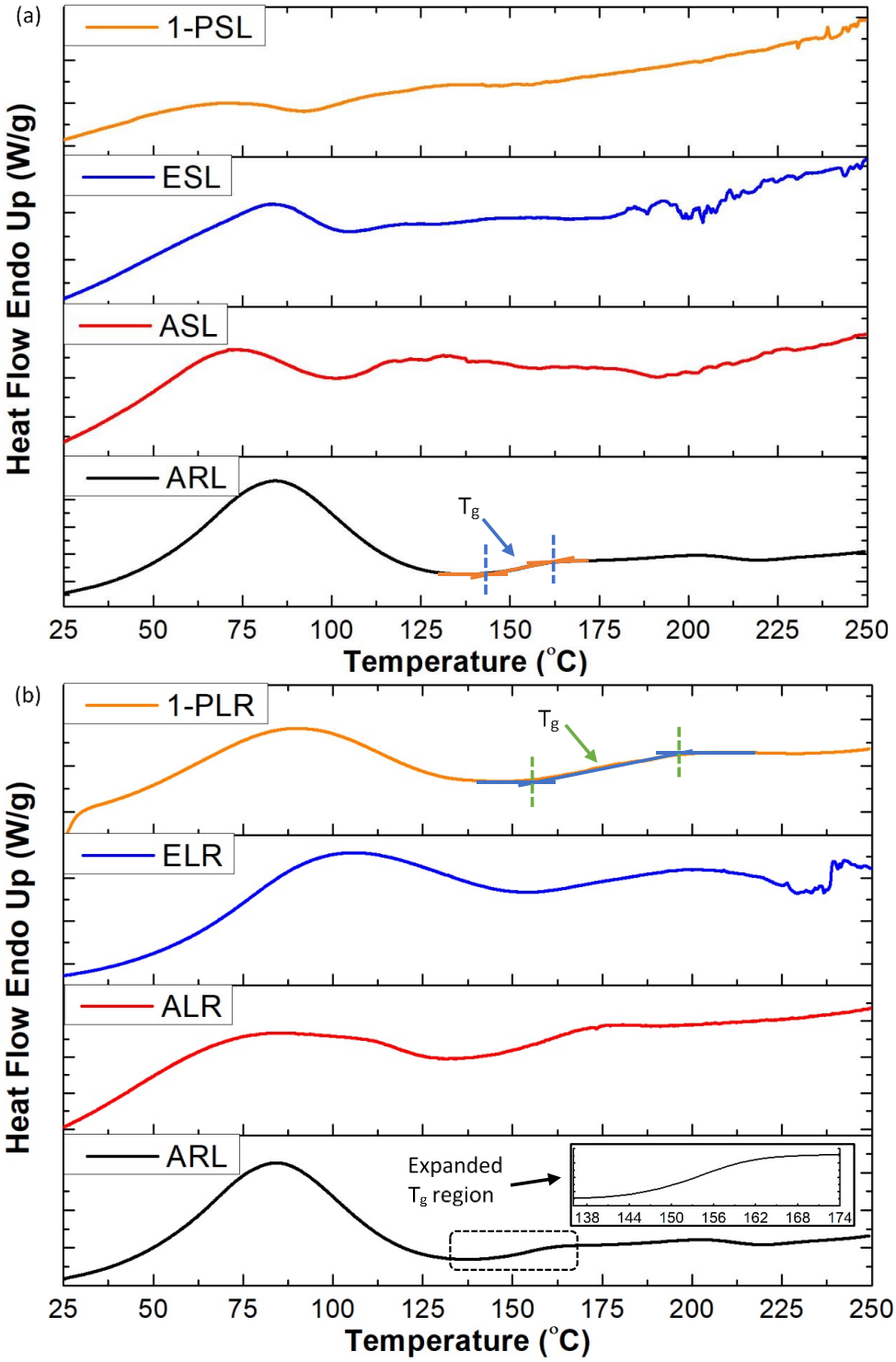

Figure 4.9 DSC traces for first heating scan of as-received lignin: (a) soluble; and (b) insoluble fractions using acetone, ethanol and 1-propanol.

The DSC traces from the second heating scan for the ARL, soluble and insoluble lignin fractions is shown in Figure 4.10. In the second heating scan, only the T_g is detected without the presence of an endothermic peak suggesting that the sample is free of moisture and low-molecular weight components. This is reasonable as in the first scan, the sample was heated to 250 °C. All the solvent soluble lignin (ASL, ESL and 1-PSL) exhibit a lower T_g when compared to the as-received (ARL) lignin whilst insoluble lignin fractions exhibit higher T_gs.

The T_g of lignin can be affected by various factor including the following: molecular weight (101, 108); thermal histories (337, 338); species (softwood, hardwood or agricultural residues) (220); the existence of lower molecular weights contaminants including water/solvents (339, 340) and chemical functional groups (122, 325, 341, 342). Hence, the typical value of T_g for lignin is generally found to be in the region between 140-180 °C (343-345).

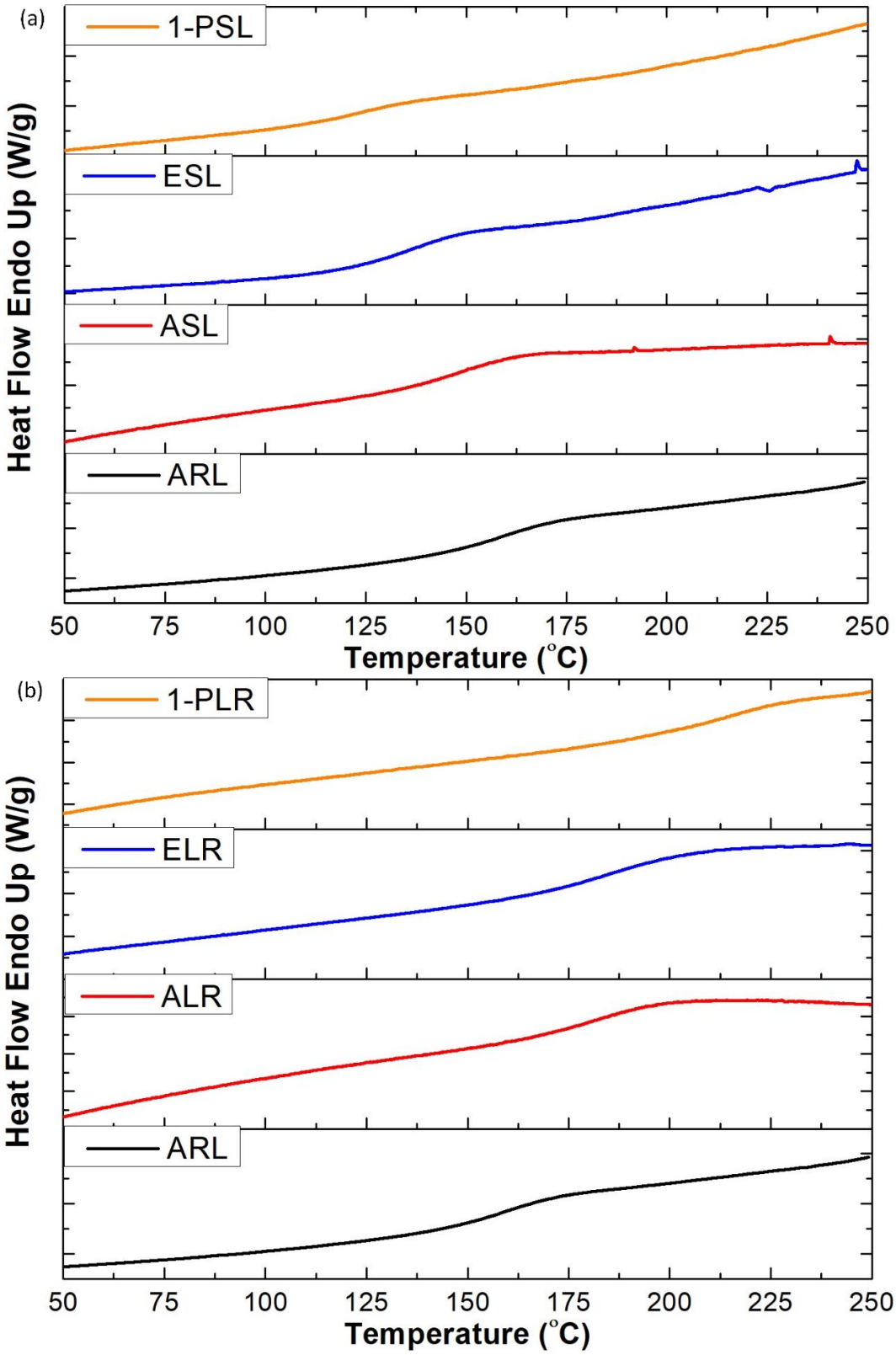

Figure 4.10 DSC traces for the second heating scan of as-received lignin: (a) soluble; and (b) insoluble fractions.

The second heating scan showed that the T_g of the as-received lignin, after heating to 250 °C in the first scan, is approximately 155 °C. The glass transitions temperatures of fractionated lignin consisting of soluble fractions in second heating scans are as follows:, acetone-soluble lignin (ASL) showed the highest T_g of 146 °C; the T_g for ethanol-soluble lignin (ESL) is around 134 °C whereas the lowest T_g of approximately 122 °C was observed for the soluble lignin fraction with 1-propanol (1-PSL).

The lignin residues (insoluble solvent fractions), ALR, ELR, and 1-PLR exhibit substantially higher T_gs when compared to the as-received (ARL) lignin. The glass transitions temperature of the lignin insoluble fractions are as follows: acetone lignin residue (ALR) exhibits the lowest T_g of all the solvents involved ~181 °C; the T_g for the ethanol lignin residue (ELR) is ~187 °C whilst the highest T_g values were found for lignin insoluble fraction with 1-propanol (1-PLR) which is ~211 °C. Generally, high T_g values are expected of higher molecular weight fractions (101, 122, 346).

The T_gs for the lignin fractions including that of the as-received lignin obtained in the 3rd heating scan are shown in Figure 4.11. There is gradual increase in the T_g for each sample after each sequential heating. This shift in the T_g after each scan could be due to the sequential heating of lignin to 250 °C ($T > T_g$) causing a structural change and thus resulting in a higher T_g in the subsequent scan. At temperature higher than the T_g, the molecular motion is restricted due to thermally induced cross-linking and rigid groups in the macromolecular chains within the lignin framework leading to an increase in the T_g (347, 348). This structural change could be attributed to a plausible non-reversible thermal event such as condensation reactions occurring between 160-250 °C causing an increase in molecular weight (325). This trend can be assigned due to irreversible cross-linking via a free-radical cross coupling of lignin leading to a cross-linked structure (286, 348). Thus through rearrangement/free-radical coupling, lignin forms new bonds which can result in irreversible changes in the T_g (349-351). These results are found to be in

accordance with the literature where GPC analysis was performed to determine the molecular weight of the heat-treated samples (101, 103, 349).

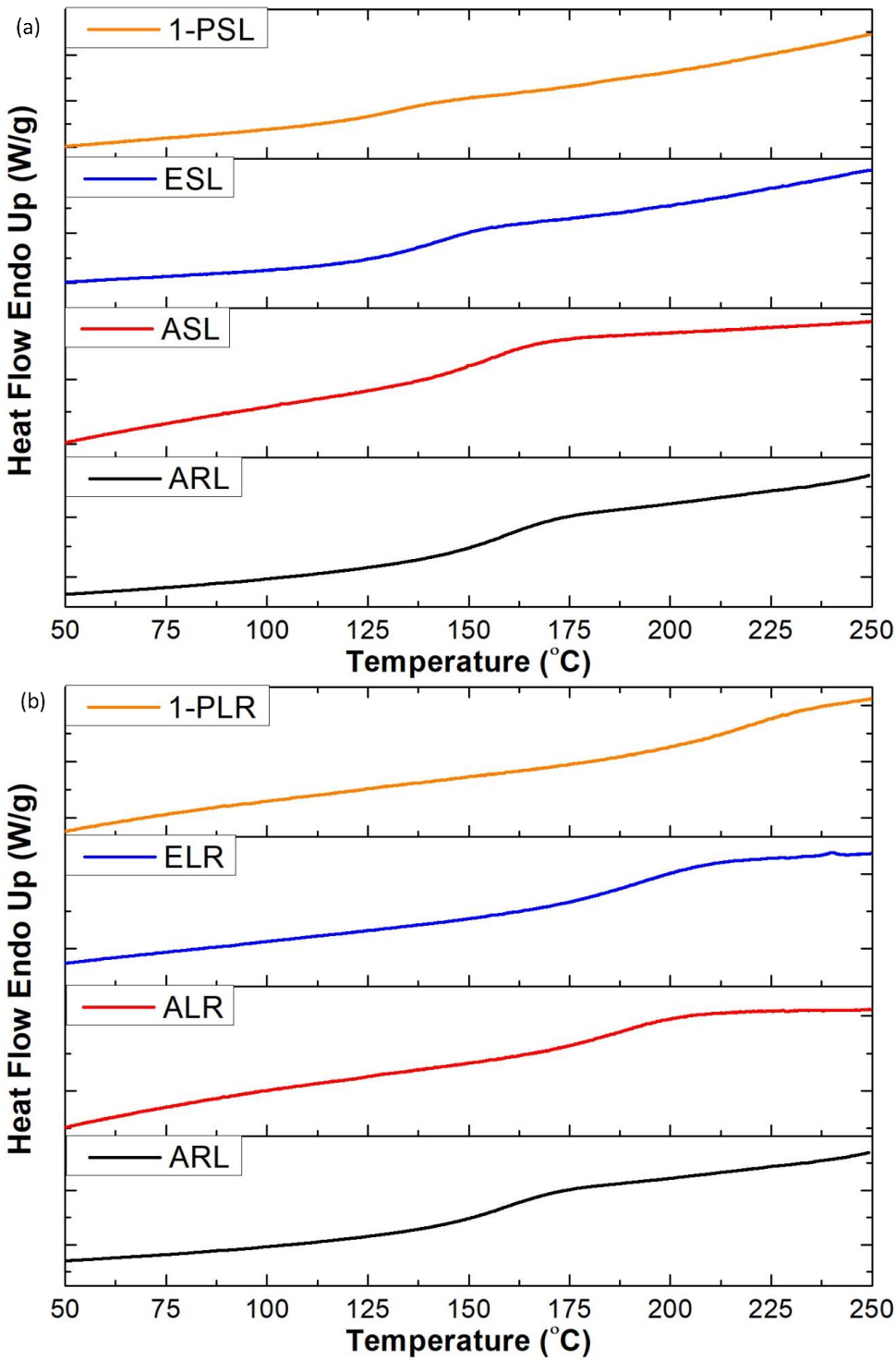

Figure 4.11 DSC traces for the 3rd heating scan of as-received lignin: (a) soluble; and (b) insoluble fractions.

The T_g for the soluble and insoluble lignin fractions of lignin are summarised in Table 4.7. Figure 4.12 shows histogram plot for T_g variation between as-received, soluble and insoluble lignin fractions. The observed trend in the glass transition temperature could be attributed to the lignin fractions having different molecular weight distributions and this is in agreement with that reported in the literature (101, 122, 346). It is also reported that the soluble fractions with lower molecular weights and reduced T_gs are attributed to the larger excess free-volume of chains-ends (101, 103). This shows that solvent extraction represents an efficient and convenient way to obtain low-molecular weight lignin with a low T_g without any chemical modifications of the as-received (ARL) lignin.

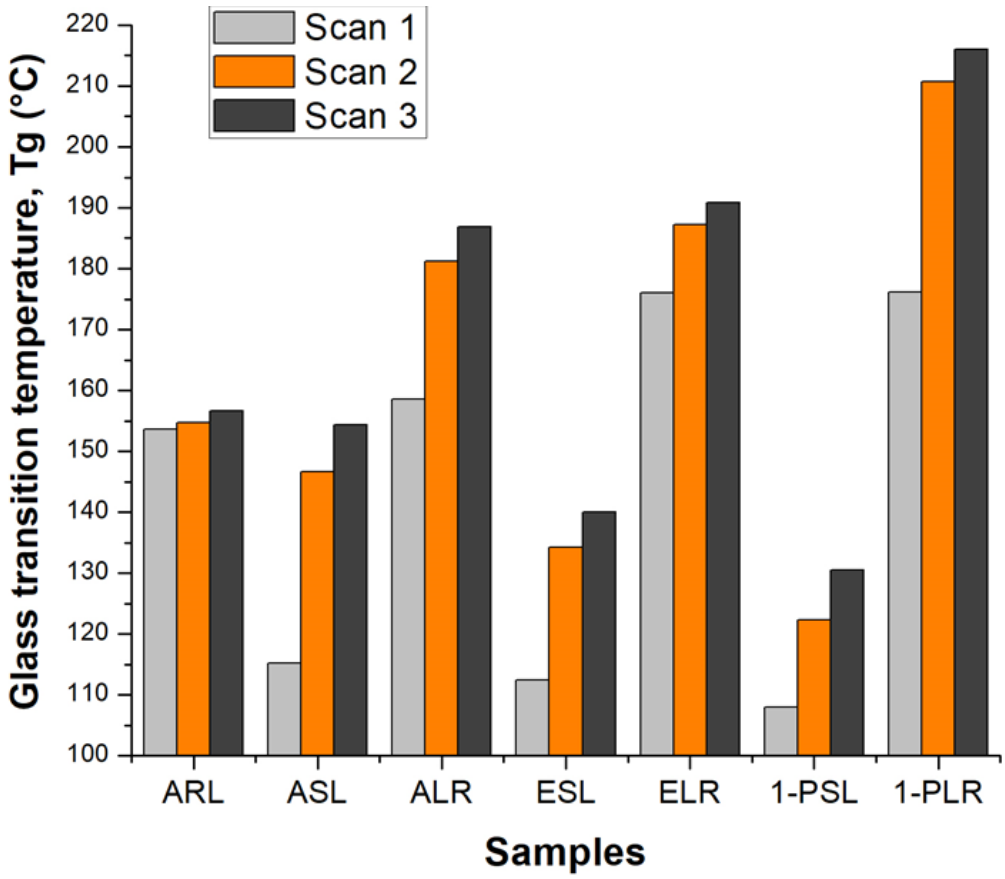

Figure 4.12 Glass transition temperature of as-received (ARL), soluble and insoluble lignin fractions in each heating scan.

Table 4.7 The T_g of as-received lignin and fractionated samples.

Samples	Heating Scan 1			Heating Scan 2	Heating Scan 3
	Peak (°C)	Peak area (J/g)	T_g (°C)	T_g (°C)	T_g (°C)
ARL	88.8	161.0	153.6	154.7	156.6
ASL	71.1	35.9	115.2	146.7	154.4
ALR	86.1	43.4	158.5	181.2	186.9
ESL	81.3	27.1	112.5	134.2	140.0
ELR	106.5	54.5	176.1	187.3	190.9
1PSL	71.7	29.7	107.9	122.3	130.5
1PLR	89.2	49.4	176.1	210.8	216.1

4.9 The Effect of Molecular weight on the Glass Transition Temperature

The lignin being an amorphous polymer undergoes a transition from glassy to a rubbery state upon heating passing at a particular temperature range. The temperature range where this transition occurs is referred to as the T_g. The molecular chains of a polymer experience increased segmental mobility at T_g (352). As mentioned previously, the T_g value can be influenced by several factors including molecular weight of a polymer and the presence of moisture. The effect of polymers molecular weight on T_g can be described using the Fox-Flory as expressed in Equation 10:

$$T_g = T_g^{\infty} + \frac{K}{M_n} \qquad \text{Equation 10}$$

where T_g refers to the glass transition temperature and M_n is the number average molecular weight of the polymer; T_g^{∞} refers to the glass transition temperature of polymer with infinite

number-average molecular weight in which the effect of chain-ends is considered to be negligible; and K is an empirical parameter that represents the free-volume in the polymer.

The Fox-Flory model exhibiting the dependence of the T_g on the molecular weight of soluble and insoluble lignin fractions is shown in Figure 4.13. The experimental data for the T_g from each heating scan is plotted against the reciprocal of number average molecular weight (M_n). The data are fitted with a linear regression equation.

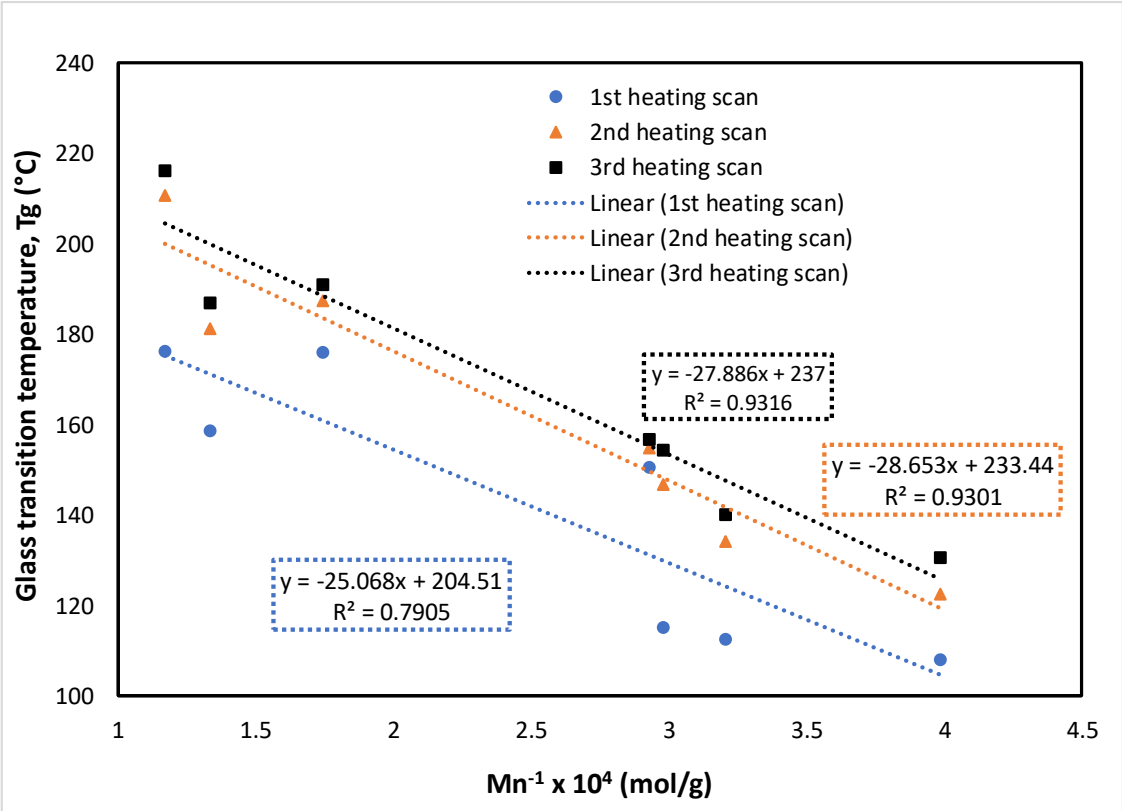

Figure 4.13 The application of the Fox-Flory model where the T_g (reported for each heating scan) is plotted against the reciprocal of number average of molecular weight (Mn) for the fractionated lignin (soluble and insoluble lignin fractions) including the parent lignin.

The relationship between the molecular weight of lignin fractions and the glass transition temperatures shows a better linear regression fit for the second and third heating scans when compared to the first heating scan. This is because, as discussed previously, the T_g is influenced by the presence of the endotherm and the difficulties in defining the baselines for determining the

beginning and end of the endotherm for the determination of T_g. The presence of residual solvent or low-molecular weight lignin chains, and their effect on the T_g was discussed previously. The empirical constant K and T_g^{∞} give an indication of the free-volume of chain-ends and the polymer stiffness corresponding to the crosslink density (101, 318). The values for K was found to increase after each successive heating scan (25.1, 27.9 and 28.7). The higher K values are taken to represent higher stiffness due to an increased cross-link density in the polymer after each subsequent heating scan.

4.10 Thermogravimetric Analysis of Fractionated Lignins

TGA was used to study the mass-loss characteristics in the lignin sample as a function of temperature in argon. The thermal decomposition of lignin is known to occur in different stages over a broad temperature range of 160-900 °C (144, 353, 354). On the other hand, components in wood such as cellulose and hemicellulose are known to degrade over 315-400 °C and 220-315 °C, respectively (353, 354).

The mass-loss data (TGA) and its derivative (DTG) for as-received lignin is shown in Figure 4.14. The mass-loss curve can be divided into three regions; in zone A (i) the mass-loss is likely to be due to the loss of absorbed water as suggested by DSC and moisture adsorption isotherm results.

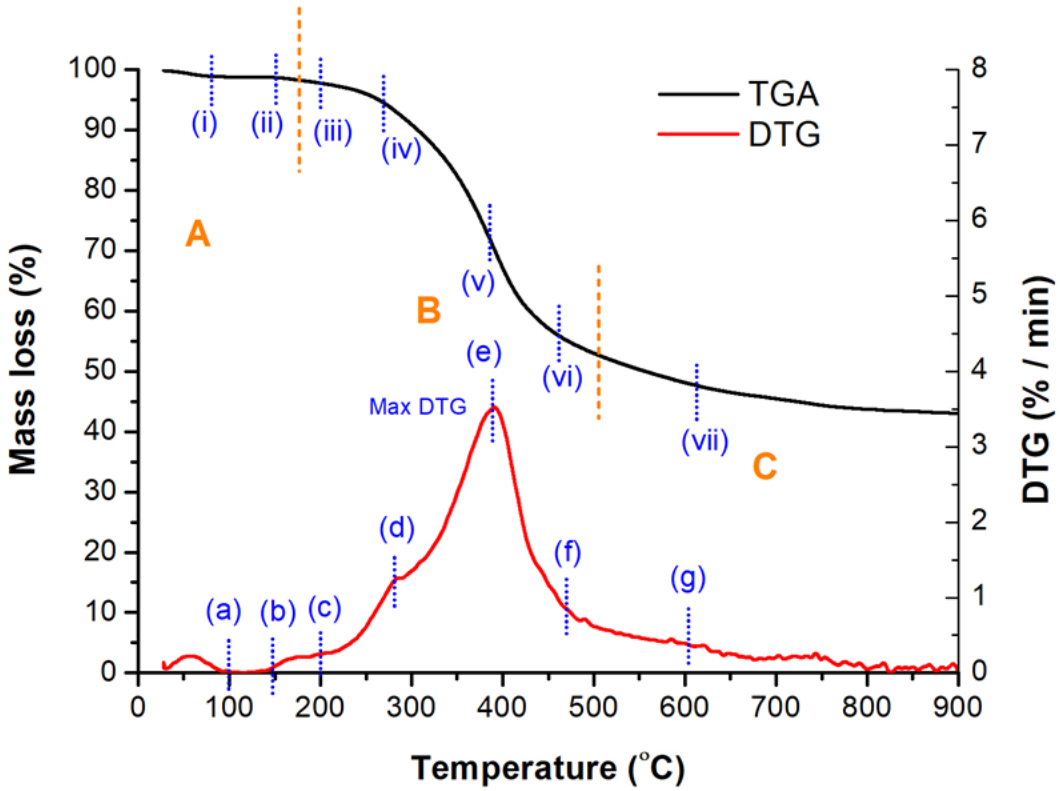

Figure 4.14 Mass loss (TGA) and DTG data for as-received lignin.

The initial mass loss of 2% in zone A: (i) may be linked to the moisture in the as-received lignin (ARL) and this may also be due to the processing conditions used isolating the lignin from wood (355). In zone A (ii) the 1% mass loss at approximately 150 °C, as the T_g is approached could be

linked to the loss of chemisorbed and/or hydrogen bonded water (144, 355). In zone B (iii) at approximately 160 °C may be attributed to the loss of low-molecular weight fragments from lignin. Zone B (iv to vi) shows maximum mass loss around 25-30% and this occurs between 250-500 °C. This region corresponds to the (e) maximum degradation (DTG max) as observed in the first derivative of the TGA data. In this region, most of the degradation products and gases are released. In zone C, the rate of mass loss slows down as only ~15% of the mass is lost between 500-885 °C. This could be attributed to the dehydrogenation (142, 144, 356) along with the evolution of condensable (acetaldehyde and acetic acid) and non-condensable (CO and CO_2) gases and finally the gradual decomposition to yield char (128, 357).

The TGA and DTG traces for soluble and insoluble lignin fractions including that for as-received lignin is shown in Figure 4.15 (a-b). The initial mass loss for the lignin fractions exhibit different thermal stabilities for the solvents used in the fractionation of lignin. The TGA traces are relatively stable until ~110 °C with minimal mass-loss due to the evaporation of absorbed water. Above this temperature, the TGA curves for soluble and insoluble lignin fractions show significant mass-loss which is also indicated by the DTG peaks between 100-150 °C. This mass loss could be due to the evaporation of solvents trapped inside the samples after fractionation. The maximum degradation (DTG) temperatures for the different lignin fractions is summarised in Table 4.8. The DTG traces for the insoluble lignin fractions show that the peak mass-loss occurs between 700-800 °C. This could be attributed to the presence of the high ash content in the insoluble lignin. The inorganic impurities especially metal oxides (CaO, MgO) (358-361) and cations such as sodium (Na^+) and calcium (Ca^{2+}) can strongly affect the degradation of lignin (362, 363). The influence of metal elements are linked to the enhancement in the catalyses of scission reactions and the accelerated formation of gaseous products (358, 359, 362, 364).

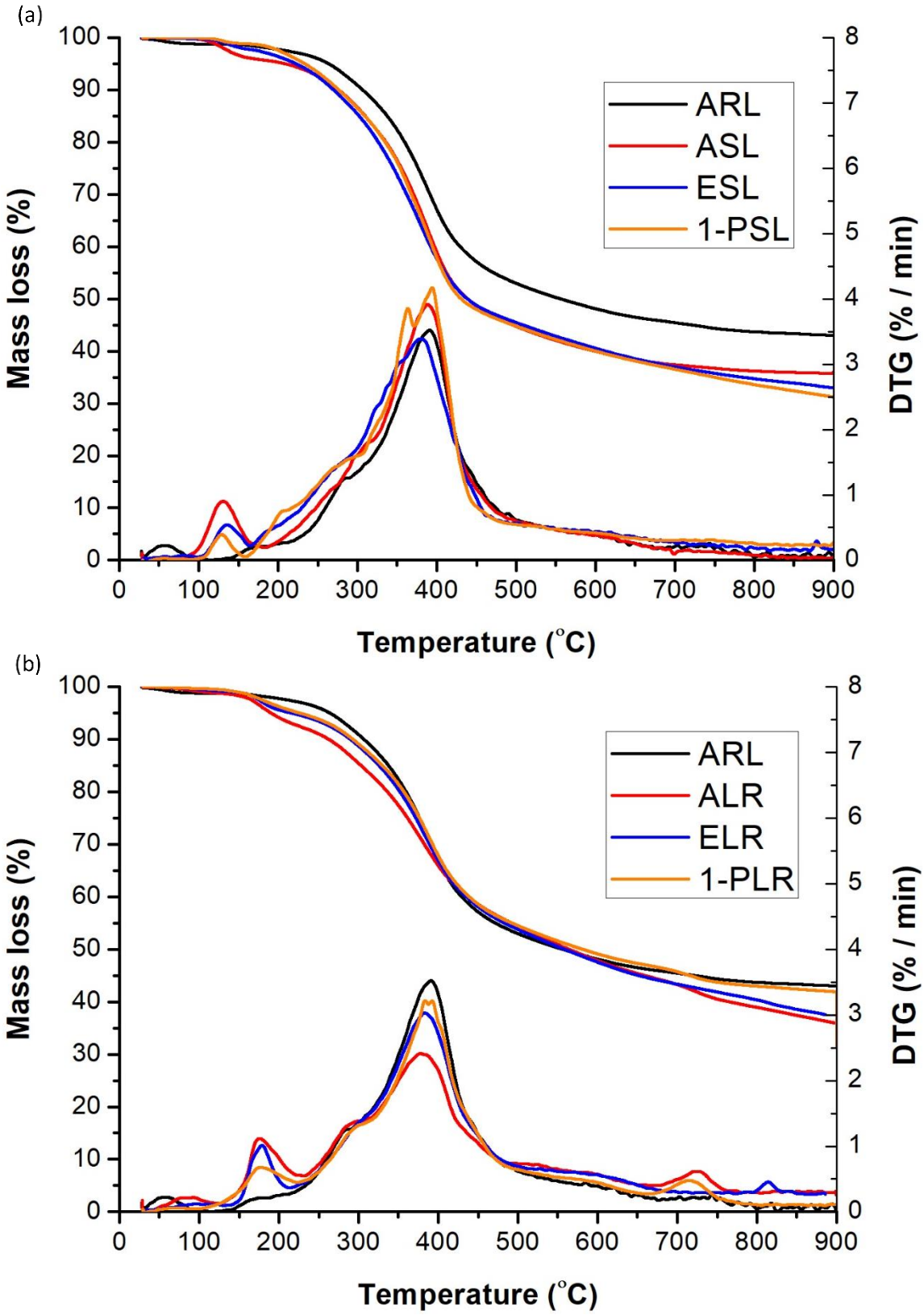

Figure 4.15 (a-b) TGA and DTG traces for as-received lignin: (a) soluble; and (b) insoluble fractions.

It is seen in Table 4.8 that the soluble fractions have a lower residue at 900 °C when compared to the as-received lignin and insoluble fractions. The char content at 900 °C can be used as a screening method to assess protentional precursors, including lignin, for the productions of carbon fibre. It is important to control the amount of char residue which is highly influenced by the heating rate and environmental conditions (355, 365, 366). For the soluble fractions, ASL has the highest char content (35.9%) at 900 °C. This could be due to the ability of the solvent to extract higher ratio of high molecular weight fractions within the parent lignin and thus resulting in higher fractionation char yield in comparison to other solvents. In the case of the insoluble lignin fractions, 1-PLR has the highest residue (42.4%) at 900 °C.

Table 4.8 Char content (%) at 900 °C including the peak mass-loss of lignin at specific temperatures for as-received lignin including the soluble and insoluble lignin fraction.

Samples	**Char at 900 °C (%)**	**DTG max (°C)**	**Mass loss of 50% at Temperature (°C)**
ARL	43.4	390.9	556.2
ASL	35.9	388.3	438.9
ALR	37.4	377.4	564.0
ESL	33.9	380.1	438.7
ELR	38.6	382.7	558.7
1-PSL	32.4	394.2	430.8
1-PLR	42.4	387.8	581.4

Some important observations can be made from the soluble fraction char yield at 900 °C as shown in Figure 4.16 and from the data presented in Table 4.8. These observations are as follows: (i) the soluble fractions exhibit a decrease in the char yield in the order: 1-PSL < ESL< ASL which correlates well with their fractionation yields. (ii) In contrast, the insoluble lignin fractions show an increase in char residue in the order: 1-PLR > ELR > ALR. (iii) The soluble lignin fractions have

low thermal stability as indicated by their 50% mass-loss which occurs at temperatures much lower than those of ARL. This indicates that the soluble fraction contains high proportions of low molecular weight lignin chains which decompose at relatively low temperatures (103). These points reaffirm the discussion in the earlier sections which stated that solvent such as 1-propanol find it harder to penetrate the lignin structural framework. Thus, the insoluble fractions with higher molecular weight and with potentially higher ratio of branched aromatic segments showed higher char residue which decomposes slowly over a broader temperature range (101, 103). The soluble fractions comprised of lower molecular weight fragments decompose at a relatively low temperature and yield lower char residue. Therefore the 1-propanol insoluble lignin (1-PLR) fraction has a higher residue (42.4 %) which is close to that in parent lignin (43.4 %). Its counterpart, the soluble fraction, 1-PSL has a relatively lower char yield (32.4 %) which could be attributed to its fractionation yield.

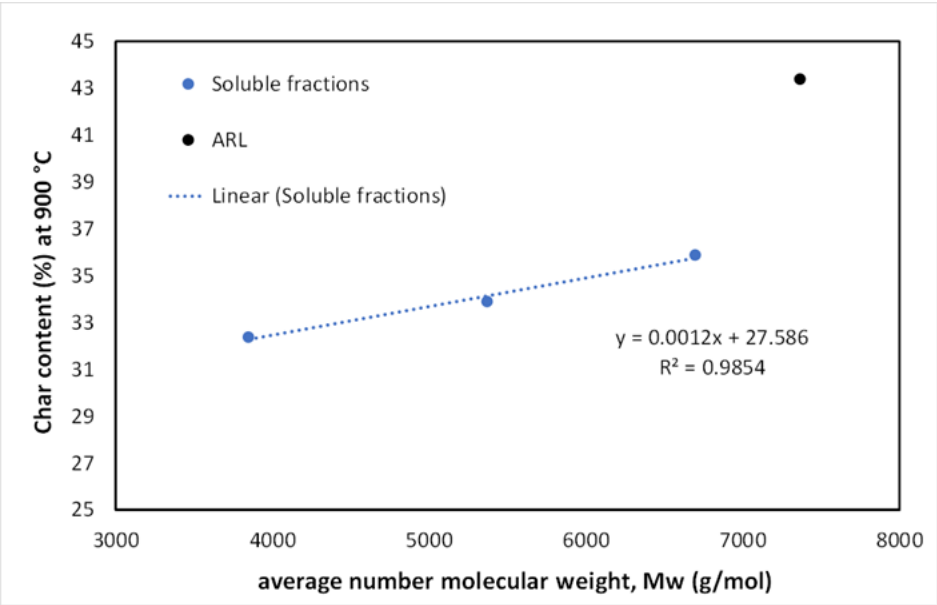

Figure 4.16 Plot showing the char residue at 900 °C as function of the Mw for soluble lignin fractions.

4.11 Pyrolysis-Gas Chromatography-Mass Spectrometry

The chromatograms for pyrolysed lignin at 320 °C and 1000 °C are shown in Figure 4.17. The pyrolytic lignin products depend on the composition and type of lignin, processing conditions including heating rate, final temperature, residence time of the pyrolysis vapours and the particle size (131, 144, 353, 354). The pyrolysed phenolic lignin products for ARL, ASL and ALR are compiled in Table 4.9 with approximately 70% or above matching quality with mass spectral reference fragments.

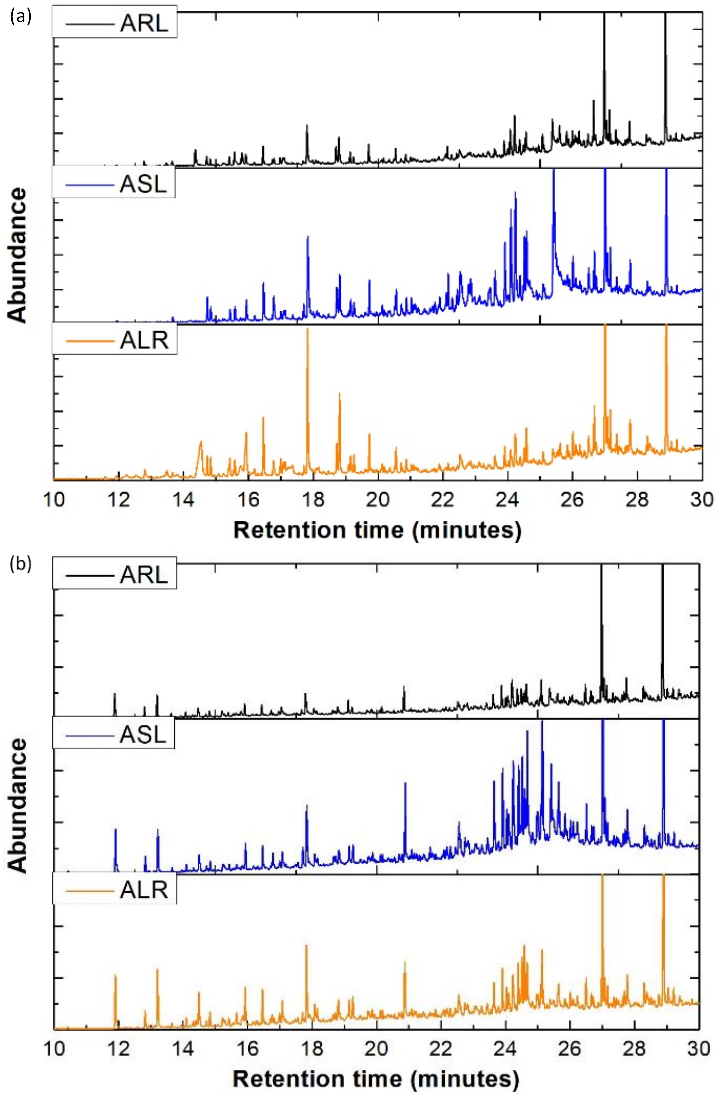

Figure 4.17 PY-GC-MS chromatogram for as-received lignin (ARL) with acetone soluble (ASL) and acetone insoluble (ALR) fractions pyrolysed at (a) 320 °C and (b) 1000 °C.

The pyrolysis products for lignin shown in Table 4.9 are mostly depolymerised components arising from the dominated G-lignin monomer unit. Dimeric and trimeric products from the pyrolysis of lignin were also observed. These include retene, naphthalene, phenanthrene, stilbene (trans), aliphatic acids such as hexadecanoic acid and octadecanoic acid, and resin acids such as dehydroabietic acid with retention time ranging from 20-30 minutes (see the chemical structures in Appendix C).

The pyrolysis products obtained are in good agreement with those reported in literature (100, 127, 136, 139, 367-370). However, the as-received lignin (ARL) and the acetone lignin residues (ARL) showed a trace of depolymerised cellulose, namely 1,6-anhydro-beta-D-glucopyranos also known as Levoglucosan. It also suggests that upon fractionation, not only is the inorganic minerals contributing to the ash content reduced, but it can also influence other impurities which can reduce the cost of separation of products from waste streams in biorefineries. The ash content has a major influence on the pyrolysis process. The higher ash content in ligno-cellulose materials can catalyse the reactions resulting in the increased formation of water and gas (144, 354, 371, 372). This in turn also adversely affects the char yield (312). The presence of metals such as potassium in inorganic impurities has a strongest affect in catalysing the reaction. Therefore, it is detrimental to the char yield including the product quality (371, 373).

As mentioned previously, softwood Kraft lignin is considered not suitable as a precursor for carbon fibre due to the presence of impurities (89, 178, 187). However, Py-GC-MS, ash content and UV/Visible spectroscopy results in Sections 4.6 and 4.14 shows that single-solvent fractionation is a cost-effective and suitable treatment method to reduce impurities.

Table 4.9 Main phenolic products from the pyrolysis of lignin at 320 °C and 1000 °C.

Retention time (minutes)	Phenolic Compounds	M^+ (m/z)	Monomer type	Area Percentange (%)		
				ARL	ASL	ALR
Pyrolysed to 320 °C						
11.97	4-Methylguaiacol	138	G	0.4	0.6	-
13.18	4-Ethylguaicol	152	G	0.7	1.6	1.1
13.67	4-vinylguaiacol	150	G	0.4	0.5	0.5
14.37	Levoglucosan	162		2.7	-	7.1
14.73	2-Methoxy-1,4 benzenediol	140	G	1.0	1.3	1.3
14.84	Vanillin	152	G	0.6	0.6	1.1
15.43	Isoeugenol (trans)/4-propenylguaicol	163	G	0.7	0.5	1.0
15.59	4-propylguaiacol/ Dihydroeugenol	166	G	2.1	0.7	0.8
15.94	Acetovanillone/ Acetoguaiacone	166	G	1.0	1.0	4.8
16.47	Guaiacyl acetone	180	G	2.0	2.0	3.4
16.78	Vanillic acid	168	G	0.5	1.7	1.3
17.00	Eugenol	180	G	3.6	5.6	8.3
17.71	Homovanillic acid	182	G	5.5	0.7	7.8
17.83	4-hydroxy-3-methoxy-benzene propanol	182	G	7.9	6.0	10.3
18.72	Methyl vanillate	196	G	1.8	1.7	1.9
18.81	Coniferyl aldehyde	178	G	3.4	1.9	4.8
19.71	3,5-Dimethoxy-4-methyl-benzoic acid	196	S	1.8	1.9	7.9
Pyrolysed to 1000 °C						
8.69	Phenol	94	G	0.4	0.8	1.9
10.42	Guaiacol	124	G	0.8	0.5	0.5
11.91	Catechol	110	G	3.6	2.4	3.9
12.83	3-Methyl catechol	124	G	1.3	0.7	1.0
13.22	4-Methyl catechol	124	G	2.5	1.8	13.2
14.50	4-Ethyl catechol	138	G	0.9	0.7	2.4
14.84	Vanillin	152	G	0.7	0.5	1.0
15.43	4-Propenylguaiacol /Isoeugenol (trans)	164	G	1.1	2.1	0.91
15.94	Acetoguaiacone/Acetovanillone	166	G	1.3	1.1	2.1
16.47	Guaiacyl acetone	180	G	1.2	1.1	2.1
16.79	4-Hydroxy-3-methoxy-benzoic acid	168	G	0.9	0.7	0.3
17.08	Propiovanillone/Propioguaiacone	180	G	0.8	0.7	1.1
17.72	4-Hydroxy-3-methoxy-benzeneacetic acid/ Homovanillic acid	182	G	2.2	1.1	0.6
17.83	4-hydroxy-3-methoxy-benzene propanol	182	G	11.4	12.1	9.7
18.79	Coniferyl aldehyde	178	G	4.0	3.8	2.9

4.12 Scanning Electron Microscopy

Image analysis was performed using a scanning electronic microscope (SEM) to investigate the effect of solvent extraction on the morphology of lignin samples as shown in Figure 4.18 (a-h).

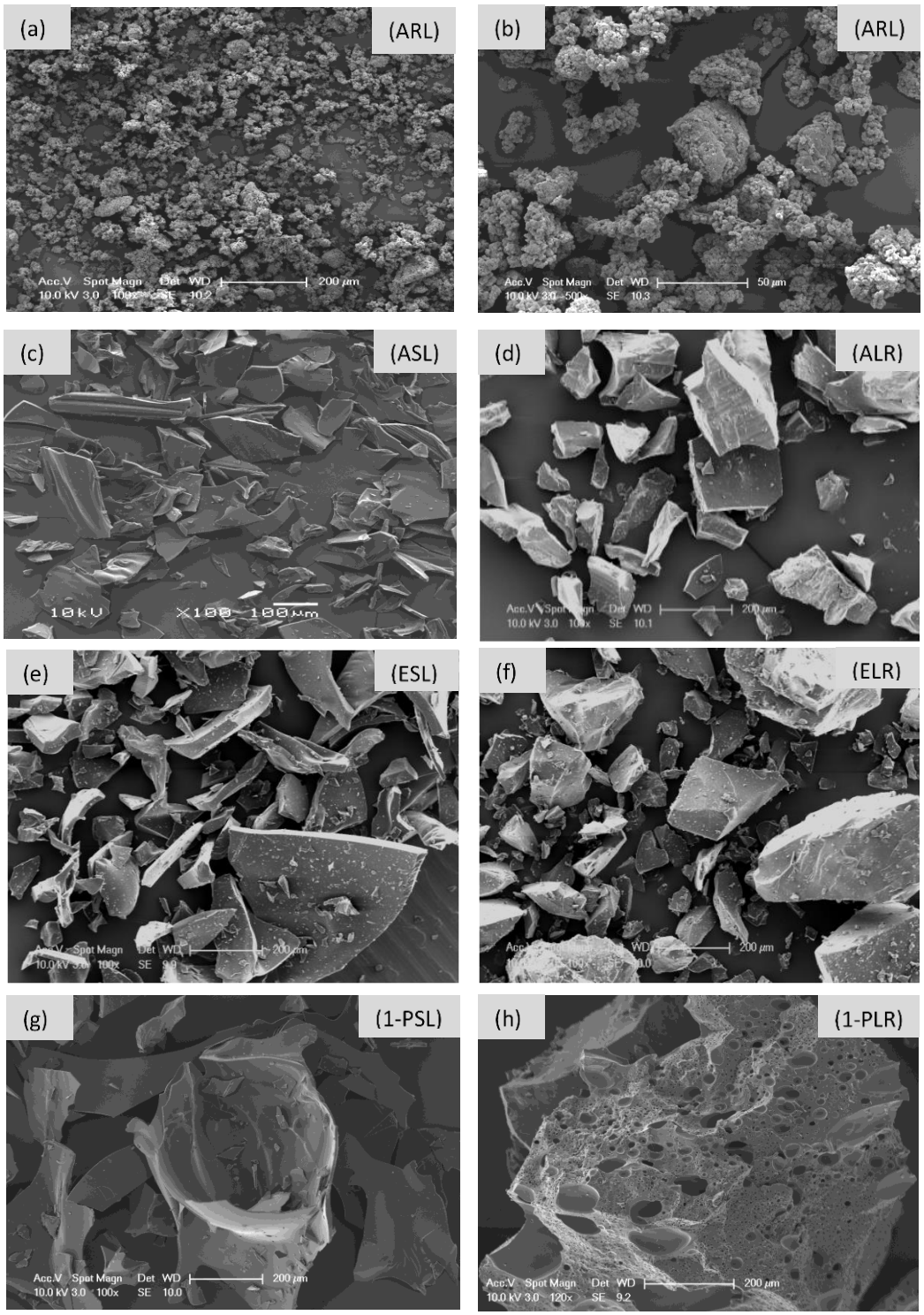

Figure 4.18 Morphology of as-received (ARL), soluble and insoluble lignin fractions.

The as-received lignin (ARL) appeared to have globular morphology with particle size between ~2-90 μm. The particles in ARL with different diameters are clustered to form agglomerates. The arrangement of particles in such a fashion is also termed as 'grape bunch' (374, 375). The distinguishable features are illustrated in the morphologies of soluble and insoluble lignin fractions upon solvent treatment. The appearance of the soluble lignin fractions (ASL, ESL and 1-PSL) resembles flaky structures whilst fused-particles are seen for insoluble lignin fractions (ALR, ELR and 1-PLR). The concentration of large diameter particle is increased in the insoluble lignin fraction. The most noticeable difference among the insoluble lignin fractions is that the 1-propanol insoluble lignin (1-PLR) showed large spherical pores and air bubbles in relatively large sized particles unlike acetone (ALR) and ethanol (ELR) insoluble lignin fractions. These results suggest that the solvent fractionation does not only alters the physico-chemical composition, but it can introduce significant changes to the morphology of the lignin particles.

4.13 Fourier Transform Infrared Spectroscopy

The FTIR spectral characterisation was performed on the lignin samples including the solvent soluble, insoluble and as-received lignin. According to the spectra presented in Figure 4.19, there were no differences in the absorbance characteristics for the different lignin samples. This indicates that the functional groups in the lignin samples were unaltered during fractionation. The spectral assignments for the functional groups present in lignin are given in Table 4.10. These correlate well with those reported in the literature (100, 101, 346, 376).

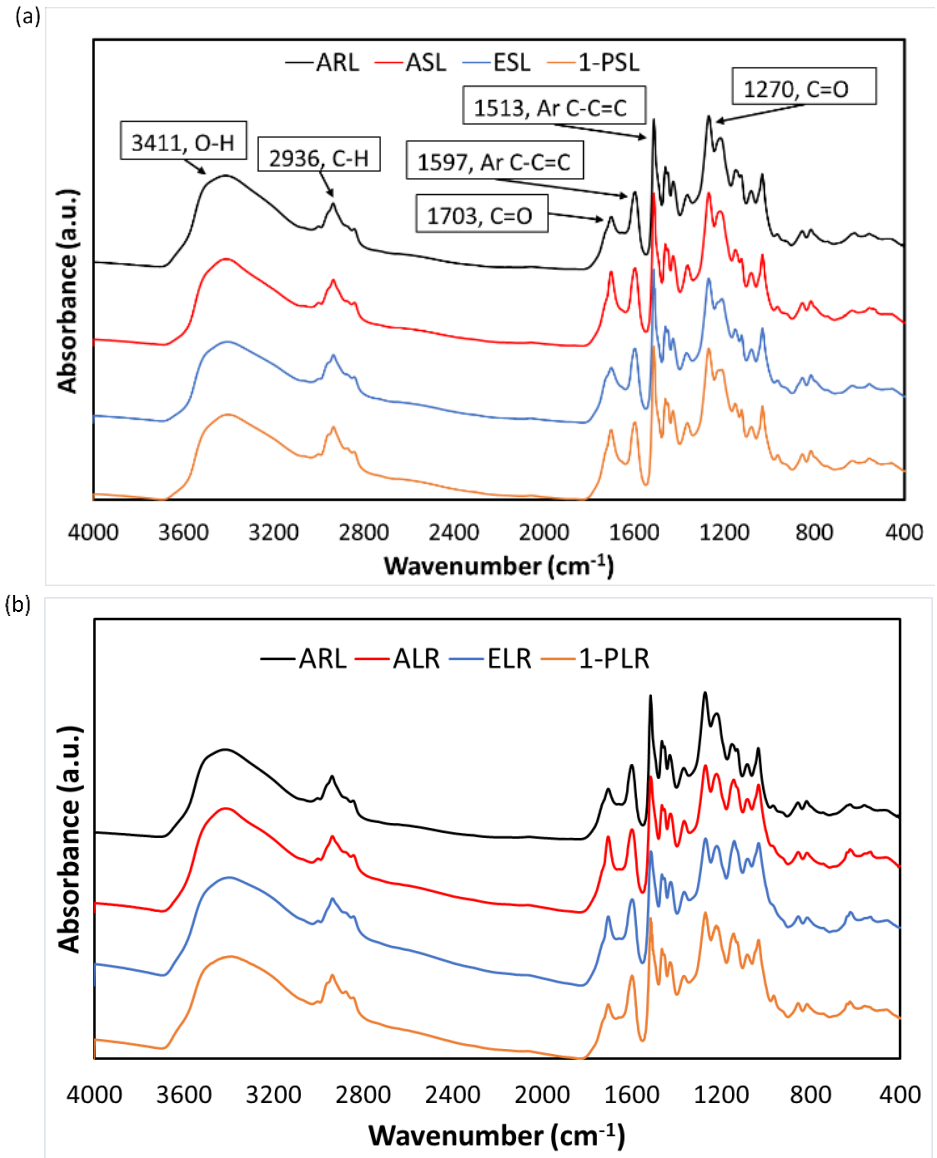

Figure 4.19 FTIR spectra of as-received lignin: (a) solvent soluble, and (b) insoluble fractions.

The lignin fractions including the as-received lignin exhibit a broad absorption peak centred at ~3400 cm^{-1} with a variable intensity which is assigned to the stretching vibration band of hydroxyl groups (O-H). These are found commonly in aliphatic and phenolic moieties. The triplet peaks in the region between 3050-2800 cm^{-1} are features of typical C-H stretching vibrations that are common to methyl (CH_3) and methylene ($=CH_2$) groups. The peak at ~1700 cm^{-1} is assigned to the stretching vibration of carbonyl bonds (C=O) in conjugated ketones, aldehydes and esters groups including carboxylic acids. The unconjugated carbonyl bands show vibrations at higher wavenumber typically in the range 1710-1740 cm^{-1}. The region with medium to strong absorbance bands at wavenumber 1600 cm^{-1} and 1500 cm^{-1} are representative of vibrations associated with aromatic skeleton (C=C-C) in lignin. The peak at 1460 cm^{-1} is attributed to the asymmetric C-H bending in the methyl and methylene groups.

The characteristic peaks at 1270 cm^{-1} and 1218 cm^{-1} are indicative of Guaiacol (G-lignin) moieties associated with the combination of C-O and C=O vibrations with C-C, C-O and C=O stretching vibrations, respectively. Interestingly, the absorption bands at 1700 cm^{-1} and 1270 cm^{-1} are noticeably higher in the acetone soluble lignin (ASL) fraction as compared to the parent lignin. This implies that the solvent treatment leads to an increase in the concentration of C=O groups or it may be attributed to the solvent used for fractionation. The noticeable peak with weak absorption band at 1150 cm^{-1} is assigned to C=O deformation corresponding to conjugated ester groups in G/S/H-type lignin units. This weak absorbance band suggests that only a small concentration of the S and H lignin moieties are ascribed to the as-received lignin. The distinctive bands at 855 cm^{-1} and 816 cm^{-1} are indicative of C-H out of plane deformation typical to G-lignin units. The absence of the peak at 835 cm^{-1} accounts for the reduced concentration of S and H lignin units (377). The noticeable peak at 623 cm^{-1} can be assigned to C-S bond arising from the Kraft process used to isolate lignin.

Table 4.10 FTIR spectral assignments for specific functional groups for lignin samples compiled from the reported literature (100, 101, 346, 376).

Wavelength (cm^{-1})	**Literature wavelength (cm^{-1})**	**Signal strength**	**Functional group assignments**
3411	3411-3390	Strong Broad	O-H stretch, phenolic and aliphatic O-H group stretch
2936	3050-2800	Medium	C-H stretch methyl and methylene groups, C-H vibrations of methyl or methoxyl group
1703	1710-1700	Medium	CO stretching (in conjugated aldehydes, ketones and carboxylic acids)
1597	1600-1500	Medium	Aromatic skeletal vibration
1513	1600-1500	Strong	Aromatic skeletal vibration
1463	1460-1450	Medium	Asymmetric bending C-H in plane deformation of methyl, methylene and methoxyl ($O-CH_3$) groups
1428	1428-1420	Weak	Aromatic skeletal (ring) vibration combined with C-H in plane deformation
1365	1365-1370	Weak	C-H deformation in methyl, methoxyl ($O-CH_3$) group
1270	1270-1260	Strong	Aromatic ring (Guaiacyl moieties) breathing with CO stretch
1218	1226-1216	Medium	C-C, C-O and CO of ester stretching vibrations
1150	1155	Weak	CO deformations in conjugated ester in G, S, H units of lignin combined with aromatic C-H in plane deformation
1082	1085-1081	Weak	C-O deformation in secondary aliphatic alcohols and aliphatic ether
1032	1035-1029	Weak	C-O deformation in primary aliphatic alcohols combined with aromatic C-H in plane deformation
855	854-852	Weak	C-H deformation out of the plane in G aromatic units
816	817-814	Weak	C-H deformation out of the plane in G aromatic units

There are some hidden spectral features which can be seen upon the derivatisation of as-received lignin. For example, after acetylation of lignin, the hydroxyl group of lignin at 3400 cm^{-1} disappears. The appearance of carbonyl peaks can be used to determine the phenolic-to-aliphatic hydroxyl group ratio. The carbonyl region of acetylated lignin (Ace-ARL) can be deconvoluted as shown in Figure 4.20. These peaks are assigned as aromatic acetoxy carbonyl C=O (peak) centred at 1765 cm^{-1} and the aliphatic acetoxy carbonyl C=O (peak) centred at 1743 cm^{-1} (100, 378, 379). The calculated phenolic-to-aliphatic hydroxyl ratio is 1.15 and it can be seen from the deconvoluted spectra of the carbonyl groups that the aromatic group has a higher absorbance than aliphatic carbonyl group.

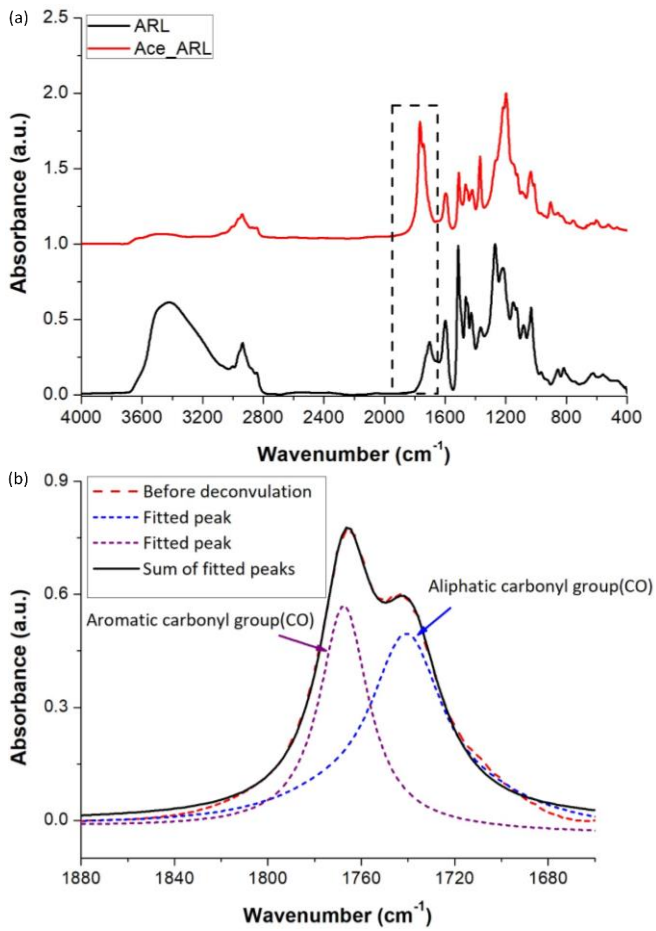

Figure 4.20 FTIR spectra for: (a) as-received lignin (ARL) and acetylated lignin (Ace-ARL); and (b) deconvoluted carbonyl peak for Ace-ARL sample.

4.14 Ultraviolet/Visible Spectroscopy

Ultraviolet/visible spectroscopy has been used widely for the quantitative determination of acid soluble lignin and semiquantitative analysis to establish the purity of lignin based on the Beer-Lambert law (380-383). UV/visible absorption spectroscopy of lignin is also used to undertake qualitative studies on aromatic structures, conjugated aliphatic bonds in side chain and carbonyl groups for qualitative analysis (89, 380). The Beer-Lambert law was applied to obtain the extinction coefficient (ε) at a given wavelength (~280 nm) as listed in Section 3.6.11. Figure 4.21 (a-b) shows the UV/visible spectra of soluble and insoluble lignin fractions.

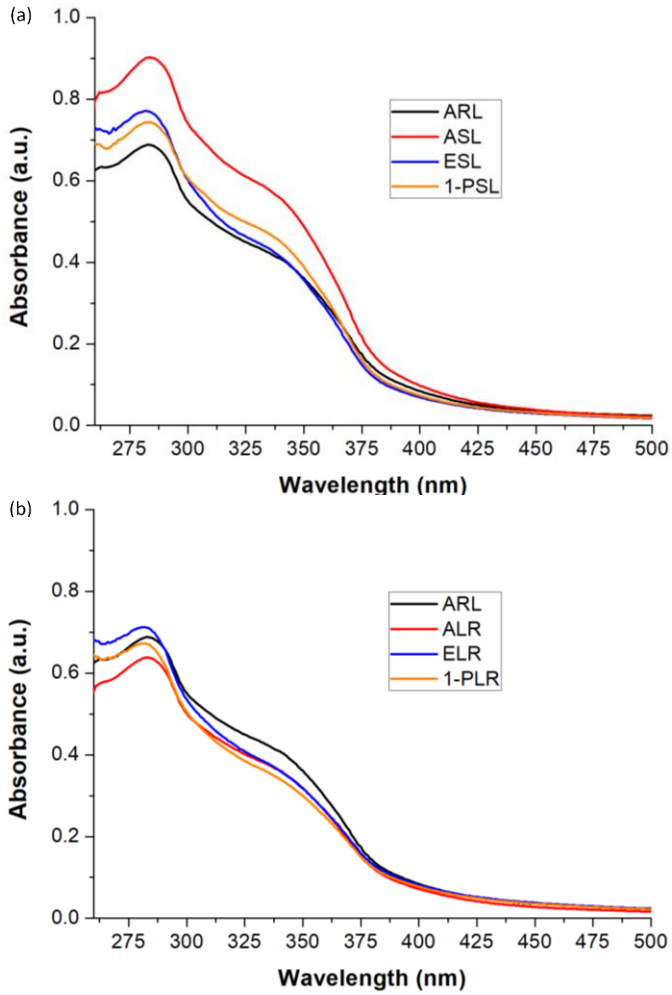

Figure 4.21 UV/vis spectra of (a) soluble and (b) insoluble lignin fractions including as-received lignin.

The structural moieties of lignin give different absorption maxima and extinction coefficients. The conjugated aromatic (non-condensed phenolic units) groups exhibit π-π* electronic transitions at a given wavelength. For the G-lignin (guaiacyl) unit this transition occurs at ~280 nm and its extinction coefficient is found to be three times higher than that of the S-lignin (syringyl) unit. In the case of the S-lignin (syringyl) unit, this transition is seen at a lower wavelength due to the additional substitution of the methoxyl (OMe) groups at the C-5 position; this shifts the absorption maxima to between 270-273 nm (89, 101, 151, 384-386). Since softwood Kraft lignin is mainly comprised of G-lignin units, the absorption maxima are observed at approximately 280 nm.

The absorption maximum at ~320 nm is ascribable to the π-π* electronic transition assigned to the conjugated carbon (C=C) bonds (89, 383). Another absorption maximum for the lignin samples is observed at 340 nm. This absorption corresponds to α-carbonyl groups and esters of hydroxycinnamic acids (e.g., ferulic acid). The calculated maximum absorption coefficients at given wavelength are shown in Table 4.11. The higher extinction coefficients are indicative of a higher lignin content (385). All the soluble fractions specifically acetone soluble lignin fraction (ASL) exhibit higher extinction coefficient in comparison to the as-received lignin (ARL). The extinction coefficients for the insoluble lignin fractions are relatively similar or slightly lower as compared to the parent lignin. The higher absorbance and extinction values for the soluble fraction could be related to the lower concentration of impurities (89, 382, 383), this assumption correlates well with the reduced ash content upon fractionation as shown in Table 4.5. This provides further evidence to support the view that the solvent fractionation can be used to refine and purify lignin before undertaking secondary operations such as fibre spinning.

Table 4.11 Extinction coefficients for as received (BioChoice ® lignin) and fractionated lignin samples at 280 nm.

Samples	**Extinction coefficient ($l\ g^{-1}cm^{-1}$)**
ARL	27.5
ASL	36.1
ALR	25.5
ESL	30.8
ELR	28.5
1-PSL	29.7
1-PLR	26.9

4.15 Proton Nuclear Magnetic Resonance Spectroscopy (1H NMR)

The ^{1}H NMR spectrum for as-received lignin (ARL) is shown in Figure 4.22. The ^{1}H NMR was used to identify hydrogen-rich lignin moieties. The proton spectrum of lignin shows extensive overlapping of hydrogen signals due to the high hydrogen content with influence of cross-coupling, proton spin-spin splitting and numerous proton moieties at closely packed chemical shifts within the lignin structure.

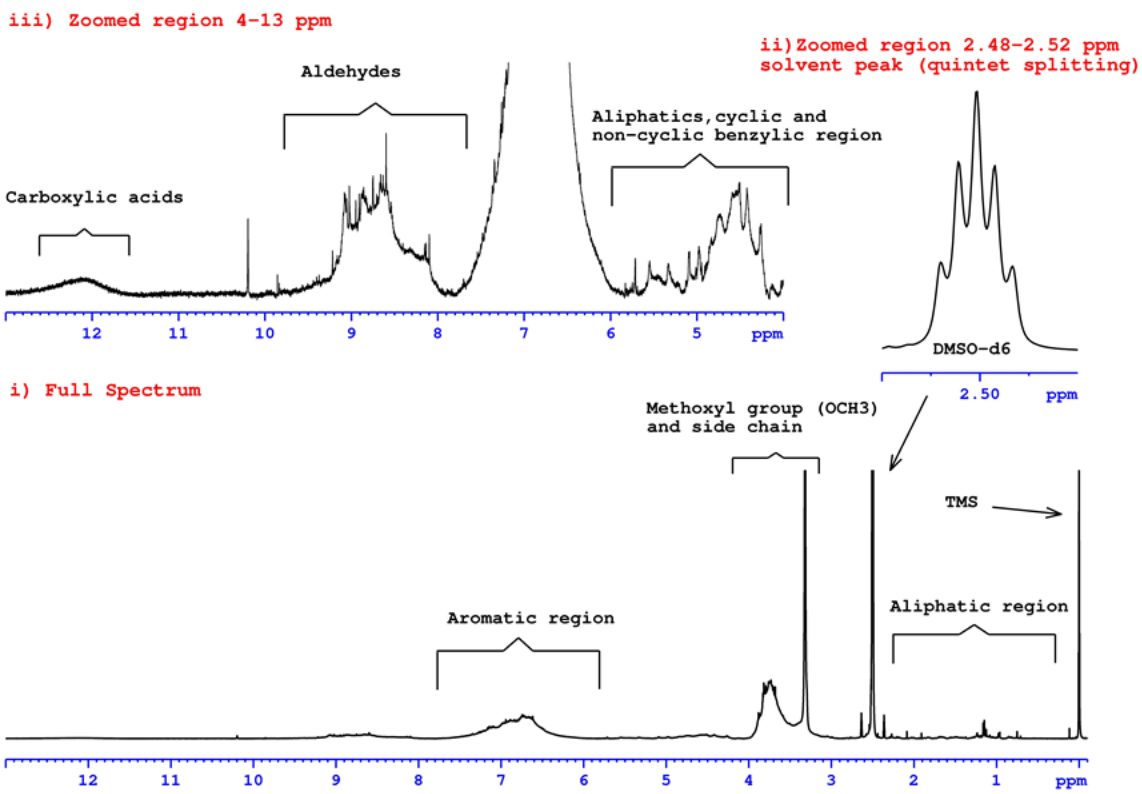

Figure 4.22 ^{1}H NMR of as-received (ARL) lignin.

The main chemicals shift in the ^{1}H NMR spectra for the ARL with the corresponding proton assignments are illustrated in Figure 4.22 and Table 4.12 . The assignment of these chemical shifts is based on the literature (89, 151, 163, 164, 174, 386, 387). The tetramethylsilane (TMS) is used as an internal standard with signal at 0 ppm. The chemical shift between 0-2.5 is assigned to aliphatic and phenolic hydroxy group protons with some contribution from

side chain and hydrocarbon contaminants. The signal at 1.9 ppm is attributed to C-H_β due to secoisolariciresinols type moieties in the lignin (see the structure in Section 4.19). The signal at 2.5 ppm corresponds to a solvent peak of DMSO with a characteristic quintet splitting as showed in (ii) zoomed region of Figure 4.22. The signal at 3.4 ppm is ascribed to methoxy (OCH_3) groups with some overlapping signals of side chain.

Table 4.12 The assignments of chemical shifts in the ^1H NMR spectra for as-received lignin (ARL).

Chemical shift, δ (ppm)	Assignment of hydrogen-1 nuclei
0.0	Tetramethylsilane (TMS) internal standard
0.0 – 2.4	Hydrocarbon contaminants
	Aliphatic and phenolic hydroxyl (OH) groups
2.5	Dimethylsulfoxide (DMSO) solvent peak
3.4-4.0	Methoxyl (OCH_3) group
4.0-5.0	Aliphatics (H_γ in several structures including in β-O-4 and β-5), H_β in β-O-4, H of xylan residue (carbohydrates)
5.0-6.0	H_α in β-O-4, β-5 and β-1
6.0-7.0	Aromatic protons in guaiacyl and syringyl ring
7.0-8.0	Stilbenes, aromatic protons ortho to carbonyl groups (C=O)
8.0-10.0	Aromatics and Aldehydes (Benzaldehydes and Cinnamaldehydes)
12.0	Carboxylic acids (hydroxycinnamic acids)

The chemical shifts in the region of 4.0-6.0 ppm are mainly attributable to the lignin linkages including the aliphatic region. This includes H_γ from 4.0-4.5 region in mainly β-O-4 and β-5 linkages that are present in the structure of resinol. The signal at 4.4 ppm is assigned to the H_α of guaiacyl hydroxy acetic acid. The chemical shift at 4.6 ppm is assigned to H_β in β-O-4

linkages including CH_2 of cinnamyl alcohol. The chemical shift at 4.7 ppm is attributed H_α of β-β linkages in pinoresinols structures including CH_2 of cinnamyl alcohol. The chemical shift at 4.8 ppm could be attributed to H_α of β-O-4 linkages to structure of arylgylcerol-β-aryl ethers. The signal at 4.9 ppm is assigned to H_α of β-O-4 linkage in dibenzodioxocin structure. The chemical shift between 4.9-5.1 ppm could also be linked to carbohydrates proton specifically of xylan residues. The signals at 5.4 ppm and 5.5 ppm are assigned to H_α of β_5 linkage including phenylcoumaran structures. The signal at 5.6-5.7 ppm is assigned to H_α of aryl enol ethers.

The chemical shifts from 8.0-10.0 is attributable to aromatic hydrogens. The chemical shift between 9.0-10.0 ppm is assigned to hydrogen corresponding to aldehydes structures indicating the presence of benzaldehyde and cinnamaldehydes. The signal from 12.0-13.0 is indicative of hydrogen contributing to existence of carboxylic acids within lignin structure. These carboxylic acids could be derivates of hydroxycinnamic acid as indicated by the results obtained using UV/Visible spectroscopy.

4.16 Carbon Nuclear Magnetic Resonance Spectroscopy

^{13}C NMR spectroscopy was used to identify and quantify certain carbon lignin moieties in as-received lignin (ARL). The ^{13}C NMR spectra showed better signal resolution upon the derivatisation (acetylation) of lignin. The ^{13}C NMR spectra for as-received lignin and its acetylated counterpart (Ace-ARL) are shown in Figure 4.23. The ^{13}C NMR spectra show lignin signals over broad chemical shift range with no coupling effects but it still suffers from overlapping of signals specifically in the lignin side chain and aromatic region.

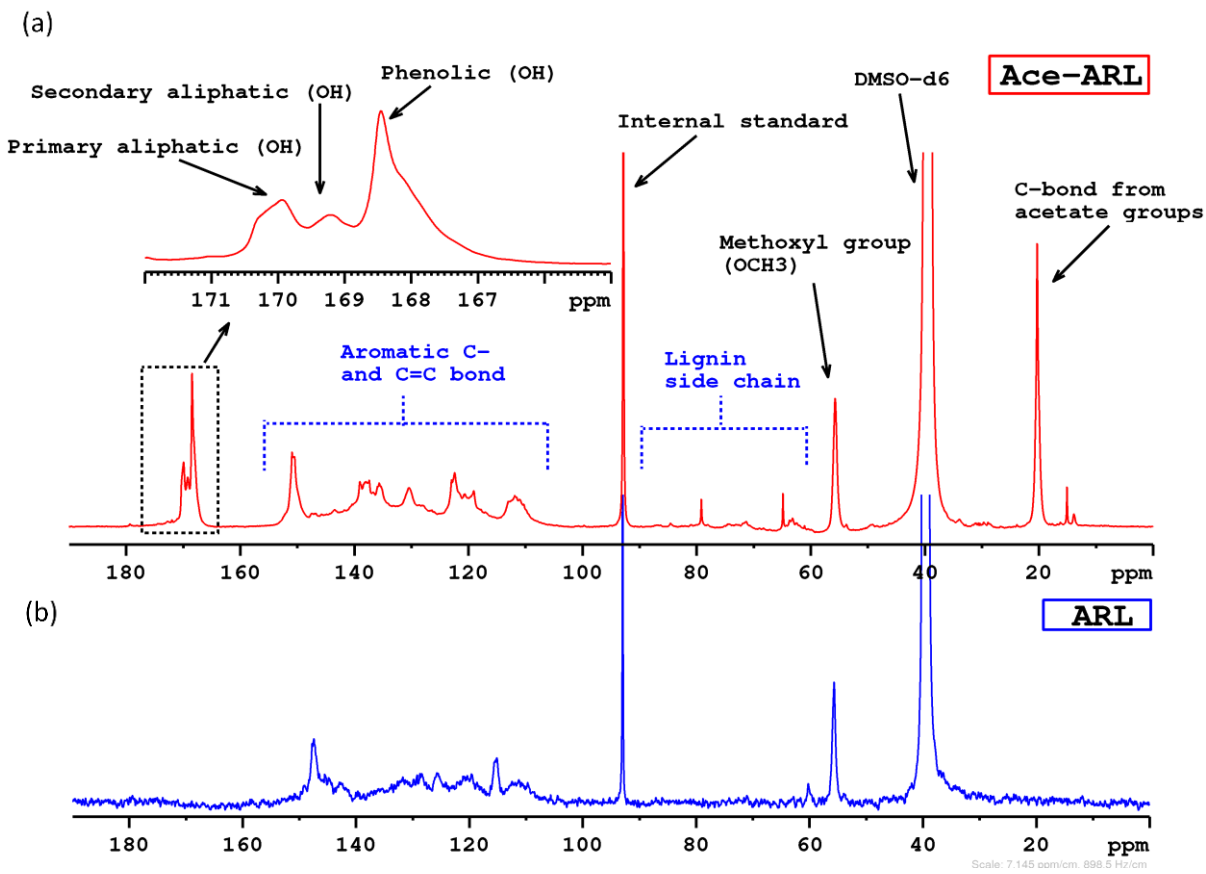

Figure 4.23 ^{13}C NMR of (a) as-received (ARL) and (b) acetylated lignin.

The spectrum for acetylated (Ace-ARL) lignin shows that upon derivatisation, it uncovers hidden features such as hydroxyl groups; these can be assigned and used for the quantification of aliphatic and phenolic hydroxyl (OH) groups. The assignments with integration of certain carbon moieties in the structure of lignin are shown in Figure 4.23 and Table 4.13. The chemical shift at 20 ppm is

attributed to the carbon in the methyl group (CH_3) which is directly attached to the carbonyl of the acetate group. The signal at 39.52 ppm corresponds to the solvent peak (DMSO). The chemical shift at 56 ppm is ascribed to the methoxyl (OMe) peak. The chemical shifts from 60-102 ppm is linked to aliphatic side chain including the signals corresponding to possible existence of low traces of polysaccharides. The weak signal close to 60 ppm is associated with Υ-CH_2 in aliphatic side region of structures that are linked with carbohydrates including hexoses and xylan (174). The chemical shift at 60 ppm could also be linked to the presence of coniferyl alcohol and dihydroconiferyl alcohol (387). The signal at 79-80 ppm region is linked to C_β-(H_β) of spirodienone structures in lignin (152). The chemical shift at 92 ppm corresponds to the internal standard (1,3,5- trioxane) which can be used for the quantification of lignin carbon moieties. There are signals with weak intensities between 102-98 ppm and this could be indicative of the presence of carbohydrates. This correlates well with the composition of BioChoice® lignin. Previously, researchers have reported the presence of small impurities of sugars in technical lignins (151, 155). The chemical shifts between 102-160 ppm are attributed to aromatic carbon moieties within the lignin structure. The characteristic peaks in acetylated lignin trace from 165-172 ppm are assigned to hydroxyl groups in lignin.

Table 4.13 Integration and assignment of ^{13}C NMR chemical shifts for acetylated as-received lignin (Ace-ALR).

Chemical Shift, δ (ppm)	Assignment	Number of carbon atoms per aromatic group Ace-ARL
171.8-165.6	Total OH groups	1.29
171.8-169.6	Primary Aliphatic	0.34
169.6-168.9	Secondary Aliphatic	0.20
168.9-165.6	Phenolic	0.75
163.0-102.0	Aromatic carbons	6.12
90.0-58.5	Aliphatic carbon side chain or C-O	0.46
58.0-54.0	Methoxyl (OMe) group	0.80

The most noticeable difference is in the ratio of hydroxyl groups in phenolic and aliphatic region. This ratio correlates well with the FTIR spectroscopy results for acetylated lignin which also shows high ratio of phenolic-to-aliphatic hydroxyl groups.

4.17 Derivation of the Empirical Formula for Lignin

The elemental analysis of as-received lignin (ARL) was used to derive the empirical formula for lignin as shown in Table 4.14. The empirical formula was calculated based on C_9 lignin units which means that lignin contains nine carbons per methoxylated phenylpropane lignin unit. The methoxy content was determined through quantitative ^{13}C per aromatic ring assuming that the majority of the lignin units in softwood Kraft lignin are guaiacyl (G) lignin units. Therefore, one methoxy group per C_9 lignin unit, as estimated through ^{13}C NMR is 0.8. The empirical formula is then calculated on the basis of each elemental atomic mass ratio and then eventually normalised

to C_9 lignin unit. The double bond equivalence (DBE) was calculated according to the relation in Equation 11;

$$\text{DBE} = \frac{(2a+2)-b}{2} \qquad \text{Equation 11}$$

where "a" refers to carbon atom ratio and "b" corresponds to hydrogen atom ratio in the C9-formula. The DBE value yields the number of double bonds and reveals the presence of aromatic rings with the extent of interunit linkages in the lignin phenylpropanoid units. The DBE also refer to the degree of unsaturation which in this case suggests that Kraft lignin contains a moderate level of unsaturated bonds. The empirical formula for BioChoice ® lignin corresponds well with that reported in the literature (316, 388-390). The small discrepancies in elemental composition such as for hydrogen may be attributed to the presence of impurities such as polysaccharides.

Table 4.14 Empirical formula for C_9 lignin unit derived from elemental composition and methoxyl content as inferred via ^{13}C NMR.

Element	**Average (%)**	**Atomic Mass (M_w)**	**M_w ratio**	**OMe (per C_9)**	**Empirical Formula (C_9)**	**M_w per C_9 unit (g/mol)**	**DBE**
C	64.70	12.01	5.38	0.80	$C_9H_{9.5}S_{0.07}O_{2.96}(OCH_3)_{0.8}$	192.17	4.85
H	5.73	1.01	5.67				
S	1.40	32.06	0.044				
O	28.30	15.99	1.77				

4.18 Phosphorous Nuclear Magnetic Resonance Spectroscopy (^{31}P NMR) of Lignin

^{31}P NMR was used to quantify the OH moieties in the structure of lignin upon derivatisation via phosphorylation. The advantage of using ^{31}P NMR is that it allows better spacing of the chemical shifts for the quantification and identification of each of lignin-OH moiety including the lignin monomeric units. The internal standard, N-hydroxy-5-norbornene-2,3-dicarboximide, was used for the quantification of lignin moieties in as-received and fractionated lignin samples. The ^{31}P NMR spectra of ARL with specific lignin moieties is shown in Figure 4.24.

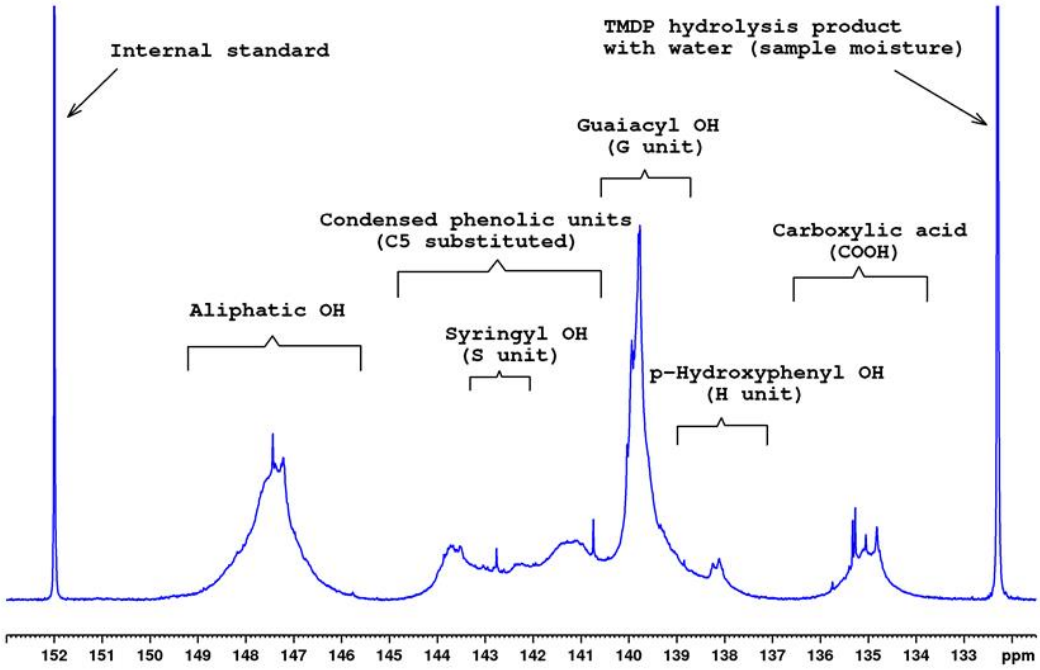

Figure 4.24 ^{31}P NMR of as-received lignin (ARL).

The OH moieties of each lignin unit (G, H and S) including the carboxylic acid, aliphatic (OH) and condensed phenolic units are labelled along with their respective chemical shifts (δ) are shown in Figure 4.24 and Table 4.15. The interunit ether linkages are not observed in the ^{31}P NMR spectra. The signal at 132.2 ppm is due the phosphorylating agent (TMDP) reacting with the moisture in the sample. The lignin OH moieties in the ^{31}P NMR spectra are in the range 134 -150 ppm. The chemical shifts between 136.4-133.6 ppm are related to the carboxylic acids. The signal at 134.8

ppm corresponds to the unconjugated carboxylic acids such as fatty acids. The signal at 135.06 ppm could be attributed to the conjugated carboxylic acids groups including benzoic acids or hydroxycinnamic acids and the derivates such as p-coumaric acid, ferulic acids, sinapic acids and vanillic acids (378). The chemical shift ranging from 138.5-137.6 ppm is ascribed to the presence of H-lignin units. The chemical shift ranging from 140.5-138.6 ppm is attributed to G-lignin moieties. The composition of H-lignin unit is reported to be comparatively low in-comparison to the G-lignin units in softwood Kraft lignin (103, 156, 163). This is found to be the case in the ^{31}P NMR spectra for as-received lignin. The chemical shift between 139-138 is attributed to the presence of catechol types structures (391). The peaks within 145.0-140.5 ppm are attributed to condensed C-5 substituted phenolic units including S-lignin units with their methoxylated substitution at the C-3 and C-5 positions. The peak signals with chemical shifts at 150.0-143.3 ppm and 151.9 ppm correspond to aliphatic hydroxyl groups and internal standard. In addition to the aliphatic moieties in lignin, some impurities such as sugar containing hydroxyl groups can also be derivatised upon phosphorylation and they exhibit signals in this chemical shift region (165, 309).

The integration of the internal standard (IS), N-hydroxy-5-norbornene-2,3-dicarboximide, was set at 1 because it has one hydroxyl group which was modified upon derivatisation. The concentration of the specific hydroxyl lignin moiety was measured relative to the peak area of the modified internal standard. The integration ranges with the associated peak assignments and the content of OH groups, c_{OH} (mmol/g in lignin) is listed in Table 4.15. These OH moieties were calculated using the Equation 12 (165, 304, 309);

$$c_{OH} = \frac{A c_{IS} V_{IS} P}{M_{IS} m_L} \qquad \text{Equation 12}$$

where A is peak area of the certain lignin moiety to be determined, the peak for IS is set as 1, c_{IS} refers to the concentration of the IS solution (21.5 mg/mL), V is volume of IS solution (0.1 mL), P

is the purity of IS (0.97), M_{IS} the molar mass of IS (179.19 g/mol) and m_L refers to the dried weight of lignin used (40 mg).

Table 4.15 Hydroxyl group content for lignin (mmol/g) calculated from the ^{31}P NMR spectra.

Chemical Shift, δ (ppm)	Assignment	OH (mmol/g)						
		ARL	ASL	ALR	ESL	ELR	1PSL	1PLR
150.0-143.3	Total aliphatic	1.46	1.08	1.51	0.64	0.88	0.58	0.88
145.0-140.5	Condensed phenolic units (C-5 substituted)	0.54	1.3	1.14	1.21	0.13	0.54	0.19
143.0-142.0	Syringyl (S) OH	0.07	0.26	0.27	0.04	0.02	0.06	0.01
140.5-138.6	Guaiacyl (G) OH	1.23	1.88	0.59	0.97	0.51	0.82	0.41
138.5-137.6	p-Hydroxyphenyl (H) unit	0.09	0.15	0.14	0.05	0.02	0.06	0.01
136.4-133.6	Carboxylic acid (COOH)	0.52	0.61	0.37	0.25	0.13	0.34	0.07
-	Total phenolic units	1.86	3.33	1.87	2.23	0.66	1.42	0.61
-	Phenolic to aliphatic ratio	1.27	3.08	1.15	3.39	0.75	2.45	0.69

The higher composition of phenolic units as comparted to the aliphatic groups in ARL correlates well with the FTIR and ^{13}C NMR results. The carboxylic acids content is found to be higher in soluble fractions compared to the insoluble lignin fractions. This is in agreement with data reported in the literature (102, 103, 332). The soluble fractions have noticeably higher composition of phenolic units, particularly of the predominant softwood G-lignin (guaiacyl) moieties, when compared to the insoluble lignin fractions. The composition of the G-lignin in the lignin fractions is found to be an influential factor in the char content as indicated in Figure 4.25 (103). With reference to Table 4.8 and Table 4.15, the soluble fractions with a higher G-lignin unit show a lower char content. This observed trend of decrease in the char content with increasing concentration of G-lignin moieties could be attributed to the decomposition of the methoxyl group

in G-lignin units at higher temperatures (144, 146). The decomposition process is said to yield catechol-type structures and this assumption is supported by the Py-GC-MS results discussed in Section 4.11 (392). It is evident through the Py-GC-MS results that the methoxylated G-lignin moieties start to decompose at high temperatures to yield phenolic and catechol-type structures (144, 146). Conversely, the insoluble lignin fractions possess a low concentration of G-lignin moieties, yet, they exhibit a higher char content as shown in Figure 4.25. This suggests that the higher number of G-lignin moieties are more susceptible to thermal devolatisation at high temperatures during heat-treatment (103).

The hydroxyl groups represent an important functional groups within the lignin structure (393). The hydroxyl content in lignin is thought to contribute to its reactivity and affects its physical properties, including the T_g (349, 394, 395). Soluble lignin fractions have a low concentration of aliphatic hydroxyl groups in comparison with the insoluble lignin fractions as seen in Table 4.15. The reduction in aliphatic hydroxyl groups and increase in phenolic hydroxyl groups correlates with data presented in the literature (102, 103, 332, 396). Conversely, Passoni *et al*., reported a high aliphatic hydroxyl group and low phenolic hydroxyl groups in the soluble fraction (101). However, as in the current study, the decreased aliphatic hydroxyl groups in the soluble fractions could aid in reducing the intermolecular hydrogen bonding interactions (103, 348). This in turn could increase molecular motion leading to a lower T_g systems (103, 347). It is also reported that the introduction of Cγ-hydroxyl groups in the aliphatic side chain significantly increases the T_g of lignin (397). Therefore, the insoluble fractions and as-received lignin show higher aliphatic hydroxyl groups with increased T_gs in comparison to soluble fractions. This implies that the functional groups in lignin and their composition play a critical role in its thermal properties and its viability to act as a potential precursor for the production of carbon fibre (186).

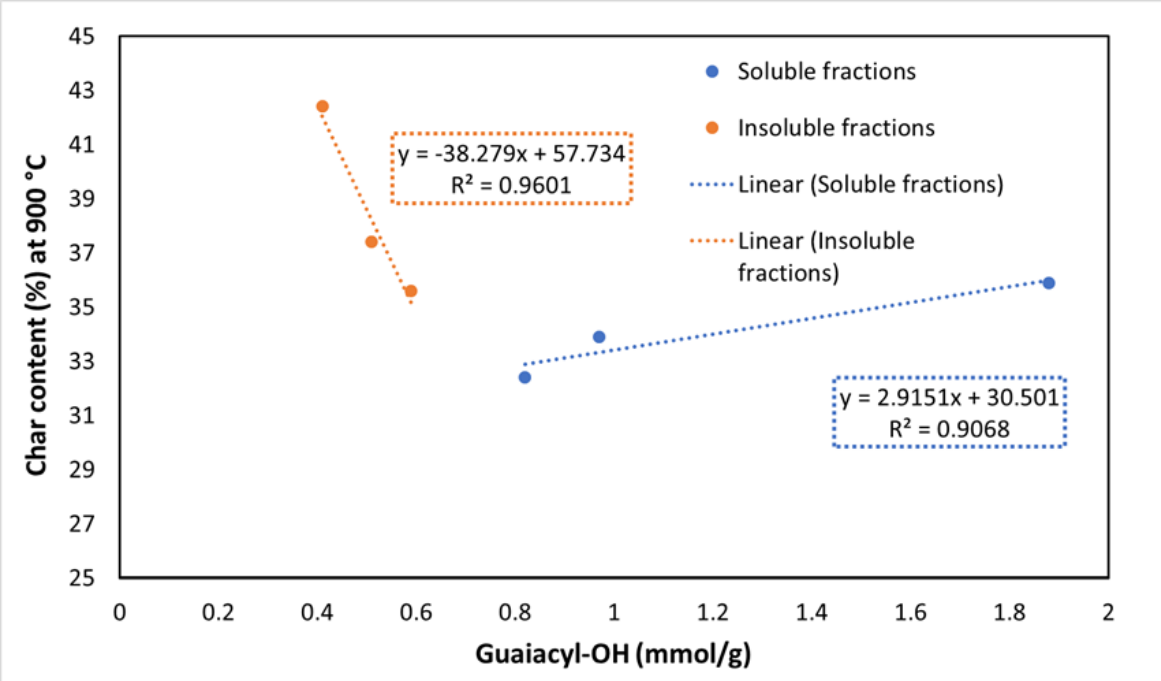

Figure 4.25 Plot the guaiacyl (G) lignin moieties concentration against the char content for the soluble and insoluble lignin fractions. The linear regression equations have been included for the two classes of materials.

4.19 Structural Evaluation of Lignin

The chemical structures for softwood Kraft lignin (ARL) are shown in Figure 4.26. These lignin moieties are confirmed through Py-GC-MS analysis and some of the structural features were also be detected through ^{31}P NMR, ^{1}H NMR and UV/Vis spectroscopy in the current study. For example, the catechol structures which are noticeable though Py-GC-MS analysis are also detected via ^{31}P NMR spectroscopy. Similarly, stilbene is detected by Py-GC-MS was also observed as small peaks using ^{1}H NMR spectroscopy. The presence of vanillic acid is seen clearly in the Py-GC-MS data and also by UV/Vis and ^{31}P NMR analysis. The presence of trace concentrations of hydroxycinnamic acids derivatives was also observed using these analytical techniques.

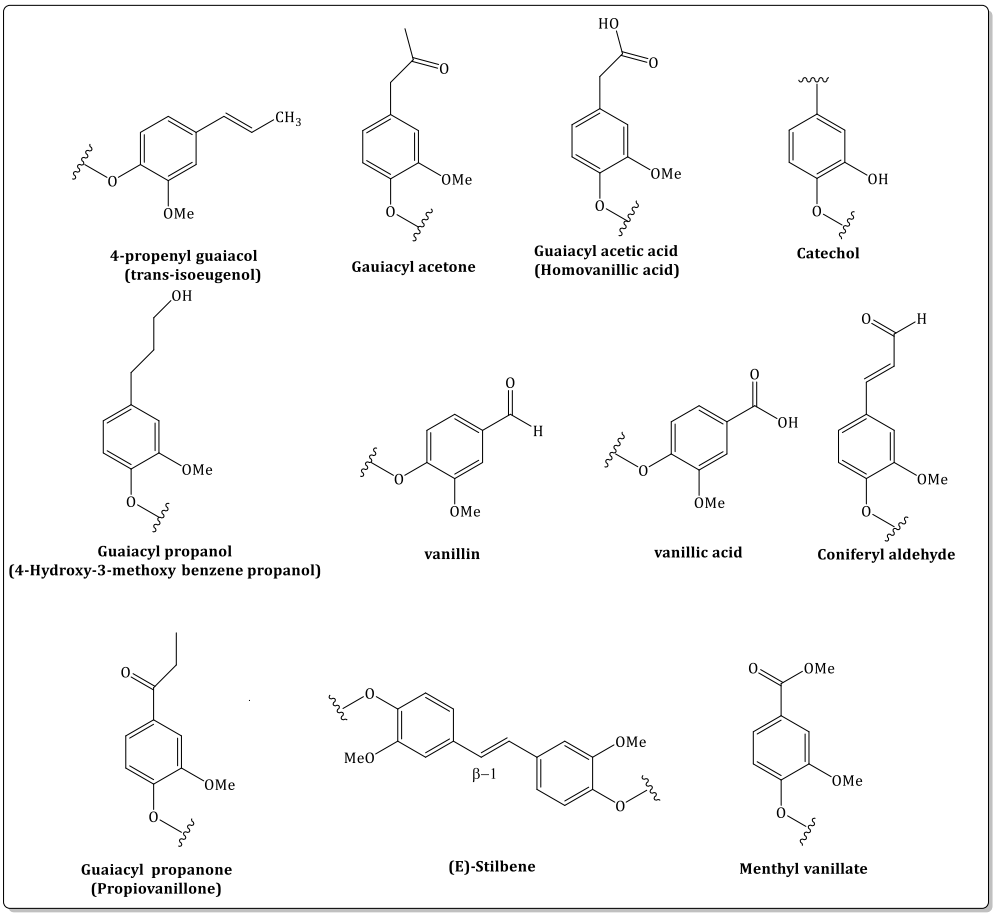

Figure 4.26 The structural components of lignin moieties as identified by PY-GC-MS, ^{31}P NMR, ^{1}H NMR and UV/Vis.

The structural elucidation of macro-molecules like lignin using 1D-nuclear magnetic spectroscopic resonance analysis is difficult due to the aforementioned reasons of cross-coupling, overlapping of signals at short chemical shift range and proton splitting. 2D-NMR techniques are employed to overcome these challenges of signal assignment for the specific lignin moieties specifically for lignin interunit linkages and side chain. The structure of the moieties in lignin shown in Figure 4.27 were compiled from the literature using ^{1}H NMR and ^{13}C NMR in relation to the 2-D NMR used for structural elucidation (151, 152, 163, 164, 174, 386, 387).

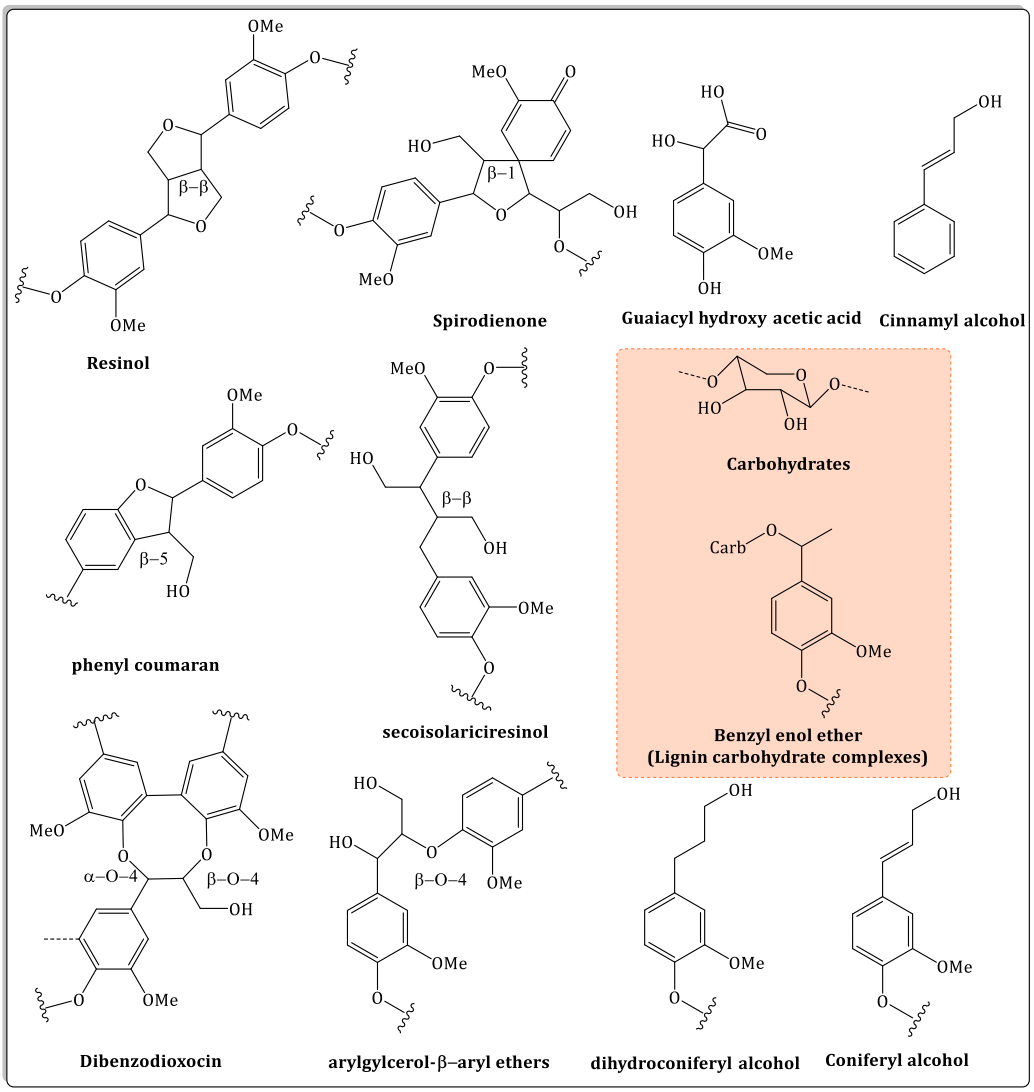

Figure 4.27 The structural moieties in lignin compiled from the literature where ^{1}H NMR and ^{13}C NMR in relation with 2-D NMR was used (151, 152, 163, 164, 174, 386, 387).

The assignment of the structural moieties in lignin is presented in Figure 4.27 which also indicates the presence of dominant β-O-4 linkages in softwood Kraft lignin. The presence of carbohydrates (sugars) was confirmed in the earlier sections and their possible structural configuration with benzol enol ether is ascribed according to the data reported in the literature (163).

The structural features of the monomeric units in lignin including derivatives of hydroxycinnamic acid and C-5 substituted condensed structures are shown in Figure 4.28. These were largely identified by ^{31}P NMR. The presence of carboxylic structural moieties was also detected using ^{13}C NMR, ^{1}H NMR and UV/Vis spectroscopy. The monomeric structural units of lignin (S, G and H-lignin units) exhibit distinctive peaks in the ^{31}P NMR spectra along with the presence of hydroxycinnamic acid derivatives and C-5 structure condensed structures. The ^{13}C NMR spectra shows the presence of G-lignin and H-lignin units. UV/Vis spectroscopy clearly indicates the presence of G-lignin moieties and hydroxycinnamic acid derivatives. The G-lignin and S-lignin units are characteristics peaks which originate from the depolymerised of lignin during pyrolysis as observed in the Py-GC-MS results.

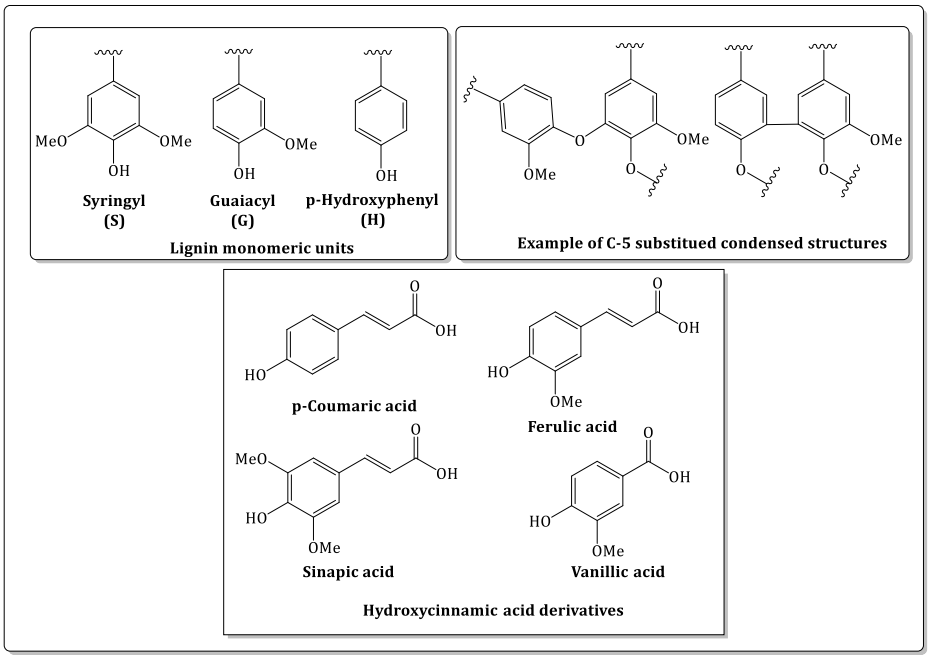

Figure 4.28 The structural moieties in the lignin as identified by ^{31}P NMR spectroscopy including ^{13}C NMR, ^{1}H NMR and UV/Vis.

4.20 Summary

The findings reported in this chapter signifies that the pre-treatment of lignin using acid washing and solvent fractionation can reduce the inorganic content. The influence of solvents fractionation on the thermal and structural properties of lignin were also discussed. The soluble fractions were found to exhibit lower molecular weight distributions with a lower T_g (122-146 °C) and reduced char content (32-36%) when compared to the insoluble fractions where the T_gs and char content were in the range 181-210 °C and 37-42% respectively. The soluble fractions tend to have higher phenolic-to-aliphatic lignin moieties where the concentrations of G-lignin units were prominent. The structural characteristics of as-received lignin revealed the presence of impurities such as polysaccharides which could be separated upon solvent fractionation. The conclusions reached in this chapter were instrumental in developing the processing conditions for electro-spinning and carbonising lignin fibres. Aspects of electro-spinning and carbonisation are discussed in Chapter 5.

Chapter 5 Electro-spinning and Carbonisation of Lignin Fibres

5.1 Optimising the Electro-spinning Parameters

The electro-spinning of a polymer solution, the resulting fibre morphology and the diameter are greatly influenced by a number of process parameters. For example, molecular weight of the polymer, viscosity of the solution, concentration, volatility of solvents/solution, electrical conductivity and surface tension. Electro-spinning parameter include the applied voltage, spinneret/needle diameter, distance between the spinneret and the collector and the flow rate of the polymer solution in conjunction with the ambient temperature and humidity (67, 254, 255, 258-260, 398, 399). A detailed insight into the electro-spinning processing conditions is presented in the literature review (Section 2.6). In order to facilitate the electro-spinning of lignin solutions, a host of polymer additives or polymer blends have been used with lignin (67, 182-184, 270, 271, 273, 276, 281, 285). Low molecular-weight additives act as plasticiser and high molecular-weight polymer blends aid in controlling the elasticity of the polymeric solution during electro-spinning (67, 277, 399, 400).

In the current research, a novel approach was adopted for electro-spinning lignin without the use of any synthetic polymer solutions. Instead, solvent-soluble fractions of lignin with different molecular weights were utilised for electro-spinning. A combination of high and low-molecular weight components of the soluble lignin fraction was used. In other words, an acetone-soluble fraction (ASL) and ethanol-soluble fraction (ESL) were solvent-blended with a composition of 95% ASL and 5% ESL (95 ASL-5 ESL) in an acetone/DMSO binary solvent. In order to identify the optimum conditions for electro-spinning, the concentration of the lignin solutions was varied as summarised in Table 5.1. The viscosity and electrical conductivity of different lignin solution concentrations (95AFL-5ESL) are also compiled in Table 5.1. The viscosity and electrical conductivity of the solution was observed to increase with the total concentration of the polymer.

Table 5.1 The viscosity and electrical conductivity of the concentrations of lignin solutions (ASL-ESL) used in the electrospinning experiments.

Experiment number	Total polymer concentration (wt%)	Viscosity (Pa.s)	Electrical conductivity (Sm^{-1}) x 10^{-4}
1	48.2 (2.5 g in 3 ml)	0.17	1.71
2	50.4 (2.5 g in 2.75 ml)	0.22	1.97
3	52.8 (2.5 g in 2.5 ml)	0.42	2.46
4	55.4 (2.5 g in 2.25 ml)	1.13	3.31

The results presented in Figure 5.1 indicate that the solution concentration is an influential parameter in controlling the fibre morphology. The SEM micrographs for experiment 1 and 2 are listed as (a-b) and (c-d), respectively in Figure 5.1 (a-d). It was observed that in experiments 1 and 2, non-continuous fibres were produced. This was mainly attributed to the low viscosity of the polymer solution which caused an intermittent spraying of the solution alongside with the production of fibres during electro-spinning. Figure 5.1 (a-b) also show the effect of low polymer concentration on the fibre morphology where large patches of solvent are observed along with beaded electro-spun fibres. Figure 5.1 (c-d) shows SEM micrographs of the beaded fibre morphology with considerably fewer solvent patches; this correspond to an increase in the polymer concentration. It was reported that viscoelastic property and the surface tension of the solution are the main factors responsible for the formation of beaded lignin fibres (277, 401).

Continuous fibre production was observed in the case of experiments 3 and 4 during electro-spinning where the polymer solution concentrations were 52.8% and 55.4 respectively. Figure 5.1(e-f) shows the fibre morphology resulting from experiment 3 where a smooth surface is seen with a relatively circular fibre cross-section. The diameter of the electro-spun fibre was in the range of 1-2 μm. Increasing the concentration of the polymer solution from 52.8% to 55.4%

resulted in a much higher viscosity which in turn lead to fibre fusion as shown in Figure 5.1 (g-h). This may be attributed to incomplete solvent evaporation from their fibre core or the formation of a skin at the fibre surface (401). The fibre diameter distribution and mean fibre diameter was also seen to increase with an increasing concentration from 52.8% to 55.4%.

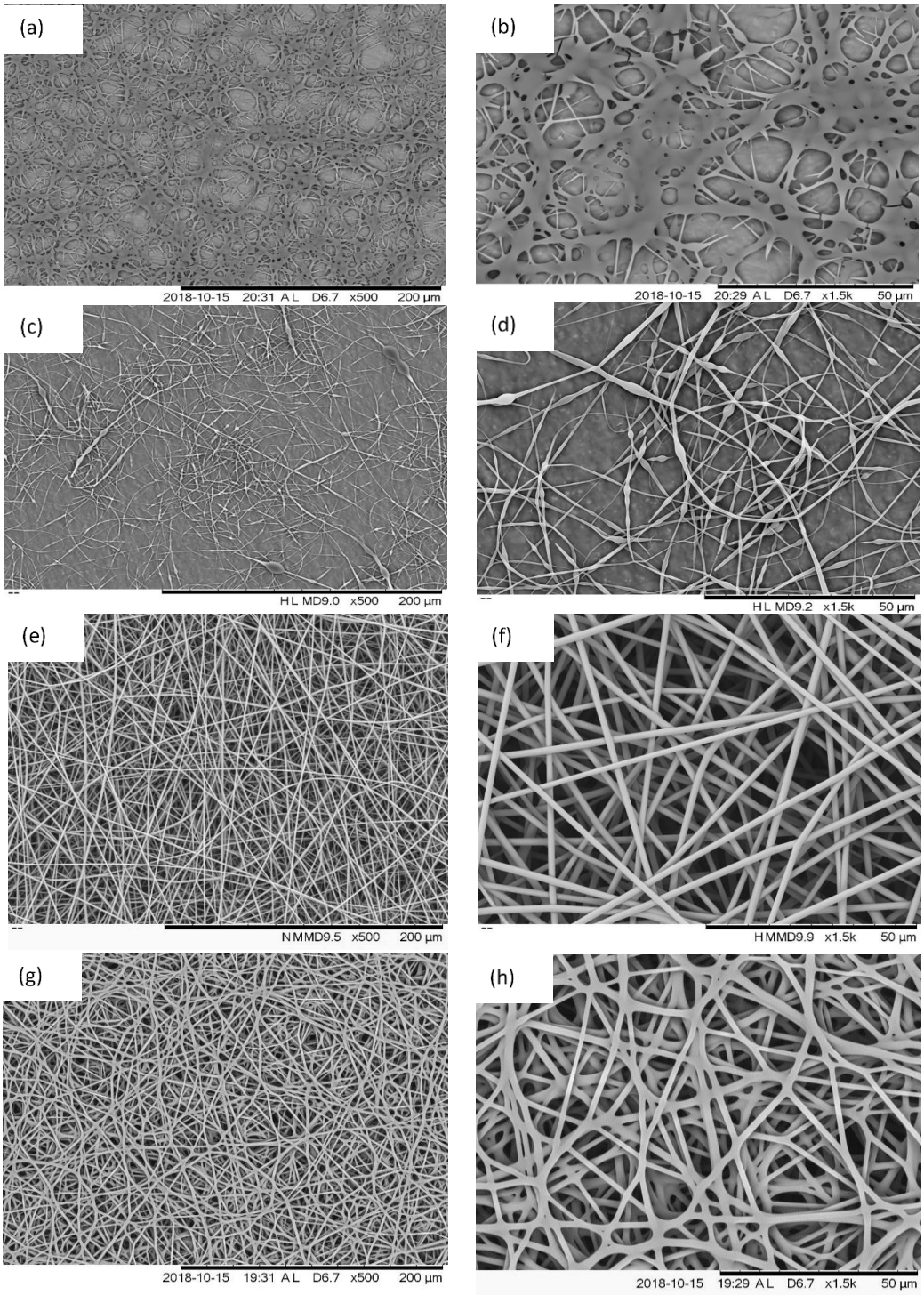

Figure 5.1 (a-g) SEM micrographs of electro-spun lignin fibres: (a-b) shows solvent rich morphology for experiment 1 (Table 5.1) with the lowest polymer concentration; (c-d) shows morphology of beaded-fibres emanating from experiment 2; (e-f) shows smooth and circular fibre morphology and this corresponds to experiment 3 with a viscosity of 0.42 Pa.s; and (c-d) shows morphology of fused fibres from experiment 4.

On inspecting Figure 5.1 (e-f) and Figure 5.2 (a-f), these suggest that a concentration of 52.8 wt% (experiment 3) produces fibres with smooth, circular and void-free morphology. This conclusion was reached after inspecting the surface and transverse sections of several individual SEM micrographs. Transverse sections of the fibres electro-spun from the 52.8 wt% total polymer concentration are shown in Figure 5.2 (a-f). With reference to the transverse sections, the maximum and minimum lengths of the cross-section were measured, and the data suggests that the majority of the fibres are circular.

In the above-mentioned experiments, the fibres were spun on to a flat plate collector and a schematic illustration of electro-spinning setup was shown in Section 3.7.3. A macroscopic image of the deposition area of the electro-spun lignin is shown in Figure 5.2 where the distance between the tip of the needle and the ground collector plate was 12 cm, and the applied voltage was 12 kV. The pale brownish fibres were deposited over a diameter of 3-4 cm. The fibres within this area were orientated randomly. Figure 5.2 (b-f) show representative micrographs for the 52.8% total polymer concentration where the fibres are unfused and orientated randomly. Figure 5.2 (e-f) shows high-magnification SEM micrographs for the transverse section where it can be seen the fibres void-free and with a smooth surface.

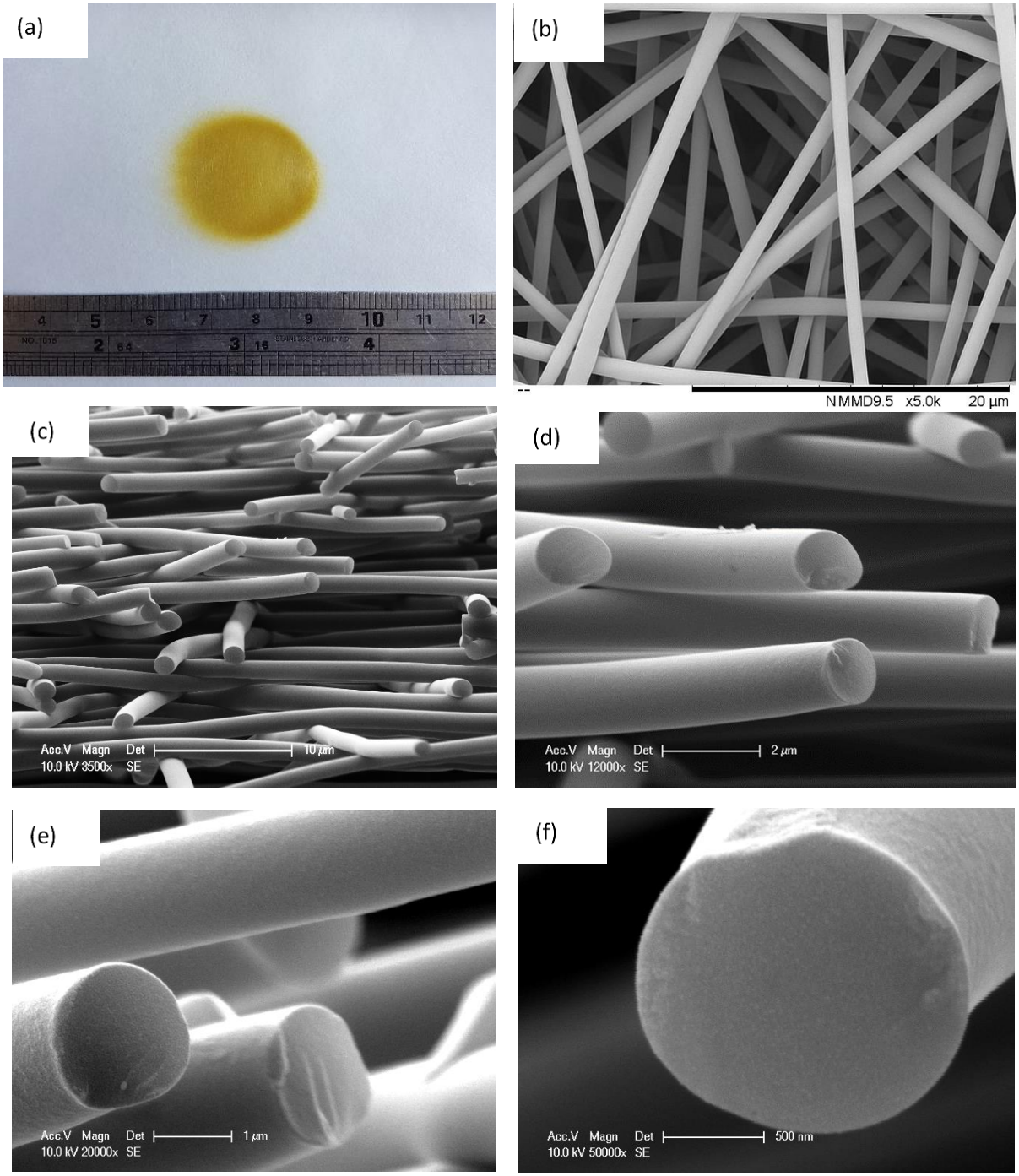

Figure 5.2 (a-f) Electro-spun lignin fibres using 95ASL–5ESL in acetone/DMSO: (a) macroscopic appearance of the deposition area (randomly oriented fibres); and (b-f) magnified SEM micrograph of fibres produced using the 52.8 wt% total polymer solution concentration.

The electro-spinning setup for obtaining unidirectional alignment of the fibres was illustrated in Section 3.7.3 where a modified parallel-edged electrode method was used. A macroscopic image of the parallel-edge electrode setup showing the aligned fibres is shown in Figure 5.3 (a). In contrast to Figure 5.2 (a) the fibres appear parallel. It is clear from Figure 5.3 (a) that there is considerable fibre deposition around the electrode and the top of graphite surface. This implies that the whipping of the polymer jet during electro-spinning results in significant deposition of the nano-fibres at the electrodes with intermittent deposition between the electrodes. Although this observation needs further investigation, it was not possible to pursue this in the current study.

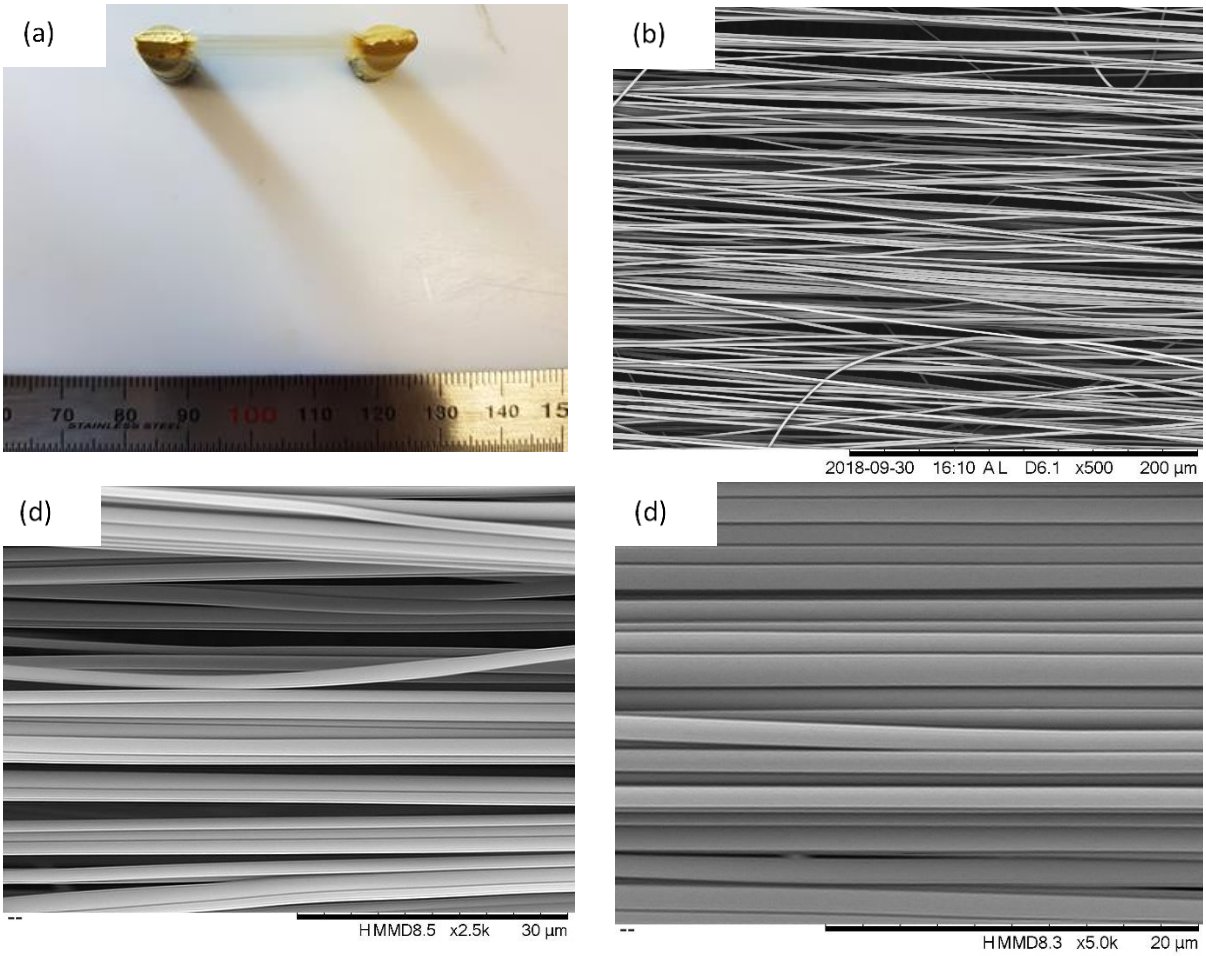

Figure 5.3 (a-d) Modified (a) parallel plate collector for alignment with SEM images (b) x500, (c) x2500 and (d) x5000 magnifications.

Higher magnification images of the electro-spun fibres from Figure 5.3 (a) are presented in Figure 5.3 (b-d). Figure 5.3 (b) indicates that the fibres are aligned within 0-10 degrees. The distribution of orientation for aligned electro-spun fibre is shown in Figure 5.4. On inspecting Figure 5.3 (b) there is a fair volume of meandering fibres in the plane of the paper and in the through-thickness directions. This is probably due to the nature of the whipping action within and between the two graphite electrodes. Nevertheless, the micrographs shown in Figure 5.3 (c-d) shown that fibres diameters are in the range 0.9-1.6 μm and that the fibres are not fused.

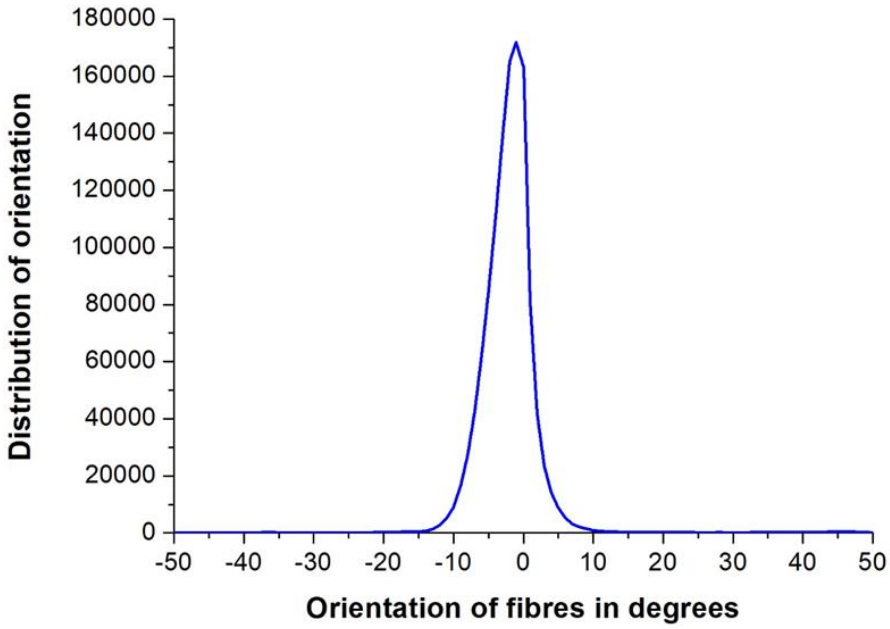

Figure 5.4 Orientation of the aligned 95ASL-5ESL electro-spun lignin fibres.

The DSC traces for the as-spun ASL-ESL lignin fibre and those dried in a vacuum oven at 140 °C for 6 hours are shown in Figure 5.5 (a-b). With reference to Figure 5.5 (a), the first heating scan shows a broad endothermic peak which could be due to the evaporation of solvents used for blending (acetone/DMSO) and absorbed moisture from the atmosphere or due to the presence of low-molecular weight volatiles in the lignin (318, 323, 325). The endothermic peak area in first heating of as-spun fibre was 58.5 J/g which was reduced to 23.8 J/g upon drying under vacuum at 140 °C for 6 hours. The presence of endothermic peak as shown in Figure 5.5 (b) for vacuum dried lignin fibre even after dying at 140 °C could be attributed the residual solvent (DMSO) which has a boiling point of approximately 189 °C or may be due to absorbed moisture. The noise on the first heating scan for vacuum-dried lignin could be due to the fact that the holes on crimped DSC top-lid may have been blocked and this may have resulted in movement in the sample holder when the trapped gases escaped. In Figure 5.5 (a), heating scan 2 shows a single T_g which is indicative of a miscible polymer blend of 95ASL-5ESL (37, 186). In general, the glass transition of a fully-miscible blend is dependent on the composition of each material present in the binary blend. The glass transition temperatures for as-spun fibre in the 1st, 2nd and 3rd heating scans are 118.5 °C, 156 °C and 162.4 °C respectively. The glass transition temperature of the vacuum dried lignin fibres in 1st ,2nd and 3rd heating scans are 132.7 °C, 152.4 °C and 157.7 °C respectively. The ASL-ESL electro-spun lignin fibre dried under vacuum at 140 °C for 6 hours were analysed by SEM to observe the morphology.

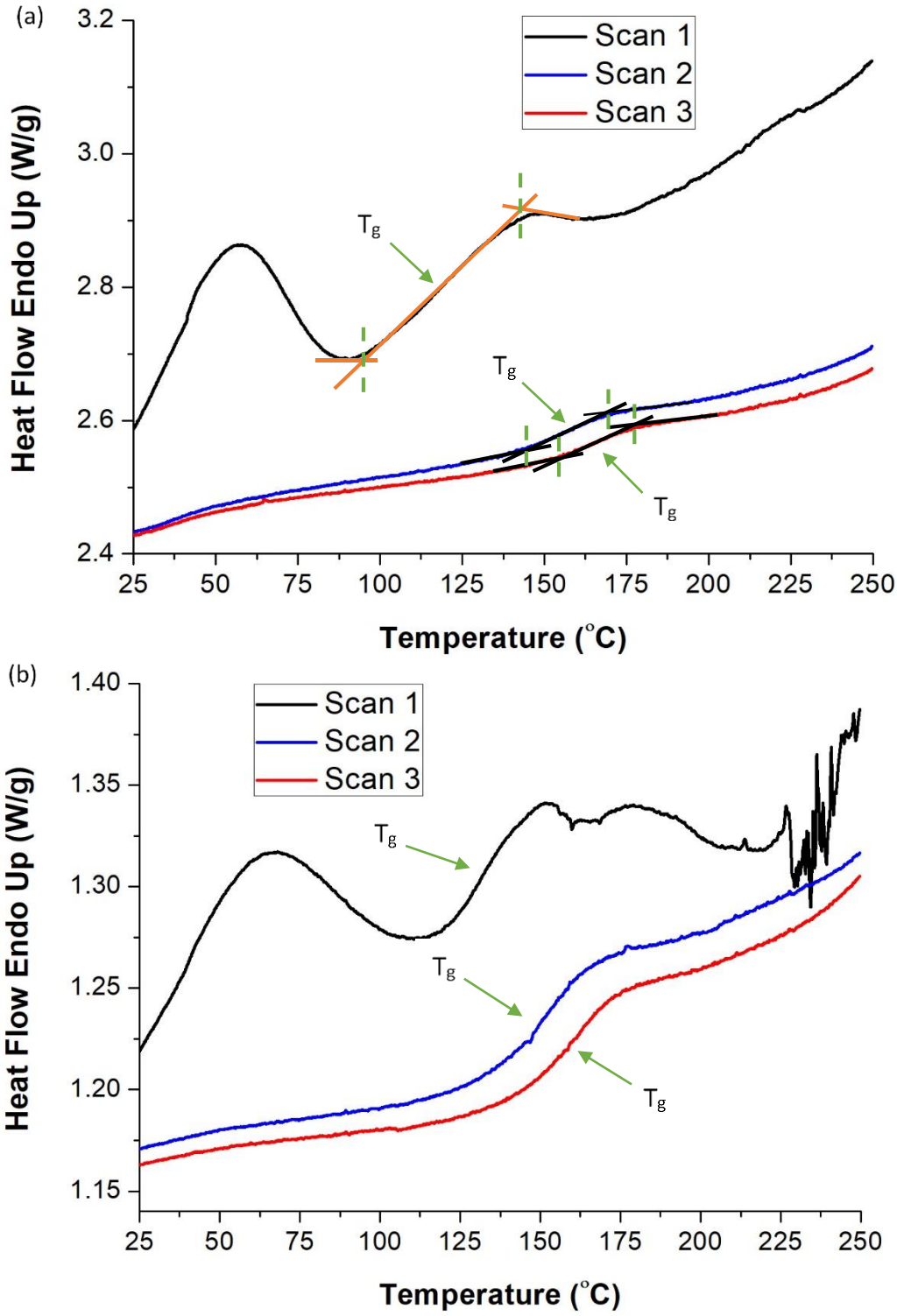

Figure 5.5 (a-b) DSC traces for electro-spun ASL-ESL lignin fibres: (a) as-spun, and (b) vacuum dried at 140 °C.

Figure 5.6 (a-b) shows SEM micrographs for vacuum-dried electro-spun ASL-ESL lignin fibre. The SEM micrographs showed an unfused and circular fibre morphology. The diameter distribution of the vacuum-dried fibres is in the range of 0.6-2.8 um. This indicates that drying lignin fibre in vacuum oven at 140 °C have no effect on the fibre diameter. The histogram plots for fibre diameter distribution are discussed in Section 5.3.1. Figure 5.6 (a-b) suggests that ASL-ESL lignin fibres dried close to the glass transition temperature in a vacuum oven, could maintained their form and shape. This preliminary result gave a good starting point for drying electro-spun lignin fibres under vacuum prior to thermo-stabilisation and carbonisation. However, this assumption was investigated in detail in the Section 5.2.

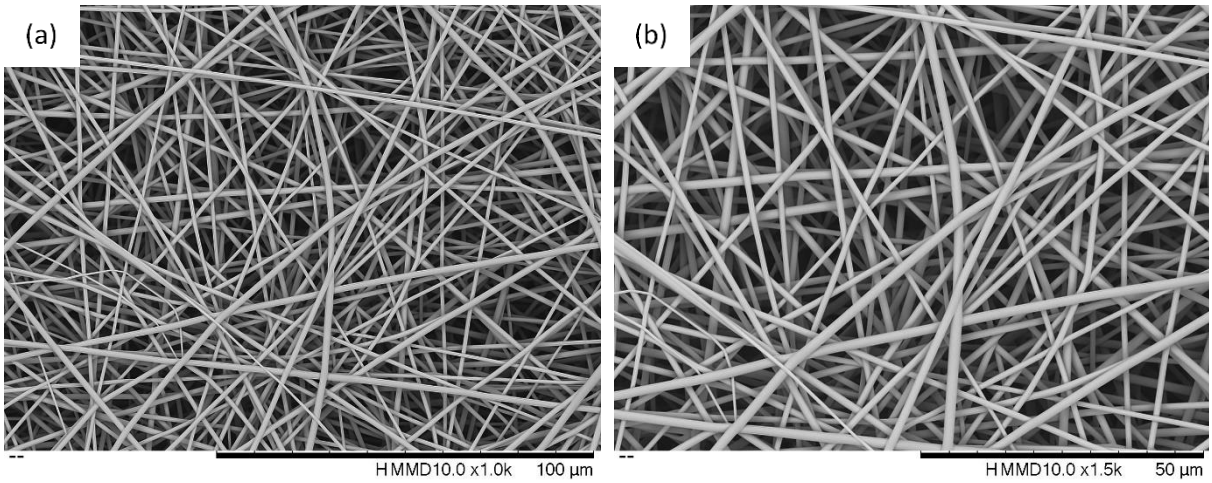

Figure 5.6 (a-b) SEM micrographs of electro-spun ASL-ESL lignin fibres that were dried under vacuum at 140 °C for 6 hours.

5.2 Thermo-stabilisation of BioChoice® Electro-Spun Lignin (95ASL-5ESL) Fibres

The electro-spun fibres contain solvents (acetone/DMSO) that needed to be removed and dried prior to thermal stabilisation in air. In order to investigate the conditions for the initial drying procedure and its effect on the fibre morphology, the electro-spun lignin fibres were dried in a vacuum oven at 100 °C, 120 °C, 140 °C, 160 °C, 180 °C and 200 °C for 6 hours. The solvent system used in the electro-spinning experiments was acetone and DMSO and the relevant properties for these solvents were presented in Section 2.4 (Table 2.4) including their boiling points. The selected drying temperatures lie below and above T_g of the ASL-ESL fibre (see DSC traces in Figure 5.5).

The experiments in the following section were carried out using the ASL-ESL lignin in acetone/DMSO. The total polymer concentration was 52.8%. The macroscopic appearance of the as-spun was shown previously in Figure 5.2 (a-f). The effect of the initial drying temperature on the macroscopic morphology of the electro-spun fibre are presented in two sets; namely, Figure 5.7 (a-f) and Figure 5.8 (a-f).

Figure 5.7 (a-f) represent micrographs of the electro-spun fibres after treatment in the vacuum oven at 100 °C, 120 °C and 140 °C for 6 hours. On comparing the morphology of the as-spun (Figure 5.2 a-f) and the fibres shown in Figure 5.7 (a-f), no prominent differences were observed visually. It can be concluded that for the initial drying at 100 °C, 120 °C and 140 °C for 6 hours, the observed changes in the morphology and diameter distribution was not obvious. This is possibly because the boiling point of DMSO is 189 °C. There was no obvious evidence to indicate fibre fusion.

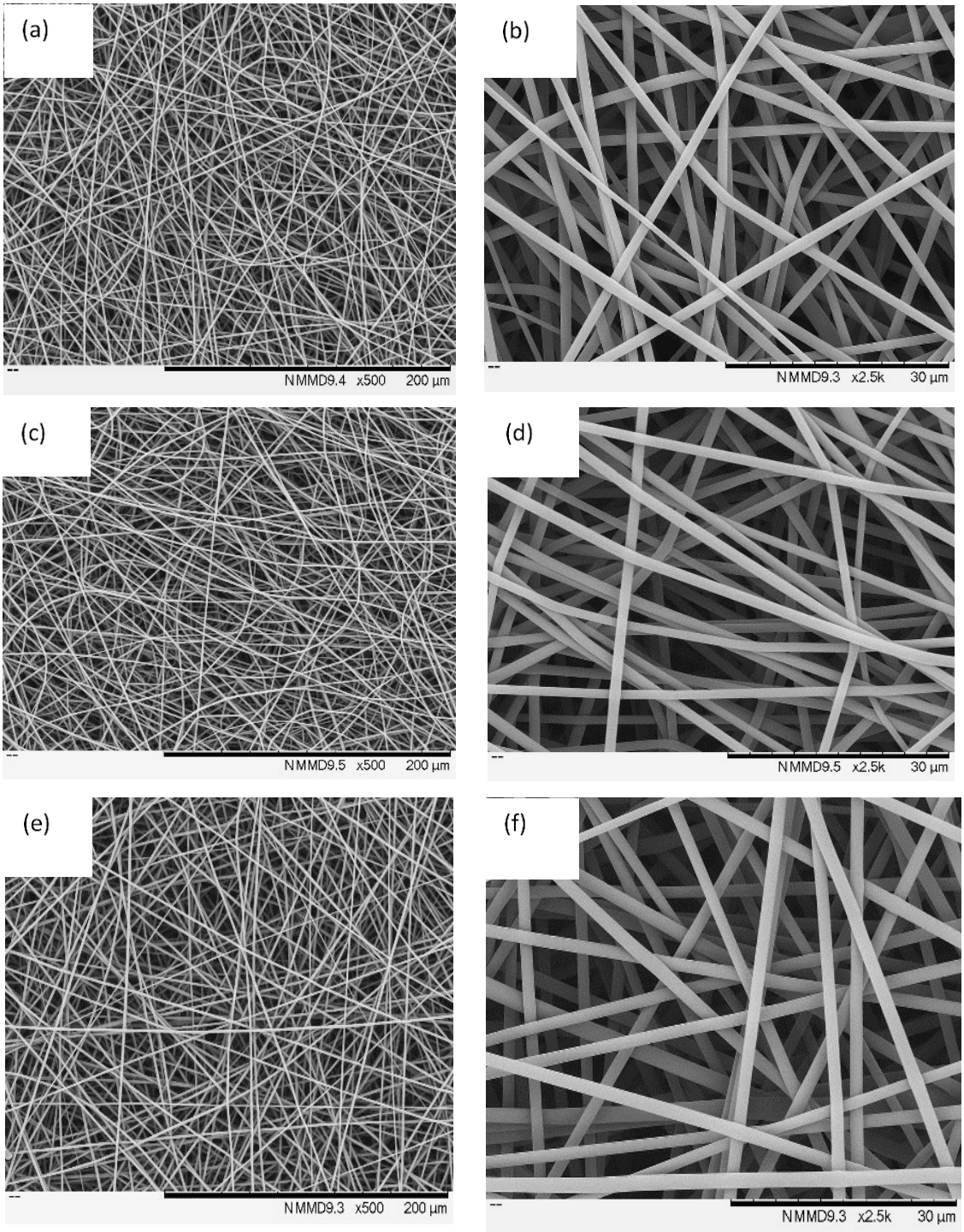

Figure 5.7 (a-f) Micrographs showing the macroscopic morphology of the electro-spun ASL-ESL lignin fibre where the initial drying was carried out in a vacuum oven at: (a-b) 100 °C; (c-d) 120 °C; and (e-f) 140 °C respectively.

The electro-spun fibres dried at 160 °C, 180 °C and 200 °C show a distinct change in fibre morphology as shown in Figure 5.8 (a-f) where significant fibre fusion is observed at 160 °C and 180 °C (see Figure 5.8 (a-b and c-d)). However, as seen in Figure 5.8 (e-f), on when the electro-spun fibres were treated at 200 °C, the fibres were fused completely.

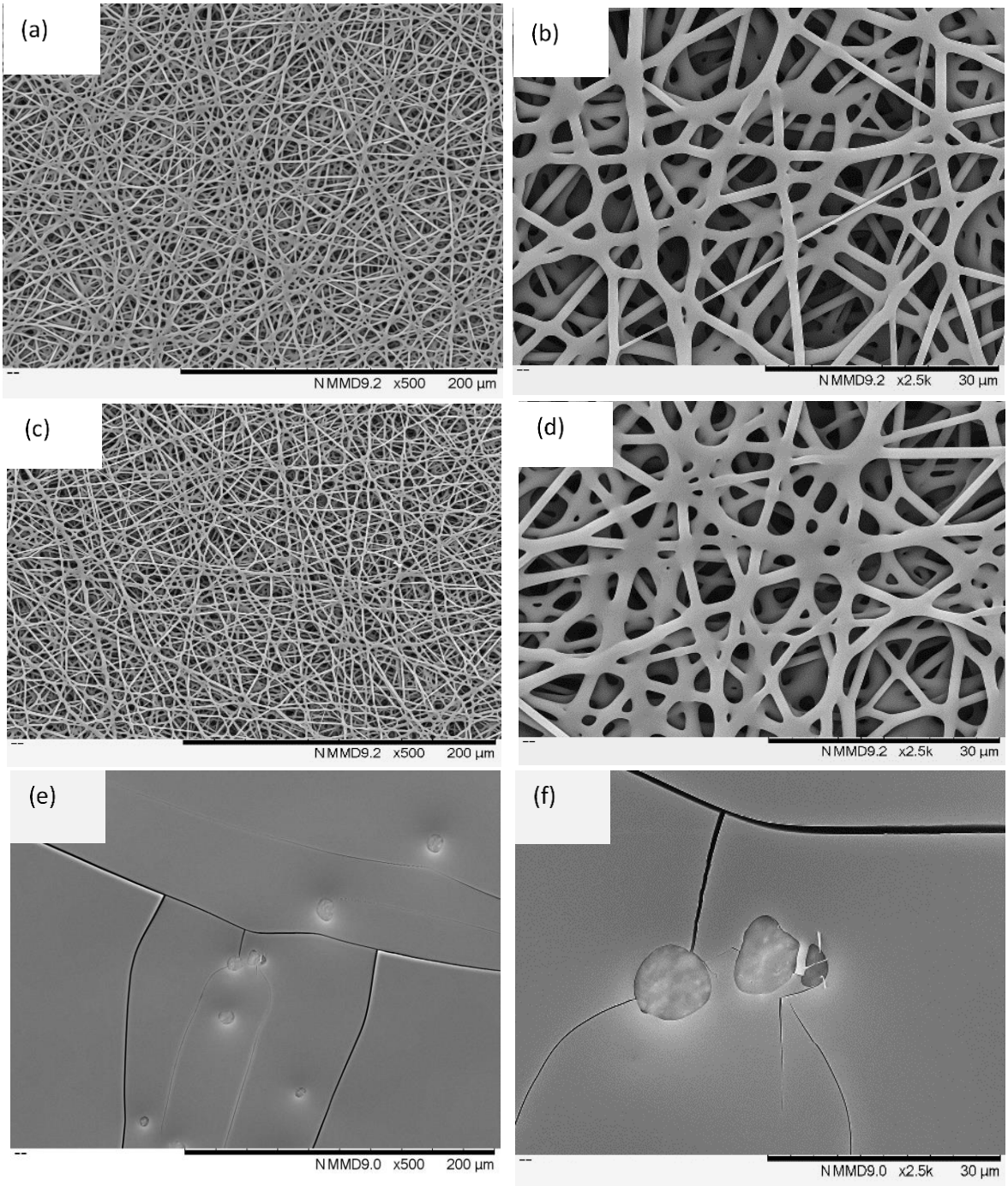

Figure 5.8 (a-f) Micrographs of electro-spun lignin fibres (95 ASL-5 ESL)- that were subjected to drying in a vacuum oven for 6 hours at: (a-b) 160 °C; (c-d) 180 °C; and (e-f) 200 °C respectively.

In the context of fibre formation and the conversion of lignin fibres to graphitic reinforcements, fibre fusion is an undesirable feature. Fibre fusion can be brought about by a number of factors including the following:

(i) Solvent-rich preforms: Solution-based electro-spinning dictates the need for a solvent. If during electrospinning, the solvent is incapable of evaporating from the jet, the formation of "skin" on the fibre will not be possible. In the current case, acetone/DMSO was used and it is reasonable to assume that some of the acetone would have evaporated partially before the fibre is deposited on the ground collector-plate. This can account for the circular and unfused profile of the as-spun (ASL-ESL) lignin fibre. However, DMSO has a boiling point of 189 °C and since the polymer content is approximately 52.8%, a significant volume of the DMSO is likely to be retained in the fibre. This may lead to the sagging of the fibres as function of storage time, fibre diameter (weight of the fibre resting on the substrate) and temperature. If a skin is present on the fibre and depending on its thickness, the retention of the shape of the fibre is likely. It is not known if the surface energy of the substrate (aluminium foil in the current case) can have an influence on the sagging or spreading of a solvent-rich fibre. In other word, further studies should be undertaken on if storing the preforms on a low surface energy substrate would be advantageous.

(ii) The heating rate and the environment: When dealing with solvent-rich fibres, rapid heating can lead to collapse of the fibres and fusion. It can also result in void formation and disruption of the smooth surface texture. Although a relatively slow heating is preferred to enable the controlled evaporation of the solvent, it may not be practical or economical. It has been reported that a slow heating rate of approximately 0.06-2 °C/minute should be adopted to avoid fibre fusion (186, 222). The effect of heating rate on the glass transition and fibre morphology was discussed in Sections 2.6.1.1 and 2.6.1.3. With reference to the environment and heating to remove the solvents, it is proposed that the environment (vacuum, air, inert gas) can lead to different outcomes with regard to the fibre morphology and the retention of its circular cross-section. In the case of heating under a vacuum, the rate of application of the vacuum can have an effect. A rapid evacuation of the chamber can cause the fibres to sag if the solvent is volatilised rapidly. It can also create porosity in the fibres. Heating the as-spun

fibre in air or an inert gas can have consequences with regard to the fibre morphology. It is proposed that if the environment (air or an inert gas) can assist the heat transfer rate (a function of the thermal conductivity of the gas), it will assist in the growth of the skin-layer, then the extent of fibre fusion can be minimised. This aspect is discussed in detail in the next section.

(iii) Inter-related parameters: In general, the heating rate and the rate of evacuation of the chamber of the vacuum oven are interrelated and so are the other parameters mentioned above. The parameters that are used for electro-spinning can also have a major influence on the fusion of fibres. For example, the temperature of the chamber, the relative humidity, the polymer concentration at the tip of the needle as a function of the electro-spinning time, the distance between the tip of the needle and the ground collector-plate, air turbulence, etc can contribute to the nature of the surface morphology and the properties and the solvent concentration in the fibres. Hence, it is difficult to attribute any parameter to the occurrence of fusion in electro-spun fibres because a number of the parameter are interrelated. Aspects relating to the surface energy and surface tension of the polymer/solvent system also need to be considered.

(iv) The glass transition temperature: The increase in the specific volume as polymer approaches and passes the T_g is a well-known phenomenon. Therefore, this volumetric expansion can lead to the fusion of fibres for a number of reasons, especially at cross-over points or where there is fibre-to-fibre contact. The increased segmental mobility in the fibre can enable inter-diffusion at the fibre-to-fibre contact points. This is readily apparent on inspecting Figure 5.8 (a-b, c-d and e-f) where increasing the initial drying temperature above 140 °C resulted in significant fibre fusion up to 180 °C and total fusion of the electro-spun fibres at 200 °C. This inter-diffusion will be influenced by the volume of solvent within the fibres and the T_g of the polymer, at the corresponding concentration of the solvent; the T_g will increase as the solvents are removed. The thickness of the skin of the fibres in this instance may not be a

factor because as the temperature is increased, the fibres will be dissolved by the solvent, primarily DMSO in this instance as the acetone would have evaporated. On the other hand, if the integrity and thickness of the skin on the fibre can be retained or increased as a function of temperature, for example by a cross-linking mechanism, then the probability of the circular cross-section of the fibres being retained is high.

The relative fibres diameter for heat treatments between 100 °C, 120 °C and 140 °C showed a negligible change in fibre diameter distribution. It can be seen that for the lignin fibres that were dried at 140 °C in the vacuum oven, showed no obvious change in fibre morphology. Therefore, 140 °C was chosen for drying the as-spun lignin fibre prior to thermo-stabilisation.

The thermo-stabilisation of pre-dried lignin fibres at 140 °C was investigated at 150 °C, 180 °C, 200 °C, 220 °C and 250 °C using compressed air or moisture-free nitrogen gas. These experiments were carried out in a tube furnace as described in Section 3.8.

Micrographs of the electro-spun lignin fibres, after drying at 140 °C, and subsequently heated to 150 °C, 180 °C and 200 °C in air and nitrogen are shown in Figure 5.9 (a-f). The relative fibre diameter of Figure 5.9, Figure 5.10 and Figure 5.25 shows that oxidative thermo-stabilisation led to a negligible change in fibre diameter and morphology (Figure 5.9 a-f) when temperature was increased from 150 °C to 200 °C. Conversely, the thermo-stabilisation in a nitrogen atmosphere resulted in fused fibres. The degree of the fibre fusion was observed to increase when the thermo-stabilisation in nitrogen was increased from 150 °C to 200 °C.

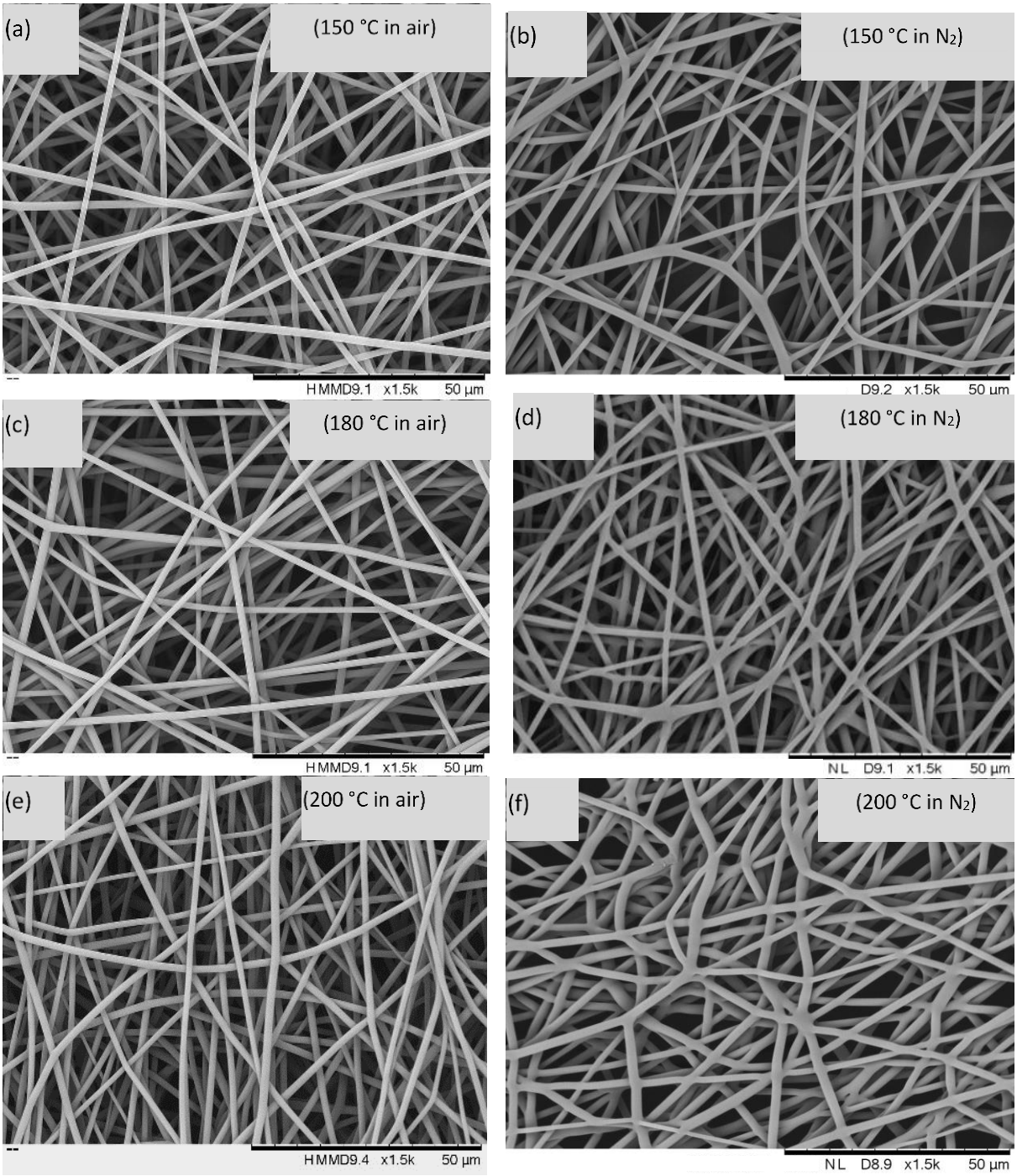

Figure 5.9 (a-f) Micrographs of electro-spun lignin fibres (95ASL-5ESL) that were previously dried at 140 °C in a vacuum oven and then thermo-stabilised in air or nitrogen at 150 °C, 180 °C and 200 °C.

Micrographs of the thermo-stabilised and dried lignin fibres at 220 °C and 250 °C in air and in nitrogen are shown in Figure 5.10 (a-d). It is clear from Figure 5.10 (a and c) and Figure 5.25 that the fibres were not fused when they were heated in air. Conversely, extensive fibre fusion and a deterioration in the desired fibre morphology is observed when the fibre were heated in nitrogen at 220 °C (see Figure 5.10 b); leading to near complete fusion of the fibres and a merger of the fibres to a flat mat at 250 °C (see Figure 5.10 d). Figure 5.10 (a and c) show that the fibres that were thermo-stabilised in air which retained their general shape and form up to 250 °C. Sections 5.2.1, 5.2.2, 5.2.3 and 5.2.4 presents a discussion on the characterisation techniques that were used to gain an insight into the observed change in the morphology of the electro-spun fibres when heat treated to 250 °C in an air or nitrogen atmosphere.

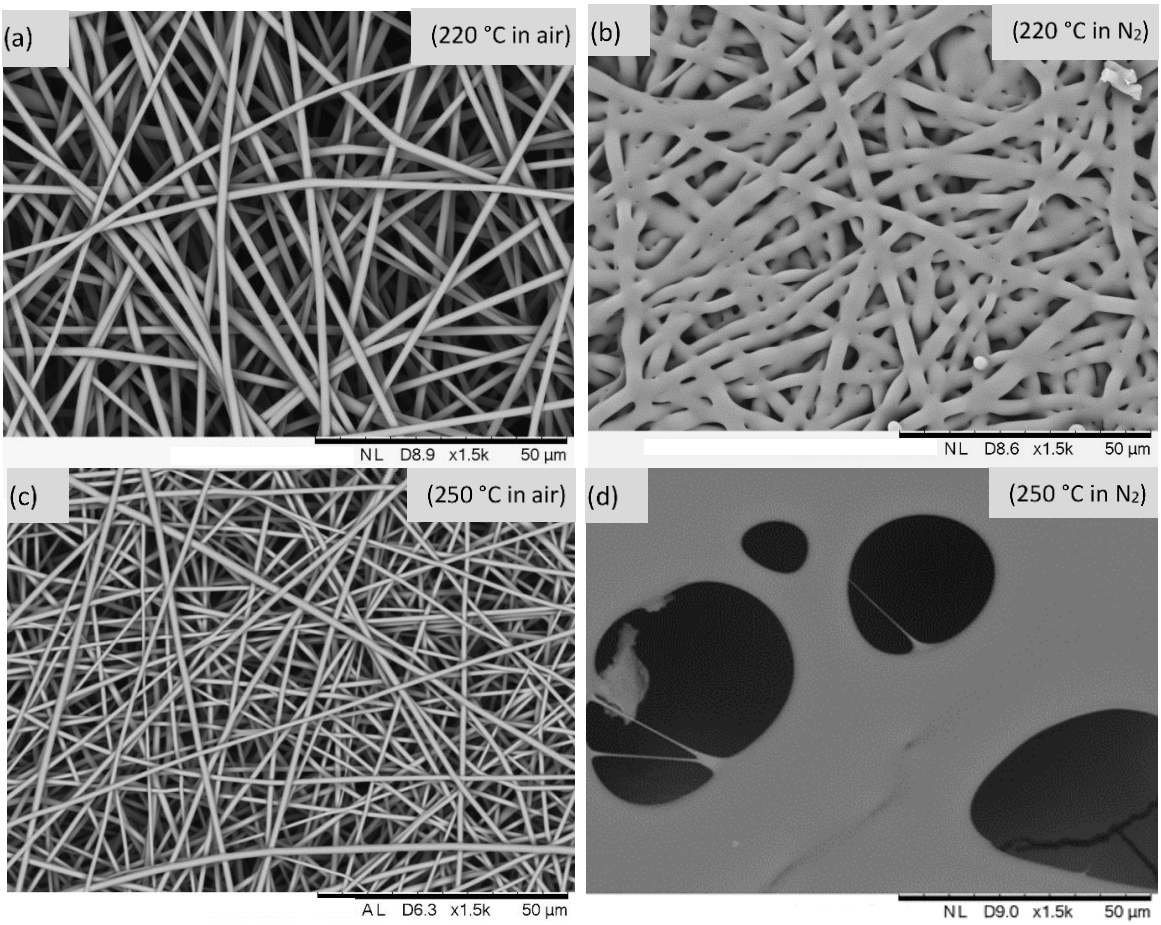

Figure 5.10 (a-d) Micrographs of thermo-stabilised electro-spun lignin fibres (95ASL-5ESL) in air or nitrogen at: (a and b) 220 °C; and (c and d) 250 °C respectively.

5.2.1 Elemental Analysis of Electro-spun Fibres from 95ASL-5ESL

The elemental analysis of as-spun, vacuum dried (140 °C) and thermo-stabilised lignin fibres at 250 °C in air or nitrogen is shown in Figure 5.11 and Table 5.2. Considering as-spun versus to 140 °C vacuum-dried fibres, the carbon content is seen to decrease. This is presumably due to the evaporation of solvents (acetone/DMSO) upon drying in a vacuum oven at 140 °C or it may be attributed to the loss of low-molecular weight volatiles components from the as-spun fibre. The hydrogen content was unchanged, however, the oxygen content showed a marginal increase and this is within the error of the measurement.

The most noticeable changes are observed during the thermo-stabilisation step in the following discussion, the comments are with reference to the vacuum dried fibres at 140 °C. The carbon content has increased significantly to 72% for the fibres that were heated in a nitrogen environment at 250 °C. A reduction in the carbon content is noticed upon thermo-stabilisation in air (59.9%) when compared to lignin fibre that were treated in nitrogen at 250 °C (72%). This is in agreement with that reported in the literature which are also discussed in Section 2.8 (146, 219, 285, 287).

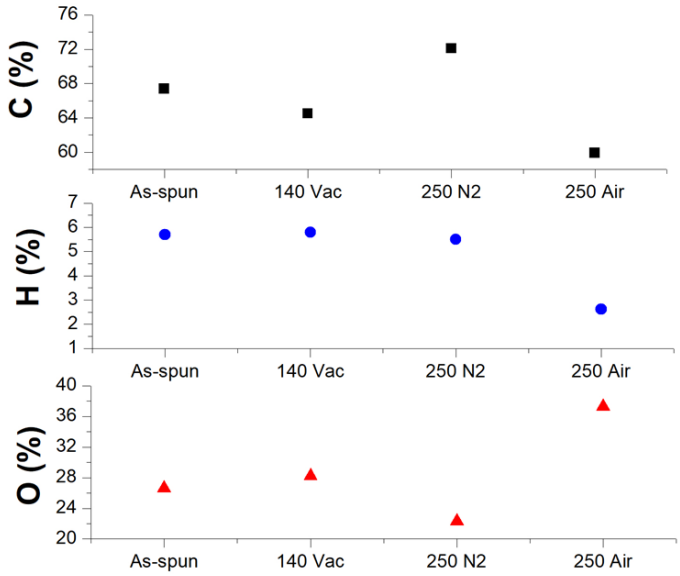

Figure 5.11 Elemental composition (carbon, hydrogen and oxygen) for electro-spun lignin fibres from 95ASL-5ESL.

A significant decrease in the hydrogen content is observed for the lignin fibres that were thermo-stabilised at 250 °C in air. This may be due to the cleavage of C-H or O-H bonds leading to the formation of free-radicals (146, 285). The increase in the oxygen content during thermo-stabilisation at 250 °C in air suggests that this promotes oxidation reactions which increase oxygen moieties in lignin and these could include carbonyl or carboxyl groups (269, 285, 287, 402, 403).

Table 5.2 Elemental analysis of 95ASL-5ESL electro-spun lignin fibres.

Samples	**Elemental analysis**		
	C	**H**	**O**
As-spun	67.4	5.7	26.6
Vacuum dried 140 °C	65.8	5.9	28.2
Thermo-stabilisation in N_2 at 250 °C	72	5.4	22.3
Thermo-stabilisation in air at 250 °C	59.9	2.63	37.3

5.2.2 Thermal Analysis of 95ASL-5ESL Electro-spun Lignin Fibres

5.2.2.1 Differential Scanning Calorimetry

DSC traces for the first heating scan for 95ASL-5ESL lignin fibres that were thermo-stabilised in air and nitrogen are shown in Figure 5.12 (a-b). This dataset represents the pre-dried (140 °C) lignin fibres that were subsequently thermo-stabilised at 150 °C, 180 °C, 200 °C, 220 °C and 250 °C. The first heating scan for the air and nitrogen thermo-stabilised lignin fibres in Figure 5.12 (a-b) shows an endothermic peak which is seen in every sample in this data set. The presence of the endothermic peak even after heat-treatment at temperatures above 150 °C could be due to desorption of the absorbed water. On inspecting the Figure 5.12 and Table 5.3, the peak area for lignin fibres thermo-stabilised in air decreases initially from 23.76 J/g to 14.55 J/g after which there was a significant increase in the endothermic peak area to 144.69 J/g for the heat-treated temperature up to 250 °C. This initial decrease could be related to the thermally induced cleavage of specific chemical linkages in lignin. However, the significant increase in the endothermic peak could relate to an increase in the hygroscopicity of lignin. This may be attributed to the introduction of new polar groups such as carbonyl and carboxyl groups during cross-linking reactions. The polar groups are known to have intermolecular interactions via hydrogen bonding with the moisture as discussed previously in the Section 4.5 (317, 320, 321, 324, 404) . This data also correlates with oxygen content reported for elemental analysis in the previous Section 5.2.1 and the data reported in literature (222, 285, 287, 402, 403). Conversely, the lignin fibres thermo-stabilised in nitrogen showed small endothermic peak area for the heat treatment up to 250 °C.

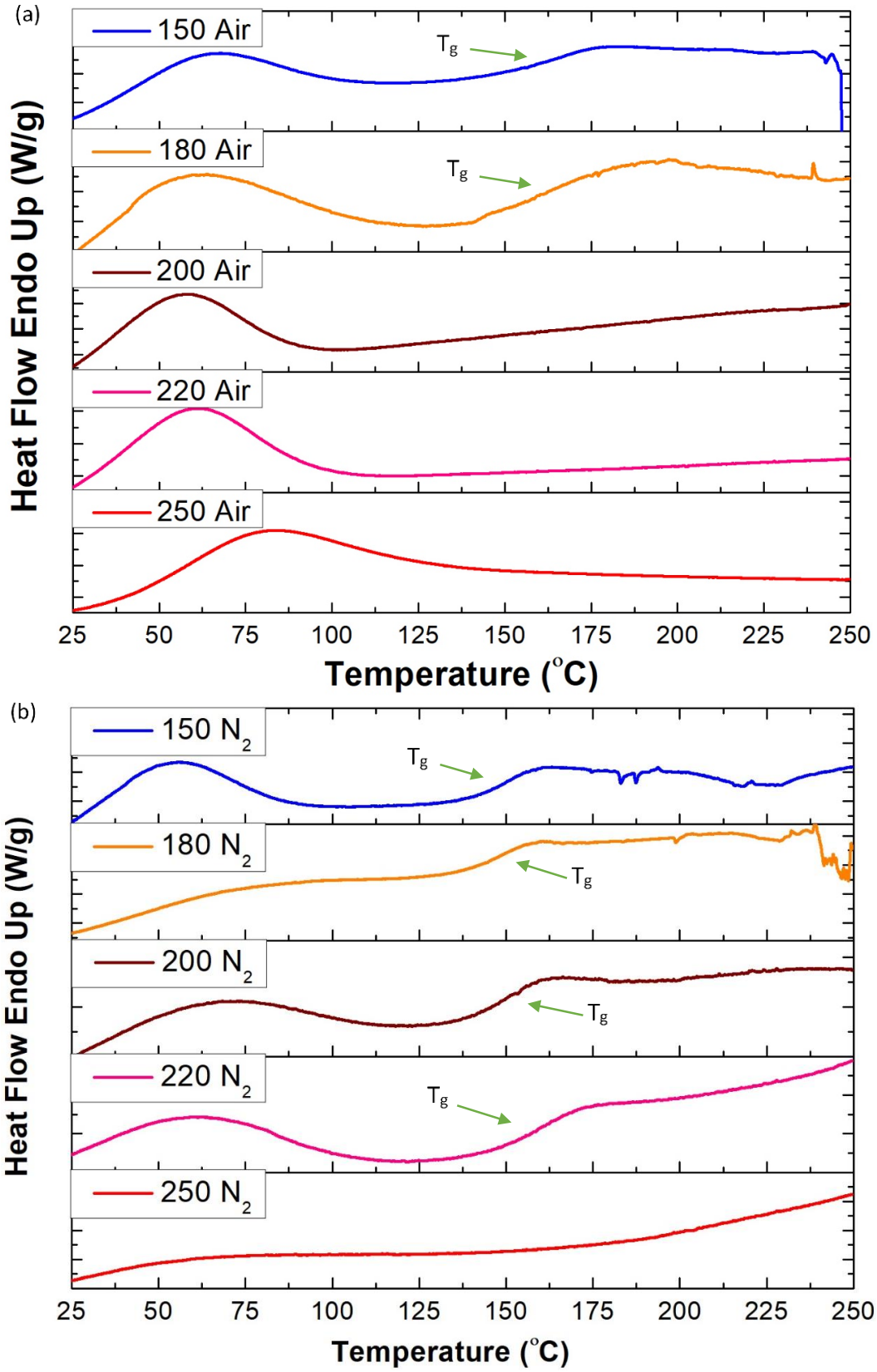

Figure 5.12 (a-b) DSC traces for the first heating scan for 95ASL-5ESL lignin fibres thermo-stabilised at 150 °C, 180 °C, 200 °C, 220 °C and 250°C: (a) in air; and (b) in nitrogen.

DSC traces of the first, second and third heating scans for ASL-ESL lignin fibres that were thermo-stabilised in air and nitrogen are shown in Figure 5.12 (a-b), Figure 5.13 (a-b) and Figure 5.14 (a-b) respectively. The T_gs for the first, second and third heating scans were observed only for lignin fibres that were thermo-stabilised in air at 150 °C and 180 °C. Whilst the T_g was not detected for temperatures at 200 °C, 220 °C and 250 °C. Similarly, Conversely, in the first, second and third heating scans, all lignin fibres that were thermo-stabilised in nitrogen show a distinct T_g except the fibres heated at 250 °C. where T_g is not detected. The disappearance for the T_g and the trend in the T_gs value is discussed later.

It is observed that the detected T_gs of lignin fibres increased gradually after each heating scan. This gradual increase in the T_g is related to the repeat heating of lignin samples to 250 °C which in turn leads to increase in molecular weight via radical cross-coupling reactions (341, 349, 405).

Table 5.3 The glass transition temperatures for 95ASL-5ESL electro-spun lignin fibres thermo-stabilised in air and nitrogen.

Samples	**Heating scan 1**		**Heating scan 2**	**Heating scan 3**
	Peak Area (J/g)	**Glass transition temperature, T_g (°C)**	**Glass transition temperature, T_g (°C)**	**Glass transition temperature, T_g (°C)**
Thermo-stabilisation in air				
150 °C	23.8	160.5	166.0	174.9
180 °C	14.6	163.1	183.4	187.1
200 °C	43.0	-	-	-
220 °C	67.8	-	-	-
250 °C	144.7	-	-	-
Thermo-stabilisation in nitrogen				
150 °C	26.6	148.0	153.5	156.6
180 °C	11.1	147.7	154.5	158.7
200 °C	18.9	149.6	157.8	162.2
220 °C	20.3	157.3	165.2	166.9
250 °C	25.8	-	-	-

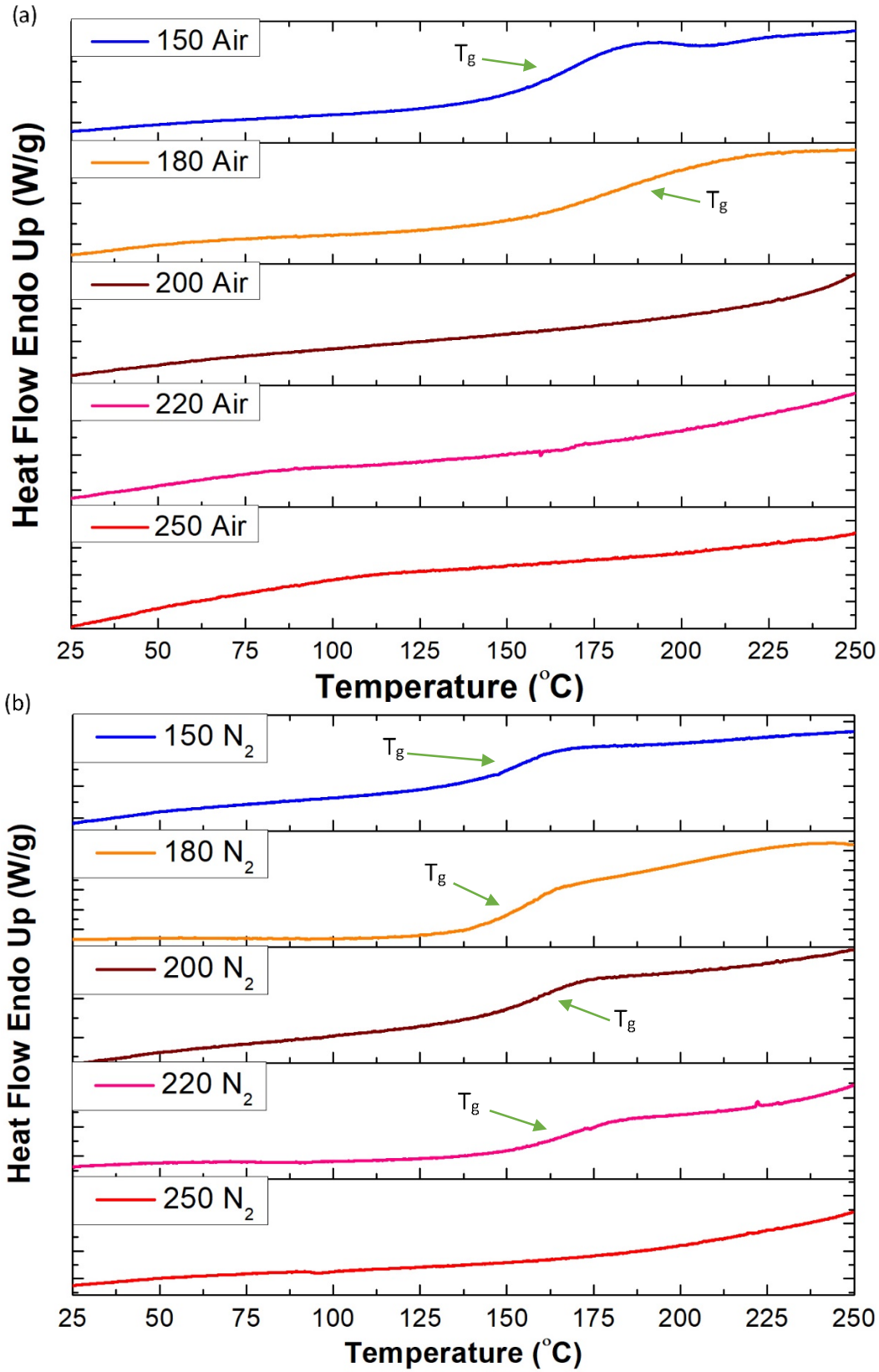

Figure 5.13 (a-b) DSC traces for the second heating scan for 95ASL-5ESL lignin fibres thermo-stabilised at 150 °C, 180 °C, 200 °C, 220 °C and 250°C: (a) in air; and (b) in nitrogen.

Inspecting the glass transition data for each heating scan, summarised in Table 5.3, the observed T_g for the lignin fibre that were thermo-stabilised in air at 150 °C and 180 °C is significantly higher when compared to pre-dried (vacuum 140 °C) lignin fibres and the lignin fibres thermo-stabilised in nitrogen. This implies that thermo-stabilisation in air which promotes cross-linking reactions leads to an increase in the molecular weights of lignin samples (186, 222, 349, 406).

Norberg *et al.*, (5) also observed the disappearance of T_g of lignin fibres that were thermo-stabilised in air. The difficulty of detecting the T_g was assumed to prevent the fibres from fusing together (222). The T_g was difficult to detect in highly cross-linked lignin fibres which is also linked to the slow heating rates employed at the thermo-stabilisation stage which allows glass transition temperature of a polymer to be higher than the processing temperature (T_g>T) (1, 201, 222). The glass transition temperature increases during slow heating rate and goes above its processing temperature which maintains the material in a glassy state (T_g>T) and this inhibits the fibres fusion (188, 202, 222, 223). The appearance of T_g in air thermo-stabilisation at low temperature such as 150 °C and 180 °C, where a significant increase in the T_g is observed but the stabilisation is incomplete. In contrast, thermo-stabilisation in nitrogen lead to a marginal increase in T_g. At 250 °C in nitrogen, the T_g is not detected but it still leads to fibre fusion because T>T_g during thermo-stabilisation processing at lower temperatures. Thus, the heating rate, the stabilisation final temperature and the atmospheric conditions play an important role in the stabilisation of lignin fibres and prevent them from fibre fusion. In general, softwood Kraft lignin is considered to be difficult for fibre spinning processes but comparatively easy to thermo-stabilise at moderate heating rates as compared to hardwood lignin (112). This is potentially due to its high T_g and ability to undergo cross-linking at a faster rate due to its composition (G-lignin units) and condensed structure which facilitates the thermo-stabilisation step and decrease the processing time for converting lignin to carbon fibre (180, 186). Therefore, 250 °C was selected for thermo-stabilisation as indicated by TGA results because above this temperature, the 95ASL-5ESL lignin (blend) starts to degrade.

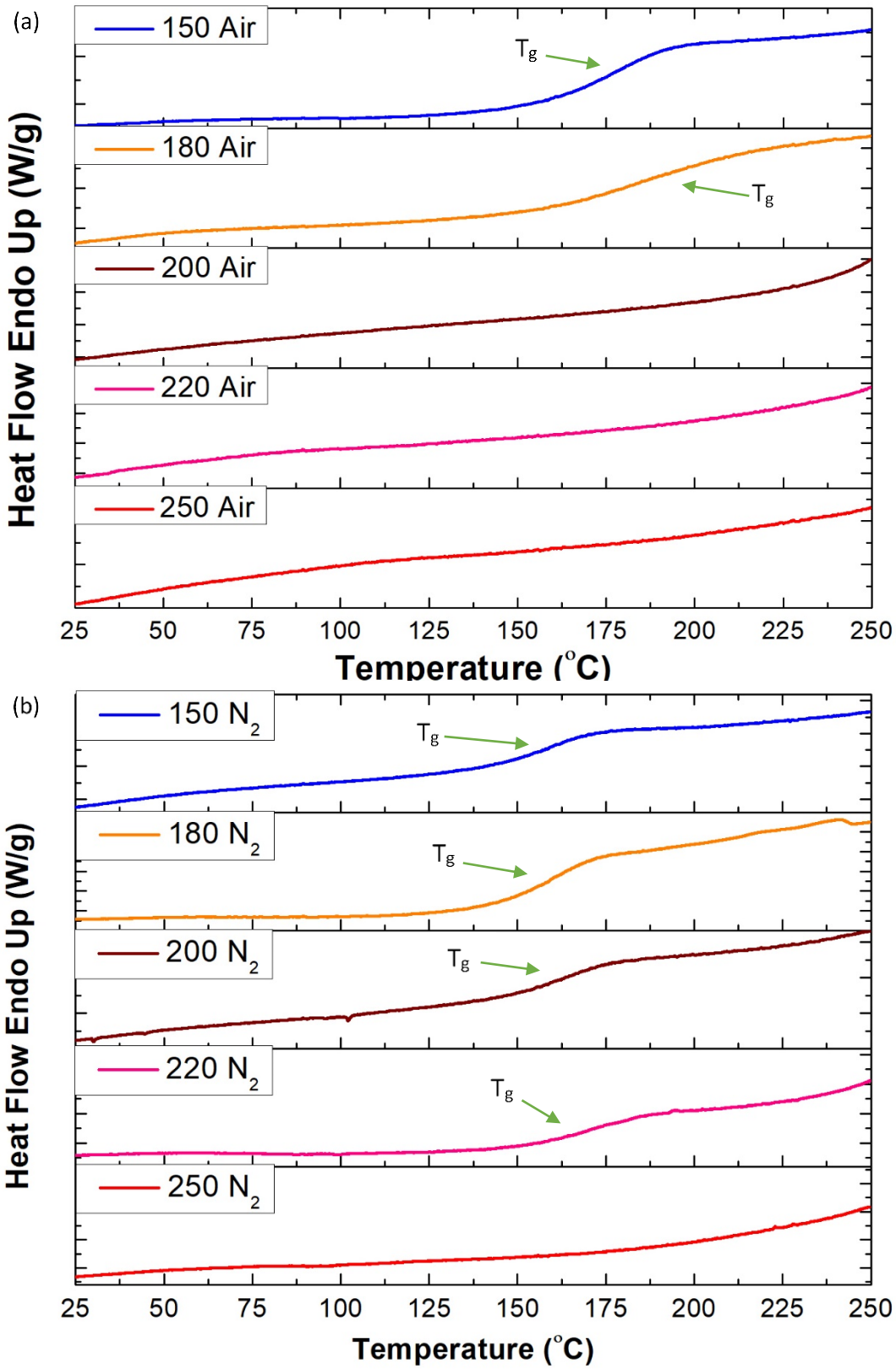

Figure 5.14 (a-b) DSC traces for the third heating scan for 95ASL-5ESL electro-spun lignin fibre thermo-stabilised at 150 °C, 180 °C, 200 °C, 220 °C and 250°C: (a) in air; and (b) in nitrogen.

5.2.2.2 Thermogravimetric Analysis of 95ASL-ESL Electro-spun Lignin Fibres

The thermogravimetric analysis (TGA) and the derivative (DTG) curves for the as-spun, vacuum dried at 140 °C and thermo-stabilised ASL-ESL lignin fibres in nitrogen or air at 250 °C are shown in Figure 5.15 (a and b) respectively. A summary of the relevant parameters are summarised in Table 5.4.

With reference to Figure 5.15 (a), the initial rapid mass-loss at between 70-110 °C for the as-spun fibre is attributed to the evaporation of solvents and absorbed moisture. The as-spun lignin fibres show a second mass-loss peak in Figure 5.15 (b) between 50-180 °C and this is attributed primarily to the DMSO being volatilised. Figure 5.15 (b) shows a high rate of mass-loss approximately between 260-450 °C. Inspecting the data for the vacuum-dried lignin at 140 °C, the peak that was assigned to absorbed moisture and residual solvent is not observed. This is reasonable as the sample was previously heated past the boiling points of acetone and water. A significantly smaller peak is observed for the loss of DMSO. The maximum value for the third peak is similar to that observed for the as-spun lignin fibres, this is at approximately 390 °C. The sample that was heat treated in a nitrogen atmosphere does not show any evidence for the presence of moisture or DMSO (as implied by the flat baseline). The sample that was treated at 250 °C in air indicates the presence of moisture and a small quantity of DMSO as indicated by the small peak but positive gradient of the baseline. The reasons for the presence of this peak is not known but it may have been due to the unintentional and unauthorised opening of the desiccator where the samples were stored. It is known that DMSO and polar groups present in lignin have an affinity for water; this affinity increases due to the increased oxygen moieties which may be due to the formation of carbonyl or carboxyl groups in air thermo-stabilised lignin fibres as indicated by elemental analysis in Section 5.2.1. Hence, with prolonged storage and intermittent exposure to the atmosphere (opening and closing of the desiccator) may have resulted in the sorption of moisture. The position of the third peak for the air-oxidised samples is observed to have shifted from 390 °C, as

observed for the other three samples, to 440 °C. Furthermore, the rate of mass-loss is significantly lower, and it is spread over a larger temperature range.

Comparing the DTG trace for the lignin fibres that were heat-treated in air and nitrogen, the following conclusion can be made:

(i) Since the rate of mass-loss for the air-oxidised lignin samples is lower and the fact that it is spread over a larger temperature range, it is likely that oxygen reacts with free-radicals produced after thermal cleavage of lignin interunit linkages. This introduces new oxygen moieties in lignin which are thermally stable at higher temperature (~250 °C); this is supported by the C, H and N analysis discussed in Section 5.2.1 where the oxygen content for the samples treated in nitrogen and air were 22.3% and 37.3% respectively. This is also supported by the data gained from FTIR and NMR spectroscopy (discussed in Section 5.2.3 and 5.2.4 respectively. The heating rates can also have an effect on the formation of products, with low heating rates favouring the formation of compounds containing oxygen along with a high char content (354, 355).

(ii) The broadening and the reduced gradient of the DTG trace suggest that the thermal stability has increased. The most likely reason for this is cross-linking of the lignin. Indirect evidence for this is found in the DSC traces where the change in the heat capacity becomes more diffuse as the sample is subjected to three successive heating regimes to 250 °C. Moreover, it is seen in Table 5.3 that the T_g also increased with successive heating. Possible mechanism for the proposed cross-linking reactions are discussed in Sections 2.7 and 5.2.5.

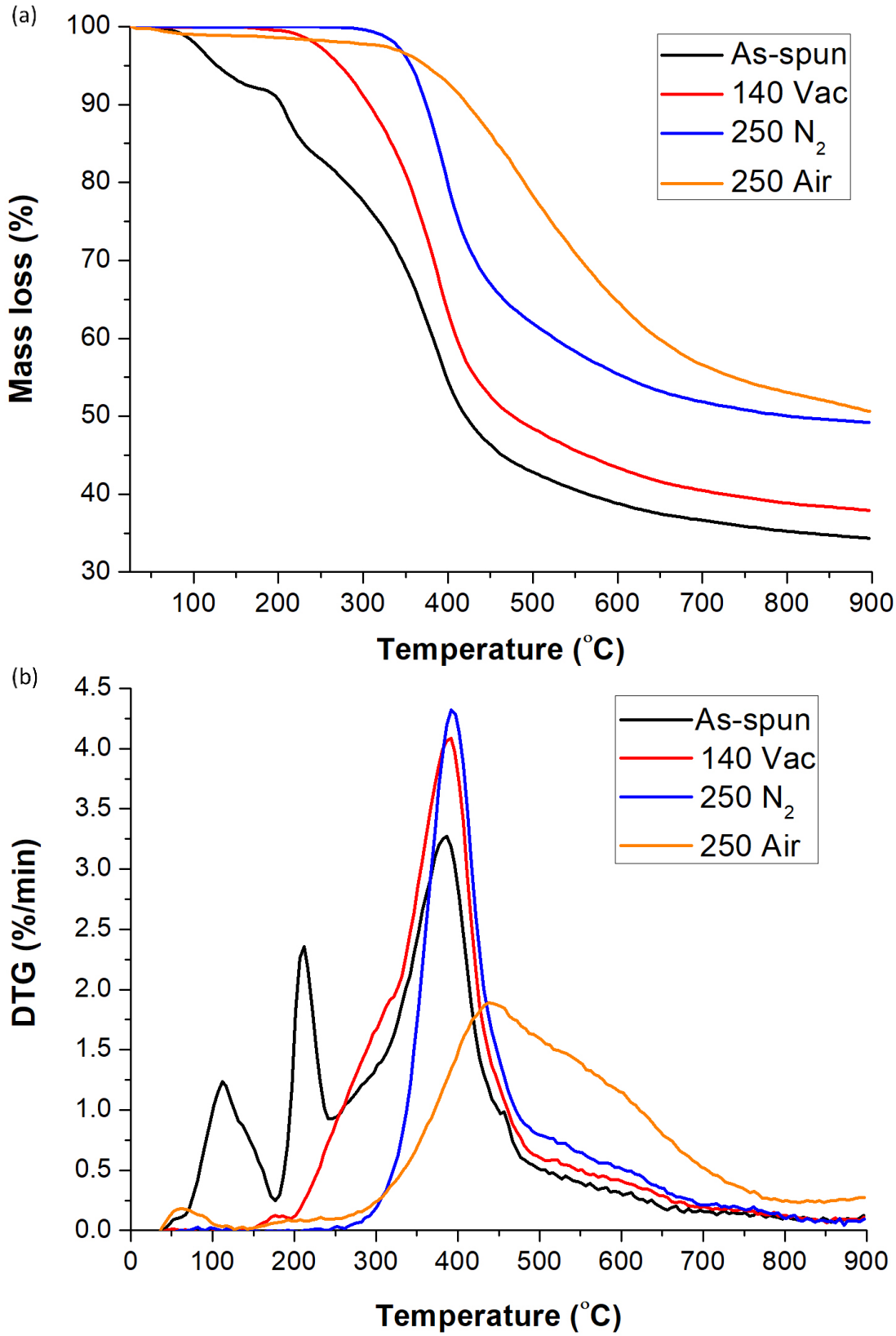

Figure 5.15 (a-b) Thermal analysis of ASL-ESL electro-spun lignin fibres that were thermo-stabilised in air or nitrogen: (a) TGA; and (b) DTG curves.

In the context of converting biomass to graphite, in the current study, the mass of the material that was retained at 900 °C was used as the guide to their suitability. In the current case, fractionated lignin was used where the inorganic content at 525 °C was 0.1% as discussed in Section 4.6. With reference to the data presented in Figure 5.15 and Table 5.4, the char content at 900 °C for the electro-spun lignin fibres that were thermo-stabilised in air and nitrogen were 50.6 and 49.2 respectively. The corresponding data for the as-spun and vacuum-dried samples are 34.3 and 37.9 respectively. The relatively higher char content for the air-oxidised lignin fibres supports the assumption that the polymer may have undergone cross-linking thus reducing the rate of thermo-oxidative degradation and enabling a higher proportion of its original mass to be retained (285, 287).

Table 5.4 Char content of lignin fibres at 900 °C, DTG max peak and the mass loss of 50% at specific temperatures.

Sample	**Temperature at 50% mass-loss (°C)**	**DTG maximum (°C)**	**Char content at 900 °C (%)**
As-spun	416.7	385.3	34.3
Vacuum dried at 140 °C	476.6	390.6	37.9
Thermostabilised in N_2 at 250 °C	801.8	393.3	49.2
Thermostabilised in air at 250 °C	900	438.5	50.6

5.2.3 Fourier Transform Infrared Spectroscopy of Electro-spun Lignin Fibres

FTIR spectra of the 95ASL-5ESL electro-spun lignin samples that were thermo-stabilised in air and nitrogen including those vacuum dried at 140 °C are shown in Figure 5.16 (a-b). The assignment of the absorption bands was discussed in Section 4.13 (Table 4.10). The noticeable changes during thermo-stabilised are summarised in this section.

The broad O-H stretching band at 3400 cm^{-1} decreases initially from 150-200 °C in the case of the air thermo-stabilised fibres. This can be attributed to the formation of formaldehyde via the loss of hydroxylated (OH) groups attached to the Cγ position(222, 285). The mechanism for the release of formaldehyde is shown in Sections 2.7.1 and 5.2.5. A slight increase in the OH groups is observed for thermo-oxidative treatment between 220-250 °C. This increase in the OH functional groups can be attributed to the H-atom transfer and formation of hydroxyl groups from the phenoxy radicals formed by the homolytic cleavage of β-O-4 ether bond linkages (222). The most significant difference observed between air and nitrogen atmosphere thermo-stabilisation steps are in concentrations of the C-H and C=O. In the air thermo-oxidised samples, the C-H absorbance bands between 3200-2800 cm^{-1} decreases as the temperature is increased and at 250 °C, this band disappears completely. When heated in air, the aliphatic side chains (alkyl groups) are believed to undergo oxidation reaction to create oxygen containing functional groups such as enol ethers and ketone products (222, 285). The carbonyl absorbance band at 1703 cm^{-1} is seen to increases significantly with heat treatment temperature which indicates the formation of new carbonyl moieties. This could be due to the formation of unconjugated carbonyl (1703 cm^{-1}), unconjugated carboxyl groups or esters (1735 cm^{-1}) (112, 407, 408). Appearance of small peak at approximately 1770 cm^{-1} is indicative of the formation of anhydride linkages (287). The increase in the oxygen content from the elemental analysis data and the formation of esters and carbonyl groups is also indicated by ^{13}C NMR and FTIR spectroscopy data.

When the electro-spun lignin fibres were thermo-stabilised in nitrogen, the relative concentration of the carbonyl groups was observed to be constant. However, in contrast, the C-H bonds remains unchanged for the lignin that was thermo-stabilised in nitrogen which indicates that only air thermo-stabilisation facilitates hydrogen abstraction reactions.

The peak at 1218 cm^{-1} which is attributed to the stretching vibrations of C-C, C-O and C=O bonds decreases slightly when the heat-treatment temperature was increased. In the samples that were thermo-stabilised in air at 250 °C, the peaks from ~1500-1000 cm^{-1} became broader making it difficult to identify and assign them to specific functional groups.

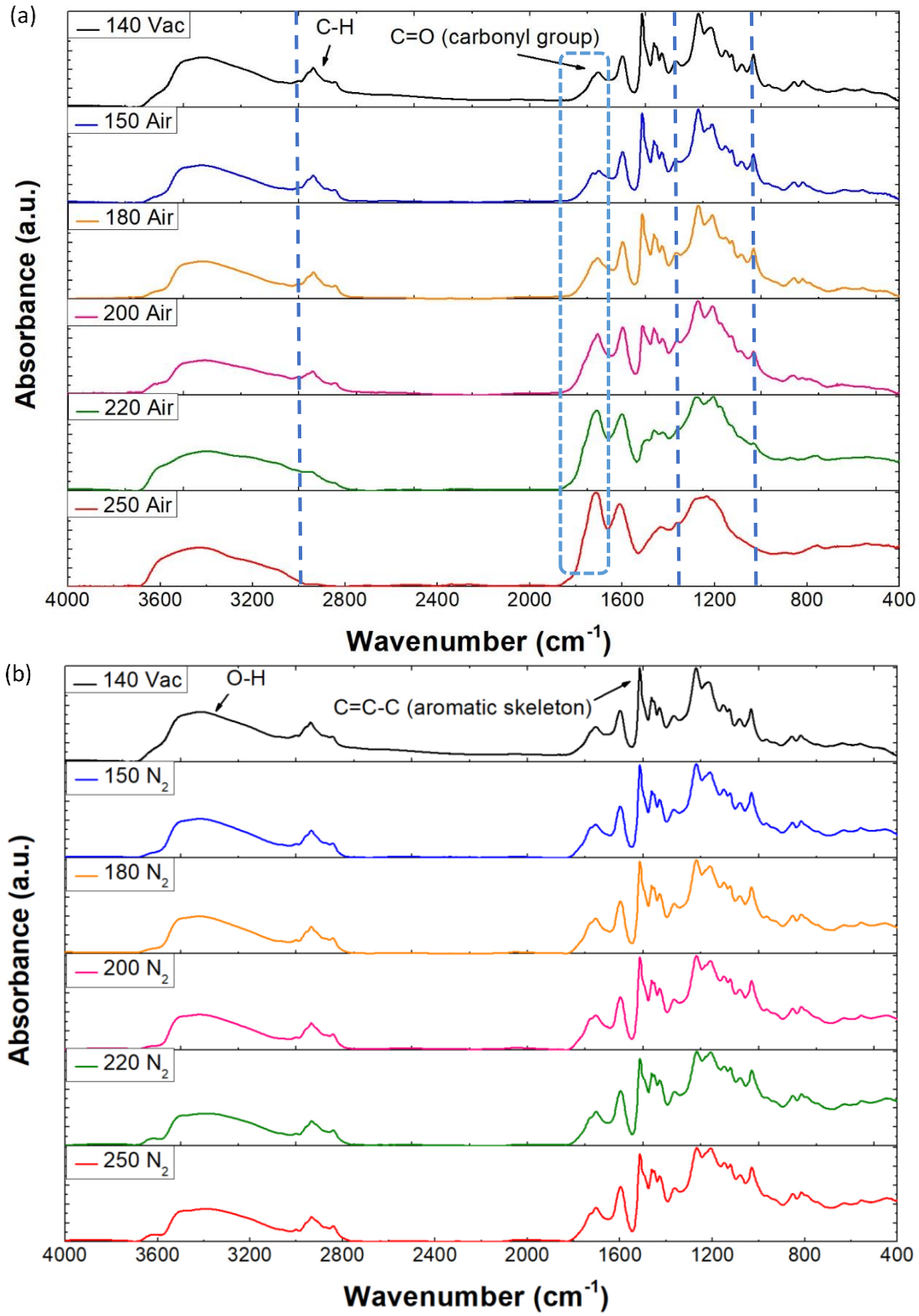

Figure 5.16 (a-b) FTIR spectra of ASL-ESL electro-spun lignin fibres that were heat-treated at selected temperature: (a) in air; and (b) nitrogen.

5.2.4 Solid State NMR (^{13}C CP/MAS NMR) Spectra of Lignin (95ASL-5ESL) Fibres

Solid state (^{13}C CP/MAS) NMR spectroscopy was used to study the structural changes in the lignin samples as a function of heat-treatment. It was observed that the electro-spun lignin ASL-ESL fibres exhibited a progressively lower solubility in DMSO as the heat-treatment temperature was increased from 140°C to 250 °C. This trend indicates an increase in molecular weight and/or cross-linking in the lignin samples; this was specifically relevant for the lignin fibres that were thermo-stabilised in air. Solid-state NMR spectra of vacuum dried (140 °C) and lignin fibres treated in nitrogen or air at 250 °C are shown in Figure 5.17. The intensity of the methoxyl (OCH_3) peak at 56 ppm for the lignin fibres oxidised in air is reduced to almost half in comparison to vacuum dried lignin (140 °C). This indicates that the cleavage of methoxyl group attributed to demethoxylation (222, 285, 287) is one of the reaction, when the treatment temperature is increased from 140 °C to 250 °C. The chemical shifts between 60-90 ppm and 20-50 ppm for the aliphatic side chain (aliphatic C-C) and interunit linkages (aliphatic C-O) disappear completely for the lignin fibre that were treated in air at 250 °C.

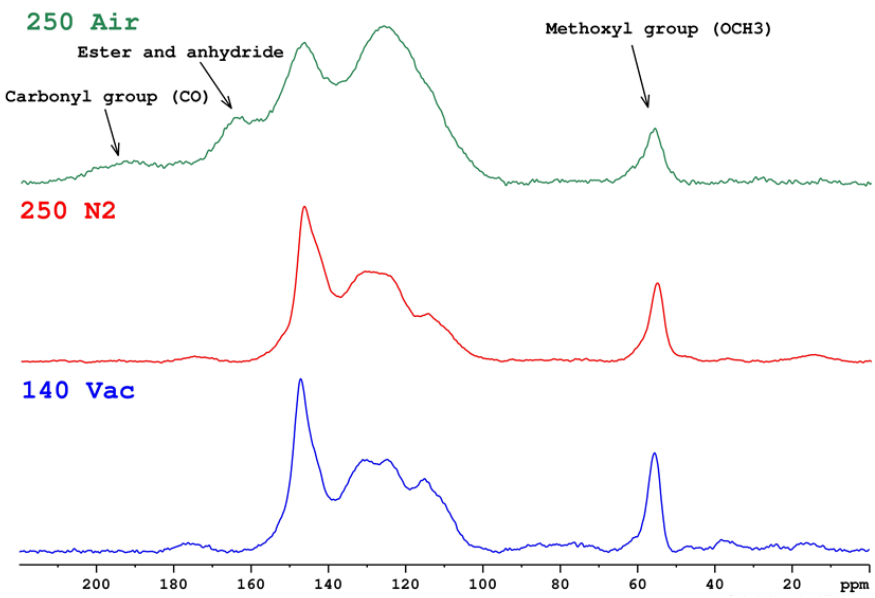

Figure 5.17 Solid state ^{13}C CP/MAS NMR spectra for the ASL-ESL electro-spun lignin fibres that were heat-treated in nitrogen and air at 250 °C.

The chemical shift between 102-160 ppm show the presence of aromaticity together with sp^2 carbon in the aliphatic side chain and interunit linkages. The increase in signal from 120-140 ppm (protonated aromatic C-C) for the lignin fibres treated in air indicates the conversion of aliphatic sp^3 to sp^2 carbons. This could be due to the formation of new oxygen moieties. The region with peaks from 160-220 ppm is attributed to the oxygen related structures. The chemical shift in between160-170 ppm shows the appearance of a new peak for the sample that was treated in air and this corresponds to the presence of esters and anhydrides (222, 285, 287).This suggests that the cross-linking reactions may lead to the formation of ester and anhydrides structure in the lignin fibres that were thermo-stabilised in air (222, 285, 287). The chemical shift in the region from 170-190 ppm shows the presence of carbonyl and carboxylic acids structures, and this is seen to increase with thermal treatment in air. This region (170-190 ppm) indicates an increase in the formation of ketone groups. In general, ketone groups appear at higher chemical shifts than carboxylic groups. This data are consistent with the increase in carbonyl (C=O) groups and increase in oxygen content as presented in earlier sections of FTIR spectroscopy and elementals analysis. The nitrogen thermostabilised lignin shows no significant change from vacuum dried lignin.

5.2.5 Evaluation of Chemical Structure of Lignin Fibres During Thermo-stabilisation in Air

As mentioned previously, the structural composition of lignin is complex, and it consists of several linkages of carbon-carbon and ether bonds with the presence of dimeric lignin units (see Figure 2.3 in Section 2.2). The composition of the BioChoice® lignin was discussed in Chapter 4. During thermo-stabilisation, the ether bonds in lignin are susceptible to thermally induced scission because of their low bond dissociation energies. The dimeric lignin units of softwood lignin undergo homolytic bond scission and one such example is the cleavage of dibenzodioxocin as shown in Figure 5.18. This homolytic cleavage could also take place in other structures such phenylcoumaran, resinol and β-aryl ethers (see Section 4.9 for the structures of lignin).

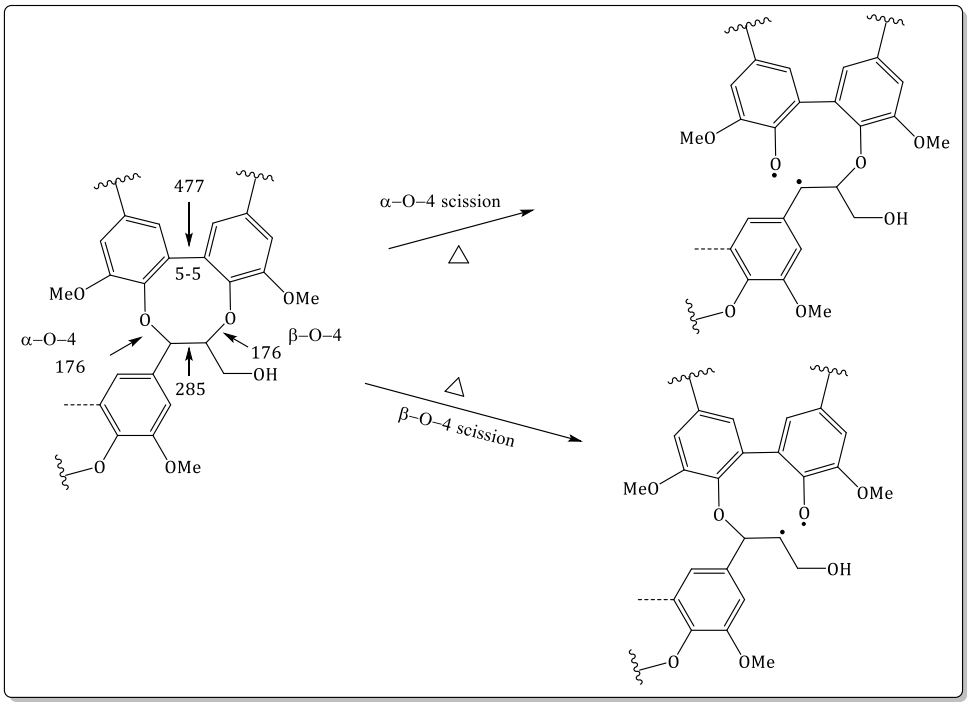

Figure 5.18 Homolytic cleavage of α-O-4 and β-O-4 in dibenzodioxocin; the numerical values of the bond dissociation energies (kJ/mol) are indicated (147).

The reduction in the hydrogen content (determined via C, H and N analysis) during thermo-stabilisation in air could be attributed to the release of formaldehyde in phenylcoumaran or

β-aryl ether type structures. An example of this reaction is shown in Figure 5.19 for phenylcoumaran with bond dissociation energies for the α-O-4 linkage which is susceptible to cleavage (147). This results in the loss of hydroxyl group from C-γ position which is also indicated by the FTIR spectral results discussed in Section 5.2.3.

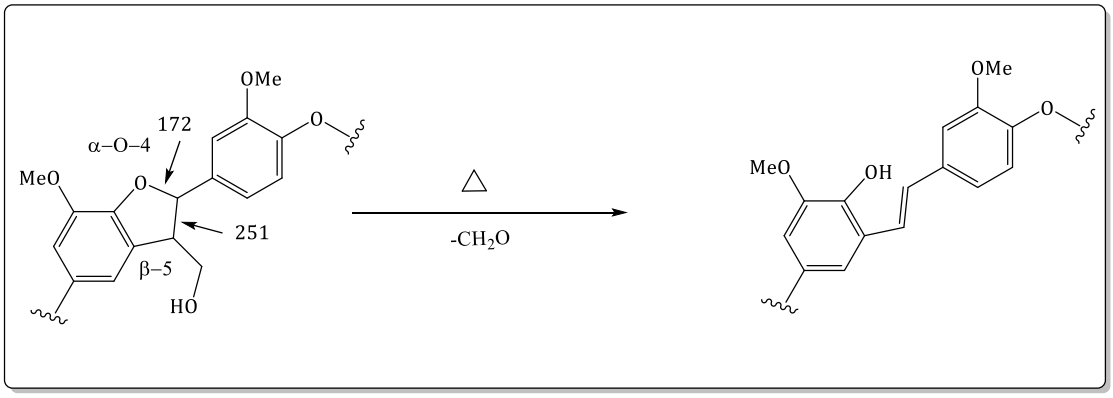

Figure 5.19 Postulated mechanism for the release of formaldehyde from a phenylcoumaran structural unit (147).

Figure 5.20 shows a thermo-oxidative reaction of a β-aryl structural unit (112). The homolytic cleavage results in the formation of free-radicals. The free-radical is delocalised over the aromatic ring which can lead to radical stabilisation as shown in Figure 5.20. The coupling of free-radicals can lead to the formation of new carbon-carbon bonds and a dimer structure. The oxidation reactions can lead to the release of volatiles such as carbon dioxide and water along with heat (112, 286). The new oxygen moieties are related to increase in carbonyl content observed in the ^{13}C NMR and FTIR spectra and the elemental composition data. This could be attributed to the formation of ketone, aldehyde or carboxylic acid as shown in Figure 5.20. Generally, aldehydes and carboxylic acids are formed from primary alcohols whilst ketones are formed from secondary alcohols.

The formation of esters and anhydride was also indicated in the thermo-stabilisation results obtained from ^{13}C NMR and FTIR spectra. These structures are believed to be formed from the aldehydes and carboxylic acids groups in lignin units (222, 285, 287, 407).

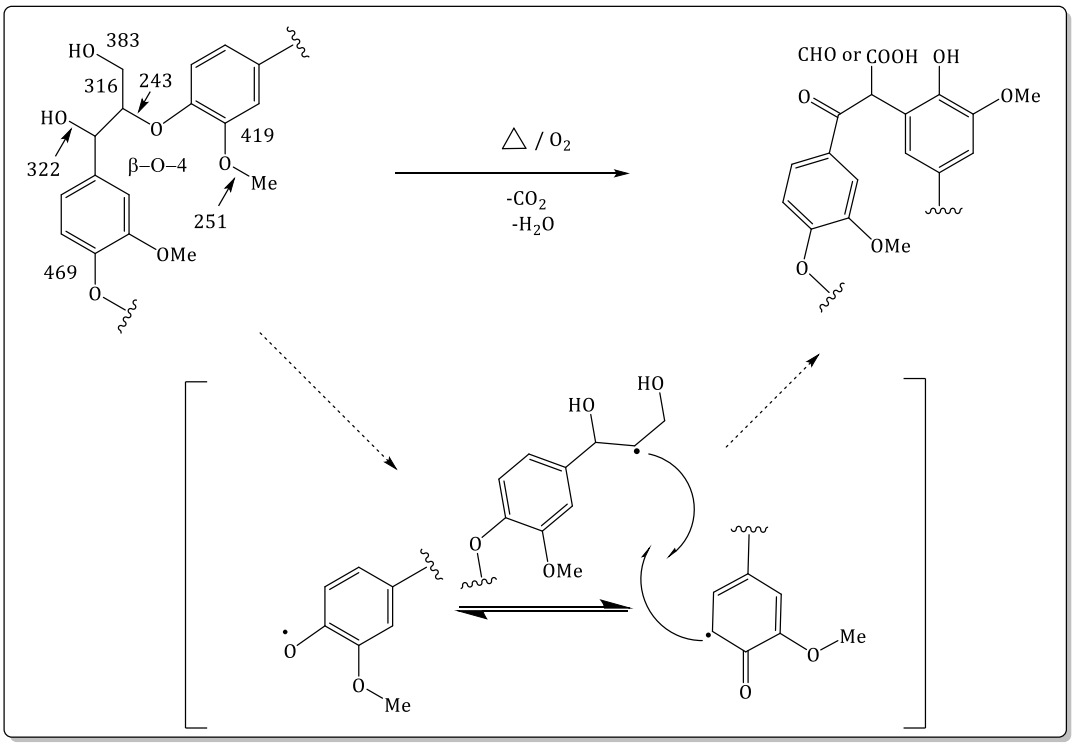

Figure 5.20 Postulated reaction of β-aryl structure with bond dissociation energies for β-O-4 (kJ/mol) (112).

It has been reported that during carbonisation at elevated temperatures the oxygen content is reduced. This may be related to the formation of condensed structures and the elimination of oxygen structural moieties (246). The evolution of such structures is revealed by the PY-GC-MS results where the evolution of phenanthrene and naphthalene is observed; these structures are shown in Figure 5.21.

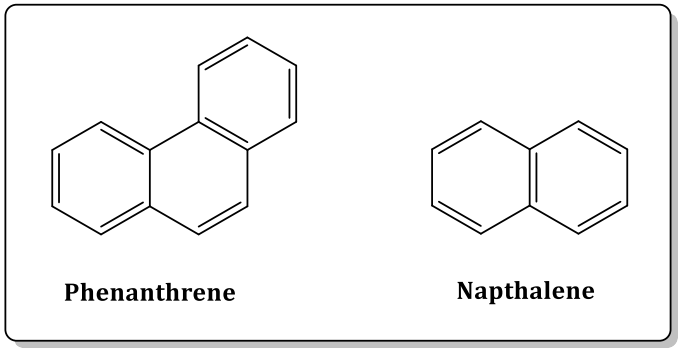

Figure 5.21 Structure of phenanthrene and naphthalene.

5.3 Carbonisation of the Electro-Spun ASL-ESL Lignin Fibres

It was discussed in Section 5.2 that the electro-spun ASL-ESL lignin fibres that were dried in a vacuum oven at 140 °C and then subsequently thermo-stabilised in air at 250 °C, maintained their form and structural shape. Therefore, the above-mentioned processing condition was adopted as the pre-treatment prior to carbonisation. The thermo-stabilised lignin fibres were carbonised in a tube furnace using a nitrogen gas flow rate of 50 ml/minute; these experiments were carried out at 1000 °C, 1200 °C and 1500 °C. The colour change observed before and after the specified heat-treatment of the electro-spun lignin fibres is shown in Figure 5.22. The as-spun fibres turn from pale yellow/brown to dark brown and eventually turned black upon carbonisation.

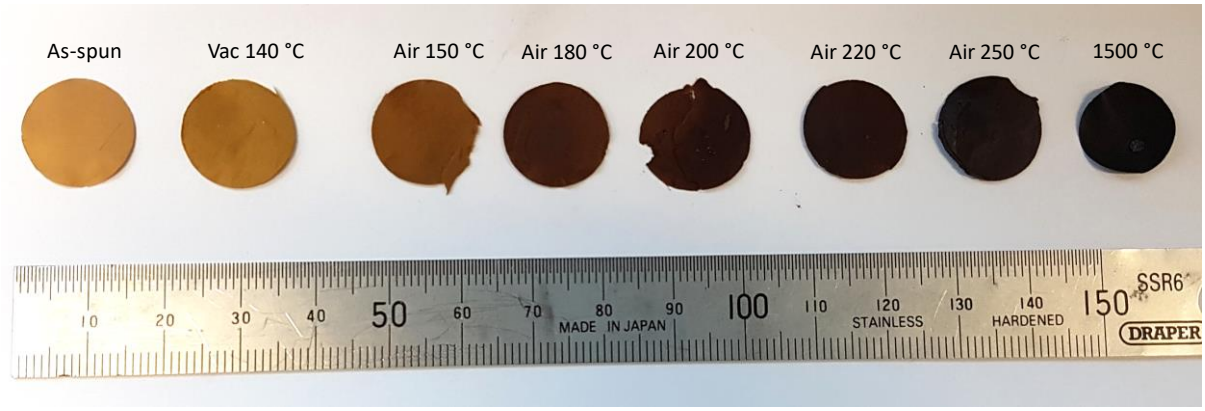

Figure 5.22 Colour changes in the electro-spun ASL-ESL lignin fibres before and after heat treatment at specified temperatures.

SEM micrographs of the carbonised lignin fibres (ASL-ESL) at 1000 °C, 1200 °C and 1500 °C are shown in Figure 5.23 (a-f). The surface morphology the fibre the fibres is seen to be smooth, circular and unfused. This demonstrates conclusively that electro-spun lignin fibres can be obtained without the use of any processing aids or synthetic polymer blends. In other words, this represents the production of electro-spun fibres using 100% lignin. At the time of writing, the author was not aware of any previous studies that reported the production of electro-spun lignin fibres from fractionated blends of lignin.

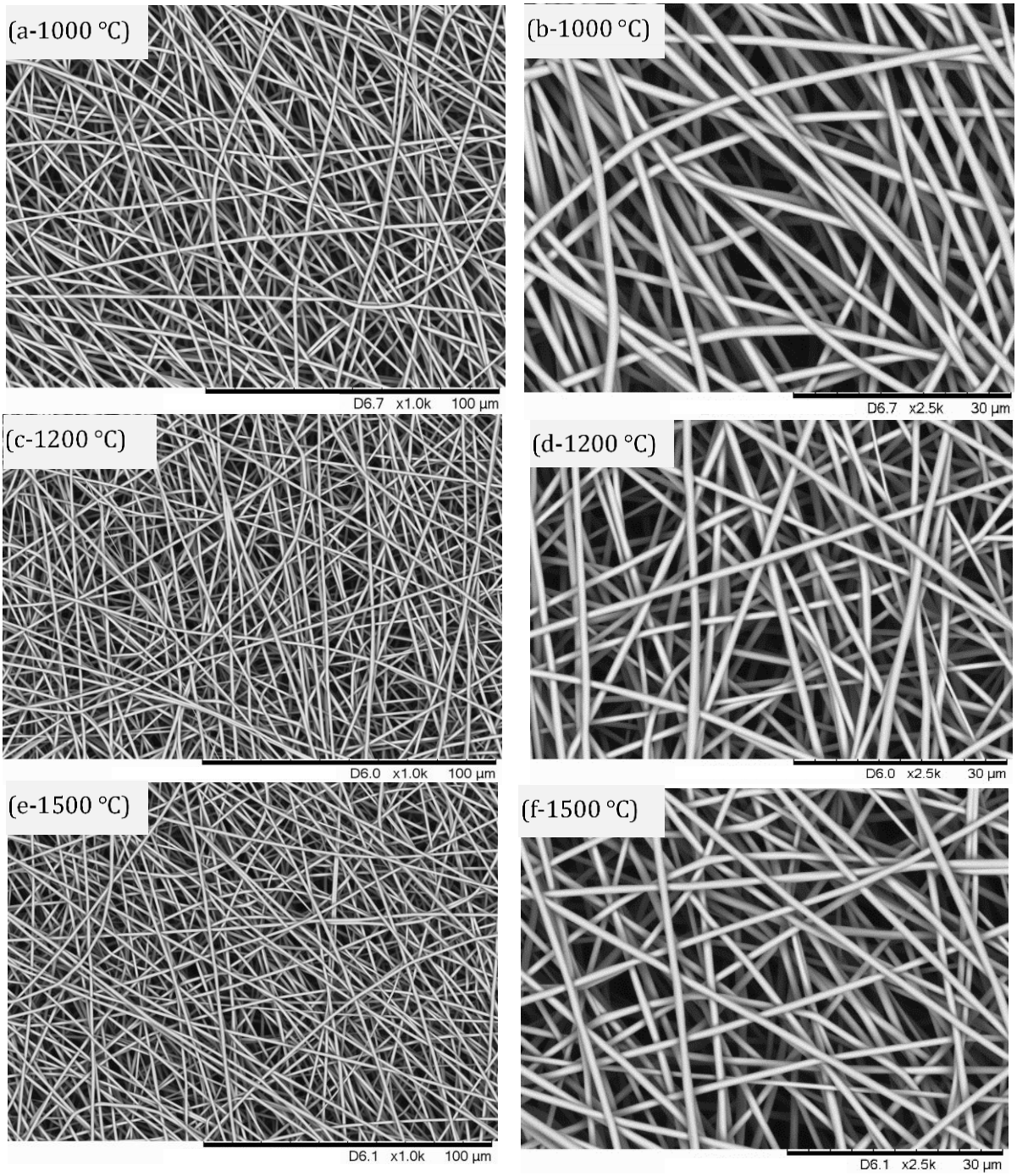

Figure 5.23 Electro-spun and carbonised (ASL-ESL) lignin fibres after carbonisation at 1000 °C, 1200 °C and 1500 °C with magnifications of x1000 and x2500.

Transverse section of the electro-spun (ASL-ESL) lignin fibres that were carbonised at 1000 °C, 1200 and 1500 °C is shown in Figure 5.24 (a-c). These micrographs demonstrate that the fibres are not fused and that their cross-section is circular. Figure 5.24 (a-c) and Figure 5.25

shows that the fibre diameter decreases as a function of the carbonisation temperature. This is expected due to shrinkage and mass-loss during carbonisation. The chemical changes and mass and the mechanism associated with the carbonisation were discussed in Sections 2.5, 5.2 and 5.2.5. Figure 5.24 (a-c) show the presence of fractured fibres. This was possibly caused when the electro-spun preform was fractured in liquid nitrogen to obtain transverse sections. However, fracture caused by fibre shrinkage during carbonised cannot be ruled out.

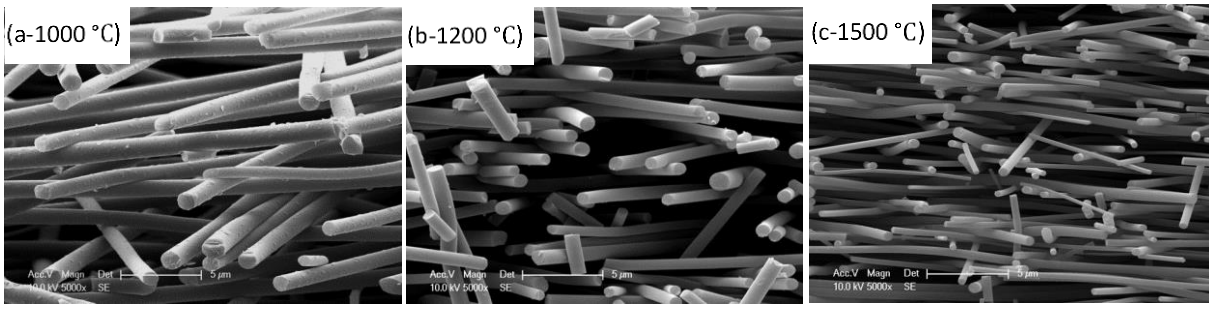

Figure 5.24 Micrographs showing transverse sections of electro-spun (ASL-ESL) lignin fibres after carbonisation at 1000 °C, 1200 °C and 1500 °C.

5.3.1 Fibre diameter distribution

The fibre diameter distribution for the electro-spun ASL-ESL lignin fibres in the as-spun and after specified heat treatments are shown in Figure 5.25 (a-f). The data sets are represented as histograms plots with an overlaid normal distribution curve per plot. The diameters for the electro-spun samples represented in Figure 5.25 are as follows: (a) as-spun = 0.6-2.8 μm; (b) vacuum-dried = 0.6-2.8 μm; (c) thermo-stabilised lignin fibre in air at 250 °C = 0.6-2.4 μm; (d) carbonised lignin fibres in nitrogen at 1000 °C = 0.6-1.4 μm; (e) 1200 °C = 0.6-1.4 μm and (f)1500 = 0.6-1.2 μm. The as-spun and vacuum dried lignin fibres showed the widest distributions ranging between 0.6-2.8 μm. There is a noticeable change in the reduction for the air thermo-stabilised lignin fibre diameter at 250 °C. The most significant change in the diameter distribution for the electro-spun fibres was observed during the carbonisation stage.

The narrowest diameter distribution (0.4-1.2 μm) was obtained from the lignin fibres that were carbonised at 1500 °C.

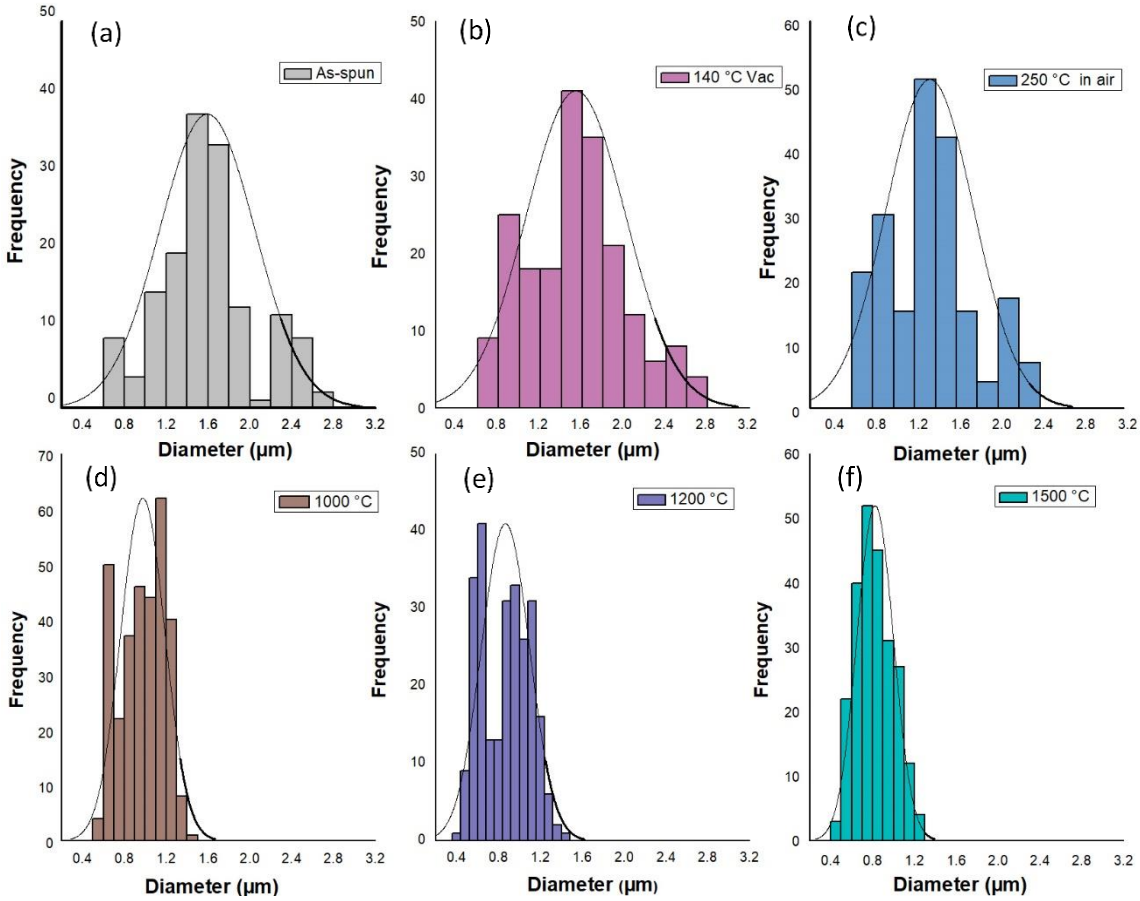

Figure 5.25 (a-f) Histogram plots for the diameter distribution for the electro-spun (ASL-ESL) lignin fibres: (a) as-spun; (b) vacuum-heated at 140 °C; (c) thermo-oxidative stabilised at 250 °C; and carbonised at (d) 1000 °C; (e) 1200 °C and (f) 1500 °C in nitrogen. The histograms have been overlaid with a normal diameter distribution curve for each data set.

The average diameter of the electro-spun ASL-ESL lignin fibre including the heat-treated samples is shown in Figure 5.26. The mean diameter of the lignin fibre is reduced noticeably during thermo-stabilisation and significantly after carbonisation. The lignin sample carbonised at 1500 °C show a mean diameter of 0.8 μm. This shrinkage in the diameter during heat-treatment which

includes thermo-stabilisation and carbonisation steps could be the result of increased mass-loss occurring at elevated temperatures.

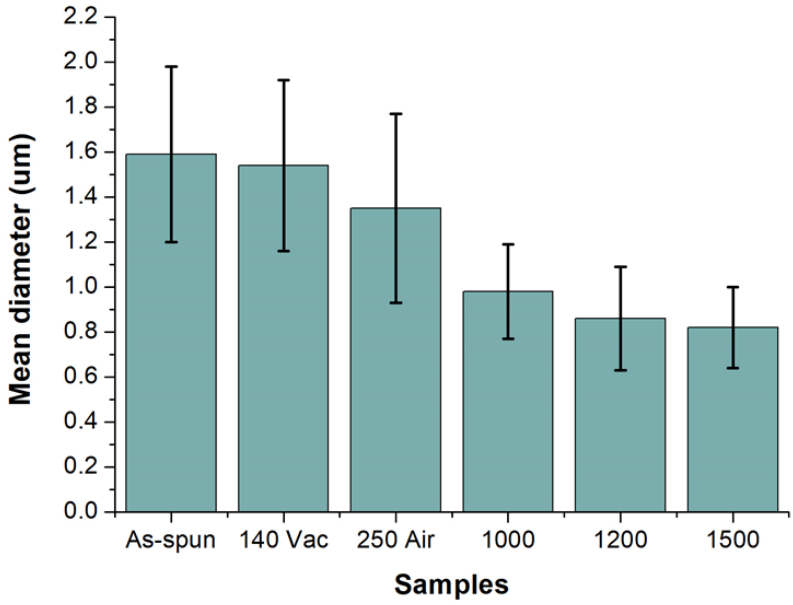

Figure 5.26 Average fibre diameter distribution for the electro-spun ASL-ESL lignin samples including the carbonised sample.

5.3.2 Electrical Conductivity of Electro-spun ASL-ESL Carbonised Lignin Fibres

The electrical properties of the carbonised lignin samples are shown in Table 5.5. The experimental details for determining the electrical conductivity of the carbonised fibres are listed in Section 3.9.1.3. The electrical properties of the solid carbonised lignin fibres are important for determining their suitability for energy storage applications such as electrodes for dye-sensitised solar cells, batteries, fuel cells, capacitors and super capacitors. As seen in Table 5.5, the electrical conductivity of the lignin fibres increased with carbonisation temperature from 1000 to 1200 and 1500 °C. The lignin fibres that were carbonised at 1500 °C show comparable electrical conductivity to those reported in literature for softwood Kraft lignin (230 S/m) (184, 285). This suggests that the carbon fibre produced from 100% lignin, without any binder as in the current case, are of comparable to those reported in literature.

Table 5.5 Electrical properties of the carbonised ASL-ESL lignin fibres that were carbonised in nitrogen at 1000, 1200 and 1500 °C for 1 hour.

Samples	**Resistivity (Ω.cm)**	**Electrical conductivity (S/m)**
1000 °C	0.96 ± 0.14	105.64 ± 14.86
1200 °C	0.51 ± 0.05	197.18 ± 20.40
1500 °C	0.49 ± 0.06	205.80 ± 24.33

5.3.3 Raman Spectroscopy of Electro-spun ASL-ESL Carbonised Lignin Fibres

Raman spectroscopy was used to evaluate the structural changes in the lignin samples as a result of carbonisation. Raman spectra of the lignin fibres that were carbonised at 1000 °C, 1200 °C and 1500 °C are shown in Figure 5.27. There are two distinct peaks present in the Raman spectra for the carbonised lignin fibres. These are characteristic peaks correspond to D and G-bands which are typical of lignin and PAN-based carbon fibres. The D-band which appears at approximately 1350 cm^{-1} is attributed to the breathing modes of carbon atoms in aromatic rings. The G-band which appears at approximately 1600 cm^{-1} is ascribed to the in plane stretching of sp^2 carbon hybridized bonds (C=C) in the aromatic rings (184, 307). Therefore, in general, the D-band indicates disorder or defects in the graphitic structure and the G-band represents sp^2 ordered graphitic carbon.

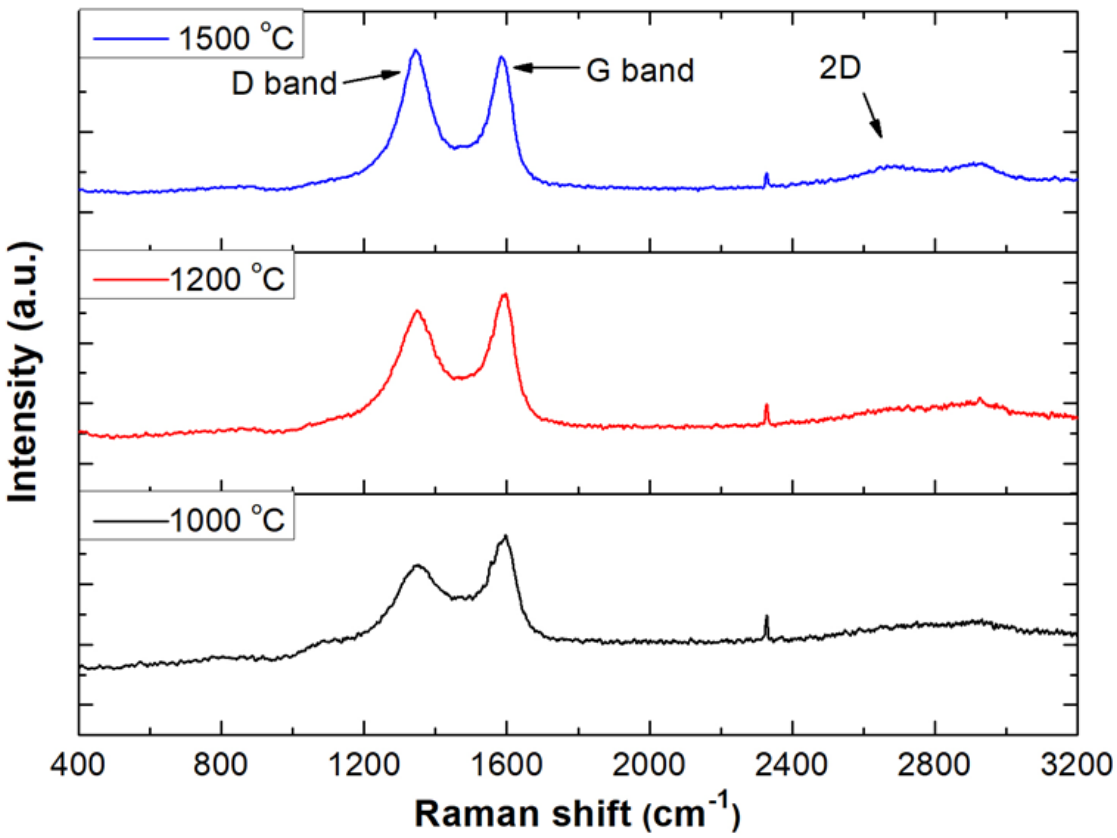

Figure 5.27 Raman spectra of electro-spun and randomly orientated lignin fibre mats that were carbonised at 1000 °C, 1200 °C and 1500 °C in nitrogen for 1 hour.

The small peak between 1000-1200 cm^{-1} could be attributed to sp^3 hybridised carbon (409). The emergence of a significant new peaks at approximately 2700 cm^{-1} is observed as the carbonisation temperature was increased from 1000 °C to 1500 °C. This band is a result of second order resonance from the D-band and it is normally referred to as the G', 2D or D* band. This 2D band is a characteristic feature of π-bonds in the layered graphitic sheets (410). This suggests that the lignin samples that were carbonised at 1500 °C show increased graphitisation.

The relative position of the D and G-bands in the Raman spectra with an analysis of the ratios of two peaks is shown in Table 5.6. The intensity of the D and G-bands increases with the processing temperature with the intensity (I_D/I_G) and area (A_D/A_G) ratios of the two bands. This suggest that more disorder is introduced in the graphitic structure upon increasing the carbonisation temperature from 1000 to 1500 °C. This is said to indicate the existence of turbostratic graphite which is thought to be composed of high condensed aromatic structure between the amorphous carbon and graphite (287, 307). The increase in the ratio of I_D/I_G is directly in contrast to carbon fibres made from PAN where this ratio is seen to decline with the increasing carbonisation temperature (411-413). However, it is reported that the higher molecular weight of lignin enhances the graphitic structure and mechanical performance (414).

Table 5.6 Analysis of the position of the D and G-band in the Raman spectra for the carbonised lignin fibres and the FWHM for these bands along with their intensity and area ratios.

Sample	D band (cm^{-1})	G band (cm^{-1})	Width (FWHM) (cm^{-1})		I_D/I_G	A_D/A_G
			D band	G band		
1000 °C	1352.91	1597.02	164.52	135.18	0.82	0.96
1200 °C	1348.61	1597.02	146.19	89.85	0.91	1.07
1500 °C	1342.88	1583.11	107.59	77.97	1.04	1.13

The full width at half maximum (FWHM) of the D and G- bands is attributed to the degree of structural disorder. It is seen in Table 5.6 that the D and G-bands experience a decrease in the FWHM values, but G-band shows more a narrower line width as the carbonisation temperature is increased. This indicates the lignin sample carbonised at higher temperature start to attain a graphitic structure (415).

5.3.4 X-ray Diffraction of Electro-spun ASL-ESL Carbonised Lignin Fibres

X-ray diffraction (XRD) was used to obtained preliminary results for the lignin fibres that were carbonised at 1000 °C, 1200 °C and 1500 °C. The XRD patterns for the carbonised lignin samples are shown in Figure 5.28. Two main diffraction peaks are observed at 22° and 44° in each of the carbonised lignin samples which correspond to (0 0 2) and (1 0 0 and 1 0 1) crystallographic planes in nano-crystallite graphitic structure, respectively (246, 307, 414, 416). The intensity of these diffraction peaks increases gradually which implies that the degree of graphitisation increases with increasing carbonisation temperature. This correlates well with Raman results where the line width of the G-band becomes narrower with the emergence of new peak (2D) at 2700 cm^{-1} for the lignin fibres that were carbonised at 1500 °C. The appearance of a new diffraction peak for lignin carbonised at 1500 °C corresponding to the (1 1 0) plane also indicates the increase in graphitic content (307, 414).

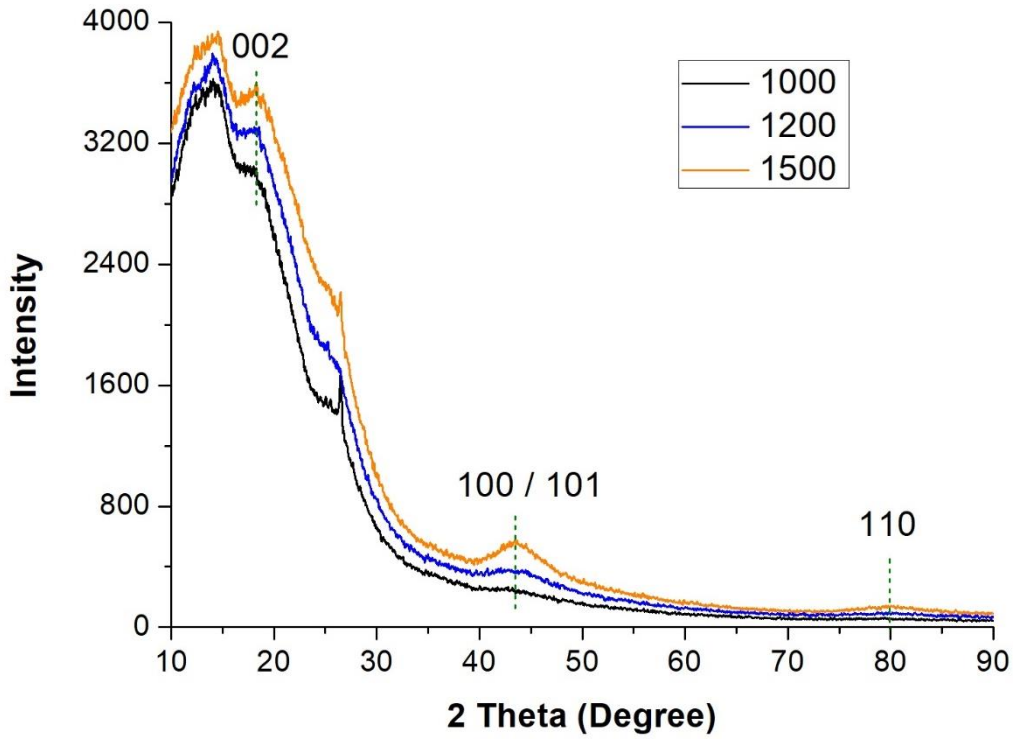

Figure 5.28 X-ray diffraction results for ASL-ESL lignin fibres carbonised at 1000 °C, 1200 °C and 1500 °C in nitrogen for 1 hour.

5.4 Electro-spinning of Lignin with Tannic Acid

As part of the initial screening of additives to aid the electro-spinning of lignin, a shortlist of possible bio-based materials was compiled (see Appendix E). The selection criteria for the processing aid was: (i) the structure of the processing aid had to be similar to that of lignin; (ii) the molecular weight was chosen to be lower than that of lignin such that it could potentially serve as a plasticiser; (iii) the char content upon pyrolysis had to be similar to that of lignin at 900 °C; (iv) its cost had to be reasonable; (v) it had to be soluble in organic solvents; and (vi) its electrical properties had to be conductive for electro-spinning.

The processing aids that proved to be the effective in terms of fibres formation via electro-spinning were Daemonorops draco resin, benzoin (Styrax) resin and tannic acid. Of these, tannic acid (TA), a derivative of tannin which exist in lignocellulosic biomass could be electro-spun in a repeatable and consistent manner. As with the 95ASL-5ESL blend, the total polymer concentration was maintained 52.8 wt% where the composition was 95% ASL and 5% TA (coded as 95 ASL-5 TA) in an acetone/DMSO solvent mixture. The conductivity and viscosity of the polymer solution were 2.68 x 10^{-4} (Sm^{-1}) and 0.43 Pa.s respectively. The conductivity and viscosity of the ASL-TA polymer solution is similar to that of 100% lignin (ASL-ESL) blend presented in Table 5.1.

SEM micrographs of the electro-spun lignin fibres are shown in Figure 5.29 (a-b). This is an exciting proposition because it opens up a whole library of naturally occurring compounds which could be utilised to produce bio-based fibres.

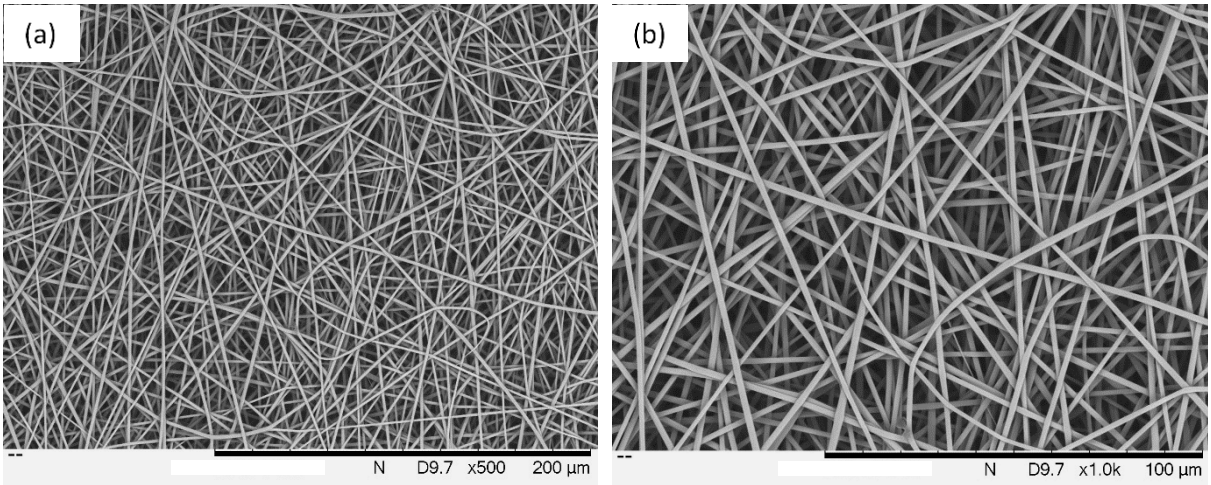

Figure 5.29 (a-b) SEM images of electro-spun lignin-based fibres (95 ASL-5 TA).

Figure 5.30 (a-b) shows transverse section of carbonised ASL-TA fibres that were thermo-stabilised at 250 °C in air followed by carbonisation at 1500 °C in nitrogen. The carbonised fibres show a smooth, circular and void-free morphology with diameter ranging from 280-790 nm.

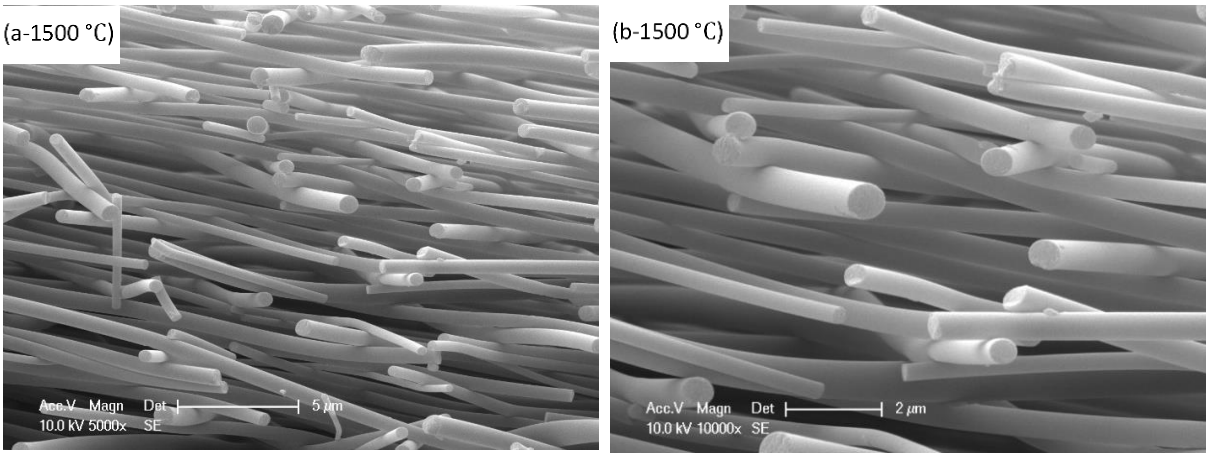

Figure 5.30 Micrographs showing transverse sections of electro-spun (ASL-ESL) lignin fibres after carbonisation at 1500 °C.

5.5 Summary

A novel production method for the production of carbonised fibres from 100% lignin was developed. The carbonised fibres had a smooth surface morphology and a circular cross-section. The presence of voids was not detected in the SEM micrographs. The experimental conditions required for maintaining the structural form and morphology of the fibres were established and the production method was reproducible. Increased in carbonisation temperature for electro-spun lignin fibres produced carbon fibres with higher graphitic content. The physical and electrical properties of 100% lignin-based carbon fibres were determined.

Chapter 6 Quantification, Extraction, Characterisation and Electro-spinning of Lignin from Coir

The electro-spinning a blend of ASL-ESL lignin was demonstrated in the previous chapter where the lignin was purchased. In the current chapter, the lignin was extracted from coir fibres and "coir dust". With reference to Table 2.1 (Section 2.1) it seen that coir fibres contain the highest lignin content for the plant-based materials cited. The fibres are extracted from the coconut husk and in general, they can be purchased in three forms: (i) "three-tie"; (ii) "two-tie"; and (iii) loose fibres of variable length. The three-ties fibres are sold as bundles and they represent the premium grade. The term tie is used because the bundle is secured by three bands of coir fibres (see Section 3.11,1). During the extraction of fibres from the husk, a significant volume of coir dust and short fibre 10-40 mm is generated, and this generally referred to as coir pith. The coir pith is compressed into briquettes of dimensions 220 x 80 x 50 mm. This chapter reports on the extraction and characterisation of coir pith and coir fibre. The extracted lignin was blended with cellulose acetate and electro-spun to produce fibres with diameter in the range between 300-600 nm.

6.1 Characterisation of Coir Pith and Fibres

6.1.1 Scanning Electron Microscopy

SEM micrographs of coir pith is presented in Figure 6.1 (a-d) which shows two distinct and contrasting morphologies. Figure 6.1 (a-b) show the flaky morphology of coir pith. The morphology in Figure 6.1 (b) is attributed to the cellulose microfibrils (374). The micrographs presented in Figure 6.1 (c-d) are most likely compressed sections of coir pith, possibly formed as a consequence of the production of the briquettes via hydraulic compaction in a mould. However, the morphology in Figure 6.1 (c-d) may be attributed to the agglomerates of cellulose microfibrils and lignin particles (374, 417).

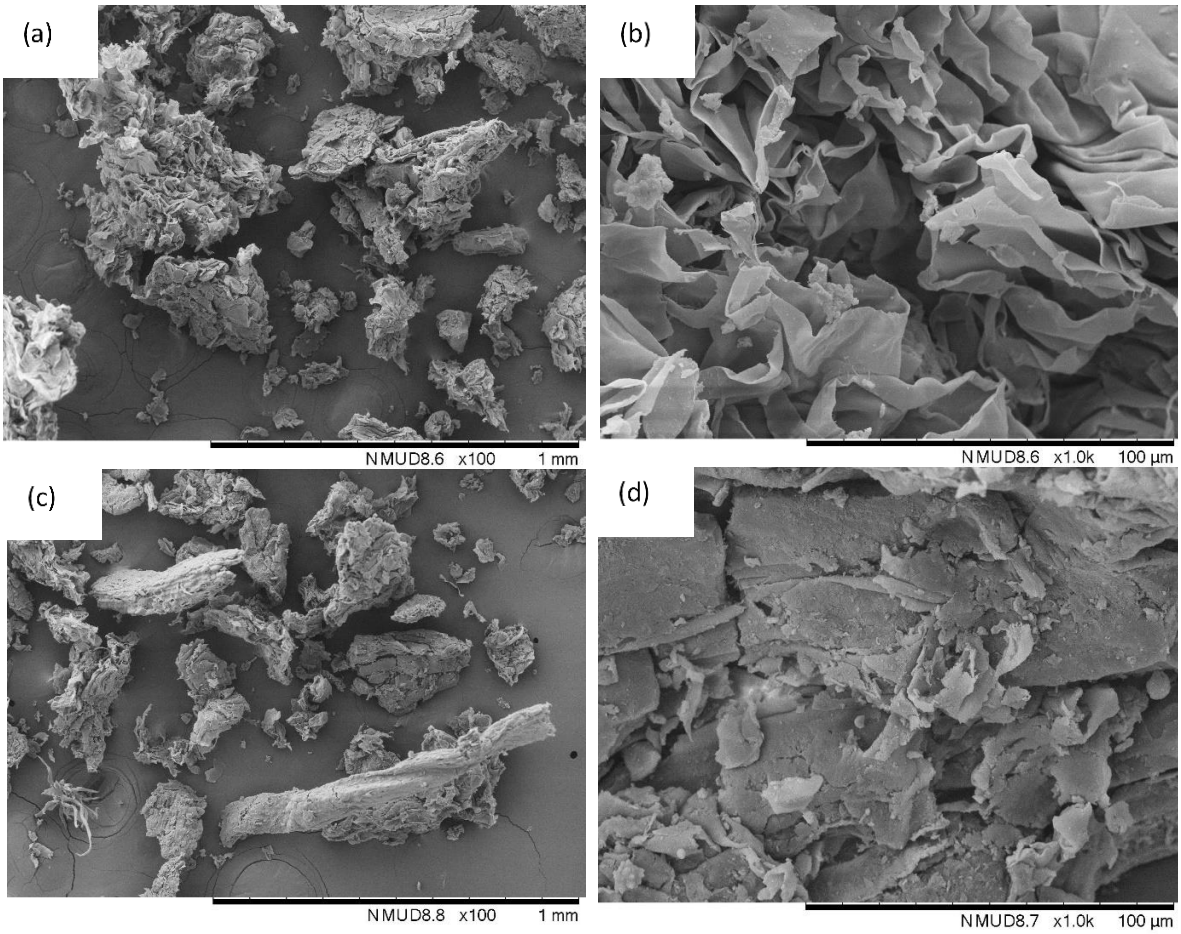

Figure 6.1(a-d) SEM micrographs of as-received coir pith showing: (a-b) a flaky morphology attributed to the cellulose microfibrils (374); and (c-d) a compacted version of the flaky morphology which is thought to be comprised of agglomerates of cellulose microfibrils and lignin particles (374, 417).

A representative transverse cross-section of a coir fibre is shown in Figure 6.2 (a-d). The diameter of the coir fibre was variable as a function along its length. The average diameter of the coir fibre was between 200-300 µm. The key structural features of the coir fibre are indicated in Figure 6.2 (a-b). Coir fibre is comprised of several elementary fibres that surround the lumen. Each elementary fibre is composed of a cell wall and microfibrils (418). The feature at the centre of the fibre in Figure 6.2 (a) is called a Lacuna (419). Figure 6.2 (c-d) shows the surface morphology of a coir fibre that contains globular protrusions on the surface called tylose. This is comprised of fatty acids (420).

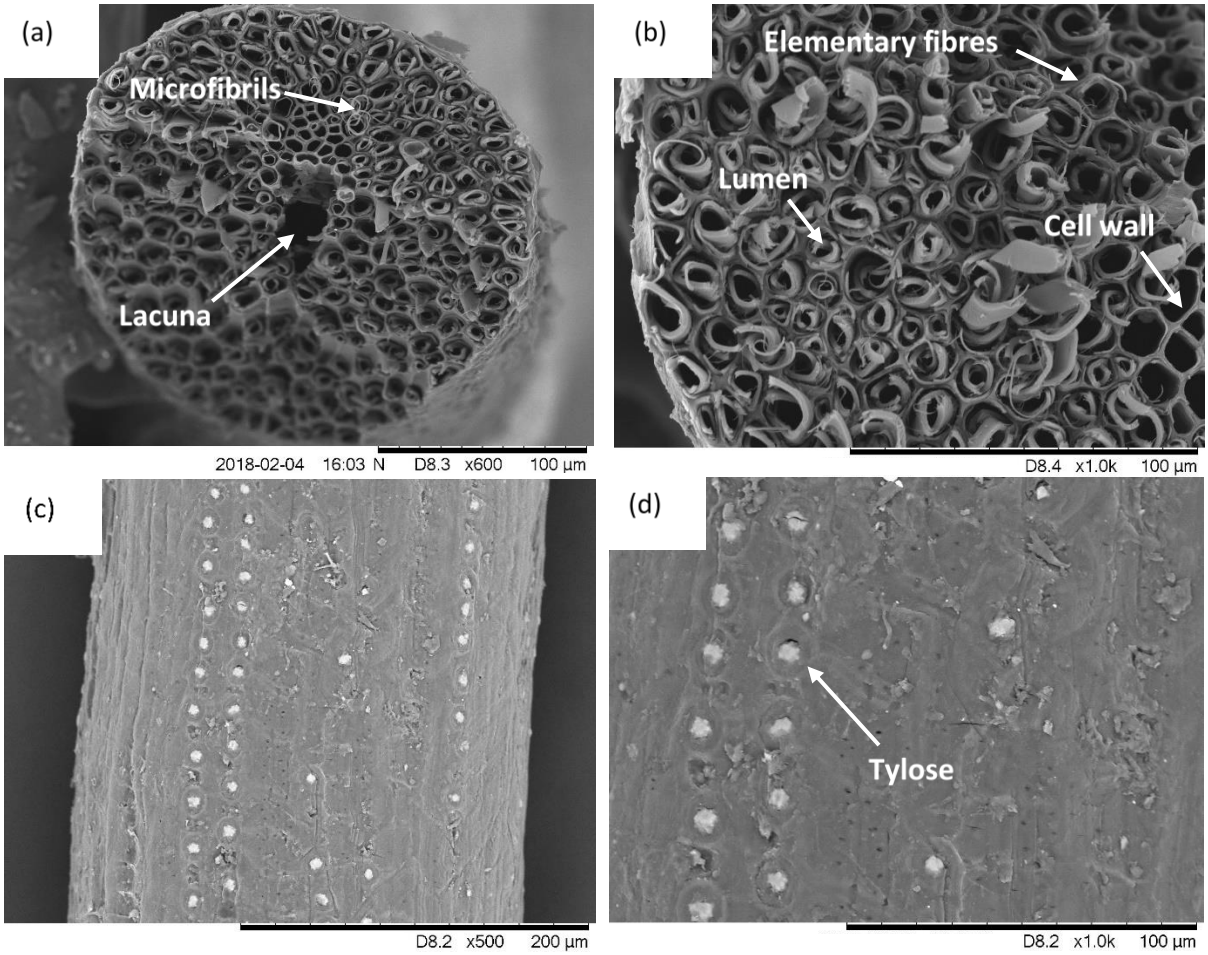

Figure 6.2 (a-d) SEM micrographs of as-received coir fibres: (a-b) transverse section; and (c-d) surface morphology.

The coir pith and fibres were subjected to cryo-milling as described in Section 3.11.1. In the case of the coir fibres, they were guillotined to produce short fibres of length between 20-30 mm. The cryo-milling was carried out to reduce the particle size distribution of the samples. SEM micrographs of the cryo-milled coir pith and fibres after processing are shown in Figure 6.3 (a-d) to enable comparison. On comparing the figures of as-received and cryo-milled coir it is seen that the cryo-milling reduces the particles size. In the case of the coir fibres, cryo-milling was seen to crush and fracture of the material in the longitudinal and transverse directions.

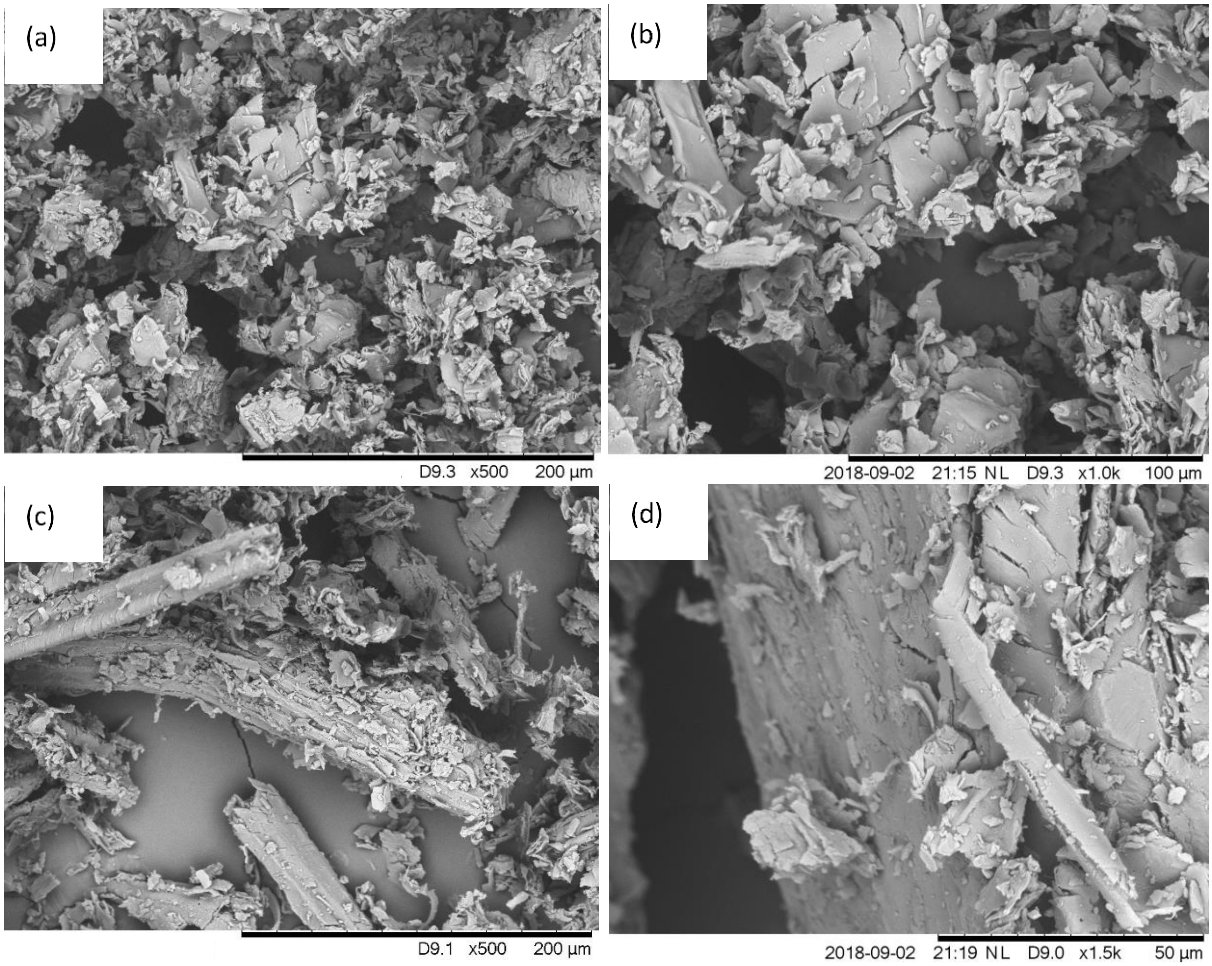

Figure 6.3 (a-d) SEM micrographs showing morphologies of: (a-b) cryo-milled coir pith; and (c-d) cryo-milled coir fibres.

6.1.2 Particle Size Distributions for Cryo-milled Coir Pith and Fibres

The particle size distribution curves for cryo-milled coir pith and fibres are shown in Figure 6.4 (a-b) respectively. The particle size distribution curves for the cryo-milled coir pith shows a relatively high volume of smaller particles when compared to the cryo-milled coir fibres.

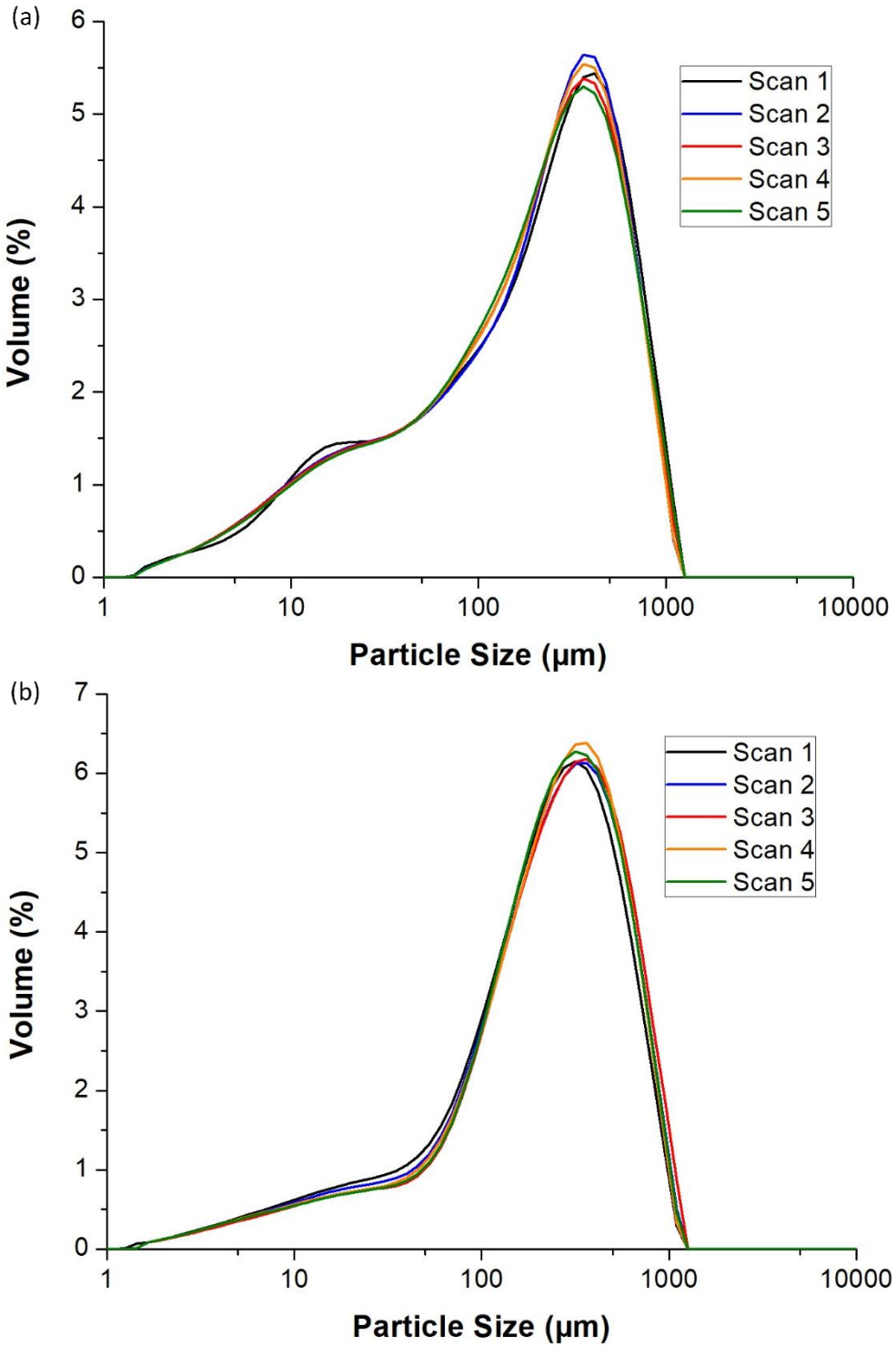

Figure 6.4 (a-b) Particle size distribution for: (a) cryo-milled coir pith; and (b) cryo-milled coir fibre.

The analysis for particle size distribution for two classes of materials after cryo-milling is summarised in Table 6.1 where a difference is observed between the particle size range. This

suggests that cryo-milling was effective in reducing the particle size. The standard percentiles d (0.1), d (0.5) and d (0.9) for the coir pith are smaller than those obtained for coir fibre.

Table 6.1 Particle size distribution analysis for cryo-milled coir pith and cryo-milled coir fibre.

Coir material	**Particle size distribution (µm)**			
	d (0.1)	d (0.5)	d (0.9)	Particle size range
Cryo-milled coir pith	14.4	191.2	579.5	1.3-1096
Cryo-milled coir fibre	28.6	223.9	583.7	1.6-1096

6.1.3 The Compositions of Coir Pith and Coir Fibre

The composition of the coir pith and fibre including the lignin content were determined in accordance with TAPPI methods as discussed in Section 3.11.2 and the results are summarised in Table 6.2. It is seen that coir pith contained a relatively higher moisture content and ash content when compared to coir fibre. However, the total lignin content was found to be significantly higher in the coir fibre. Different concentrations for lignin and carbohydrates in coir are reported in the literature (421). However, the values presented in Table 6.2 correlate well with the composition of coir (422, 423). The ash content in coir pith is also reported to be higher than that of coir fibre (424, 425). It is observed that the maturity of the nut may influence the composition of the coconut husk including the coir pith and fibre (424, 426). For instance, it is known that upon ripening of the nut, the extractives content is significantly reduced whilst lignin and polysaccharides (carbohydrates) content are increased (424, 426). Given the higher lignin content in the coir fibre, it was used as a preferred material to extract the lignin.

Table 6.2 The composition of coir pith and coir fibre in accordance with TAPPI methods.

Biomass	Moisture	Ash	Acetone soluble extractive	Acid insoluble 'Klason' lignin	Acid soluble lignin	Total lignin content	Carbohydrates
Coir pith	21.7	9.6	2.6	20.5	3.1	23.5	42.6
Coir fibre	8.6	1.2	1.9	29.8	1.8	31.6	56.7

Figure 6.5 shows the elemental composition of the ash from coir pith and coir fibre obtained using SEM-EDS. The observed minerals composition of ash in coir pith and fibre correlates with the data reported in literature where potassium and silicon are the key elements (425, 427). The reasons for the absence of chlorine in the coir fibres is not known. The presence of chlorine content is common in herbaceous and agricultural residues (428). The existence of alkali/alkaline metals in biomass is mainly in the form of inorganics salts and they generally also exist as the corresponding oxides, nitrates and chlorides (429).

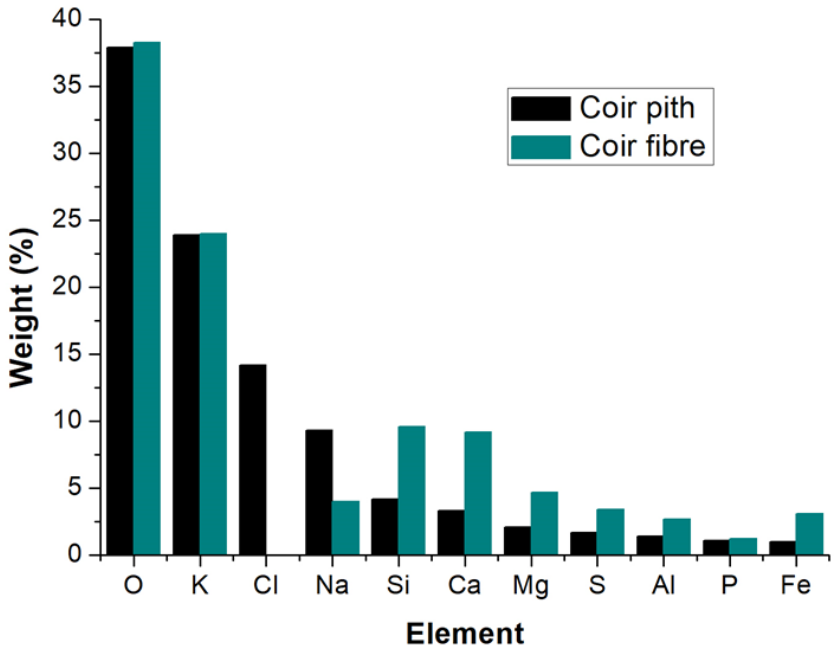

Figure 6.5 Elemental composition of the ash in oxidised coir pith and fibres.

6.2 Elemental Composition of Alkali Lignin from Coir and its Molecular Weight Distribution

Lignin was extracted from the coir fibres using the procedures outlined in Section 3.11.3. Figure 6.6 shows the appearance of the pale brownish alkali lignin that was extracted from coir fibre. SEM micrographs of the lignin that was extracted from coir fibres are presented in Figure 6.7 (a-b). The alkali lignin yield recovered from the coir fibre was 16.7%. The low yield for alkali lignin can be attributed to a lower concentration of sodium hydroxide and processing temperature used for the extraction of lignin. It is reported that the lignin yield is greatly affected by the processing temperature and the concentration of sodium hydroxide (430-432). Nevertheless, use of high temperature and high concentration can increase the yield but alters the lignin structure during delignification (430).

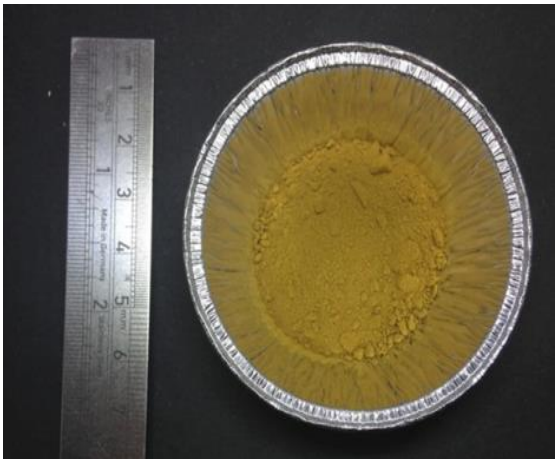

Figure 6.6 Alkali lignin extracted from coir fibre.

SEM micrographs of the alkali lignin extracted from the coir fibre is shown in Figure 6.7 (a-b). The morphology of lignin alkali shows globular morphology which is typical characteristic for lignin morphology (374). Figure 6.7 (a-b) shows that these globules are agglomerated.

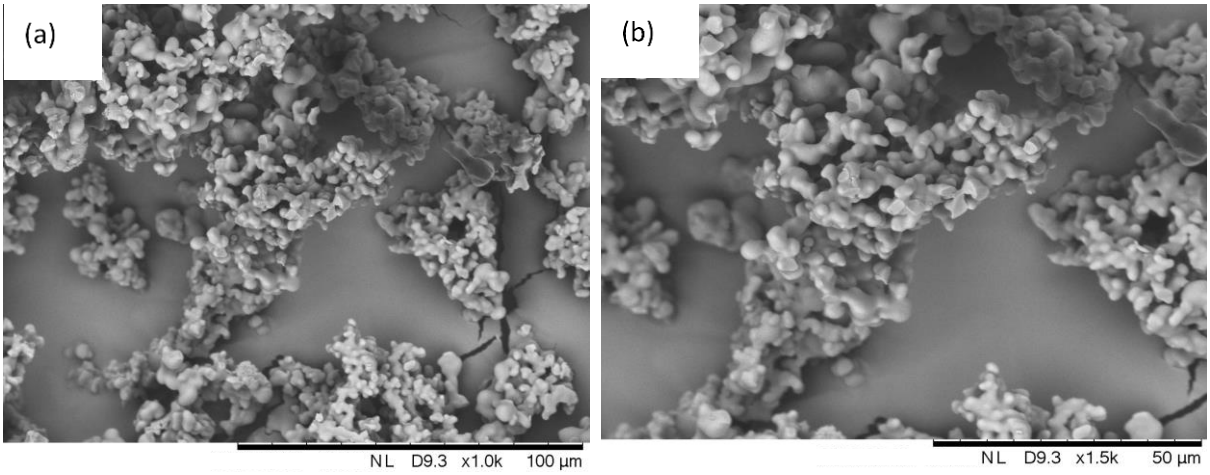

Figure 6.7 (a-b) SEM micrographs alkali lignin extracted from coir fibre.

The elemental composition and molecular weight distribution of the alkali lignin from coir fibres is summarised in Table 6.3. The elemental composition correlates well when compared with industrial softwood Kraft (BioChoice®) lignin as shown in Section 4.3. However, alkali lignin shows no sulphur content when compared to BioChoice® lignin. This is expected as Kraft pulping process for BioChoice® lignin employs sodium hydroxide and sodium sulphide (Na_2S) as a chemical solution for the extraction of lignin from softwood. The weight-average molecular weight (M_W) of alkali lignin that was extracted from the coir fibres is 5925 g/mol with a polydispersity index (PDI) of 11.7. This implies that alkali lignin has wider molecular weight distribution compared to BioChoice® lignin. This may be attributed to the presence of branched polymer chains in high concentration. This suggest that the lignin from coir has a branched structure. This is supported by the high aliphatic-to-phenolic ratio in the ^{31}P NMR spectra (see Table 6.3). The lignin from coir was further characterised using a range of techniques to determine the thermal and structural properties.

Table 6.3 Elemental composition and molecular weight of alkali lignin.

Lignin	**C, H, N, S and O content**					**Molecular weight distribution (GPC)**		
	C (%)	H (%)	N (%)	O (%)	S (%)	M_n (g/mol)	M_W (g/mol)	PDI (M_W/M_n)
Alkali lignin (coir)	58.8	5.5	0.3	35.4	0	515	5925	11.7
BioChoice ® lignin	64.7	5.7	0	28.3	1.4	3413	7367	2.16

6.3 Thermal Analysis of Alkali Lignin Extracted from Coir Fibres

TGA and DTG traces for coir pith, coir fibre, alkali and Klason lignins are shown in Figure 6.8 (a and b) respectively and the following conclusion can be drawn:

The Klason and alkali lignin showed a higher thermal stability when heated in argon when compared to that of coir pith and fibres. These samples also have a higher char content after pyrolysis at 900 °C. A contributing reason for this may be due to the higher ash and carbohydrates concentration (see Table 6.2). The higher char content in the pyrolysed coir fibre when compared to the pith indicates that the former has higher lignin content, and this also correlates well with the results determined using the TAPPI methods. Figure 6.8 (b) shows the DTG curves which indicates that the coir pith and fibres samples start to decompose at lower temperature whilst the lignin samples decompose significantly slower over a broader temperature range. This is because the coir pith and fibres contain a relatively higher concentration of carbohydrates (cellulose and hemicellulose) which decompose at lower temperatures (<400 °C) yielding a lower char residue (353, 354). This is exhibited by the high intensity DTG (maximum) peak of coir pith and fibre between 200-400 °C. The Klason lignin samples from coir fibre and coir pith yielded a char of 43.3% and 37.2% respectively whereas the char yield for the alkali lignin that was extracted from coir fibres was 34.2%.

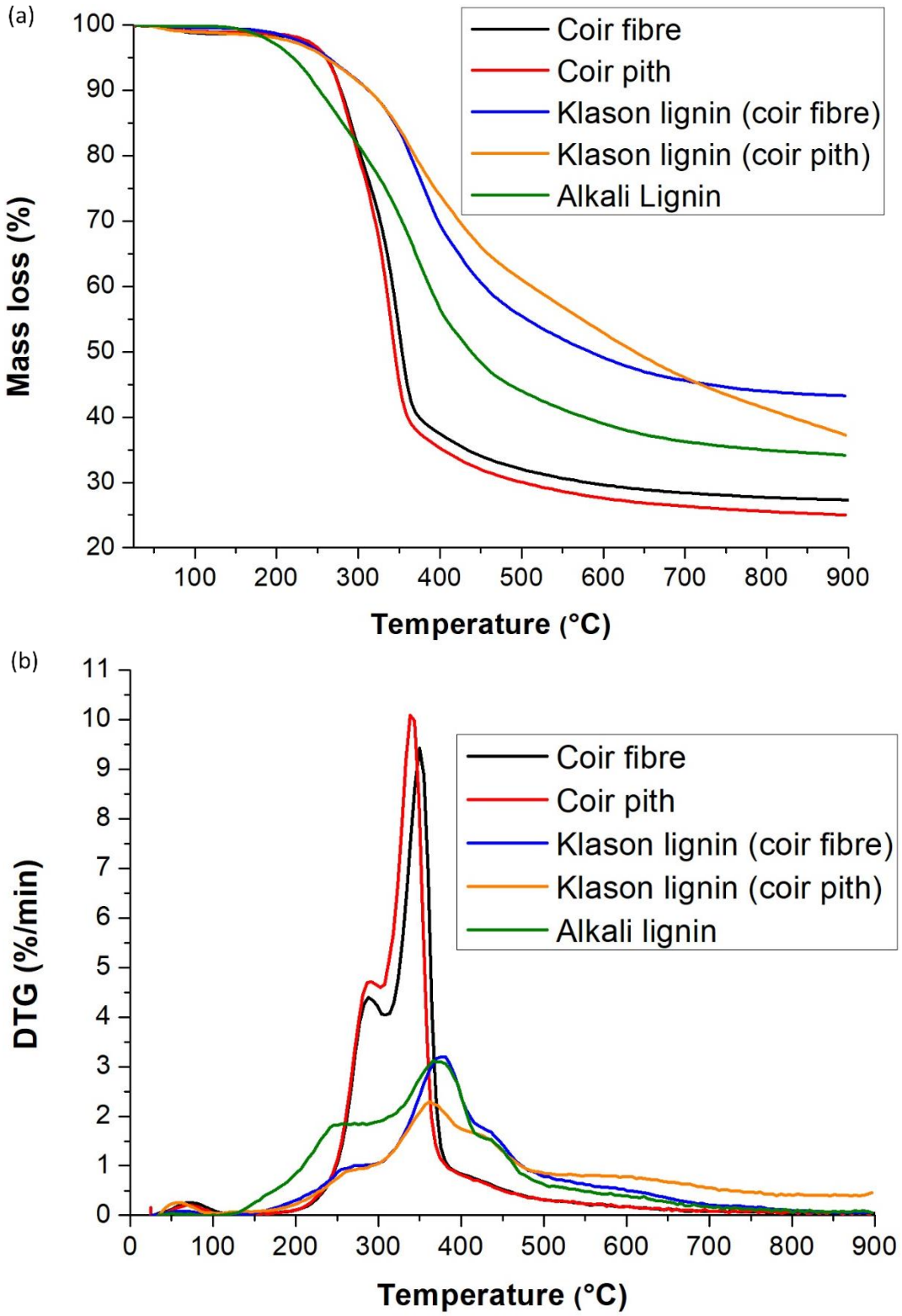

Figure 6.8 (a) TGA and (b) DTG data for coir fibre, coir pith, Klason and alkali lignin.

A summary of the char content after pyrolysis in argon at 900 °C and the DTG peak temperatures for coir pith, coir fibre, Klason, alkali and BioChoice® lignins are presented in Table 6.4. On comparing lignin samples, alkali lignin extracted from coir fibre show the lower char content. This may be attributed to the higher mass loss between 250-400 °C which is indicated by the intensity of DTG peak. Nevertheless, the char content achieved at 900°C of alkali lignin from coir is higher than those reported in the literature (433, 434).

Table 6.4 Char residue at 900 °C and maximum DTG peak temperature of biomass including Klason and alkali lignin.

Samples	**Char at 900 °C (%)**	**DTG max (°C)**
Coir pith	25.1	338.5
Coir fibre	27.3	349.7
Klason lignin (coir pith)	37.2	361.6
Klason lignin (coir fibre)	43.3	381.0
Alkali lignin	34.2	366.0
BioChoice ® lignin	43.4	566.2

The DSC traces for three successive heating scans in nitrogen for alkali lignin that was extracted from coir fibres are shown in Figure 6.9. As discussed previously, the T_g was calculated using the midpoint method (see Section 4.4). The T_g for alkali lignin in the 1st, 2nd and 3rd heating scans are 140.8, 155.8 and 160.2 °C respectively. Whilst the T_g for BioChoice® lignin heated to 200 °C in the 1st and 2nd heating scan were 120.1 and 153.4. Thus, the glass transition temperature of alkali lignin is comparable to the BioChoice® lignin. However, T_g for alkali lignin is significantly higher than those reported after fractionation in Sections 4.7 and 4.8 where the variation in the T_g correlates with molecular weight of the lignin samples.

Klason lignins were used for quantification purposes in accordance with TAPPI methods. However, the T_g was not detected for the Klason lignin. This may due to the treatment of coir fibre with a strong acid during quantification of lignin.

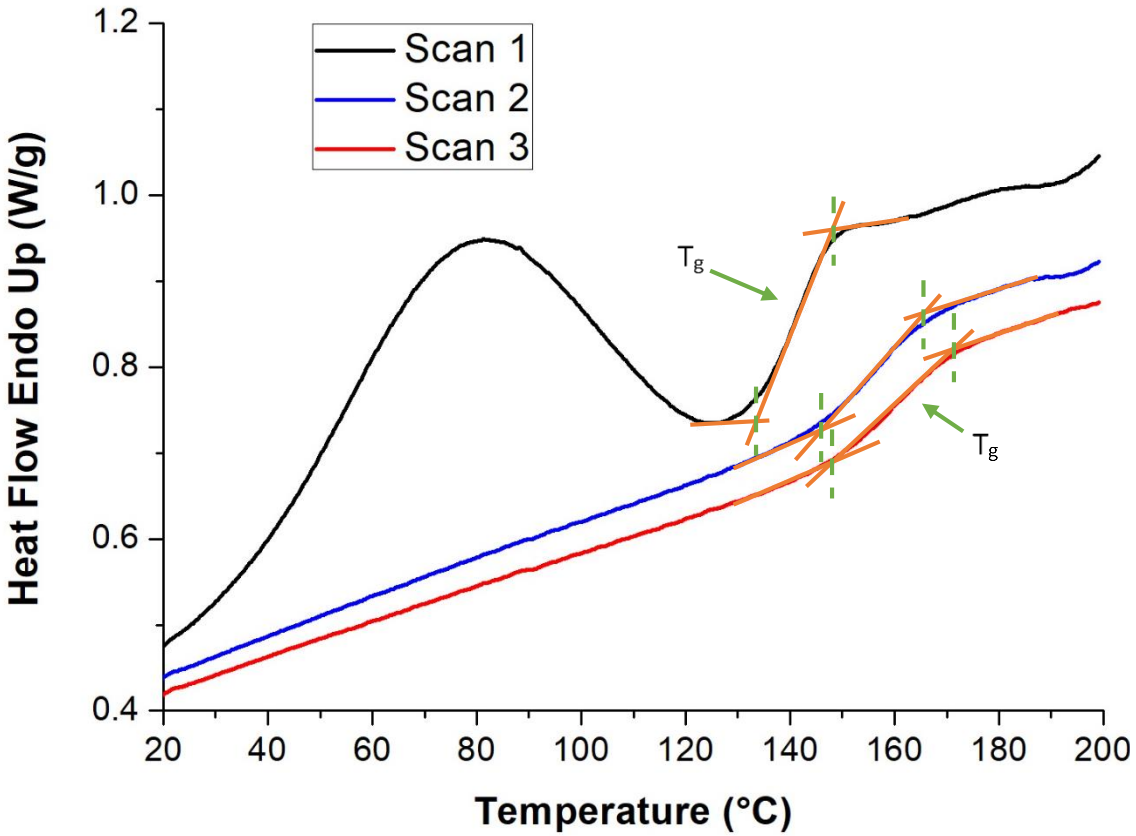

Figure 6.9 DSC traces of heating scans of alkali lignin.

6.4 Spectral Analysis of Alkali Lignin Extracted from Coir Fibres

6.4.1 Ultraviolet/Visible Spectroscopy

A representative UV/Vis spectrum for BioChoice® and alkali lignin extracted from coir fibres is shown in Figure 6.10. Alkali lignin shows an absorption peak at ~280 nm due to π-π* electronic transition of the conjugated aromatic G-lignin unit (380, 381). Assuming the absence of any contamination in the form of aromatic macromolecules, the presence of this peak suggests the presence of lignin as only it exhibits such electronic transitions whilst cellulose and hemicellulose does not contain aromatic groups. The absorption at ~320 nm is attributed to the electronic

transition of π-π* along with n-π* transition. This is due to the conjugated carbon (C=C) bonds in the aromatic ring and carbonyl groups (C=O) on the aromatic ring. The absorption at ~340 nm is due to electronic transitions of n-π* attributed to the α-carbonyl groups and esters of hydroxycinnamic acids (e.g., ferulic acid and p-coumaric acid) (89, 101, 386).

As mentioned previously, that the purity of lignin can be determined through UV/Visible spectroscopy which is based on Beer-Lambert's law (89, 383). The method for the calculation of extinction coefficient is discussed in Section 3.6.11. The extinction coefficients at 280 nm for alkali and BioChoice® lignin are 26.7 and 27.5 respectively. There is a marginal difference in the extinction coefficients which suggests that the alkali lignin is of a comparable quality to that of BioChoice® lignin.

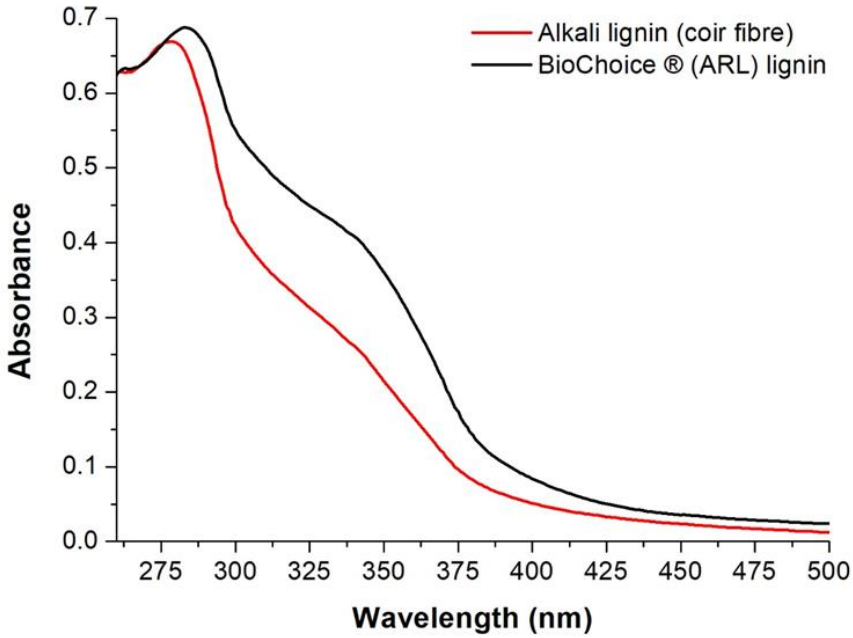

Figure 6.10 UV/Visible spectra of BioChoice® and alkali lignin that was extracted from coir fibres.

6.4.2 Fourier Transform Infrared Spectroscopy of Alkali Lignin Extracted from Coir Fibre

FTIR spectra of BioChoice® lignin (discussed in Sections 4.13) was presented in Figure 4.19 (a-b) and Table 4.10 where the major peaks were labelled and the assignments for each of the absorbance band was stated. The same assignment procedure has been used in Figure 6.11 (a-b)

where (a) represents coir pith and fibre and (b) represents the FTIR spectra for alkali, BioChoice® and Klason lignins. Table 6.5 has been reproduced here and the associated peak assignments have been extended.

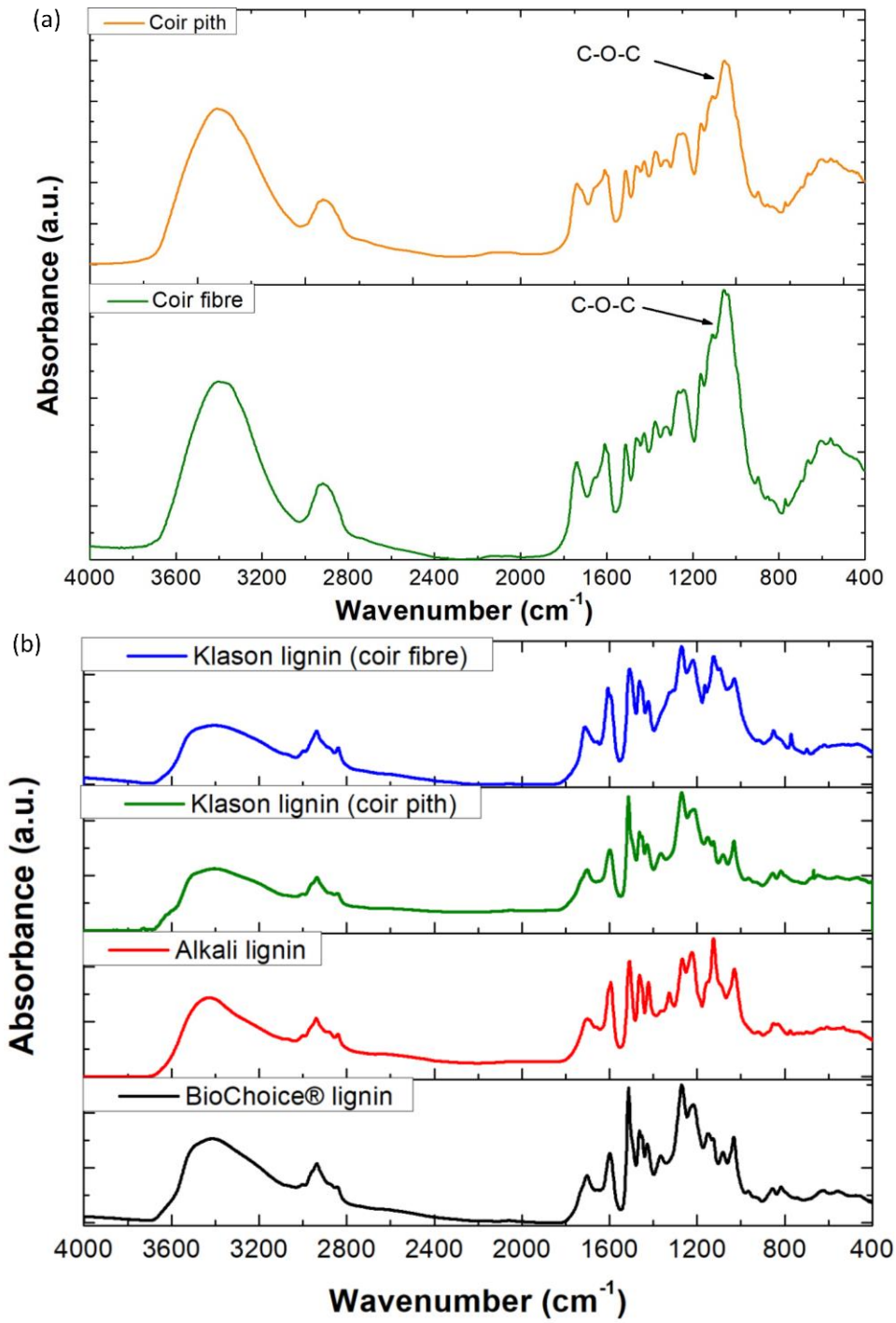

Figure 6.11 (a-b) FTIR spectra of: (a) coir pith and fibre; and (b) alkali, BioChoice® and Klason lignin.

Figure 6.11 (a) shows the fingerprint region between 1000-1200 cm^{-1} in coir pith and coir fibre which is attributed to C-O-C stretching vibration of pyranose (carbohydrates) ring skeletal vibration (353). Figure 6.11 (b) shows the FTIR spectra for alkali, BioChoice® and Klason lignin with distinct fingerprints for the structural moieties present in lignin. The quality of alkali lignin from coir and the corresponding spectrum produced is finer than those reported in the literature. The strong peak at ~1120 cm^{-1} could be attributed to secondary alcohol present in alkali lignin. The noticeable difference between the alkali and BioChoice® lignins are the absorbance peaks at 1460 cm^{-1} and 1270 cm^{-1}. The peak intensity at 1460 cm^{-1} for alkali lignin is higher that for BioChoice® lignin. This peak corresponds to C-H bending in O-CH_3 which may be attributed to higher concentration of methoxyl group in alkali lignin. The peak intensity at 1270 cm^{-1} corresponds to aromatic G-unit breathing. This peak intensity is reduced in alkali lignin when compared to that of BioChoice® lignin. This suggests that alkali lignin contains higher proportion of syringyl (S)-unit than gauiacyl (G)-unit lignin structures. This data correlates well with S/G ratios determine by ^{31}P NMR in Section 6.4.5 and the literature where a high S/G ratio is reported for alkali lignin when compared to the BioChoice® lignin (435).

Table 6.5 FTIR spectral assignments for specific functional groups for lignin samples compiled from the reported literature (100, 101, 346, 376).

Wavelength (cm^{-1})	**Literature values (cm^{-1})**	**Signal strength**	**Functional group assignments**
3411	3411-3390	Strong Broad	O-H stretch, phenolic and aliphatic O-H group stretch
2936	3050-2800	Medium	C-H stretch methyl and methylene groups, C-H vibrations of methyl or methoxyl group
1703	1710-1700	Medium	CO stretching (in conjugated aldehydes, ketones and carboxylic acids)
1597	1600-1500	Medium	Aromatic skeletal vibration
1513	1600-1500	Strong	Aromatic skeletal vibration
1463	1460-1450	Strong	Asymmetric bending C-H in plane deformation of methyl, methylene and methoxyl ($O-CH_3$) groups
1428	1428-1420	Weak	Aromatic skeletal (ring) vibration combined with C-H in plane deformation
1365	1365-1370	Weak	C-H deformation in methyl, methoxyl ($O-CH_3$) group
1270	1270-1260	Strong	Aromatic ring (Guaiacyl moieties) breathing with CO stretch
1218	1226-1216	Medium	C-C, C-O and CO of ester stretching vibrations
1150	1155	weak	CO deformations in conjugated ester in G, S, H units of lignin combined with aromatic C-H in plane deformation
1120	-	Strong	C-O stretching in secondary alcohol
1082	1085-1081	Weak	C-O deformation in secondary aliphatic alcohols and aliphatic ether
1032	1035-1029	Weak	C-O deformation in primary aliphatic alcohols combined with aromatic C-H in plane deformation
855	854-852	Weak	C-H deformation out of the plane in G aromatic units
816	817-814	Weak	C-H deformation out of the plane in G aromatic units

6.4.3 Proton Nuclear Magnetic Resonance Spectroscopy of Alkali Lignin from Coir Fibre

The ^{1}H NMR spectra of alkali lignin is shown in Figure 6.12 for the fingerprint region of the aliphatic and aromatic lignin structural moieties. The assignment of the complete structural moieties in lignin is discussed in the previous Section 4.15. The chemical shifts for the ^{1}H NMR spectra are assigned according to the database in the literature (152, 378, 435). The prominent structures in alkali lignin (coir fibre) are found to be β-O-4 aryl ethers (arylgylcerol-β-aryl ethers), phenylcoumarans, resinol and dibenzodioxocins. The chemical shift at 10.2 ppm could be attributed to cinnamaldehyde (435). The peak intensity of cinnamaldehyde is significantly higher when compared to that of BioChoice® lignin.

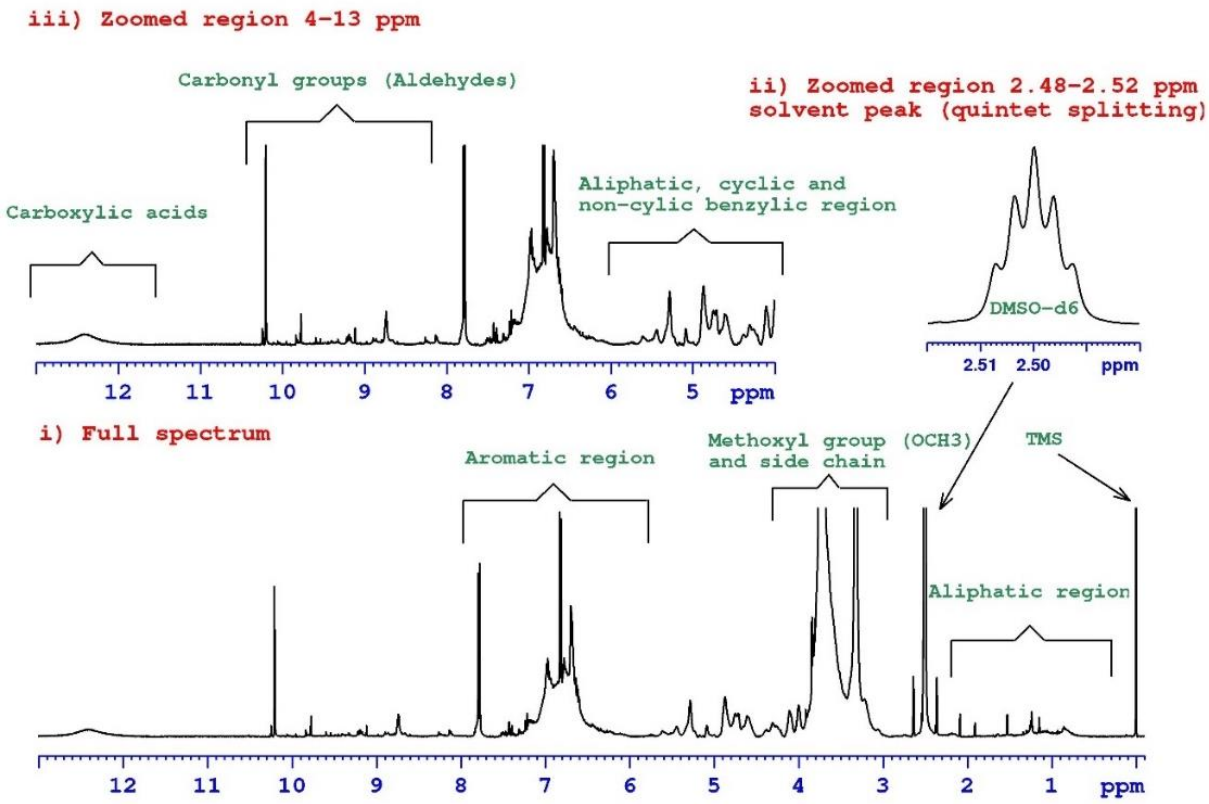

Figure 6.12 ^{1}H NMR of alkali lignin from coir fibres.

6.4.4 ^{13}Carbon Nuclear Magnetic Resonance Spectroscopy of Alkali Lignin from Coir Fibre

^{13}C NMR spectra of alkali lignin from coir fibre is shown in Figure 6.13. The chemical shift between 90-102 ppm suggests the absence of carbohydrates in alkali lignin (153, 301). The aromatic region shows increased concentration of peaks compared to softwood Kraft (BioChoice®) lignin. These peaks correspond to the presence of S, G, H-lignin units along with cinnamyl alcohol and cinnamaldehyde end-groups. The peak assignments are based on that reported literature (152, 435). The increased number of peaks in the aromatic region could be also due to the increased ratio and presence of hydroxycinnamates (p-Coumarate, ferulate and sinapate) lignin units (378). The chemical shift at 161 and 167 ppm could be due to the presence of methyl ester and carboxylic acids groups. The complete chemical shift assignment for lignin is listed in Section 4.16.

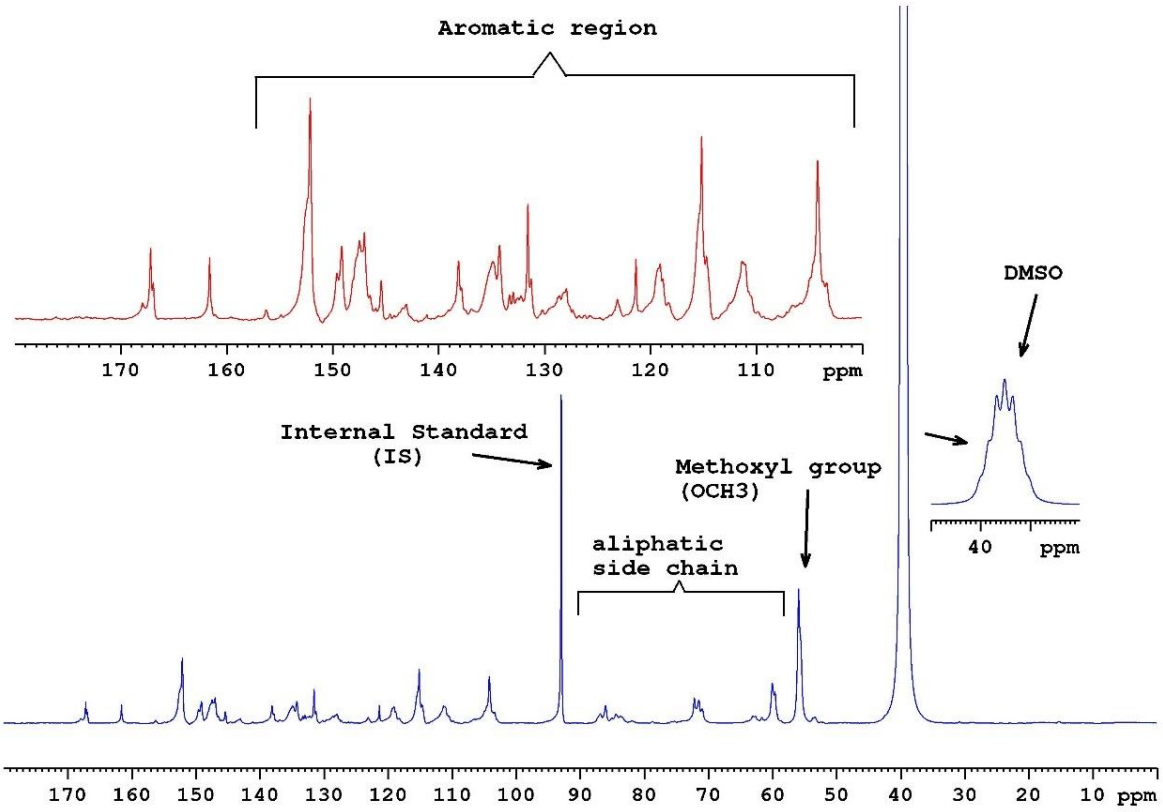

Figure 6.13 ^{13}C NMR of alkali lignin that was extracted from coir fibre.

6.4.5 ^{31}Phosphorous Nuclear Magnetic Resonance Spectroscopy of Alkali Lignin Extracted from Coir Fibre

^{31}P NMR spectra of alkali lignin from coir fibre and the structural assignment of the moieties is shown in Figure 6.14. The ^{31}P NMR spectra shows distinctively higher concentrations of carboxylic acids and aliphatic groups compared to the other lignin moieties.

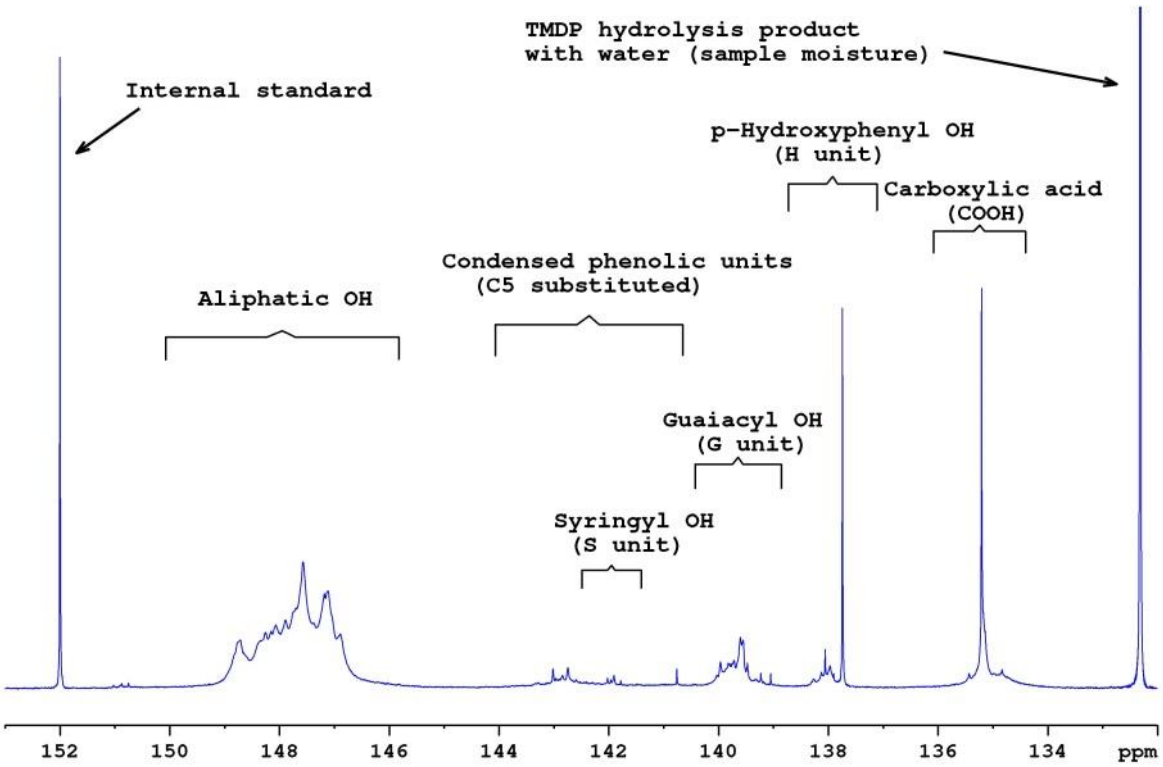

Figure 6.14 ^{31}P NMR of alkali lignin extracted from coir fibre.

The lignin structural moieties show significantly higher ratio of aliphatic-to-phenolic lignin groups as shown in Table 6.6. This suggests that alkali lignin has a highly branched structure which was also indicated by its higher polydispesity index (103). The carboxylic acid concentration was relatively higher, and it correlates well with the ^{13}C NMR spectral results. The high concentration of carboxylic acid is due to the presence of hydroxycinnamic acid derivates which was also indicated in the UV/Visible spectrum. The guaiacyl (G) lignin unit predominates in the phenolic structural units of coir lignin. The ratio of G/H/S was found to be 51/35/14. This

was in agreement with the reported S/G lignin ratio in coir (435). However, the ratio of S/G lignin unit is significantly higher when compared to that of BioChoice® lignin (Section 4.17).

Table 6.6 Hydroxyl group content in alkali lignin from coir fibre (mmol g^{-1}) moieties using ^{31}P NMR.

Chemical Shift, δ (ppm)	Assignment	Alkali lignin coir
150.0-143.3	Total aliphatic	4.42
145.0-140.5	Condensed phenolic units (C-5 substituted)	0.22
143.0-142.0	Syringyl (S)	0.14
140.5-138.6	Guaiacyl (G)	0.52
138.5-137.6	p-Hydroxyphenyl (H) unit	0.36
136.4-133.6	Carboxylic acid (COOH)	0.89
-	Total phenolic units	1.10
-	Phenolic to aliphatic ratio	0.25

6.5 Electro-spinning of Alkali Lignin Extracted from Coir Fibres

In the previous section on electro-spinning, a novel approach was used for electro-spinning lignin blends. In the current case, the electro-spinning of alkali lignin from coir was carried out with cellulose acetate in acetone/DMSO. The reasons for this is the yield obtained for the alkali lignin and the electro-spinning was carried out without the lignin being fractionated. This was because the mass of coir (alkali) lignin that was available. The experimental details of alkali lignin blending with cellulose acetate and the electro-spinning procedure is discussed in Section 3.11.5. SEM micrographs of the electro-spun alkali lignin and cellulose acetate blends are shown in Figure 6.15. The morphology of the electro-spun fibre shows production of bead-free smooth and circular fibres with diameter ranging from 300-600 nm. The fibre spinning of alkali lignin without the need of solvent fractionation may be facilitated by higher S-lignin compared to softwood Kraft (BioChoice®) lignin (180). As mentioned previously in Section 2.6.1.1, the higher concentration of S-lignin units in hardwood lignin facilitates fibre spinning (179, 186). However, hardwood lignin takes a longer time to thermo-stabilise (178, 186, 218, 219). Therefore, alkali lignin from coir fibre presents a suitable alternative with a lower concentration of S-lignin units than hardwood lignin but higher concentration when compared to BioChoice® (softwood Kraft) lignin.

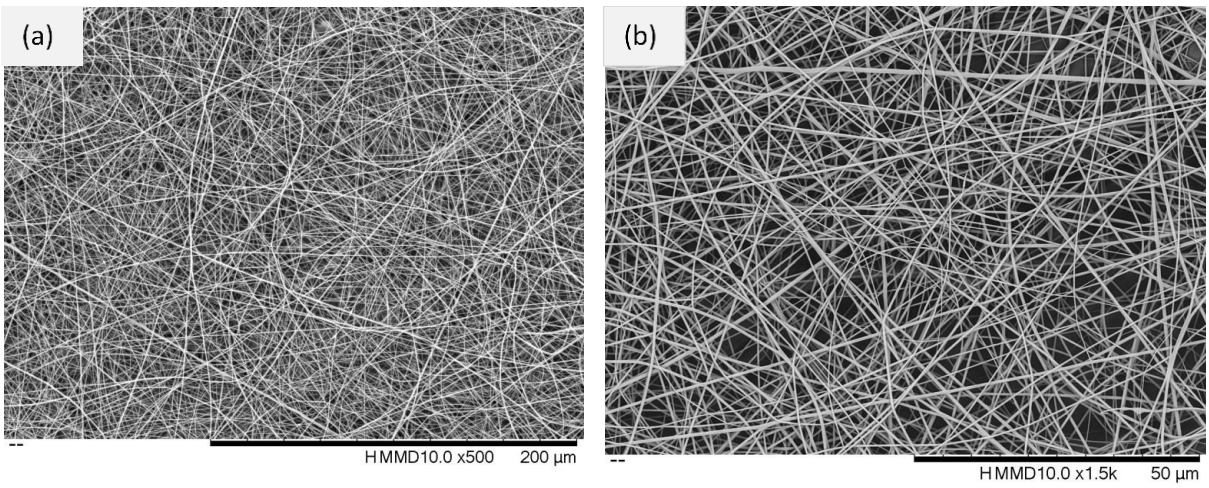

Figure 6.15 SEM micrographs of electro-spun fibres from lignin extracted from coir.

The production of electro-spun fibres confirms that lignin can be extracted from waste coconut husk and it can be used to manufacture preforms and can subsequently be converted to carbon fibres. This is the first time where lignin that was extracted from coir fibres has been used for producing electro-spun fibres.

Chapter 7 - Conclusions and Future Work

7.1 Conclusions

The focus of this research was to improve lignin processability and make 100 % lignin-based carbon fibres. The production of carbon fibres from 100 % lignin was demonstrated. The study demonstrated a pre-treatment methodology of lignin followed by an optimised thermo-stabilisation procedure for the conversion of precursor fibres into carbon fibres.

The measure of the performance can be evaluated by the comparison of aim and objectives outlined in Chapter 1 with the achieved output of results presented in previous chapters.

This chapter provides a conclusive summary of the main results obtained in each chapter. It also presents the recommendations for future work.

7.1.1 Solvent Fractionation and Characterisation of Softwood Kraft lignin

This chapter demonstrated that solvent fractionation can effectively reduce inorganic impurities down to 0.1% in comparison to the dilute acid treatment (0.34%). The fractionation also results in the removal of levoglucosan-a depolymerised product of cellulose. This implies that the solvent fractionation can be used to purify lignin by reducing the ash content which in turn can play an important role in the char content. A high inorganic or ash content can catalyse the reactions at elevated temperatures leading to the generation of water and gasification. The reduction of ash content by fractionation also facilitates the fibre spinning of lignin as discussed in Chapter 5 and Section 7.1.2. The as-received lignin was also found to be hygroscopic which was attributed due to the presence of hydroxyl groups in lignin structural framework.

The solvent fractionation with acetone, ethanol and 1-propanol leads to reduction of the molecular weight average (7367 to 3848 g/mol) and glass transition temperature (155 to 122 °C). The glass transition temperature of lignin fractions was found to be highly dependent on the molecular weight. It was also found that the soluble fractions have less branched structure with

higher phenolic to aliphatic ratio in comparison to the insoluble lignin fractions. The phenolic-to-aliphatic ratio was found to be a highly influential factor in the char yield.

7.1.2 Electro-spinning and Carbonisation of Lignin-based Fibres

The electrospinning of 100% precursor lignin without any additives was successfully demonstrated by using non-toxic solvents (acetone/DMSO). The lignin-based fibres thus produced were subjected to a series of experiment to optimise thermo-stabilisation process. The nitrogen thermostabilised fibres were found to fuse whilst the air thermo-stabilisation facilitated structural integrity of lignin fibres. The characterisation of lignin fibre revealed that the fibre undergoes significant structural changes during air thermo-stabilisation. The oxygen content was found to increase due to the formation of carbonyl and carboxyl groups whilst the hydrogen content decreased in air thermostabilised lignin fibres. The air thermostabilised lignin fibres were found to decompose slowly over a broader temperature range (250-900 °C) in comparison to nitrogen thermostabilised fibres. The disappearance of T_g associated with the structural changes were found to be hugely important to the successful completion of the thermo-stabilisation step.

The lignin-based carbon fibres showed a smooth and circular fibre morphology with electrical conductivity comparable to those reported in the literature. An increase in carbonisation temperature lead to an increase in the graphitic structure and the crystallinity of the lignin fibres. The surface roughness was also found to increase with carbonisation temperature (see Appendix Section A and B). All carbonised lignin samples showed good hydrophobicity with contact angle greater than 90° (see Appendix Section A and B). This correlates well with the general concept that the roughness is proportional to the contact angle for non-wettable surfaces (436). The diameter of lignin-based fibre was found to reduce with the increase in carbonisation temperature due to the apparent mass loss. The mean fibre diameter observed after carbonisation at 1500 °C was found to be 0.8 μm.

7.1.3 Quantification, Extraction and Electrospinning of Lignin from Coir

The determination of coconut coir composition (coir pith and coir fibre) showed the presence of relatively high lignin content (32 wt%). The lignin produced from coir fibre showed a T_g of 156 °C and char content of 34%. The alkali lignin has a branched structure due to the relatively high polydispersity index (11.7) with molecular weight average of 5925 g/mol. The aliphatic-to-phenolic ratio (4.42:1.10) of alkali lignin was found to be relatively high and is also an indicative of a branched structure. The concentration of S-lignin units was found to be higher than that of softwood Kraft lignin. It is reported that higher ratio of S-lignin unit facilitates in the formation of fibres. The electro-spun coir alkali lignin showed that the waste coconut coir can be a potential raw material for the production of carbon fibres.

7.2 Future Work

In this research, the softwood Kraft lignin was treated with a single solvent fractionation using acetone, ethanol and 1-propanol. Thus, to increase the yield of soluble fraction, the softwood Kraft lignin can be sequentially fractionated using acetone, ethanol and 1-propanol. This will increase the yield for lignin soluble fractions and reduce the content of insoluble residue. These soluble lignin fractions could contain a higher phenolic-to-aliphatic ratio with less branched structure which was demonstrated by soluble lignin fractions obtained using single solvent fractionation. The sequentially fractionated soluble lignin can be combined and used for electrospinning process. This will not only increase the soluble fraction yield but could also improve lignin char content.

It is reported that the interconnected fibres have much higher electrical conductivity than the non-fused (non-bonded) fibres (183). In this research, the investigations of thermo-stabilisation showed that atmospheric conditions influence the fibre morphology of lignin-based fibres. The thermo-stabilisation in nitrogen at a specific temperature results in fibre fusion (interconnected fibres) and the degree of fusion can be controlled by the processing temperature. This suggest that the electrical properties of lignin-based carbon fibre can be improved by introducing a controlled degree of fibre fusion. The mechanical properties of lignin electro-spun fibre also need to be explored.

The lignin-based carbon fibres showed good electrical conductivity and hydrophobicity. These properties including the surface area and porosity which can be tailored via surface activation and control of carbonisation temperature. The carbon fibres thus produced can be tested for their electrochemical, photovoltaic and capacitance performance which can determine their suitability for energy storage devices such as electrode materials for supercapacitor, solar and fuels cells.

High carbonisation temperature can also increase the crystallinity and graphitic structural domain. The mechanical properties of carbon fibre can also be improved using high carbonisation

temperature and reinforcement additives such as nanocrystalline cellulose (NCC) and carbon nanotubes (CNTs).

The successful electrospinning of 100 % lignin and other biomass derivatives such as tannic acid was demonstrated. This shows that carbon fibres can be made from a range of renewable precursors and thus opens up a library of new materials which can be utilised to produce bio-based carbon fibres.

The lignin fibres produced from coconut coir via electrospinning can be converted into carbon fibres. For future work, the properties of carbon fibre produced from coir lignin can also be compared with those produced from other lignin sources.

Appendices

Appendix A: Experimental Method for Atomic Force Microscopy and Surface Wettability

This section presents the experimental methods used for the analysis of electro-spun ASL-ESL lignin fibre using atomic force microscopy (AFM) and surface wettability (contact angle).

Appendix A1: Atomic Force Microscopy

A JPK NanoWizard II AFM (USA) was used to observe the surface morphology including the surface roughness of the electro-spun lignin fibres. The basic AFM setup is shown in Figure A.1 (437). In general, the setup consists of a mountable probe near to the end of a flexible Si based cantilever (with a reflective upper surface). The cantilever is mounted on a piezocrystal which allows the detection movement of the probe in relation to the surface of the sample. The cantilever moves vertically in the Z-direction pressing the fibre downwards and in turn gets deflected upwards. The deflection of the cantilever is observed by a photodetector through the change in the path of a laser light beam which is deflected by the top surface of the end of the cantilever. The controllable movement of piezocrystal allows the tip to come into the contact with the sample surface which results in the deflection of the laser light. This deflection can be used to generate topographic features and by calculating the interaction forces between the probe and the surface of the sample. The surface topography of randomly orientated lignin electro-spun fibres was monitored using tapping-mode. A Bruker RTESPA-300 probe (thickness: 3.4 μm; length =125 μm and width: 40 μm) was used to study the surface topography. The electro-spun fibres were mounted on silicon wafer using double-sided tape attached to both ends of the fibre mat. The following parameters were used in the tapping-mode experiments: resonance frequency = 325 kHz; and the force constant was = 40 N/m. The surface area considered to investigate the sample surface roughness was 20 x 20 μm. The surface roughness of the lignin fibres that was vacuum dried at 140 °C, thermostabilised at 250 °C in air and carbonised at 1000 °C, 1200 °C and 1500 °C

was determined using a line scan along the longitudinal fibre axis. The Ra values which represents the average roughness across the scan line were recorded (438). Total of five-line scans was obtained at different locations of the fibre to measure the roughness. The average roughness from five measurements for each sample is reported.

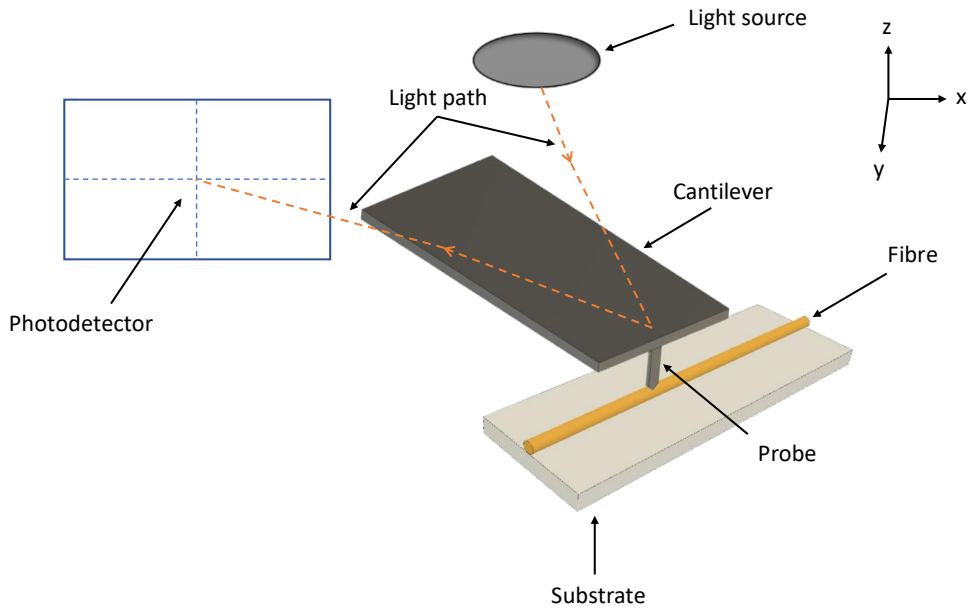

Figure A.1 Schematic illustration of the basic AFM setup to characterise the topography imaging of the electro-spun and carbonised lignin fibres.

Appendix A2: Surface Wettability

The surface wettability of the electro-spun fibres that were carbonised at 1000 °C, 1200 °C and 1500 °C was evaluated using an Opti-Tekscope (DirctNine, UK). This was achieved by obtaining high-resolution images (1600 x 1200 pixels) of water droplet on the surface of the carbonised electro-spun lignin fibre mat. A glass slide was used to mount the lignin samples. A 1 µL droplet of deionised water was deposited on the surface of the carbonised lignin fibre mate using an adjustable pipette. Three images were captured for each of the carbonised lignin fibre. A new sample was used for the acquisition of each image. The static contact angles were measured by processing the image through ImageJ software to find theta (θ) (see Figure A.2).

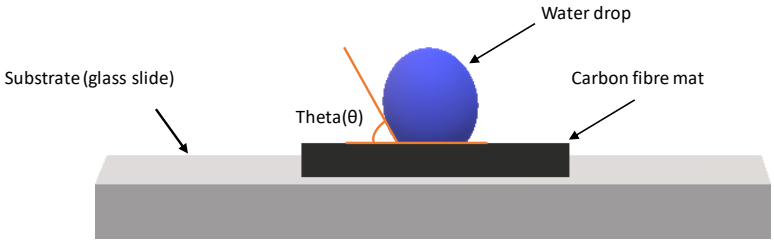

Figure A.2 Schematic illustration of the contact angle measurement involving a drop of deionised water of the surface of an electro-spun and carbonised lignin fibre mat.

Appendix B: Results and Discussion for AFM and Surface Wettability

This section presents the results of ASL-ESL electro-spun lignin fibres obtained using AFM and contact angle.

Appendix B1: Atomic Force Microscopy of Electro-spun ASL-ESL Lignin Fibres

The preliminary results for the topography of randomly orientated electro-spun ASL-ESL lignin samples using AFM in the contact mode are shown in Figure B.1 (a-e). Figure B.1 (a-b) shows the topography of vacuum dried lignin and the line scan which is obtained across the fibres to highlight the profile height of the sample in a specified dimension (20 x 20 μm).

Figure B.1 (c) shows the 3-D profile of the electro-spun fibre topography over a 20 x 20 μm scan area. The experimental details for obtaining the topography and the calculation of surface roughness is listed in Section Appendix A1. Figure B.1 (d) represents the topography image of electro-spun fibre using a line scan along the fibre axis to determine the average roughness. The surface roughness was averaged from the five line scan measurements which along with the standard deviation for the heat treated lignin samples is shown in Figure B.1 (f). The average roughness of vacuum dried lignin is 1.31 $\pm$ 0.29 nm. Figure B.1 (f) shows a gradual increase in the average roughness of the electro-spun lignin fibre upon heat treatment. This moderate increase in the roughness of lignin electro-spun fibre could be attributed to the mass-loss and shrinkage in

the fibre diameter during heat treatment. The roughness for the carbonised lignin fibre at 1500 °C was found to be the highest when compared to the other heat-treated samples.

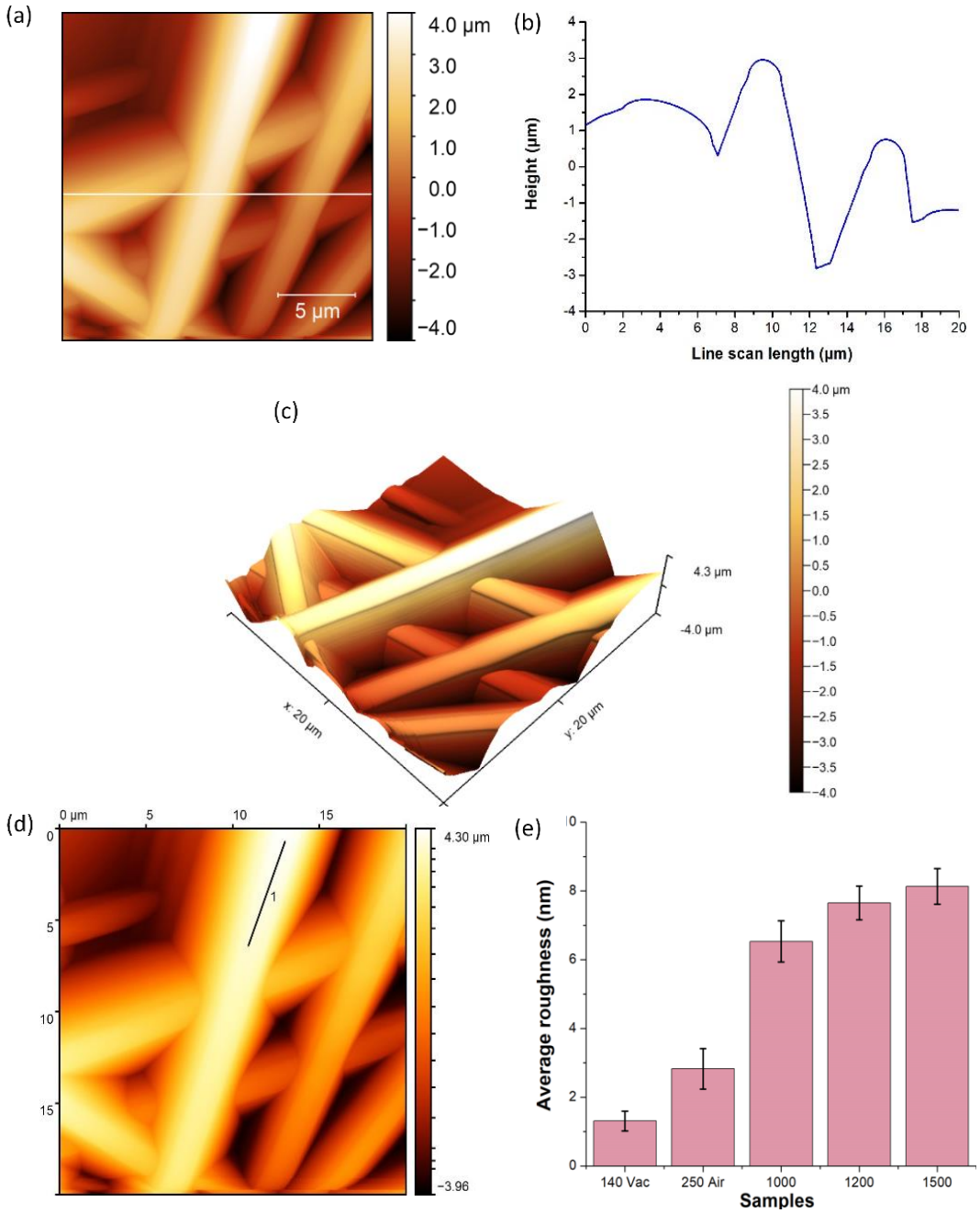

Figure B.1 Topography of lignin samples with (a-b) shows the topography and the profile of randomly orientated vacuum dried lignin electro-spun; (c) shows 3-D profile of electro-spun profile; (d) shows the calculation of surface roughness (f) show the comparison of surface roughness for different heat treated lignin samples measured along the fibre axis.

The surface topography of an aligned electro-spun lignin fibre using AFM in tapping mode is shown in Figure B.2 (a-c). Figure B.2 (a) shows the topography of an aligned single fibre with a line scan to show the profile height of scan region as shown in Figure B.2 (b). The 3D image of the single electro-spun fibre is shown in Figure B.2 (c). The surface roughness of vacuum dried aligned lignin sample was found to be 1.78 nm which is comparable to that of randomly oriented fibres.

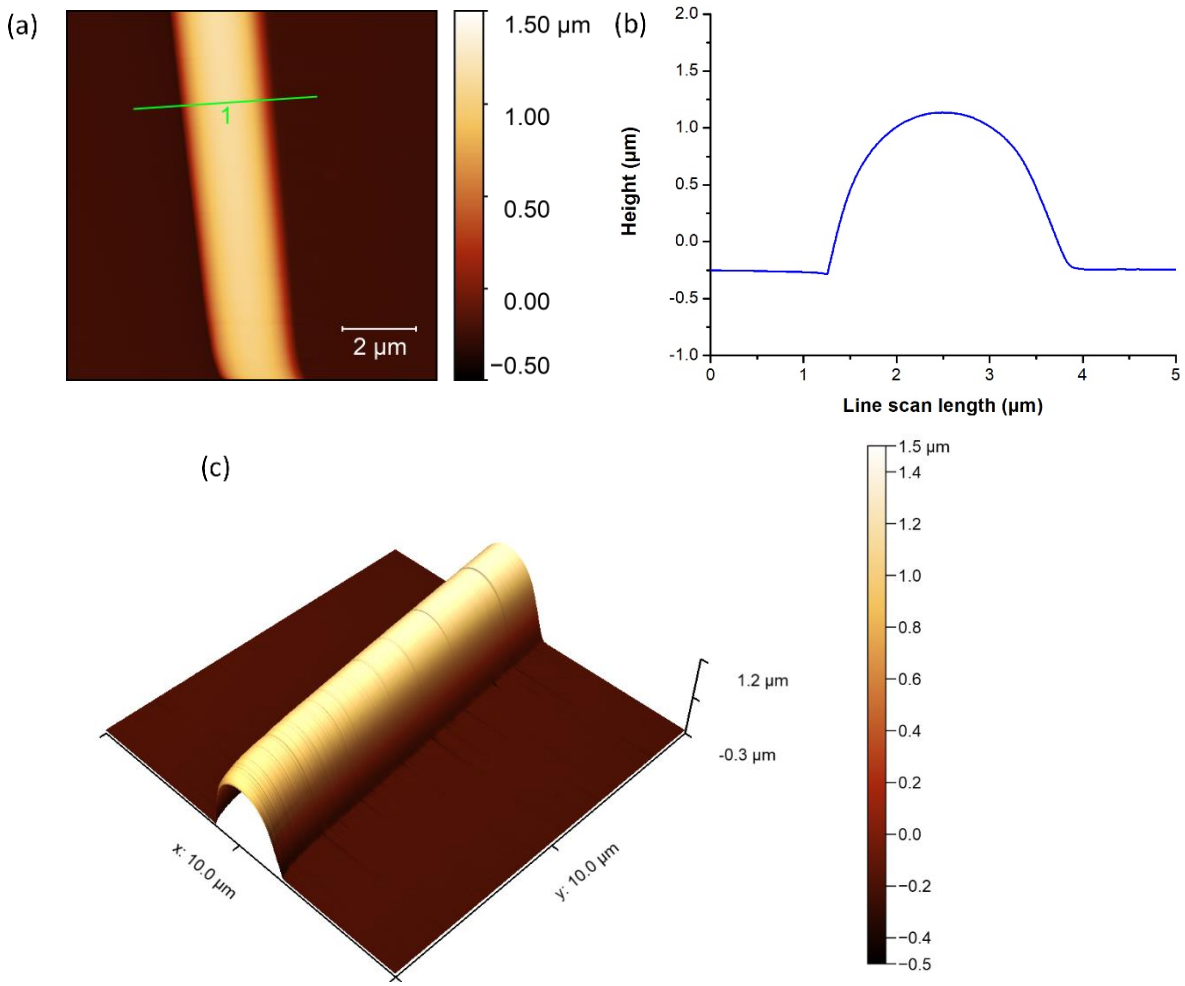

Figure B.2 Topography of (a) aligned singled electro-spun fibre with (b) its profile height and 3D image of electro-spun fibre.

Appendix B2: Wettability of Electro-spun ASL-ESL Carbonised Lignin Fibres

Surface wettability is another important factor in determining potential applications for carbon fibre derived from carbonised lignin. Surface wettability can give the measure of hydrophilic or hydrophobic nature of carbonised electro-spun lignin carbon fibre. The contact angle measurement gives an indication of the surface wettability of the carbonised fibre mat. The experimental method to measure the contact angle is presented in Section Appendix A2. Figure B.3 (a-b) shows images of a de-ionised water drop placed on a carbonised lignin fibre mat and the measurement of the contact angle using ImageJ software.

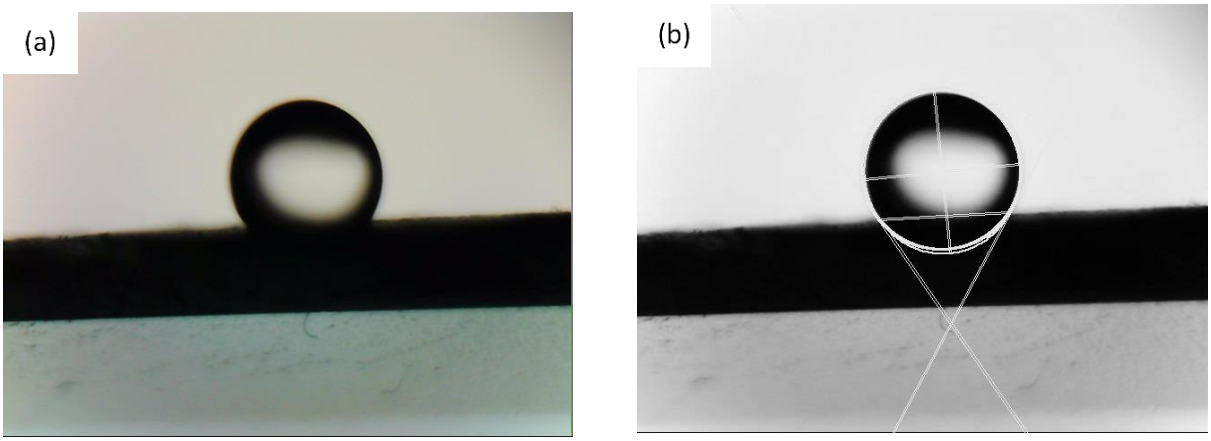

Figure B.3 Contact angle measurement with (a) showing a water droplet on carbonised electro-spun lignin fibre mat and (b) shows the processing of image for theta (θ) measurement using ImageJ software.

The measured contact angle for carbonised lignin samples is summarised in Table B.1. The material is said to be hydrophobic if it does not wet the surface making a contact angle that is greater than 90° (439). All the carbonised lignin samples show a hydrophobic nature with contact angle greater than 90°. The contact angle was found to increase with carbonisation temperature. The contact angle measured for the carbonised lignin samples is comparable to those reported in literature where a polymer blend was used (440). The variation in the contact angle among the carbonised lignin samples can be attributed to sample variations

and the loss of polar groups. The wettability of surface depends on the surface free energy and the surface roughness (441). As mentioned in the previous section, the surface roughness was found to be increased with the carbonisation temperature. Therefore, the contact angles for electro-spun carbonised lignin fibres correlates well with the general concept that the roughness is proportional to the contact angle for non-wettable surfaces (436).

Table B.1 Contact angle of electro-spun and carbonised lignin fibres.

Sample	**Theta (θ)**	**Contact angle**
1000 °C	70.90 ° ± 3.69 °	109.10 ° ± 3.69 °
1200 °C	62.53 ° ± 1.27 °	117.47 ° ± 1.27 °
1500 °C	59.07 ° ± 2.53 °	120.93 ° ± 2.53 °

Appendix C: List of Structures

This section shows the structures of materials discussed in the previous chapters specifically in results and discussion section. Figure C.1 shows the structures of carbohydrates (cellulose and hemicellulose) which were present in coir and softwood Kraft lignin as impurities. It also shows the structure of quinone methide intermediate formed during Kraft pulping process as discussed in Chapter 2.

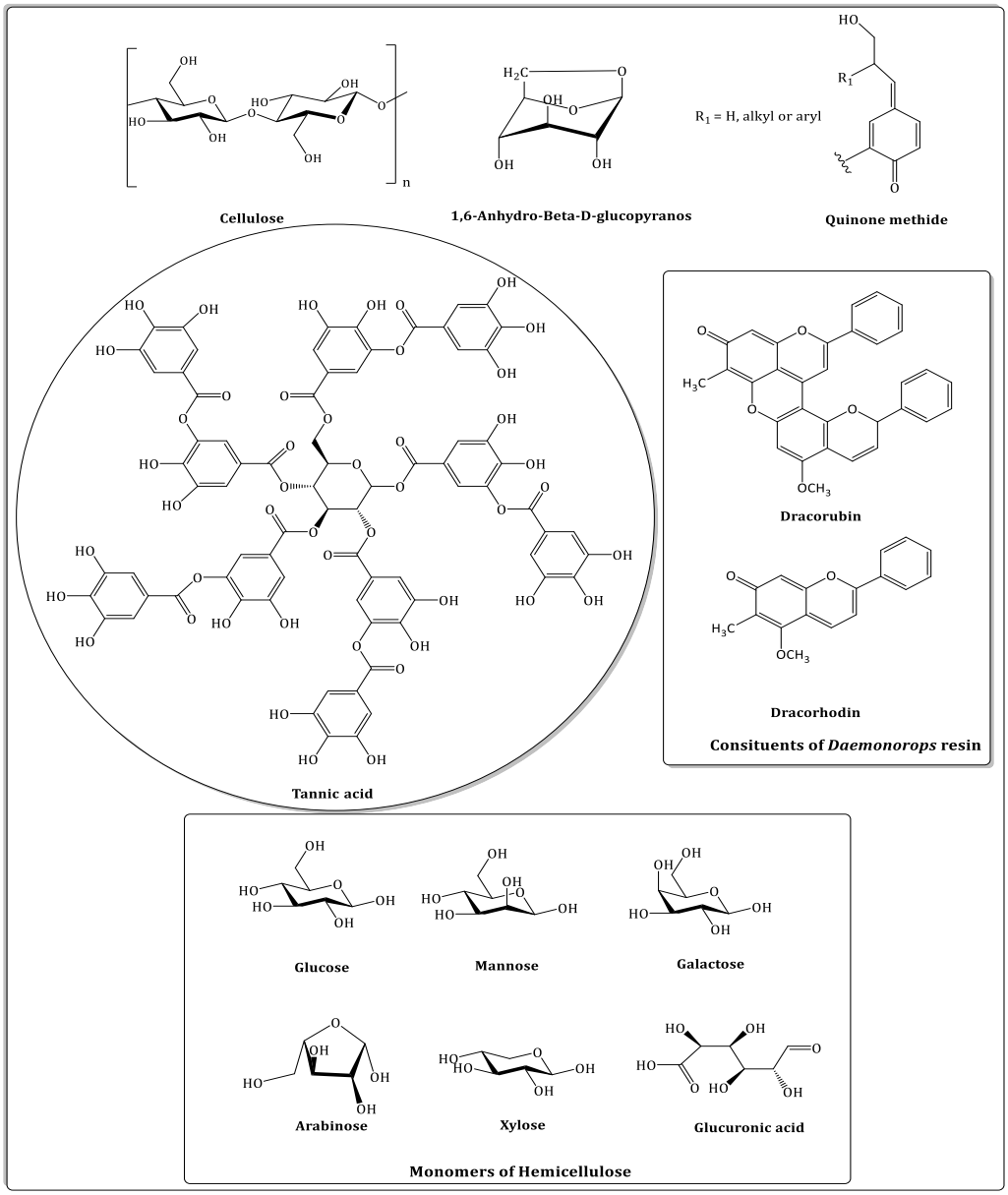

Figure C.1 Structures of carbohydrates (cellulose and hemicellulose), tannic acid and daemonorops (dragons' blood) resin.

Figure C.1 also shows the structure of tannic acid which was blended with lignin to electro-spun lignin-based fibres as shown in Chapter 5. *Daemonorops* resin was also used for initial screening as a potential bio-based material for the production of carbon fibres. Figure C.2 and Figure C.3 shows the structures of products released during lignin pyrolysis (PY-GC-MS) as discussed in Chapter 4.

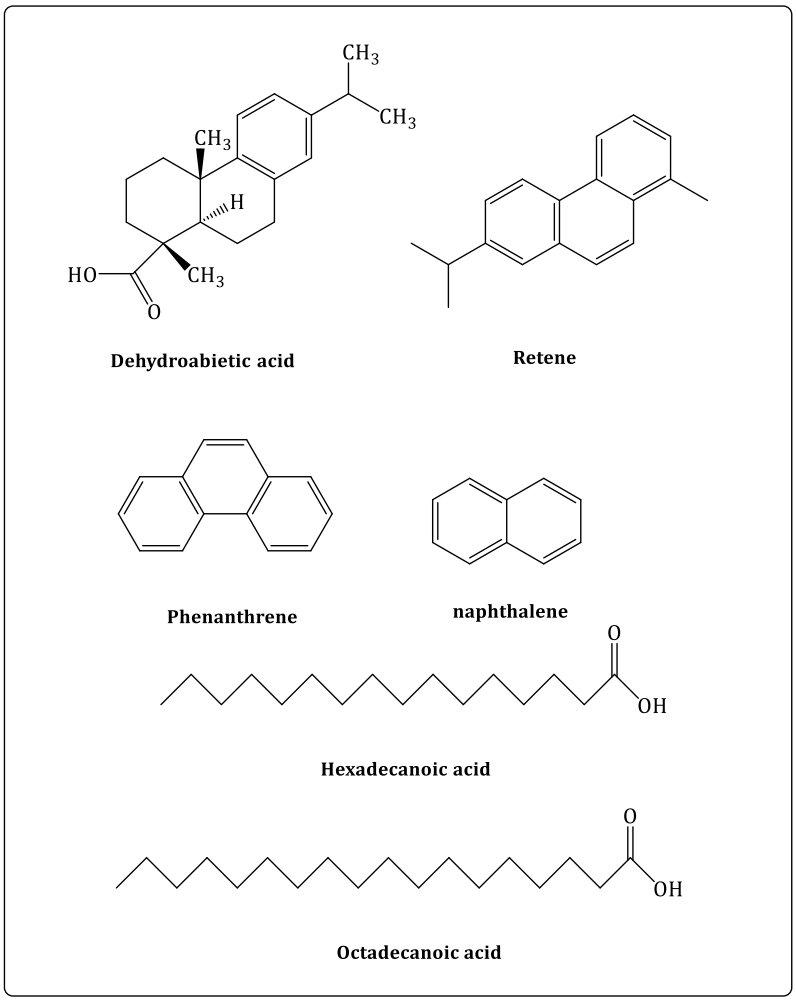

Figure C.2 Structures of pyrolysis products (Py-GC-MS) discussed in Chapter 4.

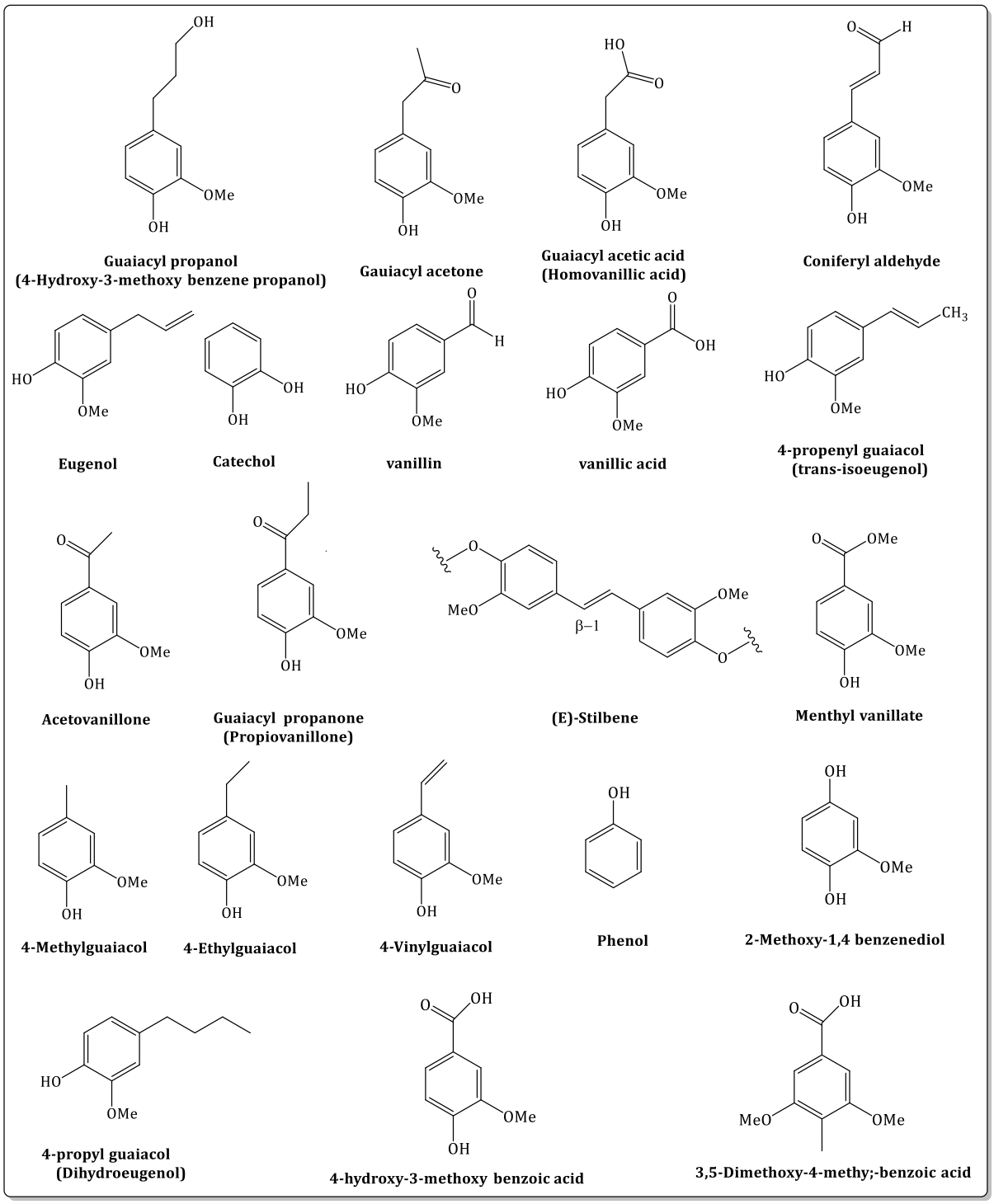

Figure C.3 Structures of pyrolysis products (Py-GC-MS) discussed in Chapter 4.

.

Figure C.4 and Figure C.5 shows the structural moieties present in lignin that were discussed in Chapter 4 and Chapter 6.

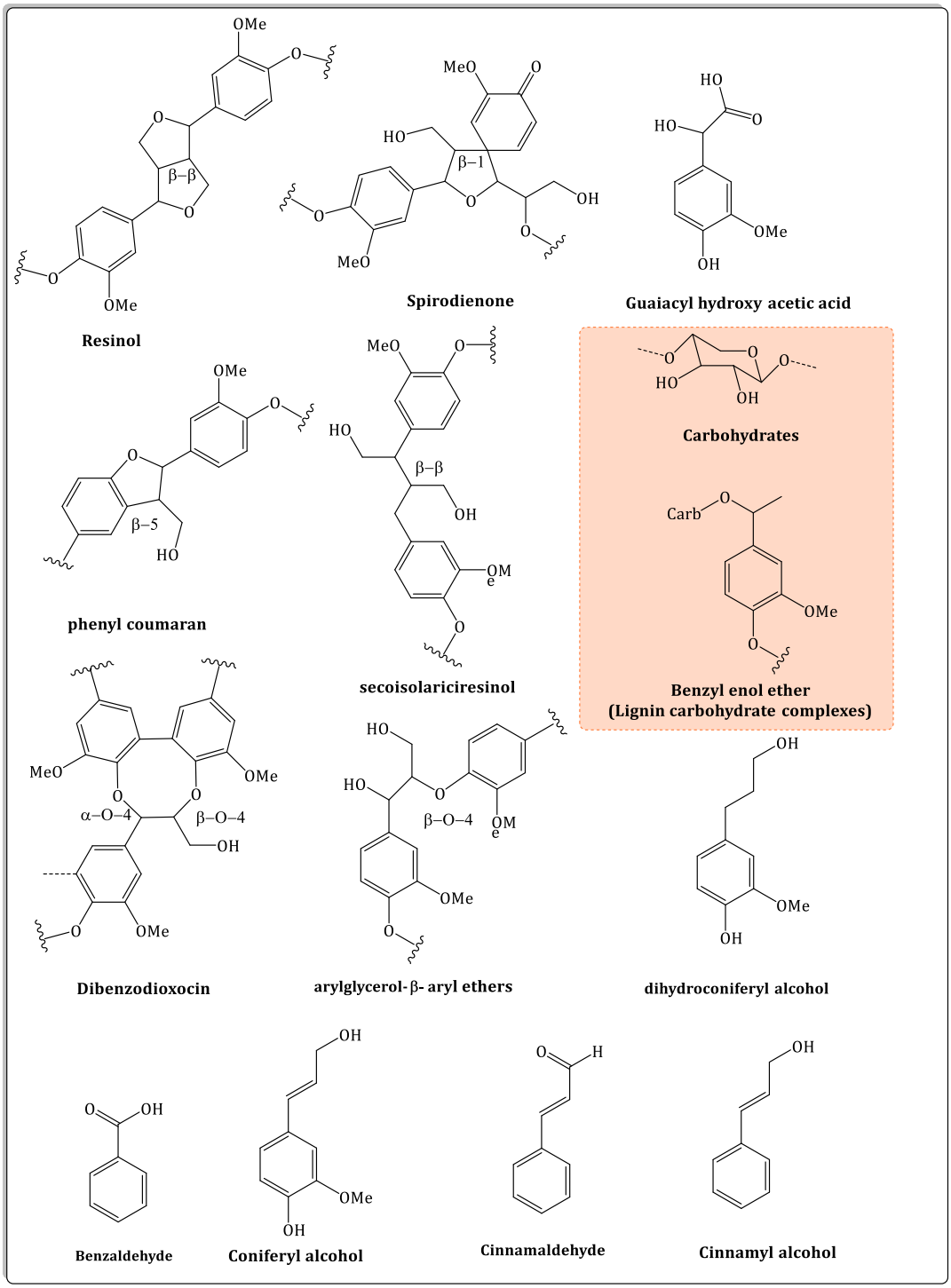

Figure C.4 Structures of products discussed in results and discussion section (Chapter 4 and Chapter 6).

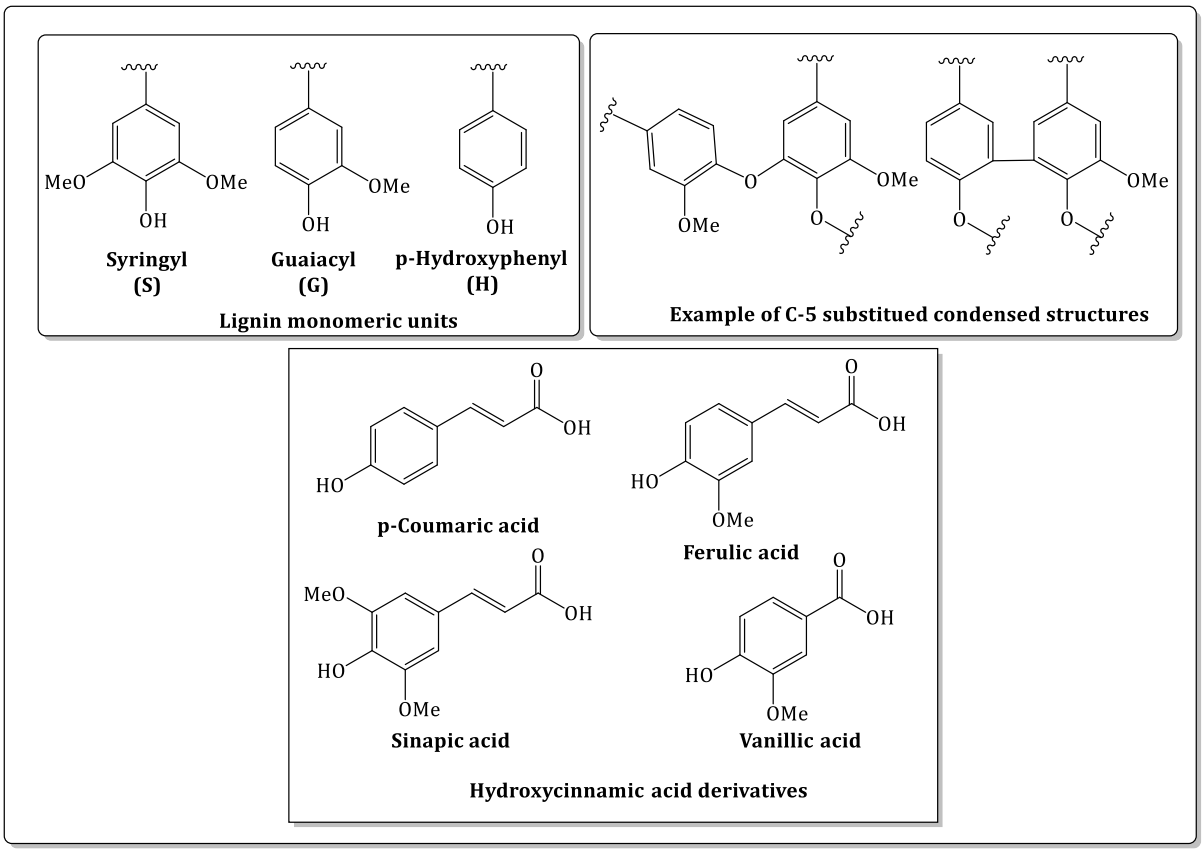

Figure C.5 Structures of products discussed in results and discussion section (Chapter 4 and Chapter 6).

Appendix D: Chemical Structure and Solubility of Bio-based Precursors

This section shows the list of chemical structure and solubility of bio-based precursors screened including lignin in Table D.1.

Table D.1 Chemical structure and solubility of bio-based precursors including lignin.

Bio-based Precursors	Solubility	Structure
Daemonorops draco	Soluble in acetone, ethanol and DMSO	See structure in Appendix C
Black storax resin (liquidambar orientalis)	Non-soluble in acetone, ethanol and DMSO	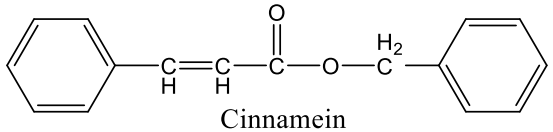 Cinnamein (Benzyl Cinnamate)
Liqourice (glycyrrhiza glabra)	Soluble in DMSO	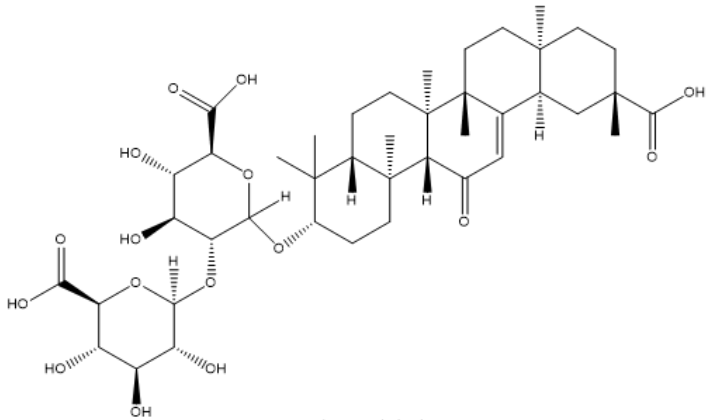 Glycrrhizin

Tannic acid (tannin)	Soluble in water, acetone, ethanol and DMSO	See structure in Appendix C
Benzoin Resin (styrax benzoin)	Non-soluble in acetone, ethanol and DMSO	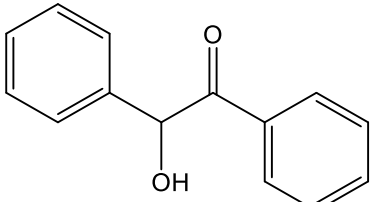 Benzoin
Myrrh resin (commiphora myrrha)	Non-soluble in acetone, ethanol and DMSO	Mixture of various compounds(442)
Elemi resin (canarium luzonicum)	Soluble in ethanol	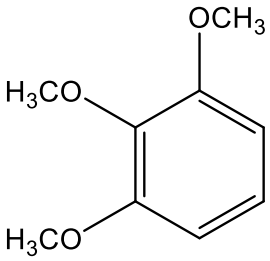 Elemicin
Lignin	Soluble in DMSO and DMF	See structure in Appendix C
Cellulose acetate	Soluble in acetone and DMSO	See structure in Appendix C

Appendix E: Thermogravimetric Analysis and Properties of Bio-based Precursors

Figure E.1 shows the TGA data for bio-based precursors including lignin. The char and inorganic content as shown in Table E.1 were influential paraments in the investigation of bio-based precursors.

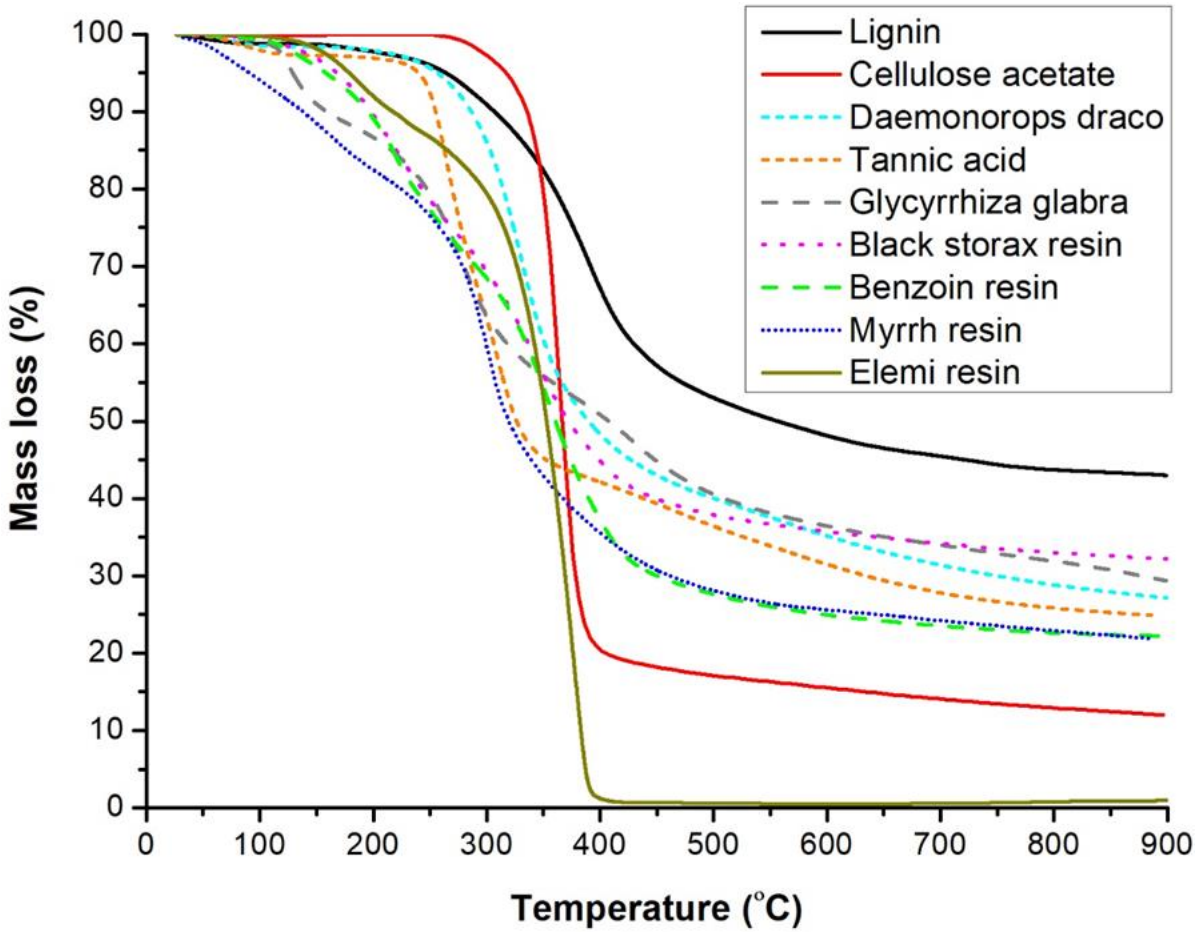

Figure E.1 TGA data of bio-based precursors including lignin.

Table E.1 Char and ash content of bio-based precursors including lignin.

Bio-based precursors	**Char at 900 °C**	**Moisture (%)**	**Ash at 525 °C (%)**
Daemonorops draco	27.1	1.4	1.5
Black storax resin (liquidambar orientalis)	32.1	2.4	3.9
Glycyrrhiza glabra	29.4	9.2	9.9
Tannic acid (tannin)	24.9	5.9	0.1
Benzoin resin (styrax benzoin)	22.2	3.0	0.4
Myrrh resin (commiphora myrrha)	21.9	8.4	9.4
Elemi resin (canarium luzonicum)	0.9	-	-
Lignin	43.4	28	1.3
Cellulose acetate	12.1	-	-

References

1. Baker DA, Gallego NC, Baker FS. On the characterization and spinning of an organic-purified lignin toward the manufacture of low-cost carbon fiber. Journal of Applied Polymer Science. 2012;124(1):227-34.

2. Baker DA, Rials TG. Recent advances in low-cost carbon fiber manufacture from lignin. Journal of Applied Polymer Science. 2013;130(2):713-28.

3. Chatterjee S, Saito T, Bhattacharya P. 11 - Lignin-Derived Carbon Fibers. Lignin in Polymer Composites: William Andrew Publishing; 2016. p. 207-16.

4. Xu Z, Gao C. Graphene fiber: a new trend in carbon fibers. Materials Today. 2015;18(9):480-92.

5. Norberg I, Nordström Y, Drougge R, Gellerstedt G, Sjöholm E. A new method for stabilizing softwood kraft lignin fibers for carbon fiber production. Journal of Applied Polymer Science. 2013;128(6):3824-30.

6. Dong X, Lu C, Zhou P, Zhang S, Wang L, Li D. Polyacrylonitrile/lignin sulfonate blend fiber for low-cost carbon fiber. RSC Advances. 2015;5(53):42259-65.

7. Seydibeyoğlu M. A Novel Partially Biobased PAN-Lignin Blend as a Potential Carbon Fiber Precursor. Journal of biomedicine & biotechnology. 2012;2012:598324.

8. Huang X. Fabrication and Properties of Carbon Fibers. Materials. 2009;2(4).

9. Kumar S. Recent Progress in Fabrication, Structure, and Properties of Carbon Fibers AU - Liu, Yaodong. Polymer Reviews. 2012;52(3):234-58.

10. Bader MG. Composites Fabrication Processes. Handbook of Materials Selection: John Wiley & Sons, Inc.; 2007. p. 1037-111.

11. Dumanlı AG, Windle AH. Carbon fibres from cellulosic precursors: a review. Journal of Materials Science. 2012;47(10):4236-50.

12. Jeon Y-P, Alway-Cooper R, Morales M, Ogale AA. Chapter 2.8 - Carbon Fibers. In: Somiya S, editor. Handbook of Advanced Ceramics (Second Edition). Oxford: Academic Press; 2013. p. 143-54.

13. Inagaki M. CHAPTER 4 - Carbon Fibers. In: Inagaki M, editor. New Carbons - Control of Structure and Functions. Oxford: Elsevier Science; 2000. p. 82-123.

14. Park S-J, Seo M-K. Chapter 6 - Element and Processing. In: Park S-J, Seo M-K, editors. Interface Science and Technology. 18: Elsevier; 2011. p. 431-99.

15. Ellringmann T, Wilms C, Warnecke M, Seide G, Gries T. Carbon fiber production costing: a modular approach. Textile Research Journal. 2015;86(2):178-90.

16. Paris O, Peterlik H. 10 - The structure of carbon fibres. In: Eichhorn SJ, Hearle JWS, Jaffe M, Kikutani T, editors. Handbook of Textile Fibre Structure. 2: Woodhead Publishing; 2009. p. 353-77.

17. Shirvanimoghaddam K, Hamim S, Karbalaei Akbari M, Fakhrhoseini S, Khayyam H, Ghasali E, et al. Carbon Fiber Reinforced Metal Matrix Composites: Fabrication Processes and Properties2017. 70-96 p.

18. Matsuhisa Y, Bunsell AR. 16 - Tensile failure of carbon fibers. In: Bunsell AR, editor. Handbook of Tensile Properties of Textile and Technical Fibres: Woodhead Publishing; 2009. p. 574-602.

19. Jiménez V, Sánchez P, Romero A. 2 - Materials for activated carbon fiber synthesis. In: Chen JY, editor. Activated Carbon Fiber and Textiles. Oxford: Woodhead Publishing; 2017. p. 21-38.

20. Zhang XH, Li QW. 3 - Carbon fiber spinning. In: Chen JY, editor. Activated Carbon Fiber and Textiles. Oxford: Woodhead Publishing; 2017. p. 39-60.

21. Grassie N. Pyrolysis of polyacrylonitrile and related polymers—VI. Acrylonitrile copolymers containing carboxylic acid and amide structures1972. 257-69 p.

22. Grassie N, McGuchan R. Pyrolysis of polyacrylonitrile and related polymers—I. Thermal analysis of polyacrylonitrile. European Polymer Journal. 1970;6(9):1277-91.

23. Clarke AJ, Bailey JE. Oxidation of Acrylic Fibres for Carbon Fibre Formation. Nature. 1973;243(5403):146-50.

24. Morita K, Murata Y, Ishitani A, Murayama K, Ono T, Nakajima A. Characterization of commercially available PAN (polyacrylonitri1e)-based carbon fibers1986. 455-68 p.

25. Paliwal DK, Bajaj P. Acrylic Precursors for Carbon Fibers AU - Gupta, A. K. Journal of Macromolecular Science, Part C. 1991;31(1):1-89.

26. Morgan P. Carbon Fibres and Their Composites. 1st Edition ed: CRC Press; 2005.

27. Rahaman MSA, Ismail AF, Mustafa A. A review of heat treatment on polyacrylonitrile fiber. Polymer Degradation and Stability. 2007;92(8):1421-32.

28. Yue Z, Economy J. 4 - Carbonization and activation for production of activated carbon fibers. In: Chen JY, editor. Activated Carbon Fiber and Textiles. Oxford: Woodhead Publishing; 2017. p. 61-139.

29. Fitzer E. Pan-based carbon fibers—present state and trend of the technology from the viewpoint of possibilities and limits to influence and to control the fiber properties by the process parameters. Carbon. 1989;27(5):621-45.

30. Frank E, Hermanutz F, Buchmeiser MR. Carbon Fibers: Precursors, Manufacturing, and Properties. Macromolecular Materials and Engineering. 2012;297(6):493-501.

31. Alekhina M, Ershova O, Ebert A, Heikkinen S, Sixta H. Softwood kraft lignin for value-added applications: Fractionation and structural characterization. Industrial Crops and Products. 2015;66:220-8.

32. Hodásová Ľ, Jablonsky M, Andrea S, Haz A. Lignin, potential products and their market value. Wood research. 2015;60:973-86.

33. Frank E, Steudle LM, Ingildeev D, Spörl JM, Buchmeiser MR. Carbon Fibers: Precursor Systems, Processing, Structure, and Properties. Angewandte Chemie International Edition. 2014;53(21):5262-98.

34. Demuner IF, Colodette JL, Demuner AJ, Jardim CM. Biorefinery Review: Wide-Reaching Products Through Kraft Lignin. 2019. 2019;14(3):39.

35. Zakzeski J, Bruijnincx PCA, Jongerius AL, Weckhuysen BM. The Catalytic Valorization of Lignin for the Production of Renewable Chemicals. Chemical Reviews. 2010;110(6):3552-99.

36. Kai D, Jiang S, Low ZW, Loh XJ. Engineering highly stretchable lignin-based electrospun nanofibers for potential biomedical applications. Journal of Materials Chemistry B. 2015;3(30):6194-204.

37. Kubo S, Kadla JF. Lignin-based Carbon Fibers: Effect of Synthetic Polymer Blending on Fiber Properties. Journal of Polymers and the Environment. 2005;13(2):97-105.

38. Choi D, Kil H-S, Lee S. Fabrication of low-cost carbon fibers using economical precursors and advanced processing technologies. Carbon. 2019;142:610-49.

39. Wertz JL, Deleu, M., Coppee, S., Richel, A. Hemicelluloses and Lignin in Biorefineries. Boca Raton: CRC Press; 2018. 1-20 p.

40. Calvo-Flores FG, Dobado, J. A., Isac-Garcia, J. and Martin-Martinez, F, J. Lignin and Lignans as Renewable Raw Materials. First Edition ed. Singapore: John & Wiley Sons, Ltd; 2015. 1-42 p.

41. Haghdan S, Renneckar S, Smith GD. 1 - Sources of Lignin. In: Faruk O, Sain M, editors. Lignin in Polymer Composites: William Andrew Publishing; 2016. p. 1-11.

42. Donald D. Overview. Lignin and Lignans: CRC Press; 2010. p. 1-10.

43. Sarkanen KV, Ludwig, C. H. Lignins: Occurrence, Formation, Structure and Reactions. United States of America: John Wiley & Sons, Inc; 1971. 1-38 p.

44. Suchy M, Argyropoulos DS. Catalysis and Activation of Oxygen and Peroxide Delignification of Chemical Pulps: A Review. Oxidative Delignification Chemistry. ACS Symposium Series. 785: American Chemical Society; 2001. p. 2-43.

45. Novaes E, Kirst M, Chiang V, Winter-Sederoff H, Sederoff R. Lignin and Biomass: A Negative Correlation for Wood Formation and Lignin Content in Trees. Plant Physiology. 2010;154(2):555-61.

46. Cotana F, Cavalaglio G, Gelosia M, Nicolini A, Coccia V, Petrozzi A. Production of Bioethanol in a Second Generation Prototype from Pine Wood Chips2014.

47. Wang S, Dai G, Haiping Y, Luo Z. Lignocellulosic biomass pyrolysis mechanism: A state-of-the-art review2017. 33-86 p.

48. Nitsos C, Rova U, Christakopoulos P. Organosolv Fractionation of Softwood Biomass for Biofuel and Biorefinery Applications. Energies. 2018;11(1).

49. Musule R, Alarcón-Gutiérrez E, Houbron EP, Bárcenas-Pazos GM, del Rosario Pineda-López M, Domínguez Z, et al. Chemical composition of lignocellulosic biomass in the wood of Abies religiosa across an altitudinal gradient. Journal of Wood Science. 2016;62(6):537-47.

50. Pan X, Xie D, Yu RW, Saddler JN. The bioconversion of mountain pine beetle-killed lodgepole pine to fuel ethanol using the organosolv process. Biotechnology and Bioengineering. 2008;101(1):39-48.

51. Pasangulapati V, Ramachandriya KD, Kumar A, Wilkins MR, Jones CL, Huhnke RL. Effects of cellulose, hemicellulose and lignin on thermochemical conversion characteristics of the selected biomass. Bioresource Technology. 2012;114:663-9.

52. Sannigrahi P, Ragauskas AJ, Tuskan GA. Poplar as a feedstock for biofuels: A review of compositional characteristics. Biofuels, Bioproducts and Biorefining. 2010;4(2):209-26.

53. Le Floch A, Jourdes M, Teissedre P-L. Polysaccharides and lignin from oak wood used in cooperage: Composition, interest, assays: A review. Carbohydrate Research. 2015;417:94-102.

54. Ghaffar SH, Fan M. Structural analysis for lignin characteristics in biomass straw. Biomass and Bioenergy. 2013;57:264-79.

55. Zheng Q, Zhou T, Wang Y, Cao X, Wu S, Zhao M, et al. Pretreatment of wheat straw leads to structural changes and improved enzymatic hydrolysis. Scientific Reports. 2018;8(1):1321.

56. Cabral MMS, Abud AKdS, Silva CEdF, Almeida RMRG. Bioethanol production from coconut husk fiber. Ciência Rural. 2016;46:1872-7.

57. Kumar AK, Sharma S. Recent updates on different methods of pretreatment of lignocellulosic feedstocks: a review. Bioresources and Bioprocessing. 2017;4(1):7.

58. Guilherme AA, Dantas PVF, Santos ES, Fernandes FAN, Macedo GR. EVALUATION OF COMPOSITION, CHARACTERIZATION AND ENZYMATIC HYDROLYSIS OF PRETREATED SUGAR CANE BAGASSE. Brazilian Journal of Chemical Engineering. 2015;32:23-33.

59. Koch G. Raw Material for Pulp. Handbook of Pulp: Wiley-VCH Verlag GmbH; 2008. p. 21-68.

60. Lu F, Ralph J. Chapter 6 - Lignin A2 - Sun, Run-Cang. Cereal Straw as a Resource for Sustainable Biomaterials and Biofuels. Amsterdam: Elsevier; 2010. p. 169-207.

61. Calvo-Flores FG, Dobado JA. Lignin as Renewable Raw Material. ChemSusChem. 2010;3(11):1227-35.

62. Laurichesse S, Avérous L. Chemical modification of lignins: Towards biobased polymers. Progress in Polymer Science. 2014;39(7):1266-90.

63. Paiva L, Goldbeck R, dos Santos W, Squina F. Ferulic acid and derivatives: Molecules with potential application in the pharmaceutical field. 2014.

64. Hanjie W, Frits Pde V, Yongcan J. A win-win technique of stabilizing sand dune and purifying paper mill black-liquor. Journal of environmental sciences (China). 2009;21(4):488-93.

65. Doherty WOS, Mousavioun P, Fellows CM. Value-adding to cellulosic ethanol: Lignin polymers. Industrial Crops and Products. 2011;33(2):259-76.

66. Gillet S, Aguedo M, Petitjean L, Morais ARC, da Costa Lopes AM, Łukasik RM, et al. Lignin transformations for high value applications: towards targeted modifications using green chemistry. Green Chemistry. 2017;19(18):4200-33.

67. Dallmeyer I, Ko F, F. Kadla J. Electrospinning of Technical Lignins for the Production of Fibrous Networks2010. 315-29 p.

68. Chakar FS, Ragauskas AJ. Review of current and future softwood kraft lignin process chemistry. Industrial Crops and Products. 2004;20(2):131-41.

69. Patil ND, Tanguy NR, Yan N. 3 - Lignin Interunit Linkages and Model Compounds. Lignin in Polymer Composites: William Andrew Publishing; 2016. p. 27-47.

70. Mosier N, Wyman C, Dale B, Elander R, Lee YY, Holtzapple M, et al. Features of promising technologies for pretreatment of lignocellulosic biomass. Bioresource Technology. 2005;96(6):673-86.

71. Vázquez G, Antorrena G, González J, Freire S. The Influence of Pulping Conditions on the Structure of Acetosolv Eucalyptus Lignins. Journal of Wood Chemistry and Technology. 1997;17(1-2):147-62.

72. Sun Z, Fridrich B, de Santi A, Elangovan S, Barta K. Bright Side of Lignin Depolymerization: Toward New Platform Chemicals. Chemical Reviews. 2018;118(2):614-78.

73. Upton BM, Kasko AM. Strategies for the Conversion of Lignin to High-Value Polymeric Materials: Review and Perspective. Chemical Reviews. 2016;116(4):2275-306.

74. Bozell JJ, Chmely SE, Hartwig W, Key R, Labbé N, Venugopal P, et al. Chapter 2 Lignin Isolation Methodology for Biorefining, Pretreatment and Analysis. Lignin Valorization: Emerging Approaches: The Royal Society of Chemistry; 2018. p. 21-61.

75. Berlin A, Balakshin M. Chapter 18 - Industrial Lignins: Analysis, Properties, and Applications. In: Gupta VK, Tuohy MG, Kubicek CP, Saddler J, Xu F, editors. Bioenergy Research: Advances and Applications. Amsterdam: Elsevier; 2014. p. 315-36.

76. Miller J, Marina, Falerois., Lori, Pilla. Lignin: Technology, Applications and Markets 2016.

77. Calvo-Flores FG, Dobado, J. A., Isac-Garcia, J. and Martin-Martinez, F, J.,. Isolation of Lignins. Lignin and Lignans as Renewable Raw Materials. First ed. Singapore: John & Wiley Sons, Ltd.; 2015. p. 113-36.

78. Wallberg O, Jönsson A-S, Wimmerstedt R. Fractionation and concentration of kraft black liquor lignin with ultrafiltration. Desalination. 2003;154(2):187-99.

79. Ohman F, Theliander H, Tomani P, Axegard P. Method for separating lignin from black liquor, a lignin product, and use of a lignin product for the production of fuels or materials. Google Patents; 2010.

80. Tomani P. The LignoBoost Process. Cellulose Chemistry and Technology. 2010;44(1-3):53-8.

81. Strassberger Z, Tanase S, Rothenberg G. The pros and cons of lignin valorisation in an integrated biorefinery. RSC Advances. 2014;4(48):25310-8.

82. Chung H, Washburn NR. 2 - Extraction and Types of Lignin. In: Faruk O, Sain M, editors. Lignin in Polymer Composites: William Andrew Publishing; 2016. p. 13-25.

83. Houtman C. Chapter 3 Lessons Learned from 150 Years of Pulping Wood. Lignin Valorization: Emerging Approaches: The Royal Society of Chemistry; 2018. p. 62-73.

84. Li T, Takkellapati S. The current and emerging sources of technical lignins and their applications. Biofuels, Bioproducts and Biorefining. 2018;12(5):756-87.

85. Tan SSY, MacFarlane DR, Upfal J, Edye LA, Doherty WOS, Patti AF, et al. Extraction of lignin from lignocellulose at atmospheric pressure using alkylbenzenesulfonate ionic liquid. Green Chemistry. 2009;11(3):339-45.

86. Alvira P, Tomás-Pejó E, Ballesteros M, Negro MJ. Pretreatment technologies for an efficient bioethanol production process based on enzymatic hydrolysis: A review. Bioresource Technology. 2010;101(13):4851-61.

87. TAPPI 222 Acid-insoluble lignin in wood and pulp (Technical Association of Pulp and Paper Industry). 2006.

88. Schutyser W, Renders T, Van den Bosch S, Koelewijn SF, Beckham GT, Sels BF. Chemicals from lignin: an interplay of lignocellulose fractionation, depolymerisation, and upgrading. Chemical Society Reviews. 2018;47(3):852-908.

89. Lu Y, Lu Y-C, Hu H-Q, Xie F-J, Wei X-Y, Fan X. Structural Characterization of Lignin and Its Degradation Products with Spectroscopic Methods. Journal of Spectroscopy. 2017;2017:15.

90. Huang F, Singh PM, Ragauskas AJ. Characterization of Milled Wood Lignin (MWL) in Loblolly Pine Stem Wood, Residue, and Bark. Journal of Agricultural and Food Chemistry. 2011;59(24):12910-6.

91. Bu L, Tang Y, Gao Y, Jian H, Jiang J. Comparative characterization of milled wood lignin from furfural residues and corncob. Chemical Engineering Journal. 2011;175:176-84.

92. Zhang A, Lu F, Sun R-C, Ralph J. Isolation of Cellulolytic Enzyme Lignin from Wood Preswollen/Dissolved in Dimethyl Sulfoxide/N-Methylimidazole. Journal of Agricultural and Food Chemistry. 2010;58(6):3446-50.

93. Tu M, Pan X, Saddler JN. Adsorption of Cellulase on Cellulolytic Enzyme Lignin from Lodgepole Pine. Journal of Agricultural and Food Chemistry. 2009;57(17):7771-8.

94. Li J, Gellerstedt G, Toven K. Steam explosion lignins; their extraction, structure and potential as feedstock for biodiesel and chemicals. Bioresource Technology. 2009;100(9):2556-61.

95. Matsakas L, Raghavendran V, Yakimenko O, Persson G, Olsson E, Rova U, et al. Lignin-first biomass fractionation using a hybrid organosolv – Steam explosion pretreatment technology improves the saccharification and fermentability of spruce biomass. Bioresource Technology. 2019;273:521-8.

96. Lee SH, Doherty T, Linhardt R, S Dordick J. Ionic Liquid-Mediated Selective Extraction of Lignin From Wood Leading to Enhanced Enzymatic Cellulose Hydrolysis2009. 1368-76 p.

97. Fort DA, Remsing RC, Swatloski RP, Moyna P, Moyna G, Rogers RD. Can ionic liquids dissolve wood? Processing and analysis of lignocellulosic materials with 1-n-butyl-3-methylimidazolium chloride. Green Chemistry. 2007;9(1):63-9.

98. pu Y, Jiang N, Ragauskas A. Ionic Liquid as a Green Solvent for Lignin2007. 23-33 p.

99. Chatterjee S, Saito T. Solvent Fractionation of Lignin. Polymer Precursor-Derived Carbon. ACS Symposium Series. 1173: American Chemical Society; 2014. p. 153-68.

100. Li H, McDonald AG. Fractionation and characterization of industrial lignins. Industrial Crops and Products. 2014;62:67-76.

101. Passoni V, Scarica C, Levi M, Turri S, Griffini G. Fractionation of Industrial Softwood Kraft Lignin: Solvent Selection as a Tool for Tailored Material Properties. ACS Sustainable Chemistry & Engineering. 2016;4(4):2232-42.

102. Cui C, Sun R, Argyropoulos DS. Fractional Precipitation of Softwood Kraft Lignin: Isolation of Narrow Fractions Common to a Variety of Lignins. ACS Sustainable Chemistry & Engineering. 2014;2(4):959-68.

103. Saito T, Perkins JH, Vautard F, Meyer HM, Messman JM, Tolnai B, et al. Methanol Fractionation of Softwood Kraft Lignin: Impact on the Lignin Properties. ChemSusChem. 2014;7(1):221-8.

104. Mussatto SI, Fernandes M, Roberto IC. Lignin recovery from brewer's spent grain black liquor. Carbohydrate Polymers. 2007;70(2):218-23.

105. Toledano A, Serrano L, Garcia A, Mondragon I, Labidi J. Comparative study of lignin fractionation by ultrafiltration and selective precipitation. Chemical Engineering Journal. 2010;157(1):93-9.

106. Sivasankarapillai G, McDonald AG. Synthesis and properties of lignin-highly branched poly (ester-amine) polymeric systems. Biomass and Bioenergy. 2011;35(2):919-31.

107. Sivasankarapillai G, McDonald AG, Li H. Lignin valorization by forming toughened lignin-co-polymers: Development of hyperbranched prepolymers for cross-linking. Biomass and Bioenergy. 2012;47:99-108.

108. Yoshida H, Mörck R, Kringstad Knut P, Hatakeyama H. Fractionation of Kraft Lignin by Successive Extraction with Organic Solvents. II. Thermal Properties of Kraft Lignin Fractions. Holzforschung - International Journal of the Biology, Chemistry, Physics and Technology of Wood1987. p. 171.

109. Mörck R, Reimann A, Kringstad Knut P. Fractionation of Kraft Lignin by Successive Extraction with Organic Solvents. III. Fractionation of Kraft Lignin from Birch. Holzforschung - International Journal of the Biology, Chemistry, Physics and Technology of Wood1988. p. 111.

110. Argyropoulos DS, Sadeghifar H, Cui C, Sen S. Synthesis and Characterization of Poly(arylene ether sulfone) Kraft Lignin Heat Stable Copolymers. ACS Sustainable Chemistry & Engineering. 2014;2(2):264-71.

111. Arshanitsa A, Ponomarenko J, Dizhbite T, Andersone A, Gosselink RJA, van der Putten J, et al. Fractionation of technical lignins as a tool for improvement of their antioxidant properties. Journal of Analytical and Applied Pyrolysis. 2013;103:78-85.

112. Brodin I, Ernstsson M, Gellerstedt G, Sjöholm E. Oxidative stabilisation of kraft lignin for carbon fibre production. Holzforschung2012. p. 141.

113. Brodin I, Sjöholm E, Gellerstedt G. The behavior of kraft lignin during thermal treatment. Journal of Analytical and Applied Pyrolysis. 2010;87(1):70-7.

114. Miller-Chou BA, Koenig JL. A review of polymer dissolution. Progress in Polymer Science. 2003;28(8):1223-70.

115. M. Hansen C. Hansen Solubility Parameters: A User's Handbook, Second Edition2012. 546 p.

116. Melro E, Alves L, Antunes F, Medronho B. A brief overview on lignin dissolution. Journal of Molecular Liquids. 2018;265.

117. Pan X, Sano Y. Atmospheric Acetic Acid Pulping of Rice Straw IV: PhysicoChemical Characterization of Acetic Acid Lignins from Rice Straw and Woods. Part 1. Physical Characteristics. Holzforschung. 1999;53:511-8.

118. Schuerch C. The Solvent Properties of Liquids and Their Relation to the Solubility, Swelling, Isolation and Fractionation of Lignin. Journal of the American Chemical Society. 1952;74(20):5061-7.

119. Ramluckan K, Moodley K, Bux F. An evaluation of the efficacy of using selected solvents for the extraction of lipids from algal biomass by the Soxhlet extraction method. Fuel. 2013;116:103-8.

120. Wyatt V. The Effects of Solvent Polarity and pKa on the Absorption of Solvents into Poly(glutaric acid- glycerol) Films. Journal of Applied Polymer Science. 2014;131.

121. Dodd AP, Kadla JF, Straus SK. Characterization of Fractions Obtained from Two Industrial Softwood Kraft Lignins. ACS Sustainable Chemistry & Engineering. 2015;3(1):103-10.

122. Gregorova A. Application of Differential Scanning Calorimetry to the Characterization of Biopolymers: INTECH Open Access Publisher; 2013.

123. Banerjee G, DIAS PM, Kalathil R. Plant extract of inula racemosa. Google Patents; 2014.

124. Gogolewski S. Resorbable polymeric medical goods with improved mechanical properties and method for producing same. Google Patents; 2005.

125. Belmares M, Blanco M, Goddard WA, Ross RB, Caldwell G, Chou SH, et al. Hildebrand and Hansen solubility parameters from Molecular Dynamics with applications to electronic nose polymer sensors. Journal of Computational Chemistry. 2004;25(15):1814-26.

126. Crowley JD, Teague, G. S., Jr., and Lowe, Jack W., Jr. A three-dimensional approach to solubility. Journal of Paint Technology. 1966;38(496):269-80.

127. Nowakowski DJ, Bridgwater AV, Elliott DC, Meier D, de Wild P. Lignin fast pyrolysis: Results from an international collaboration. Journal of Analytical and Applied Pyrolysis. 2010;88(1):53-72.

128. Patwardhan PR, Brown RC, Shanks BH. Understanding the Fast Pyrolysis of Lignin. ChemSusChem. 2011;4(11):1629-36.

129. Amini E, Safdari M-S, DeYoung JT, Weise DR, Fletcher TH. Characterization of pyrolysis products from slow pyrolysis of live and dead vegetation native to the southern United States. Fuel. 2019;235:1475-91.

130. Zhou S, Pecha B, van Kuppevelt M, McDonald AG, Garcia-Perez M. Slow and fast pyrolysis of Douglas-fir lignin: Importance of liquid-intermediate formation on the distribution of products. Biomass and Bioenergy. 2014;66:398-409.

131. Xu CaF, F. . Conversion of Lignin into Bio-Based Chemicals and Materials: Springer Nature; 2017.

132. Bridgwater AV. Renewable fuels and chemicals by thermal processing of biomass. Chemical Engineering Journal. 2003;91(2):87-102.

133. Bridgwater AV. Review of fast pyrolysis of biomass and product upgrading. Biomass and Bioenergy. 2012;38:68-94.

134. Bridgwater T. Biomass for energy. Journal of the Science of Food and Agriculture. 2006;86(12):1755-68.

135. Basu P. Chapter 11 - Production of Synthetic Fuels and Chemicals from Biomass. In: Basu P, editor. Biomass Gasification, Pyrolysis and Torrefaction (Second Edition). Boston: Academic Press; 2013. p. 375-404.

136. Wang W-L, Ren X-Y, Chang J-M, Cai L-P, Shi SQ. Characterization of bio-oils and bio-chars obtained from the catalytic pyrolysis of alkali lignin with metal chlorides. Fuel Processing Technology. 2015;138:605-11.

137. Piskorz J, Majerski P, Radlein D, Scott DS. Conversion of lignins to hydrocarbon fuels. Energy & Fuels. 1989;3(6):723-6.

138. Sukhbaatar B, Steele PH, Ingram LI, Kim MG. USE OF LIGNIN SEPARATED FROM BIO-OIL IN ORIENTED STRAND BOARD BINDER PHENOL-FORMALDEHYDE RESINS2009.

139. de Wild PJ, Huijgen WJJ, Heeres HJ. Pyrolysis of wheat straw-derived organosolv lignin. Journal of Analytical and Applied Pyrolysis. 2012;93:95-103.

140. Bährle C, Custodis V, Jeschke G, van Bokhoven JA, Vogel F. In situ Observation of Radicals and Molecular Products During Lignin Pyrolysis. ChemSusChem. 2014;7(7):2022-9.

141. Sharma RK, Wooten JB, Baliga VL, Lin X, Geoffrey Chan W, Hajaligol MR. Characterization of chars from pyrolysis of lignin. Fuel. 2004;83(11):1469-82.

142. Brebu M, Cazacu G, Chirila O. Pyrolysis of lignin - A potential method for obtaining chemicals and/or fuels2011. 43-50 p.

143. Xu C, Ferdosian F. Degradation of Lignin by Pyrolysis. 2017. p. 13-33.

144. Brebu M, Tamminen T, Spiridon I. Thermal degradation of various lignins by TG-MS/FTIR and Py-GC-MS. Journal of Analytical and Applied Pyrolysis. 2013;104:531-9.

145. Zhao J, Xiuwen W, Hu J, Liu Q, Shen D, Xiao R. Thermal degradation of softwood lignin and hardwood lignin by TG-FTIR and Py-GC/MS. Polymer Degradation and Stability. 2014;108:133–8.

146. Kim J-Y, Hwang H, Oh S, Kim Y-S, Kim U-J, Choi JW. Investigation of structural modification and thermal characteristics of lignin after heat treatment. International Journal of Biological Macromolecules. 2014;66:57-65.

147. Kawamoto H. Lignin pyrolysis reactions. Journal of Wood Science. 2017;63(2):117-32.

148. Kim J-Y, Oh S, Hwang H, Kim U-J, Choi JW. Structural features and thermal degradation properties of various lignin macromolecules obtained from poplar wood (Populus albaglandulosa). Polymer Degradation and Stability. 2013;98(9):1671-8.

149. Hosoya T, Kawamoto H, Saka S. Role of methoxyl group in char formation from lignin-related compounds. Journal of Analytical and Applied Pyrolysis. 2009;84(1):79-83.

150. Qu W, Xue Y, Gao Y, Rover M, Bai X. Repolymerization of pyrolytic lignin for producing carbon fiber with improved properties. Biomass and Bioenergy. 2016;95:19-26.

151. Hu Z, Du X, Liu J, Chang H-m, Jameel H. Structural Characterization of Pine Kraft Lignin: BioChoice Lignin vs Indulin AT. Journal of Wood Chemistry and Technology. 2016;36(6):432-46.

152. Yuan T-Q, Sun S-N, Xu F, Sun R-C. Characterization of Lignin Structures and Lignin–Carbohydrate Complex (LCC) Linkages by Quantitative 13C and 2D HSQC NMR Spectroscopy. Journal of Agricultural and Food Chemistry. 2011;59(19):10604-14.

153. Balakshin M, Capanema E, Santos R, Chang H-M, Jameel H. Structural analysis of hardwood native lignins by quantitative 13C NMR spectroscopy. Holzforschung. 2015;70.

154. Argyropoulos DS. Quantitative Phosphorus-31 NMR Analysis of Six Soluble Lignins. Journal of Wood Chemistry and Technology. 1994;14(1):65-82.

155. Balakshin M, Capanema E. On the Quantification of Lignin Hydroxyl Groups With 31P and 13C NMR Spectroscopy. Journal of Wood Chemistry and Technology. 2015;35(3):220-37.

156. Faix O, Argyropoulos Dimitris S, Robert D, Neirinck V. Determination of Hydroxyl Groups in Lignins Evaluation of 1H-, 13C-, 31P-NMR, FTIR and Wet Chemical Methods. Holzforschung - International Journal of the Biology, Chemistry, Physics and Technology of Wood1994. p. 387.

157. Lundquist K. Proton (1H) NMR Spectroscopy. In: Lin SY, Dence CW, editors. Methods in Lignin Chemistry. Berlin, Heidelberg: Springer Berlin Heidelberg; 1992. p. 242-9.

158. Ding R, Wu H, Thunga M, Bowler N, Kessler MR. Processing and characterization of low-cost electrospun carbon fibers from organosolv lignin/polyacrylonitrile blends. Carbon. 2016;100:126-36.

159. Argyropoulos D. Heteronuclear NMR Spectroscopy of Lignins2010. 245-65 p.

160. Kanitskaya LV, Gogotov AF, Khai DTT, Rokhin AV. Quantitative 13C NMR spectroscopy. Chemical structure of kraft and nitrosated lignins. Russian Journal of Bioorganic Chemistry. 2012;38(7):720-5.

161. Xia Z, Akim LG, Argyropoulos DS. Quantitative 13C NMR Analysis of Lignins with Internal Standards. Journal of Agricultural and Food Chemistry. 2001;49(8):3573-8.

162. Wen J-L, Sun S-L, Xue B-L, Sun R-C. Recent Advances in Characterization of Lignin Polymer by Solution-State Nuclear Magnetic Resonance (NMR) Methodology. Materials. 2013;6(1).

163. Crestini C, Lange H, Sette M, Argyropoulos DS. On the structure of softwood kraft lignin. Green Chemistry. 2017;19(17):4104-21.

164. Capanema E, Balakshin M, Chen C-L, S. Gratzl J, Gracz H. Structural Analysis of Residual and Technical Lignins by 1H-13C Correlation 2D NMR-Spectroscopy2001. 302-8 p.

165. Pu Y, Cao S, Ragauskas AJ. Application of quantitative 31P NMR in biomass lignin and biofuel precursors characterization. Energy & Environmental Science. 2011;4(9):3154-66.

166. MacMillan CP, Birke H, Chuah A, Brill E, Tsuji Y, Ralph J, et al. Tissue and cell-specific transcriptomes in cotton reveal the subtleties of gene regulation underlying the diversity of plant secondary cell walls. BMC Genomics. 2017;18(1):539.

167. da Costa Sousa L, Foston M, Bokade V, Azarpira A, Lu F, Ragauskas AJ, et al. Isolation and characterization of new lignin streams derived from extractive-ammonia (EA) pretreatment. Green Chemistry. 2016;18(15):4205-15.

168. Li Y, Akiyama T, Yokoyama T, Matsumoto Y. NMR Assignment for Diaryl Ether Structures (4–O–5 Structures) in Pine Wood Lignin. Biomacromolecules. 2016;17(6):1921-9.

169. Ralph J, Lundquist K, Brunow G, Lu F, Kim H, F. Schatz P, et al. Lignins: Natural polymers from oxidative coupling of 4-hydroxyphenyl- propanoids2004. 29-60 p.

170. Yue F, Lu F, Regner M, Sun R, Ralph J. Lignin-Derived Thioacidolysis Dimers: Reevaluation, New Products, Authentication, and Quantification. ChemSusChem. 2017;10(5):830-5.

171. Ibarra D, Chávez MI, Rencoret J, Del Río JC, Gutiérrez A, Romero J, et al. Lignin Modification during Eucalyptus globulus Kraft Pulping Followed by Totally Chlorine-Free Bleaching: A Two-Dimensional Nuclear Magnetic Resonance, Fourier Transform Infrared, and Pyrolysis–Gas Chromatography/Mass Spectrometry Study. Journal of Agricultural and Food Chemistry. 2007;55(9):3477-90.

172. Lancefield CS, Wienk Hans LJ, Boelens R, Weckhuysen BM, Bruijnincx PCA. Identification of a diagnostic structural motif reveals a new reaction intermediate and condensation pathway in kraft lignin formation. Chemical Science. 2018;9(30):6348-60.

173. Yue F, Lu F, Sun R, Ralph J. Synthesis and Characterization of New 5-Linked Pinoresinol Lignin Models. Chemistry – A European Journal. 2012;18(51):16402-10.

174. Balakshin MY, Capanema EA, Chen, Gracz HS. Elucidation of the Structures of Residual and Dissolved Pine Kraft Lignins Using an HMQC NMR Technique. Journal of Agricultural and Food Chemistry. 2003;51(21):6116-27.

175. Nishimura H, Kamiya A, Nagata T, Katahira M, Watanabe T. Direct evidence for α ether linkage between lignin and carbohydrates in wood cell walls. Scientific Reports. 2018;8(1):6538.

176. Lancefield C, Wienk Hans L, Boelens R, Weckhuysen B, Bruijnincx P. Identification of a diagnostic structural motif reveals a new reaction intermediate and condensation pathway in kraft lignin formation. Chemical Science. 2018;9.

177. Liu H, Dai Z, Cao Q, Shi X, Wang X, Li H, et al. Lignin/Polyacrylonitrile Carbon Fibers: The Effect of Fractionation and Purification on Properties of Derived Carbon Fibers. ACS Sustainable Chemistry & Engineering. 2018;6(7):8554-62.

178. Ghosh T, Ngo T-D, Kumar A, Ayranci C, Tang T. Cleaning carbohydrate impurities from lignin using Pseudomonas fluorescens. Green Chemistry. 2019;21(7):1648-59.

179. Steudle L, Frank E, Ota A, Hageroth U, Henzler S, Schuler W, et al. Carbon Fibers Prepared from Melt Spun Peracylated Softwood Lignin: an Integrated Approach2017. 1600441 p.

180. Fang W, Yang S, Wang X-L, Yuan T-Q, Sun R-C. Manufacture and application of lignin-based carbon fibers (LCFs) and lignin-based carbon nanofibers (LCNFs). Green Chemistry. 2017;19(8):1794-827.

181. Liu HC, Chien A-T, Newcomb BA, Liu Y, Kumar S. Processing, Structure, and Properties of Lignin- and CNT-Incorporated Polyacrylonitrile-Based Carbon Fibers. ACS Sustainable Chemistry & Engineering. 2015;3(9):1943-54.

182. Cho M, Karaaslan MA, Renneckar S, Ko F. Enhancement of the mechanical properties of electrospun lignin-based nanofibers by heat treatment. Journal of Materials Science. 2017;52(16):9602-14.

183. Cho M, Karaaslan M, Chowdhury S, Ko F, Renneckar S. Skipping Oxidative Thermal Stabilization for Lignin-Based Carbon Nanofibers. ACS Sustainable Chemistry & Engineering. 2018;6(5):6434-44.

184. Dallmeyer I, Lin LT, Li Y, Ko F, Kadla JF. Preparation and Characterization of Interconnected, Kraft Lignin-Based Carbon Fibrous Materials by Electrospinning. Macromolecular Materials and Engineering. 2014;299(5):540-51.

185. Liu J, Wang PH, Li RY. Continuous carbonization of polyacrylonitrile-based oxidized fibers: Aspects on mechanical properties and morphological structure. Journal of Applied Polymer Science. 1994;52(7):945-50.

186. Hosseinaei O, Harper PD, Bozell JJ, Rials GT. Improving Processing and Performance of Pure Lignin Carbon Fibers through Hardwood and Herbaceous Lignin Blends. International Journal of Molecular Sciences. 2017;18(7).

187. Nordström Y, Norberg I, Sjöholm E, Drougge R. A new softening agent for melt spinning of softwood kraft lignin. Journal of Applied Polymer Science. 2013;129(3):1274-9.

188. Zhang M, Ogale A. Carbon Fibers from UV-Assisted Stabilization of Lignin-Based Precursors2015. 184-96 p.

189. Jin J, Ogale AA. Carbon fibers derived from wet-spinning of equi-component lignin/polyacrylonitrile blends. Journal of Applied Polymer Science. 2018;135(8):45903.

190. Maradur SP, Kim CH, Kim SY, Kim B-H, Kim WC, Yang KS. Preparation of carbon fibers from a lignin copolymer with polyacrylonitrile. Synthetic Metals. 2012;162(5):453-9.

191. Bengtsson A, Bengtsson J, Olsson C, Sedin M, Jedvert K, Theliander H, et al. Improved yield of carbon fibres from cellulose and kraft lignin2018.

192. Liu HC, Chien A-T, Newcomb BA, Bakhtiary Davijani AA, Kumar S. Stabilization kinetics of gel spun polyacrylonitrile/lignin blend fiber. Carbon. 2016;101:382-9.

193. Demiroğlu Mustafov S, Seydibeyoğlu MÖ. Surface Treatment of Lignin Sourced Carbon Fibers: Principles, Processes, and Challenges. In: Akpan EI, Adeosun SO, editors. Sustainable Lignin

for Carbon Fibers: Principles, Techniques, and Applications. Cham: Springer International Publishing; 2019. p. 427-39.

194. Oroumei A, Naebe M. Mechanical property optimization of wet-spun lignin/polyacrylonitrile carbon fiber precursor by response surface methodology. Fibers and Polymers. 2017;18(11):2079-93.

195. Wang R, Zobeiri H, Lin H, Qu W, Bai X, Deng C, et al. Anisotropic thermal conductivities and structure in lignin-based microscale carbon fibers. Carbon. 2019;147:58-69.

196. Jia Z, Lu C, Liu Y, Zhou P, Wang L. Lignin/Polyacrylonitrile Composite Hollow Fibers Prepared by Wet-Spinning Method. ACS Sustainable Chemistry & Engineering. 2016;4(5):2838-42.

197. Zhang M, Ogale AA. Carbon fibers from dry-spinning of acetylated softwood kraft lignin. Carbon. 2014;69:626-9.

198. Aslanzadeh S, Ahvazi B, Boluk Y, Ayranci C. Carbon Fiber Production from Electrospun Sulfur Free Softwood Lignin Precursors. Journal of Engineered Fibers and Fabrics. 2017;12:33-43.

199. Lai C, Zhou Z, Zhang L, Wang X, Zhou Q, Zhao Y, et al. Free-standing and mechanically flexible mats consisting of electrospun carbon nanofibers made from a natural product of alkali lignin as binder-free electrodes for high-performance supercapacitors. Journal of Power Sources. 2014;247:134-41.

200. Roman J, Neri W, Derré A, Poulin P. Electrospun lignin-based twisted carbon nanofibers for potential microelectrodes applications. Carbon. 2019;145:556-64.

201. Ogale AA, Zhang M, Jin J. Recent advances in carbon fibers derived from biobased precursors. Journal of Applied Polymer Science. 2016;133(45).

202. Kadla JF, Kubo S, Venditti RA, Gilbert RD, Compere AL, Griffith W. Lignin-based carbon fibers for composite fiber applications. Carbon. 2002;40(15):2913-20.

203. Uraki Y, Kubo S, Nigo N, Sano Y, Sasaya T. Preparation of Carbon Fibers from Organosolv Lignin Obtained by Aqueous Acetic Acid Pulping. Holzforschung - International Journal of the Biology, Chemistry, Physics and Technology of Wood1995. p. 343.

204. Sudo K, Shimizu K. A new carbon fiber from lignin. Journal of Applied Polymer Science. 1992;44(1):127-34.

205. Kubo S, Uraki Y, Sano Y. Preparation of carbon fibers from softwood lignin by atmospheric acetic acid pulping. Carbon. 1998;36(7):1119-24.

206. Gupta VB. Melt-spinning processes. In: Gupta VB, Kothari VK, editors. Manufactured Fibre Technology. Dordrecht: Springer Netherlands; 1997. p. 67-97.

207. Ziabicki A. Physical properties of fibre spinning process. Man-made Fibres: Science and Technology. 1. Newyork: Interscience Publishers; 1967. p. 13.

208. Ziabicki A. Fundaments of Fibre Formation: The Science of Fibre Spinning and Drawing. London: Wiley-Interscience; 1976.

209. Asmatulu R, Khan WS. Chapter 1 - Introduction to electrospun nanofibers. In: Asmatulu R, Khan WS, editors. Synthesis and Applications of Electrospun Nanofibers: Elsevier; 2019. p. 1-15.

210. Thunga M, Chen K, Grewell D, Kessler MR. Bio-renewable precursor fibers from lignin/polylactide blends for conversion to carbon fibers. Carbon. 2014;68:159-66.

211. Uraki Y, Nakatani A, Kubo S, Sano Y. Preparation of activated carbon fibers with large specific surface area from softwood acetic acid lignin. Journal of Wood Science. 2001;47(6):465-9.

212. Sudo K, Shimizu K, Nakashima N, Yokoyama A. A new modification method of exploded lignin for the preparation of a carbon fiber precursor. Journal of Applied Polymer Science. 1993;48(8):1485-91.

213. Goulis P, Konstantopoulos G, Kartsonakis AI, Mpalias K, Anagnou S, Dragatogiannis D, et al. Thermal Treatment of Melt-Spun Fibers Based on High Density PolyEthylene and Lignin. C — Journal of Carbon Research. 2017;3(4).

214. Kadla JF, Kubo S. Lignin-based polymer blends: analysis of intermolecular interactions in lignin–synthetic polymer blends. Composites Part A: Applied Science and Manufacturing. 2004;35(3):395-400.

215. Kubo S, Kadla JF. The Formation of Strong Intermolecular Interactions in Immiscible Blends of Poly(vinyl alcohol) (PVA) and Lignin. Biomacromolecules. 2003;4(3):561-7.

216. Kadla JF, Kubo S, Venditti RA, Gilbert RD. Novel hollow core fibers prepared from lignin polypropylene blends. Journal of Applied Polymer Science. 2002;85(6):1353-5.

217. Yue Z, Vakili A, Hosseinaei O, Harper DP. Lignin-based carbon fibers: Accelerated stabilization of lignin fibers in the presence of hydrogen chloride. Journal of Applied Polymer Science. 2017;134(46):45507.

218. Mainka H. Lignin as an alternative precusor for a sustainable and cost-effective carbon fibre for the automotive industry. Bremen, Germany: University of Bremen; 2015.

219. Mainka H, Hilfert L, Busse S, Edelmann F, Haak E, Herrmann AS. Characterization of the major reactions during conversion of lignin to carbon fiber. Journal of Materials Research and Technology. 2015;4(4):377-91.

220. Hosseinaei O, Harper DP, Bozell JJ, Rials TG. Role of Physicochemical Structure of Organosolv Hardwood and Herbaceous Lignins on Carbon Fiber Performance. ACS Sustainable Chemistry & Engineering. 2016;4(10):5785-98.

221. Mainka H, Täger O, Körner E, Hilfert L, Busse S, Edelmann FT, et al. Lignin – an alternative precursor for sustainable and cost-effective automotive carbon fiber. Journal of Materials Research and Technology. 2015;4(3):283-96.

222. Braun JL, Holtman KM, Kadla JF. Lignin-based carbon fibers: Oxidative thermostabilization of kraft lignin. Carbon. 2005;43(2):385-94.

223. Zhang M, Ogale AA. Effect of temperature and concentration of acetylated-lignin solutions on dry-spinning of carbon fiber precursors. Journal of Applied Polymer Science. 2016;133(45).

224. Bajaj P. Acrylic fibres. In: Gupta VB, Kothari VK, editors. Manufactured Fibre Technology. Dordrecht: Springer Netherlands; 1997. p. 406-56.

225. Gupta VB. Solution-spinning processes. In: Gupta VB, Kothari VK, editors. Manufactured Fibre Technology. Dordrecht: Springer Netherlands; 1997. p. 124-38.

226. Capone GJ. Wet-spinning Technology. In: Masson J, editor. Acrylic Fiber Technology and Applications New York: Marcel Dekker Inc; 1995.

227. Jeong K, Kim DH, Chung YS, Hwang SK, Hwang HY, Kim SS. Effect of processing parameters of the continuous wet spinning system on the crystal phase of PVDF fibers. Journal of Applied Polymer Science. 2018;135(3):45712.

228. Bahrami SH, Bajaj P, Sen K. Effect of coagulation conditions on properties of poly(acrylonitrile–carboxylic acid) fibers. Journal of Applied Polymer Science. 2003;89(7):1825-37.

229. Baojun Q, Ding P, Zhenqiou W. The mechanism and characterstics of dry-jet wet-spinning of acrylic fibers. Advances in Polymer Technology. 1986;6(4):509-29.

230. Hou C, Qu R-j, Liang Y, Wang C-g. Kinetics of diffusion in polyacrylonitrile fiber formation. Journal of Applied Polymer Science. 2005;96(5):1529-33.

231. Chen J, Wang C-g, Dong X-g, Liu H-z. Study on the Coagulation Mechanism of Wet-Spinning PAN Fibers. Journal of Polymer Research. 2006;13(6):515-9.

232. Dong X-G, Wang C-G, Bai Y-J, Cao W-W. Effect of DMSO/H2O coagulation bath on the structure and property of polyacrylonitrile fibers during wet-spinning. Journal of Applied Polymer Science. 2007;105(3):1221-7.

233. Kim HC, Kim D, Lee JY, Zhai L, Kim J. Effect of Wet Spinning and Stretching to Enhance Mechanical Properties of Cellulose Nanofiber Filament. International Journal of Precision Engineering and Manufacturing-Green Technology. 2019;6(3):567-75.

234. Reddy GVR, Deopura BL, Joshi M. Dry-jet-wet spun polyurethane fibers. I. Optimization of the spinning parameters. Journal of Applied Polymer Science. 2010;118(4):2291-303.

235. Huang Z-M, Zhang YZ, Kotaki M, Ramakrishna S. A review on polymer nanofibers by electrospinning and their applications in nanocomposites. Composites Science and Technology. 2003;63(15):2223-53.

236. Zhang Y, Lim CT, Ramakrishna S, Huang Z-M. Recent development of polymer nanofibers for biomedical and biotechnological applications. Journal of Materials Science: Materials in Medicine. 2005;16(10):933-46.

237. Hammel E, Tang X, Trampert M, Schmitt T, Mauthner K, Eder A, et al. Carbon nanofibers for composite applications. Carbon. 2004;42(5):1153-8.

238. Fan Z, Yan J, Wei T, Zhi L, Ning G, Li T, et al. Asymmetric Supercapacitors Based on Graphene/MnO2 and Activated Carbon Nanofiber Electrodes with High Power and Energy Density. Advanced Functional Materials. 2011;21(12):2366-75.

239. Khandan A, Salami M, Kaveian F, Rafienia M, Saber-Samandari S, Naeimi M. Electrospun Polycaprolactone/lignin-based Nanocomposite as a Novel Tissue Scaffold for Biomedical Applications. J Med Sign Sens. 2017;7.

240. Salami MA, Kaveian F, Rafienia M, Saber-Samandari S, Khandan A, Naeimi M. Electrospun Polycaprolactone/lignin-based Nanocomposite as a Novel Tissue Scaffold for Biomedical Applications. Journal of medical signals and sensors. 2017;7(4):228-38.

241. Hsu Y-H, Chan C-H, Tang WC. Alignment of Multiple Electrospun Piezoelectric Fiber Bundles Across Serrated Gaps at an Incline: A Method to Generate Textile Strain Sensors. Scientific Reports. 2017;7(1):15436.

242. E. Tenhaeff W, Rios O, More K, A. McGuire M. Highly Robust Lithium Ion Battery Anodes from Lignin: An Abundant, Renewable, and Low-Cost Material2014.

243. Zhang H, Zhang W, Ming H, Pang J, Zhang H, Cao G, et al. Design advanced carbon materials from lignin-based interpenetrating polymer networks for high performance sodium-ion batteries. Chemical Engineering Journal. 2018;341:280-8.

244. Lima RB, Raza R, Qin H, Li J, Lindström ME, Zhu B. Direct lignin fuel cell for power generation. RSC Advances. 2013;3(15):5083-9.

245. You X, Duan J, Koda K, Yamada T, Uraki Y. Preparation of electric double layer capacitors (EDLCs) from two types of electrospun lignin fibers2016.

246. Zhao Y, Liu Y, Tong C, Ru J, Geng B, Ma Z, et al. Flexible lignin-derived electrospun carbon nanofiber mats as a highly efficient and binder-free counter electrode for dye-sensitized solar cells. Journal of Materials Science. 2018;53(10):7637-47.

247. Taylor GI, Van Dyke MD. Electrically driven jets. Proceedings of the Royal Society of London A Mathematical and Physical Sciences. 1969;313(1515):453-75.

248. Yan X, Yu M, Ramakrishna S, Russell SJ, Long Y-Z. Advances in portable electrospinning devices for in situ delivery of personalized wound care. Nanoscale. 2019;11(41):19166-78.

249. Khan W, Asmatulu R, Ceylan M, Jabbarnia A. Recent Progress on Conventional and Non-Conventional Electrospinning Processes. Fibers and Polymers. 2013;14:1235-47.

250. Reneker DH, Yarin AL, Fong H, Koombhongse S. Bending instability of electrically charged liquid jets of polymer solutions in electrospinning. Journal of Applied Physics. 2000;87(9):4531-47.

251. Li D, Wang Y, Xia Y. Electrospinning of Polymeric and Ceramic Nanofibers as Uniaxially Aligned Arrays. Nano Letters. 2003;3(8):1167-71.

252. Zhang B, Kang F, Tarascon J-M, Kim J-K. Recent advances in electrospun carbon nanofibers and their application in electrochemical energy storage. Progress in Materials Science. 2016;76:319-80.

253. Angammana CJ, Jayaram SH. Fundamentals of electrospinning and processing technologies. Particulate Science and Technology. 2016;34(1):72-82.

254. Theron SA, Zussman E, Yarin AL. Experimental investigation of the governing parameters in the electrospinning of polymer solutions. Polymer. 2004;45(6):2017-30.

255. Chang F-C, Chan K-K, Chang C-Y. The Effect of Processing Parameters on Formation of Lignosulfonate Fibers Produced using Electrospinning Technology. 2016. 2016;11(2):13.

256. Zhang C-L, Yu S-H. Nanoparticles meet electrospinning: recent advances and future prospects. Chemical Society Reviews. 2014;43(13):4423-48.

257. Beachley V, Wen X. Effect of electrospinning parameters on the nanofiber diameter and length. Materials Science and Engineering: C. 2009;29(3):663-8.

258. Ago M, Okajima K, Jakes JE, Park S, Rojas OJ. Lignin-Based Electrospun Nanofibers Reinforced with Cellulose Nanocrystals. Biomacromolecules. 2012;13(3):918-26.

259. Oroumei A, Fox B, Naebe M. Thermal and Rheological Characteristics of Biobased Carbon Fiber Precursor Derived from Low Molecular Weight Organosolv Lignin. ACS Sustainable Chemistry & Engineering. 2015;3(4):758-69.

260. Lallave M, Bedia J, Ruiz-Rosas R, Rodríguez-Mirasol J, Cordero T, Otero JC, et al. Filled and Hollow Carbon Nanofibers by Coaxial Electrospinning of Alcell Lignin without Binder Polymers. Advanced Materials. 2007;19(23):4292-6.

261. Ramakrishna S, Fujihara K, Teo W-E, Lim T-C, Ma Z. An Introduction to Electrospinning and Nanofibers: WORLD SCIENTIFIC; 2005. 396 p.

262. Hohman M, Shin M, Rutledge G, Brenner M. Electrospinning and Electrically Forced Jets. II. Applications. Physics of Fluids. 2001;13.

263. Lukáš D, Sarkar A, Martinová L, Vodsed'álková K, Lubasová D, Chaloupek J, et al. Physical principles of electrospinning (Electrospinning as a nano-scale technology of the twenty-first century). Textile Progress. 2009;41(2):59-140.

264. Matthews JA, Wnek GE, Simpson DG, Bowlin GL. Electrospinning of Collagen Nanofibers. Biomacromolecules. 2002;3(2):232-8.

265. Kim JI, Hwang TI, Aguilar LE, Park CH, Kim CS. A Controlled Design of Aligned and Random Nanofibers for 3D Bi-functionalized Nerve Conduits Fabricated via a Novel Electrospinning Set-up. Scientific Reports. 2016;6:23761.

266. Theron A, Zussman E, Yarin AL. Electrostatic field-assisted alignment of electrospun nanofibres. Nanotechnology. 2001;12(3):384-90.

267. Lei T, Peng Q, Chen Q, Xiong J, zhang F, Sun D. Alignment of electrospun fibers using the whipping instability. Materials Letters. 2017;193:248-50.

268. Kang SB, Hyuk Won S, Ji Im M, Ul Kim C, Park W, Min Baik J, et al. Enhanced piezoresponse of highly aligned electrospun poly(vinylidene fluoride) nanofibers2017.

269. Braun J, Holtman K, Kadla J. Lignin-based carbon fibers: Oxidative thermostabilization of kraft lignin. Carbon. 2005;43:385-94.

270. Nirmale TC, Kale BB, Varma AJ. A review on cellulose and lignin based binders and electrodes: Small steps towards a sustainable lithium ion battery. International Journal of Biological Macromolecules. 2017;103:1032-43.

271. Teng N-Y, Dallmeyer I, Kadla JF. Effect of Softwood Kraft Lignin Fractionation on the Dispersion of Multiwalled Carbon Nanotubes. Industrial & Engineering Chemistry Research. 2013;52(19):6311-7.

272. Ma X, Kolla P, Zhao Y, Smirnova AL, Fong H. Electrospun lignin-derived carbon nanofiber mats surface-decorated with MnO2 nanowhiskers as binder-free supercapacitor electrodes with high performance. Journal of Power Sources. 2016;325:541-8.

273. Yu B, Gele A, Wang L. Iron oxide/lignin-based hollow carbon nanofibers nanocomposite as an application electrode materials for supercapacitors. International Journal of Biological Macromolecules. 2018;118:478-84.

274. Park C-W, Youe W-J, Han S-Y, Kim Yong S, Lee S-H. Characteristics of carbon nanofibers produced from lignin/polyacrylonitrile (PAN)/kraft lignin-g-PAN copolymer blends electrospun nanofibers. Holzforschung2017. p. 743.

275. Schreiber M, Vivekanandhan S, Cooke P, Mohanty A, Misra M. Electrospun green fibres from lignin and chitosan: A novel polycomplexation process for the production of lignin-based fibres. Journal of Materials Science. 2014;49.

276. Schreiber M, Vivekanandhan S, Mohanty A, Misra M. A Study on the electrospinning behaviour and nanofibre morphology of anionically charged lignin. Advanced Materials Letters. 2012;3.

277. Fang W, Yang S, Yuan T-Q, Charlton A, Sun R-C. Effects of Various Surfactants on Alkali Lignin Electrospinning Ability and Spun Fibers. Industrial & Engineering Chemistry Research. 2017;56(34):9551-9.

278. Stojanovska E, Pampal ES, Kilic A, Quddus M, Candan Z. Developing and characterization of lignin-based fibrous nanocarbon electrodes for energy storage devices. Composites Part B: Engineering. 2019;158:239-48.

279. Deng X, Huang Y, Song A, Liu B, Yin Z, Wu Y, et al. Gel polymer electrolyte with high performances based on biodegradable polymer polyvinyl alcohol composite lignocellulose. Materials Chemistry and Physics. 2019;229:232-41.

280. Hu S, Zhang S, Pan N, Hsieh Y-L. High energy density supercapacitors from lignin derived submicron activated carbon fibers in aqueous electrolytes. Journal of Power Sources. 2014;270:106-12.

281. Ma C, Li Z, Li J, Fan Q, Wu L, Shi J, et al. Lignin-based hierarchical porous carbon nanofiber films with superior performance in supercapacitors. Applied Surface Science. 2018;456:568-76.

282. Vivo-Vilches JFC, A.; Fierro, V.; Devin-Ziegler, I.; Brosse, N.; Dufour, A.; Etienne, M. Lignin-Based Carbon Nanofibers as Electrosdes for Vanadium Redox Couple Electrochemistry. Nanomaterials. 2019;9(1):1-13.

283. Youe W-J, Kim SJ, Lee S-M, Chun S-J, Kang J, Kim YS. MnO2-deposited lignin-based carbon nanofiber mats for application as electrodes in symmetric pseudocapacitors. International Journal of Biological Macromolecules. 2018;112:943-50.

284. Zhang W, Yu C, Chang L, Zhong W, Yang W. Three-dimensional nitrogen-doped hierarchical porous carbon derived from cross-linked lignin derivatives for high performance supercapacitors. Electrochimica Acta. 2018;282:642-52.

285. Cho M, Ko F, Renneckar S. Impact of Thermal Oxidative Stabilization on the Performance of Lignin-Based Carbon Nanofiber Mats2019. 5345-55 p.

286. Wikberg H, Ohra-aho T, Pileidis F, Titirici M-M. Structural and Morphological Changes in Kraft Lignin during Hydrothermal Carbonization. ACS Sustainable Chemistry & Engineering. 2015;3(11):2737-45.

287. Li Y, Cui D, Tong Y, Xu L. Study on structure and thermal stability properties of lignin during thermostabilization and carbonization. International Journal of Biological Macromolecules. 2013;62:663-9.

288. Beste A. ReaxFF Study of the Oxidation of Lignin Model Compounds for the Most Common Linkages in Softwood in View of Carbon Fiber Production. The Journal of Physical Chemistry A. 2014;118(5):803-14.

289. Faravelli T, Frassoldati A, Migliavacca G, Ranzi E. Detailed kinetic modeling of the thermal degradation of lignins. Biomass and Bioenergy. 2010;34(3):290-301.

290. Foston M, Nunnery GA, Meng X, Sun Q, Baker FS, Ragauskas A. NMR a critical tool to study the production of carbon fiber from lignin. Carbon. 2013;52:65-73.

291. TAPPI T257 sp-14 Sampling and Preparing wood for analysis. Atlanta, GA.2014.

292. TAPPI T264 cm-07 Preparation of Wood for Chemical Analysis. Atlanta, GA.2007.

293. TAPPI T211 om-02 Ash in Wood, Pulp, Paper and Paperboard: Combustion at 525°C Atlanta, GA2002.

294. Useful Method UM 250 Acid soluble lignin in wood and pulp. Atlanta, GA1985b.

295. TAPPI T222 om-02 Acid-insoluble Lignin in Wood and Pulp Atlanta, GA2006.

296. Dence CW. The Determination of Lignin. In: Lin SY, Dence CW, editors. Methods in Lignin Chemistry. Berlin, Heidelberg: Springer Berlin Heidelberg; 1992. p. 33-61.

297. de Jong E, Gosselink RJA. Chapter 17 - Lignocellulose-Based Chemical Products. In: Gupta VK, Tuohy MG, Kubicek CP, Saddler J, Xu F, editors. Bioenergy Research: Advances and Applications. Amsterdam: Elsevier; 2014. p. 277-313.

298. Malins EL, Waterson C, Becer CR. Alternating copolymers of functionalized α-methyl styrene monomers and maleic anhydride. Polymer Chemistry. 2015;6(36):6543-52.

299. Buono P, Duval A, Verge P, Averous L, Habibi Y. New Insights on the Chemical Modification of Lignin: Acetylation versus Silylation. ACS Sustainable Chemistry & Engineering. 2016;4(10):5212-22.

300. Choi JW, Faix O. NMR study on residual lignins isolated from chemical pulps of beech wood by enzymatic hydrolysis. Journal of Industrial and Engineering Chemistry. 2011;17(1):25-8.

301. Balakshin MY, Capanema EA. Comprehensive structural analysis of biorefinery lignins with a quantitative 13C NMR approach. RSC Advances. 2015;5(106):87187-99.

302. Crestini C, Argyropoulos D. Structural Analysis of Wheat Straw Lignin by Quantitative 31P and 2D NMR Spectroscopy. The Occurrence of Ester Bonds and ??-O-4 Substructures1997.

303. Sannigrahi P, Ragauskas AJ, Miller SJ. Lignin Structural Modifications Resulting from Ethanol Organosolv Treatment of Loblolly Pine. Energy & Fuels. 2010;24(1):683-9.

304. Rönnols J, Schweinebarth H, Jacobs A, Stevanic J, Olsson A-M, Reimann A, et al. Structural changes in softwood kraft lignin during non-oxidative thermal treatment2015. 550-61 p.

305. Granata A, Argyropoulos DS. 2-Chloro-4,4,5,5-tetramethyl-1,3,2-dioxaphospholane, a Reagent for the Accurate Determination of the Uncondensed and Condensed Phenolic Moieties in Lignins. Journal of Agricultural and Food Chemistry. 1995;43(6):1538-44.

306. Ghorbani MM, Taherian R. 12 - Methods of Measuring Electrical Properties of Material**Hereby from Keithley Co. and Dr. Michael B. Heaney is appreciated due to valuable content used in this chapter. In: Taherian R, Kausar A, editors. Electrical Conductivity in Polymer-Based Composites: William Andrew Publishing; 2019. p. 365-94.

307. Zhang X, Yan Q, Leng W, Li J, Zhang J, Cai Z, et al. Carbon Nanostructure of Kraft Lignin Thermally Treated at 500 to 1000 °C. Materials. 2017;10(8).

308. TAPPI T204 cm-97 Solvent extractives of wood and pulp. Atlanta, GA2007.

309. Constant S, Wienk HLJ, Frissen AE, Peinder Pd, Boelens R, van Es DS, et al. New insights into the structure and composition of technical lignins: a comparative characterisation study. Green Chemistry. 2016;18(9):2651-65.

310. Fagerstedt VK, Saranpää P, Tapanila T, Immanen J, Serra AJ, Nieminen K. Determining the Composition of Lignins in Different Tissues of Silver Birch. Plants. 2015;4(2).

311. Vassilev SV, Baxter D, Andersen LK, Vassileva CG. An overview of the chemical composition of biomass. Fuel. 2010;89(5):913-33.

312. Sameni J, Krigstin S, Rosa D, Leao A, Sain M. Thermal Characteristics of Lignin Residue from Industrial Processes. Bioresources. 2014;9:725-37.

313. Ház A, Jablonský M, Šurina I, Kačík F, Bubeníková T, Ďurkovič J. Chemical Composition and Thermal Behavior of Kraft Lignins. Forests. 2019;10(6).

314. Rohde V, Böringer S, Tübke B, Adam C, Dahmen N, Schmiedl D. Fractionation of three different lignins by thermal separation techniques—A comparative study. GCB Bioenergy. 2019;11(1):206-17.

315. Ehrnrooth EML. Change in Pulp Fibre Density With Acid-Chlorite Delignification. Journal of Wood Chemistry and Technology. 1984;4(1):91-109.

316. Alekhina M, Erdmann J, Ebert A, Stepan AM, Sixta H. Physico-chemical properties of fractionated softwood kraft lignin and its potential use as a bio-based component in blends with polyethylene. Journal of Materials Science. 2015;50(19):6395-406.

317. Nakamura K, Hatakeyama T, Hatakeyama H. Studies on Bound Water of Cellulose by Differential Scanning Calorimetry. Textile Research Journal. 1981;51(9):607-13.

318. Sevastyanova O, Helander M, Chowdhury S, Lange H, Wedin H, Zhang L, et al. Tailoring the molecular and thermo–mechanical properties of kraft lignin by ultrafiltration. Journal of Applied Polymer Science. 2014;131(18).

319. Sun Q, Khunsupat R, Akato K, Tao J, Labbé N, Gallego NC, et al. A study of poplar organosolv lignin after melt rheology treatment as carbon fiber precursors. Green Chemistry. 2016;18(18):5015-24.

320. Berthold J, Rinaudo M, Salmeń L. Association of water to polar groups; estimations by an adsorption model for ligno-cellulosic materials. Colloids and Surfaces A: Physicochemical and Engineering Aspects. 1996;112(2):117-29.

321. Hatakeyama T, Hirose S, Hatakeyama H. Differential scanning calorimetric studies on bound water in 1,4-dioxane acidolysis lignin. Die Makromolekulare Chemie. 1983;184(6):1265-74.

322. Engelund ET, Thygesen LG, Svensson S, Hill CAS. A critical discussion of the physics of wood–water interactions. Wood Science and Technology. 2013;47(1):141-61.

323. Mansouri N, Yuan Q, Huang F. Characterization of alkaline lignins for use in penol-formaldehyde and epoxy resins2011.

324. Hatakeyama H, Hatakeyama T. Interaction between water and hydrophilic polymers. Thermochimica Acta. 1998;308(1):3-22.

325. Guigo N, Mija A, Vincent L, Sbirrazzuoli N. Molecular mobility and relaxation process of isolated lignin studied by multifrequency calorimetric experiments. Physical Chemistry Chemical Physics. 2009;11(8):1227-36.

326. Price DM, Bashir Z. A study of the porosity of water-plasticised polyacrylonitrile films by thermal analysis and microscopy. Thermochimica Acta. 1995;249:351-66.

327. Jiang Y, Lawrence M, Hussain A, Ansell M, Walker P. Comparative moisture and heat sorption properties of fibre and shiv derived from hemp and flax. Cellulose. 2019;26(2):823-43.

328. Sun B, Wang Z, Liu J. Changes of chemical properties and the water vapour sorption of Eucalyptus pellita wood thermally modified in vacuum. Journal of Wood Science. 2017;63(2):133-9.

329. Hill CAS, Norton A, Newman G. The water vapor sorption behavior of natural fibers. Journal of Applied Polymer Science. 2009;112(3):1524-37.

330. Reina JJ, Domínguez E, Heredia A. Water sorption–desorption in conifer cuticles: The role of lignin. Physiologia Plantarum. 2001;112(3):372-8.

331. Saito T, Brown RH, Hunt MA, Pickel DL, Pickel JM, Messman JM, et al. Turning renewable resources into value-added polymer: development of lignin-based thermoplastic. Green Chemistry. 2012;14(12):3295-303.

332. Jääskeläinen AS, Liitiä T, Mikkelson A, Tamminen T. Aqueous organic solvent fractionation as means to improve lignin homogeneity and purity. Industrial Crops and Products. 2017;103:51-8.

333. Deng Y, Feng X, Zhou M, Qian Y, Yu H, Qiu X. Investigation of Aggregation and Assembly of Alkali Lignin Using Iodine as a Probe. Biomacromolecules. 2011;12(4):1116-25.

334. Sadeghifar H, Argyropoulos DS. Macroscopic Behavior of Kraft Lignin Fractions: Melt Stability Considerations for Lignin–Polyethylene Blends. ACS Sustainable Chemistry & Engineering. 2016;4(10):5160-6.

335. Jiang X, Savithri D, Du X, Pawar S, Jameel H, Chang H-m, et al. Fractionation and Characterization of Kraft Lignin by Sequential Precipitation with Various Organic Solvents. ACS Sustainable Chemistry & Engineering. 2017;5(1):835-42.

336. Boeriu CG, Fiţigău FI, Gosselink RJA, Frissen AE, Stoutjesdijk J, Peter F. Fractionation of five technical lignins by selective extraction in green solvents and characterisation of isolated fractions. Industrial Crops and Products. 2014;62:481-90.

337. Hatakeyama H. Thermal analysis of lignin by defferential scanning calorimetry. Cellulose Chem Technol. 1972;6:521-9.

338. LeBoeuf EJ, Weber WJ. Macromolecular Characteristics of Natural Organic Matter. 1. Insights from Glass Transition and Enthalpic Relaxation Behavior. Environmental Science & Technology. 2000;34(17):3623-31.

339. Bouajila J, Dole P, Joly C, Limare A. Some laws of a lignin plasticization. Journal of Applied Polymer Science. 2006;102(2):1445-51.

340. Sakata I, Senju R. Thermoplastic behavior of lignin with various synthetic plasticizers. Journal of Applied Polymer Science. 1975;19(10):2799-810.

341. Hatakeyama H. Thermal Analysis. In: Lin SY, Dence CW, editors. Methods in Lignin Chemistry. Berlin, Heidelberg: Springer Berlin Heidelberg; 1992. p. 200-14.

342. Hatakeyama H, and Hatakeyama, T. Thermal properties of isolated and in situ lignin. Lignan and Lignans: Advances in Chemistry2010. p. 301-16.

343. Holladay JE, White JF, Bozell JJ, Johnson D. Top Value-Added Chemicals from Biomass - Volume II—Results of Screening for Potential Candidates from Biorefinery Lignin. 2007. Report No.: PNNL-16983; Other: BM0102070; TRN: US200805%%262 United States10.2172/921839Other: BM0102070; TRN: US200805%%262Mon Apr 07 07:21:24 EDT 2008PNNLEnglish.

344. Vural D, Smith JC, Petridis L. Dynamics of the lignin glass transition. Physical Chemistry Chemical Physics. 2018;20(31):20504-12.

345. Chen Y, Stark NM, Cai Z, Frihart CR, Lorenz LF, Ibach RE. Chemical Modification of Kraft Lignin: Effect on Chemical and Thermal Properties. BioResources; Vol 9, No 3 (2014). 2014.

346. Methacanon P, Weerawatsophon, U., Thainthongdee, M., and Lekpittaya, P. Optimum conditions for selective separation of kraft lignin. Kasetsart Journal: Natural Science. 2010;44:680-90.

347. Hatakeyama H, Tsujimoto Y, Zarubin M, Krutov S, Hatakeyama T. Thermal decomposition and glass transition of industrial hydrolysis lignin. Journal of Thermal Analysis and Calorimetry. 2010;101:289-95.

348. Zhou X, Zheng F, Liu X, Tang L, Xue G, Du G, et al. Glass transition of oxygen plasma treated enzymatic hydrolysis lignin2012.

349. Cui C, Sadeghifar H, Sen S, Argyropoulos DS. Toward Thermoplastic Lignin Polymers; Part II: Thermal & Polymer Characteristics of Kraft Lignin & Derivatives2013.

350. Argyropoulos DS, Berry RM, Bolker HI. Polymerization beyond the gel point, 2. A study of the soluble fraction as a function of the extent of reaction. Die Makromolekulare Chemie. 1987;188(8):1985-92.

351. Argyropoulos DS, Berry RM, Bolker HI. Species distribution within the soluble phase beyond the gel point. Macromolecules. 1987;20(2):357-61.

352. Gregorova A. Application of Differential Scanning Calorimetry to the Characterization of Biopolymers. Applications of Calorimetry in a Wide Context - Differential Scanning Calorimetry, Isothermal Titration Calorimetry and Microcalorimetry2013. p. 3-17.

353. Yang H, Yan R, Chen H, Lee DH, Zheng C. Characteristics of hemicellulose, cellulose and lignin pyrolysis. Fuel. 2007;86(12–13):1781-8.

354. Brebu MaV, Cornelia. Thermal degradation of lignin-A reivew. Cellulose Chemistry and Technology. 2010;44(9):353-63.

355. Watkins D, Nuruddin M, Hosur M, Tcherbi-Narteh A, Jeelani S. Extraction and characterization of lignin from different biomass resources. Journal of Materials Research and Technology. 2015;4(1):26-32.

356. Fisher T, Hajaligol M, Waymack B, Kellogg D. Pyrolysis behavior and kinetics of biomass derived materials. Journal of Analytical and Applied Pyrolysis. 2002;62(2):331-49.

357. Boateng AA, Hicks KB, Vogel KP. Pyrolysis of switchgrass (Panicum virgatum) harvested at several stages of maturity. Journal of Analytical and Applied Pyrolysis. 2006;75(2):55-64.

358. Zhang C, Hu X, Guo H, Wei T, Dong D, Hu G, et al. Pyrolysis of poplar, cellulose and lignin: Effects of acidity and alkalinity of the metal oxide catalysts. Journal of Analytical and Applied Pyrolysis. 2018;134:590-605.

359. Ryu HW, Lee HW, Jae J, Park Y-K. Catalytic pyrolysis of lignin for the production of aromatic hydrocarbons: Effect of magnesium oxide catalyst. Energy. 2019;179:669-75.

360. Yildiz G, Ronsse F, Venderbosch R, Duren Rv, Kersten SRA, Prins W. Effect of biomass ash in catalytic fast pyrolysis of pine wood. Applied Catalysis B: Environmental. 2015;168-169:203-11.

361. Gray MR, Corcoran WH, Gavalas GR. Pyrolysis of a wood-derived material. Effects of moisture and ash content. Industrial & Engineering Chemistry Process Design and Development. 1985;24(3):646-51.

362. Fahmi R, Bridgwater AV, Donnison I, Yates N, Jones JM. The effect of lignin and inorganic species in biomass on pyrolysis oil yields, quality and stability. Fuel. 2008;87(7):1230-40.

363. Jakab E, Faix O, Till F, Székely T. The effect of cations on the thermal decomposition of lignins. Journal of Analytical and Applied Pyrolysis. 1993;25:185-94.

364. Pan W-P, Richards GN. Influence of metal ions on volatile products of pyrolysis of wood. Journal of Analytical and Applied Pyrolysis. 1989;16(2):117-26.

365. Toloue Farrokh N, Suopajärvi H, Sulasalmi P, Fabritius T. A thermogravimetric analysis of lignin char combustion2018.

366. Farrokh NT, Suopajärvi H, Sulasalmi P, Fabritius T. A thermogravimetric analysis of lignin char combustion. Energy Procedia. 2019;158:1241-8.

367. Simoneit BRT, Rogge WF, Mazurek MA, Standley LJ, Hildemann LM, Cass GR. Lignin pyrolysis products, lignans, and resin acids as specific tracers of plant classes in emissions from biomass combustion. Environmental Science & Technology. 1993;27(12):2533-41.

368. Jegers HE, Klein MT. Primary and secondary lignin pyrolysis reaction pathways. Industrial & Engineering Chemistry Process Design and Development. 1985;24(1):173-83.

369. Kuroda K-I, Ashitani T, Fujita K, Hattori T. Thermal Behavior of β-1 Subunits in Lignin: Pyrolysis of 1,2-Diarylpropane-1,3-diol-type Lignin Model Compounds2007. 2770-8 p.

370. de Wild P, Van der Laan R, Kloekhorst A, Heeres E. Lignin valorisation for chemicals and (transportation) fuels via (catalytic) pyrolysis and hydrodeoxygenation. Environmental Progress & Sustainable Energy. 2009;28(3):461-9.

371. Butler E, Devlin G, Meier D, McDonnell K. A review of recent laboratory research and commercial developments in fast pyrolysis and upgrading. Renewable and Sustainable Energy Reviews. 2011;15(8):4171-86.

372. Zhang R, Chen Y, Lei K, Liu D. The effects of specific surface area and ash on char gasification mechanisms in the mixture of H2O, CO2, H2 and CO. Fuel. 2017;209:109-16.

373. Fan L, Zhang Y, Liu S, Zhou N, Chen P, Cheng Y, et al. Bio-oil from fast pyrolysis of lignin: Effects of process and upgrading parameters. Bioresource Technology. 2017;241:1118-26.

374. Brazil T, Costa R, Massi M, Rezende M. Structural, morphological, and thermal characterization of kraft lignin and its charcoals obtained at different heating rates. Materials Research Express. 2018;5.

375. Silva R, Haraguchi SK, Muniz EC, Rubira AF. Aplicações de fibras lignocelulósicas na química de polímeros e em compósitos. Química Nova. 2009;32:661-71.

376. Schorr D, Diouf PN, Stevanovic T. Evaluation of industrial lignins for biocomposites production. Industrial Crops and Products. 2014;52:65-73.

377. Faix O. Classification of Lignins from Different Botanical Origins by FT-IR Spectroscopy. Holzforschung - International Journal of the Biology, Chemistry, Physics and Technology of Wood1991. p. 21.

378. Abdelkafi F, Ammar H, Rousseau B, Tessier M, El Gharbi R, Fradet A. Structural Analysis of Alfa Grass (Stipa tenacissima L.) Lignin Obtained by Acetic Acid/Formic Acid Delignification. Biomacromolecules. 2011;12(11):3895-902.

379. Faix O. Fourier Transform Infrared Spectroscopy. In: Lin SY, Dence CW, editors. Methods in Lignin Chemistry. Berlin, Heidelberg: Springer Berlin Heidelberg; 1992. p. 83-109.

380. Wang K, Xu F, Sun R. Molecular Characteristics of Kraft-AQ Pulping Lignin Fractionated by Sequential Organic Solvent Extraction. International Journal of Molecular Sciences. 2010;11(8).

381. Sun R, Lu Q, Sun XF. Physico-chemical and thermal characterization of lignins from Caligonum monogoliacum and Tamarix spp. Polymer Degradation and Stability. 2001;72(2):229-38.

382. Prozil SO, Evtuguin DV, Silva AMS, Lopes LPC. Structural Characterization of Lignin from Grape Stalks (Vitis vinifera L.). Journal of Agricultural and Food Chemistry. 2014;62(24):5420-8.

383. Azadfar M, Gao AH, Bule MV, Chen S. Structural characterization of lignin: A potential source of antioxidants guaiacol and 4-vinylguaiacol. International Journal of Biological Macromolecules. 2015;75:58-66.

384. Sun R, Tomkinson J, Mao FC, Sun XF. Physicochemical characterization of lignins from rice straw by hydrogen peroxide treatment. Journal of Applied Polymer Science. 2001;79(4):719-32.

385. El Khaldi-Hansen B, Kusch P, Schulze M, Kamm B. Qualitative and Quantitative Analysis of Lignin Produced from Beech Wood by Different Conditions of the Organosolv Process2016.

386. Jahan M, Liu Z, Wang H, Saeed A, Ni Y. Isolation and characterization of lignin from prehydrolysis liquor of kraft-based dissolving pulp production2012. 261-7 p.

387. Liitiä TM, Maunu SL, Hortling B, Toikka M, Kilpeläinen I. Analysis of Technical Lignins by Two- and Three-Dimensional NMR Spectroscopy. Journal of Agricultural and Food Chemistry. 2003;51(8):2136-43.

388. Sameni J, Krigstin S, Sain M. Characterization of Lignins Isolated from Industrial Residues and their Beneficial Uses2016.

389. Monteil-Rivera F, Phuong M, Ye M, Halasz A, Hawari J. Isolation and characterization of herbaceous lignins for applications in biomaterials. Industrial Crops and Products. 2013;41:356-64.

390. Calvo-Flores. Functional and Spectroscopic Characterization of Lignins. Lignin and Lignans as Renewable Raw Materials2015. p. 145-87.

391. Kosa M, Ben H, Theliander H, Ragauskas AJ. Pyrolysis oils from CO2 precipitated Kraft lignin. Green Chemistry. 2011;13(11):3196-202.

392. Ben H, Ragauskas AJ. Pyrolysis of Kraft Lignin with Additives. Energy & Fuels. 2011;25(10):4662-8.

393. Jablonsky M, Strižincová P, Majová V, Andrea S, Haz A, Surina I. CONTENT OF PHENOLIC HYDROXYL GROUPS IN LIGNIN: CHARACTERISATION OF 23 ISOLATED NON-WOOD LIGNIN WITH VARIOUS ACIDS. International Journal of Scientific Research. 2016;7:11547-51.

394. Zhao X, Zhang Y, Yang M, Huang Z, Hu H, Huang A, et al. Acylation of Lignin with Different Acylating Agents by Mechanical Activation-Assisted Solid Phase Synthesis: Preparation and Properties. Polymers (Basel). 2018;10(8):907.

395. Sen S, Patil S, Argyropoulos DS. Methylation of softwood kraft lignin with dimethyl carbonate. Green Chemistry. 2015;17(2):1077-87.

396. Sadeghifar H, Wells T, Le RK, Sadeghifar F, Yuan JS, Jonas Ragauskas A. Fractionation of Organosolv Lignin Using Acetone:Water and Properties of the Obtained Fractions. ACS Sustainable Chemistry & Engineering. 2017;5(1):580-7.

397. Uraki Y, Sugiyama Y, Koda K, Kubo S, Kishimoto T, Kadla JF. Thermal Mobility of β-O-4-Type Artificial Lignin. Biomacromolecules. 2012;13(3):867-72.

398. Ruiz-Rosas R, Bedia J, Lallave M, Loscertales IG, Barrero A, Rodríguez-Mirasol J, et al. The production of submicron diameter carbon fibers by the electrospinning of lignin. Carbon. 2010;48(3):696-705.

399. Poursorkhabi V, Mohanty AK, Misra M. Electrospinning of aqueous lignin/poly(ethylene oxide) complexes. Journal of Applied Polymer Science. 2015;132(2).

400. Zhang W, Yang P, Li X, Zhu Z, Chen M, Zhou X. Electrospun lignin-based composite nanofiber membrane as high-performance absorbent for water purification. International Journal of Biological Macromolecules. 2019;141:747-55.

401. Dallmeyer I, Ko F, Kadla JF. Correlation of Elongational Fluid Properties to Fiber Diameter in Electrospinning of Softwood Kraft Lignin Solutions. Industrial & Engineering Chemistry Research. 2014;53(7):2697-705.

402. Fenner RA, Lephardt JO. Examination of the thermal decomposition of kraft pine lignin by Fourier transform infrared evolved gas analysis. Journal of Agricultural and Food Chemistry. 1981;29(4):846-9.

403. Kadla JF, Chang Hm. The Reactions of Peroxides with Lignin and Lignin Model Compounds. Oxidative Delignification Chemistry. ACS Symposium Series. 785: American Chemical Society; 2001. p. 108-29.

404. Berthold J, Desbrières J, Rinaudo M, Salmén L. Types of adsorbed water in relation to the ionic groups and their counter-ions for some cellulose derivatives. Polymer. 1994;35(26):5729-36.

405. Jääskeläinen A-S, Keyriläinen P, Liitiä T, Tamminen T. Carbohydrate-free and highly soluble softwood kraft lignin fractions by aqueous acetone evaporation fractionation. Nordic Pulp & Paper Research Journal. 2017;32:485-92.

406. Zhang Y, Wu J-Q, Li H, Yuan T-Q, Wang Y-Y, Sun R-C. Heat treatment of industrial alkaline lignin and its potential application as adhesive for green wood-lignin composites2017.

407. Drbohlav J, Stevenson WTK. The oxidative stabilization and carbonization of a synthetic mesophase pitch, part I: The oxidative stabilization process. Carbon. 1995;33(5):693-711.

408. Simms JR, Yang CQ. Infrared spectroscopy studies of the petroleum pitch carbon fiber—II. The distribution of the oxidation products between the surface and the bulk. Carbon. 1994;32(4):621-6.

409. Major I, Pin J-M, Behazin E, Rodriguez-Uribe A, Misra M, Mohanty A. Graphitization of Miscanthus grass biocarbon enhanced by in situ generated FeCo nanoparticles. Green Chemistry. 2018;20(10):2269-78.

410. Tatarova E, Dias A, Henriques J, Abrashev M, Bundaleska N, Kovacevic E, et al. Towards large-scale in free-standing graphene and N-graphene sheets. Scientific Reports. 2017;7(1):10175.

411. Kim C, Park S-H, Cho J-I, Lee D-Y, Park T-J, Lee W-J, et al. Raman spectroscopic evaluation of polyacrylonitrile-based carbon nanofibers prepared by electrospinning. Journal of Raman Spectroscopy. 2004;35(11):928-33.

412. Zhu J, Chen C, Lu Y, Ge Y, Jiang H, Fu K, et al. Nitrogen-doped carbon nanofibers derived from polyacrylonitrile for use as anode material in sodium-ion batteries. Carbon. 2015;94:189-95.

413. Lee S. Structural Evolution of Polyacrylonitrile Fibers in Stabilization and Carbonization. Advances in Chemical Engineering and Science. 2012;02:275-82.

414. Sagues WJ, Jain A, Brown D, Aggarwal S, Suarez A, Kollman M, et al. Are lignin-derived carbon fibers graphitic enough? Green Chemistry. 2019;21(16):4253-65.

415. Snowdon MR, Mohanty AK, Misra M. A Study of Carbonized Lignin as an Alternative to Carbon Black. ACS Sustainable Chemistry & Engineering. 2014;2(5):1257-63.

416. Liu J, Qu W, Xie Y, Zhu B, Wang T, Bai X, et al. Thermal conductivity and annealing effect on structure of lignin-based microscale carbon fibers. Carbon. 2017;121:35-47.

417. Santos F, Queiroz J, Colodette J, Manfredi M, Queiroz M, Caldas C, et al. OPTIMIZATION OF HYDROTHERMAL PRETREATMENT OF CANE SUGAR STRAW FOR CELLULOSIC ETHANOL PRODUCTION. Química Nova. 2014;37:56-U78.

418. Tran LQN, Minh TN, Fuentes CA, Chi TT, Van Vuure AW, Verpoest I. Investigation of microstructure and tensile properties of porous natural coir fibre for use in composite materials. Industrial Crops and Products. 2015;65:437-45.

419. Yan L, Chouw N, Huang L, Kasal B. Effect of alkali treatment on microstructure and mechanical properties of coir fibres, coir fibre reinforced-polymer composites and reinforced-cementitious composites. Construction and Building Materials. 2016;112:168-82.

420. Muensri P, Kunanopparat T, Menut P, Siriwattanayotin S. Effect of lignin removal on the properties of coconut coir fiber/wheat gluten biocomposite. Composites Part A: Applied Science and Manufacturing. 2011;42(2):173-9.

421. Khalil HPSA, Ismail H, Rozman HD, Ahmad MN. The effect of acetylation on interfacial shear strength between plant fibres and various matrices. European Polymer Journal. 2001;37(5):1037-45.

422. Hill CAS, Khalil HPSA, Hale MD. A study of the potential of acetylation to improve the properties of plant fibres. Industrial Crops and Products. 1998;8(1):53-63.

423. Abdul Khalil HPS, Siti Alwani M, Mohd Omar AK. CHEMICAL COMPOSITION, ANATOMY, LIGNIN DISTRIBUTION, AND CELL WALL STRUCTURE OF MALAYSIAN PLANT WASTE FIBERS. BioResources; Vol 1, No 2 (2006). 2007.

424. van Dam JEG, van den Oever MJA, Keijsers ERP, van der Putten JC, Anayron C, Josol F, et al. Process for production of high density/high performance binderless boards from whole coconut husk: Part 2: Coconut husk morphology, composition and properties. Industrial Crops and Products. 2006;24(2):96-104.

425. Raveendran K, Ganesh A, Khilar KC. Influence of mineral matter on biomass pyrolysis characteristics. Fuel. 1995;74(12):1812-22.

426. van Dam JEG, van den Oever MJA, Teunissen W, Keijsers ERP, Peralta AG. Process for production of high density/high performance binderless boards from whole coconut husk: Part 1: Lignin as intrinsic thermosetting binder resin. Industrial Crops and Products. 2004;19(3):207-16.

427. Bayuaji R, Kurniawan R, Yasin A, Fatoni H, Lutfi FI. The effect of fly ash and coconut fibre ash as cement replacement materials on cement paste strength. IOP Conference Series: Materials Science and Engineering. 2016;128:012014.

428. Jenkins BM, Baxter LL, Miles TR, Miles TR. Combustion properties of biomass. Fuel Processing Technology. 1998;54(1):17-46.

429. Shao Y, Wang J, Preto F, Zhu J, Xu C. Ash Deposition in Biomass Combustion or Co-Firing for Power/Heat Generation. Energies. 2012;5(12).

430. Jung W, Savithri D, Sharma-Shivappa R, Kolar P. Changes in Lignin Chemistry of Switchgrass due to Delignification by Sodium Hydroxide Pretreatment. Energies. 2018;11:376.

431. Jung W, Savithri D, Sharma-Shivappa R, Kolar P. Effect of Sodium Hydroxide Pretreatment on Lignin Monomeric Components of Miscanthus × giganteus and Enzymatic Hydrolysis. Waste and Biomass Valorization. 2019.

432. Han L, Feng J, Zhang S, Ma Z, Wang Y, Zhang X. Alkali pretreated of wheat straw and its enzymatic hydrolysis. Brazilian journal of microbiology : [publication of the Brazilian Society for Microbiology]. 2012;43:53-61.

433. Avelino F, Silva KTd, de Souza Filho MdSM, Mazzetto SE, Lomonaco D. Microwave-assisted organosolv extraction of coconut shell lignin by Brønsted and Lewis acids catalysts. Journal of Cleaner Production. 2018;189:785-96.

434. Váquez-Torres H, Canché-Escamilla G, Cruz-Ramos CA. Coconut husk lignin. I. Extraction and characterization. Journal of Applied Polymer Science. 1992;45(4):633-44.

435. Rencoret J, Ralph J, Marques G, Gutiérrez A, Martínez ÁT, del Río JC. Structural Characterization of Lignin Isolated from Coconut (Cocos nucifera) Coir Fibers. Journal of Agricultural and Food Chemistry. 2013;61(10):2434-45.

436. Wenzel RN. Surface Roughness and Contact Angle. The Journal of Physical and Colloid Chemistry. 1949;53(9):1466-7.

437. Johnson D, Hilal N, Bowen WR. Chapter 1 - Basic Principles of Atomic Force Microscopy. In: Bowen WR, Hilal N, editors. Atomic Force Microscopy in Process Engineering. Oxford: Butterworth-Heinemann; 2009. p. 1-30.

438. Szewczyk P, Ura D, Metwally S, Knapczyk-Korczak J, Gajek M, Marzec M, et al. Roughness and Fiber Fraction Dominated Wetting of Electrospun Fiber-Based Porous Meshes. Polymers. 2018;11:34.

439. Alarifi IM, Alharbi A, Khan WS, Swindle A, Asmatulu R. Thermal, Electrical and Surface Hydrophobic Properties of Electrospun Polyacrylonitrile Nanofibers for Structural Health Monitoring. Materials (Basel). 2015;8(10):7017-31.

440. Cho M, Karaaslan M, Wang H, Renneckar S. Greener transformation of lignin into ultralight multifunctional materials. Journal of Materials Chemistry A. 2018;6(42):20973-81.

441. Zhou S, Liu P, Wang M, Zhao H, Yang J, Xu F. Sustainable, Reusable, and Superhydrophobic Aerogels from Microfibrillated Cellulose for Highly Effective Oil/Water Separation. ACS Sustainable Chemistry & Engineering. 2016;4(12):6409-16.

442. Hanus L, Řezanka T, Dembitsky V, Moussaieff A. Myrrh–Commiphora chemistry. Biomedical papers of the Medical Faculty of the University Palacký, Olomouc, Czechoslovakia. 2005;149:3-27.